The Emergence of Greenland Meltwater Impacts: From Boundary Currents to the Atlantic Overturning Circulation

Dissertation
for the degree Doctor of Natural Sciences
at the Faculty of Mathematics and Natural Sciences
of the Christian-Albrechts-Universität zu Kiel

submitted by

Ilana Schiller-Weiss

Kiel, 2024

First reviewer: Prof. Dr. Arne Biastoch

Second reviewer: Prof. Dr. Joakim Kjellsson

Date of submission: April 30th, 2024

Date of oral examination: June 20th, 2024

Prof. Dr. Frank Kempken, Dean

Declaration

I hereby declare that apart from the supervisor's guidance, the content and design of the thesis is all the candidate's own work. The thesis has not been been submitted either partially or wholly as part of a doctoral degree to another examining body nor has it been published or submitted for publication other than as indicated in the thesis. The thesis has been prepared with regard to the Rules of Good Scientific Practice of the German Research Foundation and that prior to this thesis, I have not attempted and failed to obtain a doctoral degree nor have I withdrawn from an academic degree.

Ilana Schiller-Weiss

Kiel, April 2024

This thesis is dedicated
to my grandmother Jane Schiller,
whose wisdom, love,
and dedication to learning has guided me.

Cover photo by Lois Anderson.
Photo of icebergs in Disko Bay, August 2023.

Abstract

The Greenland ice sheet has been steadily losing mass over the past decades from rising air temperatures and global warming. Additional freshwater input to the subpolar North Atlantic (SPNA) has the potential to reach areas where deep waters are formed, creating a lid of low salinity water resulting in a more strongly stratified layer. This could inhibit deep convection, potentially having future implications for the global ocean circulation and heat redistribution.

This thesis aims to identify and quantify an emerging impact of enhanced Greenland meltwater runoff, at its current magnitudes, on hydrography and dynamics in the SPNA. Meltwater, upon entering the open ocean, will first reach the East and West Greenland boundary currents. Both the East and West Greenland Current (EGC/WGC) consist of two surface-intensified current cores, a coastal current and outer slope current where the coastal current contains the majority of glacial meltwater and relatively fresh Arctic-sourced polar water. Using a hindcast, eddy-rich ocean-sea ice model and an ocean reanalysis product, both validated against mooring data, it is found that freshwater remains close to the shelf forced by strong alongshore winds. In two years, 2010 and 2012, exceptionally large freshwater content anomalies primarily visible in the coastal current can be attributed to the imprint of Greenland meltwater runoff, two years of record breaking surface melt extend during the summer season. Freshwater propagates from Fram Strait to Cape Farewell on time scales of 4–8 months with freshwater anomalies originating from the Arctic Ocean and sea ice melt. The latter often masks the signal from meltwater runoff coinciding in seasonal occurrence. Sufficiently resolving the coastal and slope current and representing mesoscale dynamics are necessary to understand freshwater propagation and exchanges between the two currents and with the open ocean, particularly as the coastal current contains the freshest water and early imprint of Greenland melt. A realistic freshwater forcing is critical for correctly representing the effect of Greenland ice sheet melting in model simulations then used to determine the imprint on salinity variations in the boundary current system.

To further identify the impacts from enhanced meltwater input into the SPNA, a set of twin model experiments was conducted only differing by the amounts of freshwater input from Greenland prescribed: one with interannually varying and increasing freshwater fluxes (FWFs) and the other with continued lower runoff based on the climatological mean (1960–2000). The most significant hydrographic changes, associated with a local near surface freshening and cooling, occur along the boundary current, decreasing the along-shelf density. A stronger density gradient between the warm, saltier interior and the fresher, cooler boundary current appears to have evolved, speeding up the boundary currents primarily seen at OSNAP West. The accelerated currents show a tendency towards eddy formation

and also shedding into the interior Labrador Sea, where deep convection most often occurs. Recently, 2015–2018, the Irminger Sea experienced deep convection as well and the twin experiments showed that enhanced Greenland meltwater runoff supported the eastward shift found in the winter deep mixed layer. Prior to 2015–2018, Greenland meltwater lead to a significant freshening of the Labrador deep convection area, not inhibiting convection but resulting in a shallower mixed layer and redistributing the meltwater to shallower depths only prior to being exported to the Irminger Sea at mid depth. These fresher waters at mid to intermediate depths contributed to a weakening in stratification and deepening of the winter mixed layer in the Irminger Sea.

There are no evident impacts on the large scale circulation such as the Atlantic Meridional Overturning Circulation (AMOC) with enhanced Greenland meltwater runoff at its current magnitudes. Since imprints are anticipated, an analysis of the covariation of AMOC strength and sea surface height (SSH)—two key parameters of potential climate risks in consequence of ice sheet melt—on decadal time scales is conducted using an ensemble of six ocean model hindcast simulations plus the two additional simulations with realistic and reduced freshwater input from Greenland. There is a strong, inverse relationship between AMOC and SSH variability: as the AMOC weakens (strengthens), there is an increase (decrease) in regional SSH along the US East coast and western subpolar gyre (SPG). However this relationship is also dependent on the strength of the AMOC, which varies among the simulations. There is a pronounced increase in SSH along the East Greenland shelf and the Labrador basin with enhanced Greenland melt, particularly during a low AMOC phase (2005–2014). Greenland FWFs show a lagged, inverse relationship with the AMOC and North Atlantic Oscillation (NAO) on longer, pentadal and decadal time scales with a positive NAO phase associated with cooler winter temperatures, stronger ocean heat loss and reduced melting.

This thesis provides new insights into the local impact of Greenland meltwater runoff and its current increase. While the signal is still relatively small, there are observable hydrographic changes that occur primarily along the East and West Greenland boundary currents with potential for meltwater to reach deep convective sites. There are still open questions to as what, how, and when Greenland meltwater may tip the freshwater balance of the SPNA. Thus it is important to continue monitoring freshwater changes using both observations and models.

Zusammenfassung

Der grönländische Eisschild hat in den letzten Jahrzehnten aufgrund steigender Lufttemperaturen und globaler Erwärmung stetig an Masse verloren. Zusätzlicher Süßwassereintrag in den subpolaren Nordatlantik (SPNA) hat das Potenzial, Gebiete zu erreichen, in denen sich Tiefenwasser bildet, wodurch ein Deckel aus Wasser mit niedrigem Salzgehalt entsteht, der die Schichtung verstärkt. Dies könnte die Tiefenkonvektion hemmen, was sich in Zukunft auf die globale Ozeanzirkulation und die Wärmeumverteilung auswirken könnte. Ziel dieser Arbeit ist es, eine sich abzeichnende Auswirkung des verstärkten Abflusses von grönländischem Schmelzwasser auf die Hydrographie und Dynamik im SPNA zu identifizieren und zu quantifizieren. Wenn das Schmelzwasser in den offenen Ozean gelangt, erreicht es zunächst die ost- und westgrönländischen Randströme. Sowohl der Ost- als auch der Westgrönlandstrom (EGC/WGC) bestehen aus zwei oberflächenintensiven Strömungskernen, einem Küstenstrom und einem äußeren Hangstrom, wobei der Küstenstrom den Großteil des Gletscherschmelzwassers und relativ frisches Polarwasser aus der Arktis enthält.

Unter Verwendung eines wirbelreichen Ozean-Meereis-Modells und eines Ozean-Reanalyse-Produkts, die beide anhand von Verankerungsdaten validiert wurden, wird gezeigt, dass das Süßwasser in der Nähe des Schelfs verbleibt, was durch starke küstenparallele Winde erzwungen wird. In zwei Jahren, 2010 und 2012, können außergewöhnlich große Anomalien des Süßwassergehalts, die vor allem in der Küstenströmung sichtbar sind, auf den Einfluss des grönländischen Schmelzwasserabflusses zurückgeführt werden, zwei Jahre mit rekordverdächtiger Oberflächenschmelze während der Sommersaison. Süßwasser breitet sich von der Framstraße bis zum Kap Farewell auf Zeitskalen von 4 bis 8 Monaten aus, wobei die Süßwasseranomalien aus dem Arktischen Ozean und der Meereisschmelze stammen. Letzteres überdeckt oft das Signal des Schmelzwasserabflusses, das saisonal auftritt. Eine ausreichende Auflösung des Küsten- und Hangstroms und die Darstellung der mesoskaligen Dynamik sind notwendig, um die Ausbreitung des Süßwassers und den Austausch zwischen den beiden Strömen und mit dem offenen Ozean zu verstehen, insbesondere, da der Küstenstrom das frischeste Wasser und den frühen Einfluss der Grönlandschmelze enthält. Ein realistischer Süßwasserantrieb ist entscheidend für die korrekte Darstellung der Auswirkungen der Grönlandeisschmelze in Modellsimulationen, die dann zur Bestimmung der Auswirkungen auf die Salzgehaltsschwankungen im Grenzstromsystem verwendet werden.

Um die Auswirkungen des verstärkten Schmelzwassereintrags in die SPNA zu ermitteln, wurden zwei komplementäre Modellsimulationen durchgeführt, die sich nur durch die

Menge des vorgeschriebenen Süßwassereintrags aus Grönland unterschieden: eines mit zwischenjährlich veränderlichen und steigenden Süßwasserflüssen (FWFs) und das andere mit anhaltend geringeren Abflüssen auf der Grundlage des klimatologischen Mittels (1960-2000). Die bedeutendsten hydrographischen Veränderungen, die mit einer lokalen oberflächennahen Auffrischung und Abkühlung verbunden sind, treten entlang des Grenzstroms auf, wodurch die Dichte entlang des Schelfs abnimmt. Es scheint sich ein stärkerer Dichtegradient zwischen dem warmen, salzigeren Landesinneren und der frischeren, kühleren Grenzströmung entwickelt zu haben, der die Grenzströmungen, die vor allem entlang der OSNAP-West-Linie zu beobachten sind, beschleunigt. Die beschleunigten Strömungen zeigen eine Tendenz zur Wirbelbildung und auch zur Ablösung in das Innere der Labradorsee, wo Tiefenkonvektion am häufigsten auftritt. In den Jahren 2015 bis 2018 kam es auch in der Irmingersee zu Tiefenkonvektion, und die Zwillingsexperimente zeigten, dass der verstärkte Abfluss von grönländischem Schmelzwasser die Ostverschiebung der winterlichen tiefen Deckschicht unterstützte. Vor 2015-2018 führte das grönländische Schmelzwasser zu einer erheblichen Auffrischung des Labrador-Tiefenkonvektionsgebiets, was die Konvektion nicht hemmte, sondern zu einer flacheren Deckschicht und zu einer Umverteilung des Schmelzwassers in geringere Tiefen führte, bevor es in die Irmingersee in mittlerer Tiefe exportiert wurde. Dieses frischere Wasser in oberen bis mittleren Wassertiefen trug zu einer Schwächung der Schichtung und einer Vertiefung der winterlichen Deckschicht in der Irmingersee bei.

Es gibt keine herausstechenden Auswirkungen auf die großräumige Zirkulation wie die atlantische meridionale Umwälzzirkulation (AMOC) mit verstärktem grönländischem Schmelzwasserabfluss in ihren derzeitigen Ausmaßen. Da aber Auswirkungen zu erwarten sind, wird eine Analyse der Kovariation der AMOC-Stärke und der Meeresoberflächenhöhe (SSH) - zwei Schlüsselparameter für potenzielle Klimarisiken infolge der Eisschmelze - auf dekadischen Zeitskalen durchgeführt, wobei ein Ensemble aus sechs Ozeanmodell-Hindcast-Simulationen und den zwei zusätzlichen Simulationen mit realistischem und reduziertem Süßwassereintrag aus Grönland verwendet wird. Es besteht eine starke, umgekehrte Beziehung zwischen AMOC und SSH-Variabilität: Wenn die AMOC schwächer (stärker) wird, kommt es zu einer Zunahme (Abnahme) der regionalen SSH entlang der US-Ostküste und des westlichen subpolaren Wirbels (SPG). Diese Beziehung hängt jedoch auch von der Stärke der AMOC ab, die in den Simulationen variiert. Es gibt einen deutlichen Anstieg der SSH entlang des ostgrönländischen Schelfs und des Labradorbeckens mit verstärkter Grönlandschmelze, insbesondere während einer Phase mit niedriger AMOC (2005-2014). Die grönländischen FWFs zeigen eine verzögerte, umgekehrte Beziehung zur AMOC und der Nordatlantischen Oszillation (NAO) auf längeren, pentadischen und dekadischen Zeitskalen, wobei eine positive NAO-Phase mit kühleren Wintertemperaturen, stärkerem Wärmeverlust des Ozeans und geringerem Schmelzen einhergeht. Diese Arbeit liefert neue Erkenntnisse über die lokalen Auswirkungen des grönländischen Schmelzwasserabflusses und seiner derzeitigen Zunahme. Obwohl das Signal noch relativ klein ist, sind bereits hydrographische Veränderungen zu beobachten, die vor allem entlang der ost- und westgrönländischen Grenzströme auftreten und dazu führen können, dass Schmelzwasser Tiefenkonvektoinsgebiete erreicht. Es gibt noch offene Fragen, ob, wie und wann grönländisches Schmelzwasser die Süßwasserbilanz der SPNA kippen könnte. Daher ist es wichtig, die Veränderungen des Süßwassers sowohl durch Beobachtungen als auch durch Modellsimulationen weiter zu verfolgen.

Contents

1 Introduction **3**
- 1.1 Atlantic Meridional Overturning Circulation . . . 3
- 1.2 Buoyancy and Circulation in the Subpolar North Atlantic . . . 5
  - 1.2.1 Wind and buoyancy changes in the SPNA . . . 5
  - 1.2.2 Current pathways . . . 7
  - 1.2.3 The Greenland Boundary Current System . . . 8
  - 1.2.4 Deep water formation and convection . . . 10
- 1.3 Greenland runoff and freshwater pathways . . . 11
  - 1.3.1 Greenland Runoff . . . 11
  - 1.3.2 Freshwater pathways . . . 12
- 1.4 Thesis aims, contributions, and structure . . . 14

2 Study 1: Do Salinity Variations Along the East Greenland Shelf Show Imprints of Increasing Meltwater Runoff? **17**

3 Study 2: Emerging influence of enhanced Greenland melting on boundary currents and deep convection regimes in the Labrador and Irminger Seas **39**

4 Study 3: Relating sea surface height changes to decadal variability of the Atlantic Meridional Overturning Circulation: a multi-centennial ocean model study using repeated forcing cycles **73**

5 Summary and Outlook **91**
- 5.0.1 Synthesis . . . 91
- 5.0.2 Summary of findings . . . 93
- 5.0.3 Emerging Challenges and Outlook . . . 95

6 Acknowledgement **97**

References **99**

1 Introduction

1.1 Atlantic Meridional Overturning Circulation

The Atlantic Ocean contains a complex web of currents transporting warm, saline upper waters northwards and fresher, deep waters southwards. This large scale current system, known as the Atlantic Meridional Overturning Circulation (AMOC), is a fundamental part of the climate system as it redistributes heat and freshwater all across the ocean (Figure 1.1).

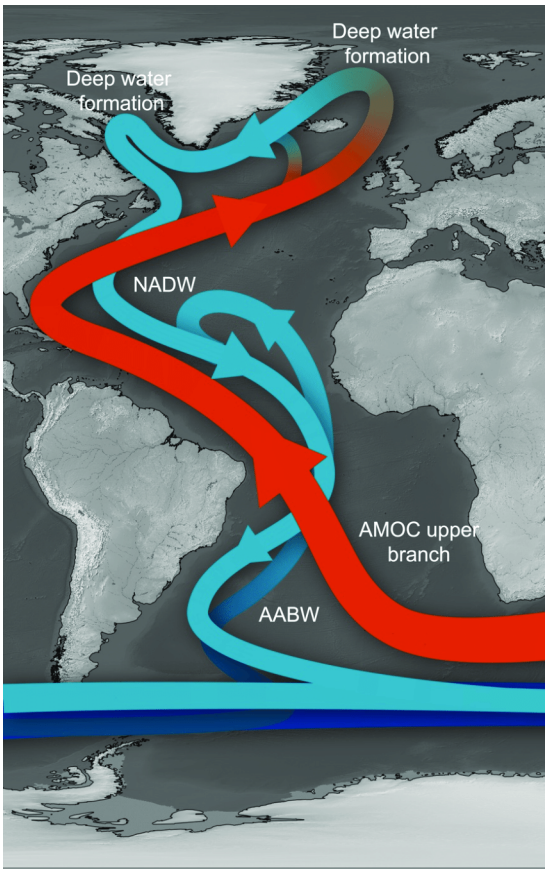

Fig. 1.1: Schematic of current pathways from AMOC. The northward/southward branch highlighted in red/blue. The areas of deep water formation are marked. Source: Crivellari, 2018.

The AMOC consists of a major source of northern heat transport, containing 20–30% of the total heat transport from the ocean and atmosphere, into the mid-latitudes (Trenberth

et al., 2019, Jackson et al., 2022), thus making the AMOC a key component in modulating regional and global climate variability. The AMOC however is also sensitive to changes in long term climate. Global warming and climate change are predicted to reduce or even halt overturning strength in the coming century, which could have far reaching impacts on the climate system from changes in precipitation patterns (Parsons et al., 2014; Jackson et al., 2015; Liu et al., 2020) to regional sea level rise (Goddard et al., 2015; Little et al., 2019; Volkov et al., 2023).

The north and southward branches of the AMOC reconnect at the high northern latitudes. Warm waters lose heat to the atmosphere and cool down as they travel northward, mixing with deeper layers and forming deep waters through a process known as deep convection (Rhein et al., 2011; Stramma et al., 2004). These colder, denser waters sink and return southwards at depth along the narrow and fast Deep Western Boundary Current (Toole et al., 2011; Buckley and Marshall, 2016). These large gradients in density, i.e. temperature and salinity, are primary drivers of AMOC, inducing deep mixing and deep water formation, referred to as thermohaline mechanisms (Kuhlbrodt et al., 2007; Buckley and Marshall, 2016). Surface winds and internal tides generate internal waves that also drive the AMOC through turbulent mixing of heat, causing heavier water masses at depth to mix with lighter, overlying waters, referred to as wind-driven mechanisms (Kuhlbrodt et al., 2007).

The subpolar North Atlantic (SPNA) has been observed to go through rapid changes in decadal temperatures trends from cooler to warmer periods (Desbruyères et al., 2021; Fox et al., 2022; Chafik et al., 2023). However with the onset of climate change, there is a projected warming of the SPNA resulting in additional freshwater input from increased net precipitation (Josey and Marsh, 2005) and warmer surface temperatures which increase the potential for melting of the Greenland ice sheet (Fichefet et al., 2003; Gerdes et al., 2006; Jungclaus et al., 2006; Swingedouw et al., 2006; Swingedouw et al., 2007; Stammer, 2008; Hanna et al., 2008; Kopp et al., 2010; Straneo and Heimbach, 2013). The growing concern is that too much Greenland-sourced freshwater upon entering the SPNA will result in a cool, fresh, and low density "lid" of water that would increase stratification and inhibit deep water formation and mixing processes. This in turn could reduce overturning strength and circulation in the SPNA (Dickson et al., 1988; Bakker et al., 2016; Böning et al., 2016).

The sensitivity of the AMOC to enhanced freshwater input in the SPNA has been a long-term topic of interest and debate. In particular, what might happen to the overturning strength with an additional increase in freshwater from accelerated Greenland ice sheet melt? Is there a quantifiable tipping point at which the AMOC will weaken or collapse in the future? And is there a certain recovery period for the AMOC when freshwater input is reduced? The AMOC's stability has been investigated under a number of ocean and climate model-based experiments where large-scale amounts of of freshwater are artificially "hosed" into the North Atlantic to simulate ocean climate responses (Fischer et al., 2004; Smith and Gregory, 2009; Kopp et al., 2010; Swingedouw, Rodehacke, et al., 2013; Jackson and Wood, 2018; Westen et al., 2024; Jackson et al., 2023). These hosing experiments reveal a range of scenarios from an AMOC weakening to recovery after the hosing ceases (Jackson et al., 2023) to a complete shutdown (Jackson et al., 2015; Westen et al., 2024). Figure 1.2 shows the weakened AMOC and tipping point from a hosing experiment with a CESM simulation (Westen et al., 2024).

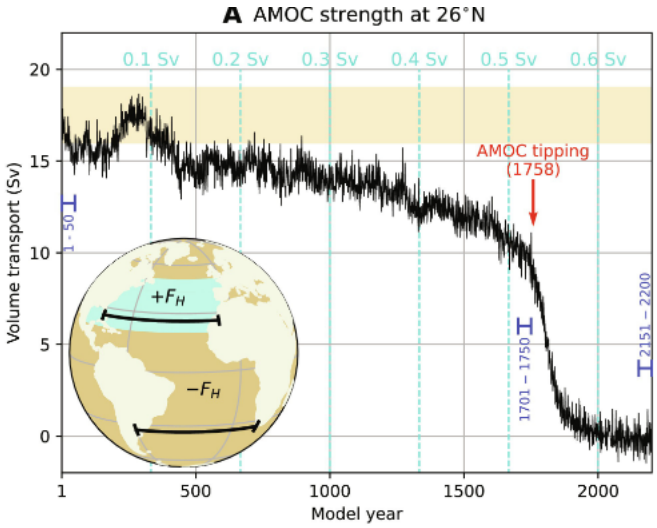

Fig. 1.2: The evolution of AMOC volume transport given in Sverdrups (Sv) at 26°N in a CSEM model version 1.0.5, after freshwater is fluxed into the North Atlantic (area marked by light blue rectangle in the globe inset). The proposed tipping point is indicated by the red arrow (source: Westen et al., 2024).

The ocean's response to these model-based freshwater perturbation experiments are sensitive to the amount and duration of freshwater being added, but also to the model configuration itself i.e. the horizontal resolution, eddy resolving capabilities, surface fluxes, atmospheric coupling and mean climatic state (Martin et al., 2022; Martin and Biastoch, 2023; Jackson et al., 2023). However, the rate of Greenland melting at present is far less and more gradual than what is prescribed in the hosing and freshwater perturbation experiments (Böning et al., 2016; Dukhovskoy et al., 2019). Greenland meltwater reaches the open ocean via the coastline where freshwater travels along Greenland's continental shelves in swift and narrow western boundary currents (Talley et al., 2011). Freshwater must be exported off the shelf to reach the interior ocean and regions where deep waters are formed (Marsh et al., 2010; Luo et al., 2016; Böning et al., 2016). Thus it is of high importance to explore whether there are any changes that we see in the SPNA, as a result of realistic estimates of freshwater input from Greenland. In order to gain further insight on the impacts of Greenland meltwater and their associated pathways, let's first delve into the wind, buoyancy forcings, and circulation patterns in the SPNA.

1.2 Buoyancy and Circulation in the Subpolar North Atlantic

1.2.1 Wind and buoyancy changes in the SPNA

The SPNA is characterized by strong westerly winds that blow over the mid-latitudes. The northern side of the westerlies cause Ekman pumping, driving the cyclonic circulation in the SPNA (Talley et al., 2011; Deshayes and Frankignoul, 2008). The SPNA sits below an

area of low atmospheric pressure, where changes in the SPNA are thought to be driven largely by the North Atlantic Oscillation (NAO) (Hurrell, 1995; Visbeck et al., 2001; Hurrell and Deser, 2010). The NAO is characterized by changes in the strength of the atmospheric pressure gradient between the Icelandic low and Azores high (Visbeck et al., 2001; Flatau et al., 2003; Hurrell et al., 2003; Hurrell and Deser, 2010) and is attributed to drive much of the interannual and decadal variability in the SPNA including the size and strength of the SPG (Koul et al., 2020).

The NAO undergoes positive and negative phases; during the positive phase, westerly winds strengthen and conditions tend to be colder and drier (Visbeck et al., 2001; Hurrell et al., 2003). These stronger winds also result in more severe outbreaks of cold and dry air from North America (Rühs et al., 2021), with enhanced cyclonic flow in the SPG. There tends to be stronger wintertime heat loss during positive phases of the NAO (Lohmann et al., 2009b), enhancing the potential for deep convective activity in the SPG (Bersch et al., 2007; Frankignoul et al., 2009; Brodeau and Koenigk, 2016; Rühs et al., 2021).

Meanwhile, the opposite occurs during a negative phase of the NAO, where conditions tend to be warmer with weaker westerly winds and cyclonic circulation. Increased Greenland melt is observed during negative phases, where warmer and wetter conditions lead to faster melt rates (Hanna et al., 2012; Bevis et al., 2019). It is not only atmospheric variability that drives changes in the SPNA, but also large scale changes in salinity and temperature, i.e. buoyancy. The Arctic is a primary source of cold and freshwater entering the SPNA through differing Arctic "gateways" i.e. Fram Strait (northeastern Greenland), Davis Strait, and the Canadian Arctic Archipelago (western Greenland) (Myers, 2005; Haine et al., 2015; Rudels, 2011).

"Great Salinity Anomalies" (GSA), patches of low salinity and cool waters, propagated around the SPNA throughout the 1970s, 80s, and 90s (Dickson et al., 1988; Belkin et al., 1998; Belkin, 2004). GSA origins stem from remote and local forcings from enhanced Arctic freshwater export (remote) and severe winters in the Labrador Sea and Baffin Bay (local) (Belkin et al., 1998). In winter of 1968/69, a temporary shut down of deep water convection was observed in the Labrador Sea, induced from the GSA freshening event coinciding with mild atmospheric winter conditions (Gelderloos et al., 2012), signifying the impact that low salinity anomalies may have on convection.

Recent changes in the Arctic freshwater system are attributed to anthropogenic warming, such as the reduction of sea ice in summer, enhanced river runoff, and freshwater from Bering Strait (Proshutinsky et al., 2009; Haine et al., 2015; Wu et al., 2005; Nummelin et al., 2016). The Arctic ocean stores a lot of freshwater, with the Beaufort Gyre being one of the largest freshwater reservoirs (Proshutinsky et al., 2009). Freshwater in the gyre has been increasing (Wang et al., 2018; Proshutinsky et al., 2009) by 40% in the past two decades (Zhang et al., 2021). A future freshwater release of the gyre would lead to enhanced freshwater export through Fram and Davis Strait, potentially having widespread impacts in the SPNA and deep water formation (Zhang et al., 2021; Lin et al., 2023).

1.2.2 Current pathways

The SPNA contains a complex interplay of different currents (schematic shown in Figure 1.3). Starting from south to north, the North Atlantic Current (NAC) transports warm and saline, tropical-sourced water northward via the eastern SPNA. The current meanders and splits into two major current branches, navigated by major topographic features along the NAC pathway (Rossby, 1996). One branch flowing through the Iceland basin and the other one via the Rockall Trough (Orvik and Niiler, 2002). These two branches of the NAC make up the major pathways of warmer, upper Atlantic Water into the North Atlantic (Fratantoni, 2001).

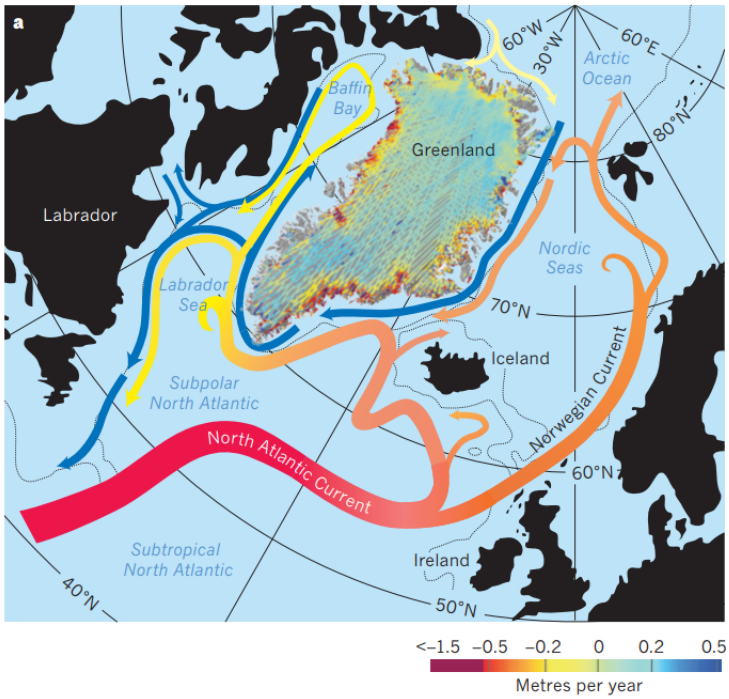

Fig. 1.3: Schematic of major surface currents and basins. Atlantic-origin pathways in red and yellow, Arctic-origin freshwater pathways marked in blue. The dynamic thinning of Greenland is superimposed (source: Straneo and Heimbach, 2013).

The northeastward branch through the Rockall Trough makes up the Norwegian Current heading into the Nordic Seas and then towards the Arctic (Orvik and Niiler, 2002). The other branch that crosses the Icelandic basin bifurcates southeast of Iceland and returns around Reykjanes Ridge circulating westward over the Denmark Strait. Through subsequent cooling via heat loss in winter, the modified, cooler return flows merge along the southeastern side of Greenland and flows cyclonically around the rim of the subpolar gyre (SPG), forming a strong boundary current system around the Labrador Sea (Orvik and Niiler, 2002; Pickart et al., 2002; Reverdin et al., 2003; Fischer et al., 2004; Böning et al., 2016). The currents described here are a part of the SPG.

The East and West Greenland Current consists of two surface-intensified currents flowing around Greenland. The East Greenland Current (EGC) flows along Greenland's eastern

continental shelf (Rudels et al., 2002; Sutherland and Pickart, 2008; Foukal et al., 2020). Starting northward and flowing southward, it rounds the southern tip of Greenland merging into the West Greenland Current (Rudels et al., 2002). The West Greenland Current (WGC) then splits into two major branches: either flowing northwards up towards Baffin Bay or cyclonically around the perimeter of the Labrador sea (Pacini et al., 2021; Gou et al., 2021), to join the Labrador Current along the Canadian coast. More details on the EGC and WGC system are discussed in the following section.

1.2.3 The Greenland Boundary Current System

Additional freshwater input from Greenland runoff will first appear along the EGC and WGC system. The Greenland shelf consists of a wide continental shelf, varying in width with the southern shelf of Greenland narrowing sharply. At the shelfbreak, the bathymetry drops rapidly in just over a few kilometers making a steep slope from the shelf to just offshore (Duyck and De Jong, 2023). Starting from east of Greenland, the EGC stems from Fram Strait and follows the shelf traveling downstream. It is a strong, surface-intensified buoyant current transporting cold and fresh Arctic polar water and Greenland meltwater southward (Rudels et al., 2002; Sutherland and Pickart, 2008; Håvik et al., 2017).

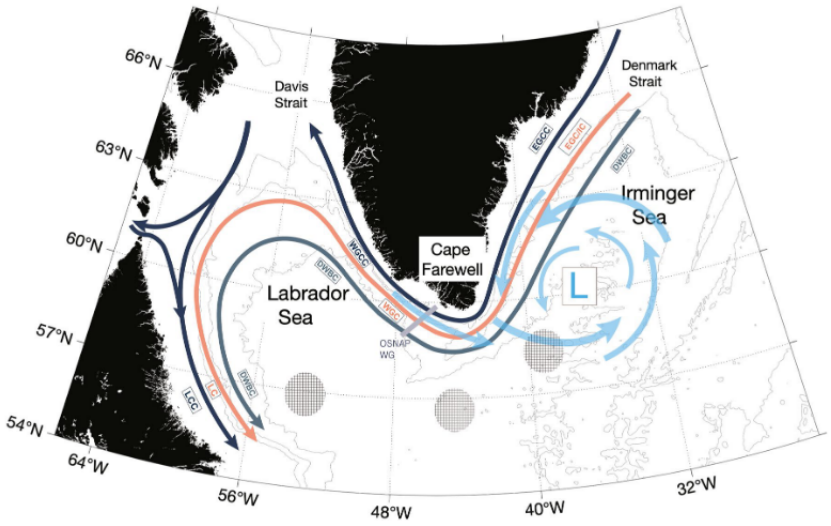

Fig. 1.4: Schematic of circulation along the East and West Greenland boundary system. EGCC: East Greenland Coastal Current, EGC/IC: East Greenland Current/Irminger Curent, WGCC: West Greenlannd coastal current, WGC: West Greenland Current (source: Pacini and Pickart, 2023).

The EGC system is made up of two currents, the one close to the coast referred to as the coastal current (EGCC). The EGCC has been observed primarily south of Denmark Strait (Bacon et al., 2002; Sutherland and Pickart, 2008; Håvik et al., 2017; Foukal et al., 2020), where two distinct current cores are observed. It is the EGCC that contains the majority of fresh polar water and Greenland melt (Foukal et al., 2020). Just beyond the shelfbreak, there is the outer EGC (Håvik et al., 2017), also referred to as the slope current (Le Bras et al., 2020). The outer EGC flows adjacent to and merges with the saltier and warmer

Irminger Current, particularly as it rounds Cape Farewell, the southern tip of Greenland (Le Bras et al., 2018). A schematic of the surface boundary currents is shown in Figure 1.4.

As the EGCC and EGC round Cape Farewell, they form the WGC and WGCC (Pacini et al., 2020; Gou et al., 2021). Similar to the EGCC, the WGCC carries cold and freshwater from the Arctic and Greenland (Gou et al., 2021). The outer WGC, situated on the shelfbreak of West Greenland, still carries buoyant freshwater near the surface with warmer, saltier Irminger water at intermediate depths (Myers et al., 2007; Fratantoni and Pickart, 2007; Pacini et al., 2020; Gou et al., 2022). Unlike the EGCC, with its clear separation from the outer EGC, the WGCC's boundary with the outer WGC is not as clearly defined, associated with a merging between the two current branches (Duyck and De Jong, 2021; Gou et al., 2021; Gou et al., 2022). The WGCC extends northward towards Baffin Bay via Davis Strait, while the outer WGC can split into two branches: flowing along the rim of the Labrador Sea, joining the Labrador Current or northwards to Baffin Bay (Myers et al., 2009; Gou et al., 2021; Gou et al., 2022) (Figure 1.4).

Along the EGC/WGC system, there is a sharp hydrographic and velocity front separating these fast moving boundary currents along Greenland from the warmer and saltier interior ocean (Sutherland and Pickart, 2008; Brearley et al., 2012; Duyck et al., 2022). As the boundary currents along Greenland are the first instances where Greenland runoff will show up in the open ocean, they are vital to understanding export off the shelf and freshwater pathways into the interior SPNA.

One way that water from the boundary current can enter the interior ocean is through mesoscale eddies. These eddies can transport heat and salt into the interior and have been observed to play a large role in determining the magnitude and location of deep convection and restratification (Lilly et al., 2003; Bracco et al., 2008; Chanut et al., 2008; Gelderloos et al., 2011; Rieck et al., 2019). Different types of eddies are found in the Labrador Sea depending on the origin, properties, and vertical structure Rieck et al., 2019. Irminger Rings (IRs) originate from the WGC, particularly near Cape Desolation (60.44°N, 48.10°W) where a steep topographical gradient along the continental slope induces local instabilities leading to the generation of warm-core, anticylonics IRs (Chanut et al., 2008; Rieck et al., 2019). IRs have a typical diameter of 30–60 km and upon shedding from the boundary current, they can mix with surrounding waters in the northern Labrador Sea increasing stratification and potentially inhibiting deep convection (Chanut et al., 2008; Rieck et al., 2019).

Boundary current eddies (BCEs) are smaller, shallower, and surface intensified, generated from baroclinic instabilities along the WGC and Labrador Current Chanut et al., 2008. BCEs are observed to form from the southern tip of Greenland at Cape Farewell to Cape Desolation, where these eddies have a pronounced seasonal cycle, with enhanced formation in winter as boundary currents strengthen (Eden and Böning, 2002; Brandt et al., 2004; Rieck et al., 2019). Numerous model studies have worked to diagnose the relative importance of eddies in transporting heat and freshwater into the interior (e.g. Chanut et al., 2008; Gelderloos et al., 2011; Rieck et al., 2019), and while results may differ, eddies shed into the interior Labrador Sea play a large role in modulating the strength of convection and subsequent restratification (Pacini et al., 2021).

1.2.4 Deep water formation and convection

There are very few locations in the open ocean where dense and deep waters are formed, a process referred to as deep convection. Deep convection takes place in the SPNA primarily from the strong ocean-atmosphere interactions, typically during winters, where the ocean undergoes strong surface heat loss leading to deep mixing and convection (Marshall and Schott, 1999; Lazier et al., 2002). Deep convection is an integral part for regional and global climate variability as it modulates the storage and uptake of heat and trace gases, such as CO2 (Rhein et al., 2017; DeGrandpre et al., 2006), and can have impacts on the strength of overturning circulation (Kuhlbrodt et al., 2007; Rhein et al., 2011).

There are several criteria that must be met to enable deep convective processes. The first begins with preconditioning, where prevailing cyclonic winds cause upwelling via Ekman pumping and push near surface waters away from the interior towards the coasts (Kuhlbrodt et al., 2007). Dense deeper waters are now closer to the surface, visible in the doming of isopycnals where weakly stratified waters are exposed (Marshall and Schott, 1999; Lilly et al., 1999; Rühs et al., 2021). The second is favorable wintertime conditions, where there is strong winter buoyancy loss over the ocean surface induced by cold and dry westerly winds (The Lab Sea Group, 1998; Marshall and Schott, 1999; Lazier et al., 2002). With the combination of strong heat and buoyancy loss from the ocean to the atmosphere and weakly stratified waters, stratification erodes even further.

The vertical density gradient is weakened and deep convection is initiated, causing cold surface waters to mix with the water below, typically over an area of about 50–100 km in diameter (Kuhlbrodt et al., 2007; Sterl and de Jong, 2022). The deep convection phase is followed by restratification, occurring in spring and/or summer. The restratification phase sets the stratification at the beginning of the following deep convection period, in turn affecting preconditioning (Sterl and de Jong, 2022). Restratification and preconditioning phases largely determine the magnitude and extent of deep convection. Deep convection has been observed in the Labrador, Irminger, and Nordic seas. It was predominantly thought to occur in the Labrador Sea but studies have shown that the Irminger Sea also undergoes phases of deep convection (Pickart et al., 2003; de Jong et al., 2012; de Jong and de Steur, 2016; Piron et al., 2016; Piron et al., 2017; de Jong et al., 2018).

The NAO has been considered a primary driver for subpolar deep water formation and convection (Lazier, 1980; Dickson et al., 1996; Ortega et al., 2017; Rühs et al., 2021), with positive phases associated with strong winter cooling, increased sea ice coverage over the Labrador Sea, and ocean to atmosphere heat loss with an increased potential for deep convection to occur. However there were periods where a temporary shut down of convection was observed (e.g. Gelderloos et al., 2012) from the GSA event in 1968–1971, not necessarily directly related to NAO variability (Rühs et al., 2021). Labrador Sea convection was markedly deep during the early 1990s, partially attributed to an extended period of excessive winter cooling associated with a positive NAO phase (Böning et al., 2023). There was minimal convection in the 2010s but a strong intensification of deep water formation occurred since 2012–2016 (de Jong and de Steur, 2016; Yashayaev and Loder, 2017; Yashayaev and Loder, 2017; Zunino et al., 2020). Intermittent deep convection occuring pentadal-to-decadal

time scales continues to generate voluminous classes of Labrador Sea Water, whose varying properties are expected to have larger-scale influences on the North Atlantic (Yashayaev and Loder, 2016, 2017)

The fact that deep convective processes occur on relatively small spatial scales and are temporally intermittent makes it difficult to observe (Frajka-Williams et al., 2014; Koenigk et al., 2021). There is limited observational data and simulating deep convection in ocean models remains a challenge. Ocean models have typically tended to overestimate deep convection in the Labrador sea, particularly coarser resolution models which did not include eddy-resolving features. Koenigk et al., 2021 found that increasing the ocean resolution improves the vertical stratification in the upper Labrador Sea but is also dependent on the model's surface fluxes. In an inter-model comparison, they suggested that deep convection may be overestimated from too shallow of a light surface layer or too much oceanic heat loss to the atmosphere. Thus to adequately represent deep convection, a sufficient horizontal resolution representing mesoscale, eddying dynamics and a realistic, high resolution atmospheric forcing is of importance (Rühs et al., 2021).

1.3 Greenland runoff and freshwater pathways

It is evident that changes in stratification can have impacts on deep water formation and convection. As freshwater from Greenland runoff and the Arctic increases, it is an open question as to how, where, and on what time scales could additional freshwater affect or disrupt circulation in the SPNA and AMOC.

1.3.1 Greenland Runoff

Greenland runoff has sharply increased since the 1990s (Hanna et al., 2008; Mouginot et al., 2019). Rising air temperatures have enhanced surface meltwater runoff (Hanna et al., 2006) and submarine melting of glaciers (Straneo and Heimbach, 2013; Slater and Straneo, 2022). The rate of Greenland mass loss has increased from 39 Gt/year in 1992–1999 to 243 Gt/year from 2010–2019 (Fox-Kemper et al., 2021). Compared to Arctic export, Greenland runoff is much smaller in magnitude. Thus, making it a challenge to identify the exact effect freshwater changes from Greenland melt alone has on the SPNA versus larger scale changes in Arctic export i.e. GSA's (Böning et al., 2016). Most of the Greenland mass loss occurs along the western coast of Greenland, as west Greenland is lower in elevation compared to east Greenland, resulting in thinning of the ice sheet to occur more rapidly (Fettweis et al., 2013; Tedesco et al., 2013; Neff et al., 2014).

Figure 1.5a shows a composite map of ice speed composed of Greenland's peripheral glaciers and ice caps (Mouginot et al., 2019). Freshwater from the Greenland ice sheet can be released as liquid runoff in the form of meltwater and submarine melting, and solid runoff through calving of icebergs (Rignot et al., 2010; Bamber et al., 2018; Slater et al., 2019). The annual freshwater fluxes from Greenland from 1958–2016, based on a combination of satellite, in-situ measurements, and a regional climate model are shown in Figure 1.5b. The

freshwater fluxes are split up into different components: solid ice discharge (D), Greenland ice sheet runoff (R_{GRIS}), tundra runoff associated with non-glaciated Greenland land (R_t), and glaier and ice cap runoff outside of Greenland (R_{GIC}) (Bamber et al., 2018).

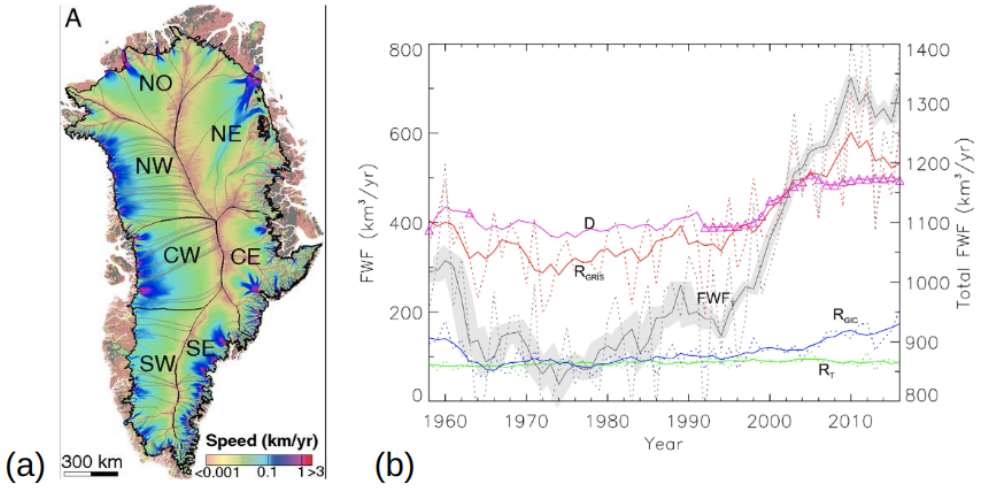

Fig. 1.5: (a) Composite map of ice speed over the Greenland ice sheet (source: Mouginot et al., 2019). (b) Annual Greenland freshwater fluxes (km^3/year) split up into runoff components (D is solid ice discharge, R_t is tundra, R_{GRIS} is Greenland ice sheet runoff, and R_{GIC} is glaicer and ice cap runoff outside of Greenland). Solid lines are 5 years moving averages (left-hand y axis), the total freshwater fluxes in the solid black line (right-hand y axis) (source: Bamber et al., 2018).

Marine terminating outlet glaciers play a significant role as they control the majority of Greenland runoff to the open ocean (Rignot et al., 2015). Greenland has large fjords, acting as link between the ice sheet and the large-scale ocean (Straneo and Cenedese, 2015). At the ice-ocean interface, there is typically a cold and fresh near surface layer and an underlying layer of warmer, salty Atlantic water below 200 m that enhance glacial melt (Straneo and Heimbach, 2013). Melting of ice by the ocean is significantly increased from entrainment where plumes of buoyant meltwater rise to the surface (Holland et al., 2008; Rignot et al., 2010; Straneo and Heimbach, 2013; Rignot et al., 2015; Slater and Straneo, 2022). This combination of surface runoff, calving icebergs, and subsurface glacial melting all contribute to the freshening of the Greenland shelf.

1.3.2 Freshwater pathways

Changes that occur in stratification from additional freshwater input can have impacts on deep water formation and convection. The majority of freshwater sticks to the Greenland shelf from the sharp hydrographic front separating cold and fresh coastal waters from the warmer and saltier interior (Duyck and De Jong, 2021), however there are ways that freshwater can be exported off the shelf. Starting from East Greenland, there are strong, alongshore northeasterly winds resulting in little export off the shelf as the winds tend to keep freshwater towards the coast via onshore Ekman transport (Duyck et al., 2022; Duyck and De Jong, 2023).

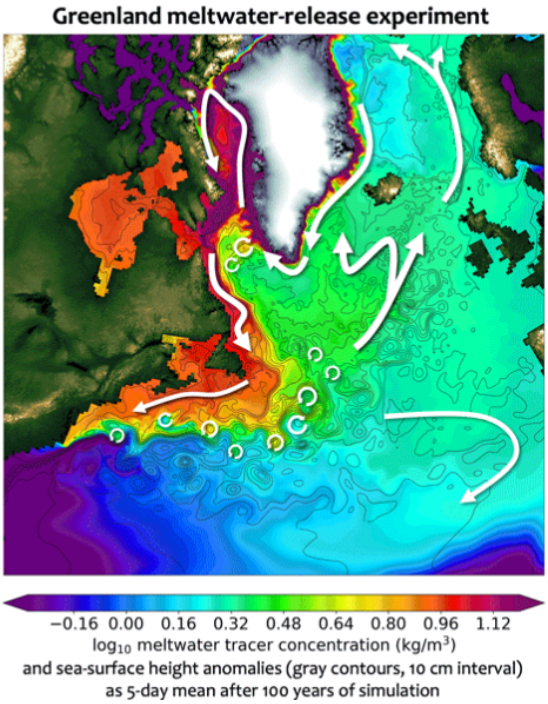

Fig. 1.6: Greenland meltwater as passive tracer content in a meltwater release experiment in a high-resolution, eddy resolving model. Largescale current pathways are marked in white, with eddies denoted by small circles. (source: Martin and Biastoch, 2023).

There are deep bathymetric troughs found along the shelf (Kangerlussuaq and Sermilik Trough) where merging and interactions between the EGC current cores (EGCC/EGC) have been observed (Sutherland and Pickart, 2008; Sutherland and Cenedese, 2009; Foukal et al., 2020; Duyck and De Jong, 2021), but offshore export along the eastern shelf remains limited. Along southeast Greenland, strong wintertime westerly and northeasterly wind events have been observed to drive freshwater off the shelf into the Irminger Sea (Moore, 2003; Moore and Renfrew, 2005; Duyck et al., 2022). Holliday et al., 2007 also observed a retroflection along southeast Greenland where freshwater can be steered away from Cape Farewell towards the interior. Exchanges of freshwater along the southeast Greenland shelf are primarily driven by winds and topography but export occurs intermittently at relatively small scales (Duyck and De Jong, 2023).

Along west Greenland, there is increasing potential for offshore transport of freshwater into the interior through winds (Luo et al., 2016; Castelao et al., 2019; Schulze Chretien and Frajka-Williams, 2018) and eddies (Lilly et al., 2003; Katsman et al., 2004; Rieck et al., 2019; Pacini and Pickart, 2022). Coastal winds off west Greenland tend to be upwelling favorable, i.e. offshore Ekman transport, particularly in winter (Castelao et al., 2019). Eddies can form from increased WGC speeds in winter as alongshore winds strengthen (Katsman et al., 2004; Chanut et al., 2008; Rieck et al., 2019), and steep topographical changes in the slope, particularly at Cape Desolation (Lilly et al., 2003; Bracco et al., 2008; Luo et al., 2011; de Jong and de Steur, 2016; Rieck et al., 2019). Eddies transport heat and freshwater into the interior and are observed to play a role in determining the location and magnitude of deep convection and restratification (Gelderloos et al., 2011; Chanut et al., 2008; Rieck

et al., 2019). Types of eddies shed from the boundary current are described further in subsection 1.2.3.

Model studies used to investigate the fate of Greenland runoff through passive tracer experiments found that meltwater released from the southeast versus the southwest of Greenland has differing pathways (Luo et al., 2016; Castelao et al., 2019). Meltwater originating from southeast Greenland was transported westwards into the northern Labrador Sea leading to salinity and stratification anomalies further offshore, while the majority of meltwater released from the southwest was transported northwards to Baffin Bay (Luo et al., 2016). As winds are a large driver of on or offshore transport, the combination of anomalous runoff along East Greenland and upwelling-favorable winds off West Greenland would likely amount in increased transport across the shelf into the Labrador Sea (Castelao et al., 2019).

The amount of freshwater reaching the interior is very dependent on the ocean model's horizontal resolution, particularly for representing the narrow boundary currents along Greenland and eddies (Gelderloos et al., 2011; Gillard et al., 2016; Rieck et al., 2019; Martin and Biastoch, 2023). The effect of eddies in simulations results in enhanced cross-frontal transport, with more freshwater being mixed from the shelf into the interior (Martin and Biastoch, 2023), where eddies also hold importance for restratification processes in Labrador and Irminger seas (Gelderloos et al., 2011; Martin and Biastoch, 2023). In passive tracer experiments simulating the evolution of Greenland meltwater fluxes over several years, meltwater first appears in the Greenland boundary currents and SPG, propagating into Baffin Bay and the Labrador Sea, with the largest accumulation in Baffin Bay (Dukhovskoy et al., 2016; Gillard et al., 2016; Dukhovskoy et al., 2019).

1.4 Thesis aims, contributions, and structure

It is evident that there are future ramifications for the SPNA with the accumulation of too much freshwater input from Greenland. The primary objective of this thesis is to investigate whether there is an emerging impact of increasing Greenland meltwater on hydrographic and dynamical changes in the SPNA. As outlined above, there remain challenges: 1) complex and narrow boundary currents export freshwater along Greenland and observing the dynamics in-situ or representing them accurately in models proves difficult, 2) Greenland runoff, at its current magnitudes, is relatively small compared to other freshwater sources in the SPNA, thus isolating a meltwater signal let alone the direct impacts on Greenland runoff alone is a challenge, and 3) given the smaller magnitudes of runoff, distinguishing long term variability from shorter time scales and its relevance to Greenland meltwater impacting large scale circulation still remains elusive. The research questions that this thesis aims to answer are as following:

What are the freshwater sources driving salinity changes along the Greenland boundary currents and how do they compare on seasonal time scales?

Are there observable changes in stratification and deep convection processes attributed to accelerated Greenland runoff?

What are the effects from increased meltwater runoff on large scale circulation changes i.e. AMOC and the SPG, particularly on pentadal to decadal time scales?

An over-arching question that this thesis aims to answer through each of the chapters is what are the necessary tools we need to study the impact of Geenland meltwater on the SPNA accurately, particularly from the focal point of ocean model. In order to answer these questions, a mixture of high resolution model output, reanalysis, and in-situ mooring data is used to first investigate freshwater variability along the East Greenland Current. Freshening sources such as sea ice, Arctic export, and Greenland meltwater are investigated and what processes drive on and offshore exchanges. Freshwater sources and alongshore winds strongly differ in seasonal timing further masking the input from Greenland meltwater. The results are presented in Chapter 2.

The mechanisms and emerging influence of enhanced Greenland runoff on the West Greenland Current and neighboring seas are explored between two, twin model simulations but with differing inputs of runoff. There is a localized imprint of enhanced runoff particularly near the Greenland boundaries along with an emerging signal of meltwater propagation into and affecting deep convective sites. The results are presented in Chapter 3.

Lastly, this thesis aims to relate changing freshwater patterns in the SPNA to changes in sea surface height by investigating the role of differing AMOC strengths on sea surface height on decadal time scales. Using an ensemble of six ocean model simulations and two additional experiments, there is a subtle but visible perturbation in sea level along with increasing trends in the Labrador Sea and Greenland shelves, suggesting that Greenland runoff may contribute to localized sea level changes in addition to large scale, decadal AMOC variability. The results are presented in Chapter 4.

Chapter 5 concludes the thesis, synthesizes the primary findings, emerging challenges, and provides a future outlook for further research and studies.

2

Study 1: Do Salinity Variations Along the East Greenland Shelf Show Imprints of Increasing Meltwater Runoff?

This study presents a detailed look into freshwater content variability and freshwater sources along the East Greenland Current (EGC) using high resolution VIKING20X model output, GLORYS12 reanalysis, and mooring observations for model validation. Two interannual extremes corresponding to strong Greenland melt were found in the summers of 2010 and 2012. Freshwater content is highest in the East Greenland Coastal Current due to its proximity to the Greenland coast and the amount of polar water exported from the Arctic. Additional freshwater sources such as Arctic export and sea ice set interannual freshwater content variations along the EGC differing in seasonality, which can mask the runoff signal. This chapter is a print of the manuscript "*Do salinity variations along the East Greenland shelf show imprints of increasing meltwater runoff?*", published in Journal of Geophysical Research: Oceans.

Schiller-Weiss, I., Martin, T., Karstensen, J., & Biastoch, A. (2023). Do salinity variations along the East Greenland shelf show imprints of increasing meltwater runoff? Journal of Geophysical Research: Oceans, 128, e2023JC019890. https://doi.org/10.1029/2023JC019890

JGR Oceans

RESEARCH ARTICLE
10.1029/2023JC019890

Do Salinity Variations Along the East Greenland Shelf Show Imprints of Increasing Meltwater Runoff?

Ilana Schiller-Weiss[1], Torge Martin[1], Johannes Karstensen[1], and Arne Biastoch[1,2]

[1]GEOMAR Helmholtz Centre for Ocean Research Kiel, Kiel, Germany, [2]Christian-Albrechts-Universität Kiel, Kiel, Germany

Key Points:

- During 1993–2019, the East Greenland Coastal Current is freshest in 2010 and 2012 notably matching years of exceptional Greenland runoff
- Freshwater anomalies from sea-ice melt and Arctic export advected along east Greenland are of similar magnitudes as those linked to runoff
- Simulation of fresh coastal waters requires improved surface boundary conditions and/or models capable of representing mesoscale dynamics

Supporting Information:

Supporting Information may be found in the online version of this article.

Correspondence to:

I. Schiller-Weiss,
ischiller-weiss@geomar.de

Citation:

Schiller-Weiss, I., Martin, T., Karstensen, J., & Biastoch, A. (2023). Do salinity variations along the East Greenland shelf show imprints of increasing meltwater runoff? *Journal of Geophysical Research: Oceans*, *128*, e2023JC019890. https://doi.org/10.1029/2023JC019890

Received 19 APR 2023
Accepted 20 SEP 2023

Abstract Accelerated melting of the Greenland Ice Sheet is considered a tipping element in the freshwater balance of the subpolar North Atlantic (SPNA). The East Greenland Current (EGC) and Coastal Current (EGCC) are the major conduits for transporting Arctic-sourced and Greenland glacial freshwater. Understanding freshwater changes in the EGC system and drivers thereof is crucial for connecting tipping elements in the SPNA. Using the eddy-rich model VIKING20X (1/20°) and Copernicus GLORYS12 (1/12°), we find that from 1993 to 2019 freshwater remains close to the shelf with interannual extremes in freshwater content (FWC) attributable to the imprint of Greenland melt only in years 2010 and 2012. Runoff increased significantly from 1995 to 2005 and Arctic freshwater export after 2005. Overall, regional wind patterns, sea ice melt and increasingly glacial ice and snow meltwater runoff along with the Arctic-sourced Polar Water set interannual FWC variations in the EGC system. We emphasize that these freshwater sources have different seasonal timing. South of 65°N sea ice melts year round and retreats to north of 65°N, where melt in summer prevails. Greenland runoff peaks in June–August with only some locations of year round discharge. Alongshore winds intensify in fall and winter where reduced onshore Ekman transport allows for freshwater to spread laterally in the EGC. We show that sea ice melt, runoff and wind can cause interannual variations of comparable magnitude. All of which makes attributing ocean freshening events to Greenland meltwater inflow at current magnitudes a major challenge.

Plain Language Summary The intensity of Greenland ice sheet melt has greatly accelerated over the past decades bringing more freshwater to the surrounding ocean. The additional freshwater has the potential to reach areas where deep waters are formed, which are an important part of the global ocean circulation. A lid of cool and low salinity water would weaken deep water formation and circulation affecting global heat redistribution. In this study we use a high-resolution model to investigate the effect of Greenland melt, sea ice export, and alongshore winds on freshwater content in the East Greenland Current and its coastal twin from Fram Strait to Cape Farewell. Two fresh extremes in 2010 and 2012 are attributable to local Greenland runoff maxima. We find that it takes 4–8 months for freshwater to propagate all along Greenland's east coast, with freshwater anomalies originating from the Arctic Ocean and additional input from sea ice melt along the journey often masking the Greenland runoff signal. Our results emphasize the need for ocean models and observations to resolve and record meltwater runoff, fjord and shelf processes, and boundary current dynamics to detect and attribute local freshening events.

1. Introduction

The East Greenland Current (EGC) provides a primary pathway of freshwater between the Arctic and North Atlantic (Haine et al., 2015). The freshening of the Arctic Ocean and the increase in ice-mass loss due to climate change on Greenland are additional sources of freshwater to the subpolar North Atlantic (SPNA) (Böning et al., 2016; Haine et al., 2015). Modulations in salinity can have far reaching impacts in the North Atlantic as changes affect the density stratification. This in turn may affect deep convection as additional freshwater input increases buoyancy, leading to a dampening of deep convection which in turn reduces aspects of the overturning circulation strength (Bakker et al., 2016; Böning et al., 2016; de Steur et al., 2016; Dickson et al., 1988; Tesdal et al., 2018; Zou et al., 2020).

While Greenland ice sheet melt has sharply accelerated during the recent decades, the contribution from melt alone is insufficient to explain the freshening trend in the SPNA (Friedman et al., 2017; Holliday et al., 2020) as there likely has not been sufficient freshwater input from Greenland to the regions that would directly affect deep convection and eventually the Atlantic Meridional Overturning Circulation (AMOC) strength (Böning

et al., 2016; Dukhovskoy et al., 2019; Jackson & Wood, 2018; Luo et al., 2016; Rahmstorf et al., 2015; Swingedouw et al., 2012). Recent high-resolution model comparisons show that the effect on meltwater redistribution and local response patterns is strongly dependent on eddy-resolving capabilities (Martin & Biastoch, 2023; Swingedouw et al., 2022). From the Greenland coastline to the open ocean, the main export pathway of liquid freshwater from Greenland melting sources and particularly Arctic export is manifested in the total freshwater content (FWC) flowing with the EGC south of Fram Strait (de Steur et al., 2018).

The freshwater pathways from the EGC to the deep convective sites in the Irminger and Labrador Sea are still not fully understood. Observational data shows that freshwater primarily flows along the boundary currents such as the EGC, the West Greenland Current, and following the Labrador Current (Bacon et al., 2002; Dickson et al., 2006; Dukhovskoy et al., 2015; Myers et al., 2009; Sutherland & Pickart, 2008). Cold and fresh waters originating from the EGC is found in the vertical structure of the West Greenland Current, where eddies form and shed along the West Greenland transporting heat and freshwater toward the interior Labrador Sea (Fischer et al., 2018; Rieck et al., 2019). South of Greenland at Cape Farewell, (Holliday et al., 2007) observed a retroflection which provides a direct pathway for freshwater to enter the interior of the gyre. Strong wintertime northeasterly wind and tip jet events can also export freshwater from East Greenland into the interior Irminger Sea (Duyck et al., 2022; Moore, 2012). As the EGC is a major conduit of freshwater from the Arctic and Greenland melt, it is of importance to unravel the complexities of the EGC system and better understand the fate of freshwater and its impact on the SPNA.

The EGC system has been observed to flow southward in two velocity cores (Le Bras et al., 2018), confirmed by moorings along the Overturning in the Subpolar North Atlantic Program (OSNAP, (Lozier et al., 2019)) East section, that extends from the Greenland shelf to Scotland through the central Irminger Sea (Le Bras et al., 2018; Lozier et al., 2019). The East Greenland Coastal Current (EGCC) is surface-intensified and carries cold and fresh water on the shelf (Le Bras et al., 2018). South of Denmark Strait, the EGCC is a well-known feature (Bacon et al., 2002; Foukal et al., 2020; Håvik et al., 2017; Sutherland & Pickart, 2008).

Just offshore is the shelfbreak branch of the EGC which separates fresh, cold shelf waters from warmer, saltier waters of the interior basin (Bacon et al., 2002; Håvik et al., 2017; Le Bras et al., 2018; Sutherland & Pickart, 2008). North of 71°N, Håvik et al. (2017) observed an offshore velocity core which they term the "outer EGC." South of 64°N where the EGC and Irminger Current merge and flow at the shelfbreak, Le Bras et al. (2018) refer to that current branch as the slope current. In order to avoid confusion between these terms, slope current and outer EGC, we will refer to EGC flowing along the slope, beyond the shelfbreak, as the outer EGC.

Freshwater transport (FWT) along the EGC system has a strong seasonality, reaching a maximum during winter in concurrence with strong northerly, downwelling-favorable winds along the shelf (Foukal et al., 2020; Le Bras et al., 2018; Luo et al., 2016). Downwelling favorable winds induce onshore Ekman transport which constrains the low salinity water near the shelf, while upwelling is associated with offshore transport and eventually allow for freshwater to intrude into the interior basin (Castelao et al., 2019; Håvik & Våge, 2018; Luo et al., 2016; Oltmanns et al., 2018; Sutherland & Pickart, 2008).

In summer, winds weaken and are less downwelling-favorable, increasing the likelihood for intermittent offshore FWT (Håvik & Våge, 2018; Våge et al., 2018) which coincides with Greenland melt during summer. As the potential for extreme Greenland summer melt episodes may increase in the future, it is of interest to determine the role onshore and offshore transport plays on freshwater.

In this study we focus on the EGCC and outer EGC from Fram Strait (78.5°N) to Cape Farewell. We take cross sections along East Greenland and isolate the EGCC/outer EGC to investigate the FWC variability from a high-resolution model (1/20°) and reanalysis product (1/12°). We look at the effect of Ekman transport and analyze the evolution of freshwater in the East Greenland boundary current system, considering associated sources that is, Greenland and sea ice melt and Arctic export. We break down the overarching question of whether Greenland Ice Sheet melting and its recent increase (i.e., (Hanna et al., 2008; Rignot et al., 2011)) adds a significant amount of freshwater into the Greenland boundary current system into the following subtopics: the imprint of Greenland runoff and freshwater propagation along the East Greenland shelf, processes which drive salinity changes and FWT along the EGC system, and the significance of freshwater sources and temporal changes.

Section 2 describes the ocean model, reanalysis, and in situ observations, as well as the methods to compute FWC and EGCC/EGC variability. Section 3 starts with potential imprints of anomalous Greenland runoff in

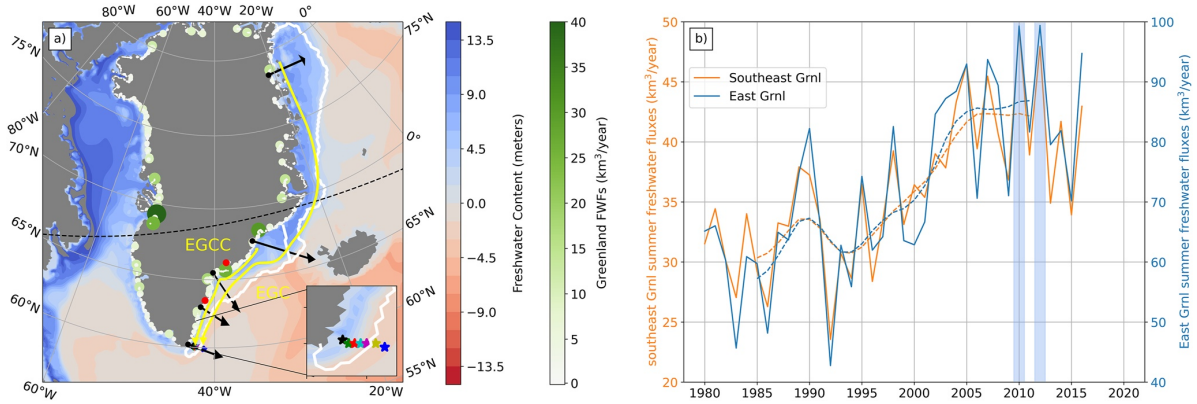

Figure 1. (a) Mean freshwater content for the years 1993–2019 computed from VIKING20X output based on a reference salinity of 34.8 psu. White to green dots encircling the Greenland coast show the integrated annual freshwater flux (FWF) estimates (Bamber et al., 2018) over the same period. The major current pathways of the East Greenland Current system are represented with yellow lines. Black arrows indicate cross sections discussed in the manuscript. The seven Overturning in the Subpolar North Atlantic Program mooring stations are marked as stars off of Cape Farewell, with an inset zooming into the Cape Farewell region. The red dots indicate the locations at Kangerlussuaq (68.63°N) and Helheim glaciers (66.35°N). The white contour shows the 1000 m isobath used to define the offshore boundary of the two regions of focus: the entire east Greenland shelf (59–80°N) and southeast Greenland shelf (59–69°N). The black dashed line indicates the extent of the regional nest, with the ocean grid refined to 1/20° south of the line. (b) Summer (June–August) FWFs along southeast Greenland (blue) and the entire east Greenland shelf (orange). The dashed blue and orange lines show the decadal running mean over the respective regions. The two extreme summers (2010 and 2012) are highlighted by the vertical blue thick lines.

the EGC system in southeast Greenland, the investigating the role of different freshening sources, such as Fram Strait export, propagation along the Greenland shelf, sea ice melt, runoff and wind regimes concluding with a composite analysis contrasting the different contributions on FWC. Lastly Section 4 considers the context and implications of freshwater variability along East Greenland.

2. Data and Methods

2.1. Description of Data Sets

2.1.1. Ocean Model

Freshwater variability along the East Greenland shelf is investigated using the ocean general circulation model VIKING20X (Biastoch et al., 2021) an updated version of the original VIKING20 model configuration (Behrens, 2013; Böning et al., 2016). VIKING20X employs the NEMO3.6 ocean (Madec et al., 2016) and LIM2 sea-ice models (Fichefet & Morales Maqueda, 1997) on a tripolar Arakawa C grid. The model uses two-way nesting with Adaptive Grid Refinement in Fortran (AGRIF, (Debreu et al., 2008)) with a global host model at 1/4° (ORCA025) and regional horizontal grid refinement to 1/20° extending from the Nordic Seas to the southernmost tip of the African continent (34°S–70°N). The northern boundary of the nest is indicated by the black dashed line in Figure 1 where any latitudes south of the dashed line have a resolution of 1/20° and north is at 1/4° (see Biastoch et al., 2021, their Figure 1). There are 46 depth levels increasing from 6 m thickness near the surface to 250 m in the deep ocean. The higher, eddy-rich resolution enables significant improvements in explicitly simulating mesoscale variability, which improves, for instance, Labrador Sea deep convection and AMOC variability (Biastoch et al., 2021; Rühs et al., 2021).

The JRA55-do reanalysis is applied for atmospheric forcing, available at a 3-hourly temporal resolution on a 1/2° horizontal grid (Tsujino et al., 2018). JRA55-do version 1.4 also provides spatially and monthly varying meltwater runoff and iceberg discharge in terms of freshwater fluxes (FWFs) from Greenland based on (Bamber et al., 2018), elsewhere daily river runoff at 1/4° resolution is applied. As the FWF data does not extend beyond 2016, JRA55-do v1.4 repeats the FWF from Greenland of 2016 thereafter. In the VIKING20X simulations solid discharge is assumed liquid and applied as a combined field with river runoff. Runoff is assumed to have sea surface temperature, that is, any heat flux associated with solid discharge or liquid runoff is omitted. Sea surface restoring is also applied based on the World Ocean Atlas 2013 (Locarnini et al., 2013; Zweng et al., 2013)

climatology at a rate of 12.2 m/yr (timescale of 183 d for the 6 m thick surface layer). The restoring flux is not applied in an 80 km radius from Greenland to avoid a local, instant compensation of the enhanced runoff from ice-sheet melt. The coastal mask and the relatively weak salinity restoring facilitate a most realistic representation of Greenland-sourced freshwater in the SPNA while maintaining stability of the simulation.

We analyze monthly output of the VIKING20X-JRA-short run (Biastoch et al., 2021) from January 1993 to December 2019, the overlap period with the GLORYS12 reanalysis (see Section 2.1.2). Figure 1a provides an overview of the general FWC in the model over this period. Runoff from the major glacier and fjord outlets is indicated by the white to green dots, the size signifying the magnitude of the cumulative FWF over the same period. Note, FWF is used synonymous with runoff throughout the study and includes the "liquified" discharge flux.

To illustrate the recent increase in runoff, its total over the southeastern shelf and entire east Greenland from summers (June–August) of 1980–2016 is shown in Figure 1b. We define the East Greenland shelf to be bounded offshore by the 1000 m isobath with a latitudinal extent from just north of Fram Strait (78.5°N) to Cape Farewell at 59°N (Figure 1a). The southeastern Greenland region is defined in agreement with (Sutherland & Pickart, 2008) and its FWF contributes ∼50% to all runoff entering the ocean from East Greenland. In both regions the runoff steadily increased starting in 1995 up to 2005 with strong interannual variability thereafter and two maxima in 2010 and 2012.

2.1.2. Ocean Reanalysis

As Greenland meltwater enters the shelf and then interacts dynamically with the EGC system on local scales, high resolution observational data and coverage on the shelf would be needed but is sparse because of access limitations and shallow depth. High latitude—cold and ice covered—seas and, in particular, coastal and shelf regions are less well represented in remote sensing products (Garcia et al., 2017; Koehler et al., 2014; Olmedo et al., 2018), highlighting the importance of using high-resolution models to capture hydrodynamical instability processes in the SPNA for example, (Handmann, 2019). As a consequence, available ocean reanalysis products such as EN4 (Good et al., 2013) and ARMOR3D (Guinehut et al., 2012; Mulet et al., 2012) are also limited in their representation of the shelf seas around Greenland. They also lack in resolution for sampling the dynamical EGC system. Only the Copernicus Marine Environment Monitoring Service (CMEMS) global ocean physical reanalysis GLORYS12V1 (referred to as GLORYS12 throughout the manuscript) provided on a 1/12° grid is an assimilation model offering a holistic, near-eddy resolving estimate of global salinity, temperature, and velocities (Lellouche et al., 2021) and is used here for cross-validation with the eddy-resolving VIKING20X simulation. In addition both VIKING20X and GLORYS12 are validated with Overturning in the Subpolar North Atlantic Program moored data, see Text S2 in Supporting Information S1.

GLORYS12 contains 50 vertical levels at 1/12° horizontal resolution, covers the period 1993 to present, and assimilates in situ measurements and along-track satellite data via a Kalman Filter with a 3D multivariate modal decomposition of the background error into the model. The model component is based on NEMO driven at the surface by atmospheric conditions from ERA interim reanalysis output. In situ measurements include sea surface temperature data from NOAA, sea ice concentration from Ifremer/CERSAT, and the salinity and temperature vertical profiles are from CMEMS Coriolis Ocean Database for ReAnalysis (CORA) database which includes various in situ data (Argo profilers, moorings, underwater gliders, surface drifters, ship data) (Lellouche et al., 2021). In general, Argo floats from 2003 onward improve the reanalysis above 2000 m; however there are no Argo floats on the East Greenland shelf. Very few in situ measurements are included in the assimilation near the shelf, for example, OSNAP East mooring measurements are excluded. However when an in situ measurement is present, spatial and temporal correlation scales are used to define a sphere of influence around that grid point where the observation is present. A multivariate bias correction is added to enhance any observations that are within this bubble of influence, for example, if there is an available observation of sea level then the temperature and salinity increments can be deduced. It is only when observational coverage is completely insufficient or there is no direct constraint from the correlation scales based on proximity to an observation, then the ocean state is based on the numerical model (Drévillon et al., 2021; Lellouche et al., 2021).

Some regional biases exist in GLORYS12 where the largest, cooler temperature bias lies in the 50–100 m layer in the North Atlantic. Sea surface salinity is generally fresher than when compared to the World Ocean Atlas (WOA) climatology, except in the Arctic where salinity tends to be higher than individual profiles suggest. While a slight

fresh bias exists, there are positive trends of sea surface salinity over most parts of the global ocean, with negative salinity trends found in the Arctic. Biases against all in situ observations decrease significantly with time as the density and number of observations increase (Lellouche et al., 2021).

GLORYS12's freshwater forcing differs from that applied to VIKING20X, particularly when replicating the additional freshwater input from ice sheet mass loss. In GLORYS12, there were two corrections made to the salinity field in order to avoid sea surface height drift from discrepancies in closing the water budget: first, the surface freshwater global budget was set to a seasonal cycle including 100 major rivers based on (Dai et al., 2008); second, a linear trend was imposed to the surface mass budget to replicate the freshwater sources from glaciers and ice sheet loss (Lellouche et al., 2021). For the period 1993–2001 the trend is 1.31 mm/yr and is increased to 2.2 mm/yr from 2002 onwards. These trends are implemented as a uniform surface FWF in ocean areas populated with observed icebergs (Lellouche et al., 2021), which for Greenland is based on the CERSAT Altiberg database for small and giant icebergs provided by Tournadre et al. (2015).

There intentions differ between the high-resolution ocean-only model VIKING20X and observation-assimilated reanalysis GLORYS12. VIKING20X is used to run a hindcast simulation (for sensitivity and process studies) based on ocean physics and constrained by surface fluxes providing a consistent though somewhat biased ocean state by construction. GLORYS12 aims to provide a holistic picture of the actual ocean state using a physical model but minimizing model biases by assimilating observations.

2.1.3. In Situ Observations

In order to examine the state of the northern boundary of our East Greenland delimited region (Figure 1a), VIKING20X and GLORYS12 are compared with 16 years of in situ salinity and velocity measurements at Fram Strait from September 2003 to August 2019 (de Steur et al., 2018; Karpouzoglou et al., 2022). The salinity and velocity measurements were collected from moorings at 78.5°N extending from 8° to 2°W by the Fram Strait Arctic Outflow Observatory (de Steur et al., 2018). The measurements are provided as monthly means on a 1/4° grid with the vertical resolution varying in depth (Karpouzoglou et al., 2022). While measurements at Fram Strait began in 1997, the mooring line was adjusted from 79°N to 78.5°N in 2002 where increased FWT was observed at the latter location. The coverage of the southward recirculating branch of the Return Atlantic Current also improved at the shifted mooring location (de Steur et al., 2018). Mooring measurements at OSNAP East were cross-validated with VIKING20X and GLORYS12 (Text S2 in Supporting Information S1).

2.2. Methods

We compute the FWC following (Haine et al., 2015; Marshall et al., 2017) using a reference salinity of 34.8 psu, which is consistent with previous studies and separates well between polar and Atlantic-origin waters (de Steur et al., 2016; Sutherland & Pickart, 2008). The FWC is presented for zonal cross-sections of specified latitude and horizontal maps, where for the latter it was integrated over the upper water column down to 200 m. For a single grid cell the FWC was computed as:

$$\mathrm{FWC} = \iiint \frac{S_{ref} - S(t,z,y,x)}{S_{ref}}\, dz\, dy\, dx, \tag{1}$$

where S is the salinity and S_{ref} is the reference salinity. FWC represents the amount of zero-salinity water that would be required to reach the observed salinity, relative to a given reference salinity (Fuentes-Franco & Koenigk, 2019; Haine et al., 2015). A positive FWC implies that the salinity is fresher than the defined reference salinity. Given a cross section over a particular width and depth, the FWC is defined as the amount of freshwater present within that cross-sectional area.

We also investigate the FWT perpendicular to a cross section, in particular at Fram Strait to determine the amount of freshwater that is exported from the Arctic (discussed further in Section 3). Freshwater transport across a section is defined as:

$$FWT = \iint v_{\perp}(x,z) \cdot \frac{S(x,z) - S_{ref}}{S_{ref}}\, dz\, dx \tag{2}$$

where $v_{\perp}(x, z)$ corresponds to the velocity normal to the section specified by distance x and depth z. FWT differs from FWC in that it describes the volumetric flow rate at which freshwater is exported from upstream of the

section whereas FWC represents cumulative salinity variations below a given threshold. The FWT across a section further upstream can impact the FWC downstream.

Further, we compute Ekman transport components using the modeled wind stresses:

$$U_{ek} = \frac{\tau_y}{f\rho_0}, V_{ek} = \frac{-\tau_x}{f\rho_0}, \tag{3}$$

where $\tau_{x,y}$ is the wind stress provided by the ocean model, $\rho_0 = 1027$ kg/m^3 is the density of sea water, and $f = 10^{-4}$ s^{-1} is the Coriolis parameter.

The method to distinguish between the EGCC and the outer EGC velocity cores at the cross sections is described in Supporting Information S1 (see Text S1).

2.2.1. Composite Analysis

In Section 3.4, we perform a composite analysis to determine the impact of Greenland FWFs, alongshore wind stress, and sea ice production on the FWC using VIKING20X output. GLORYS12 has no wind stress or sea ice production output available. We refrained from computing the wind stress with ERA-interim reanalysis due to uncertainty about the exact bulk formulae used in GLORYS12.

We high pass filter Greenland FWFs, sea ice production, and FWC subtracting a 5-year Hamming-windowed running mean from the original time series to remove any decadal trends. This removes the signal of increasing Greenland FWFs from the early 1990s to mid-2000s (see Figure 1b), the recent eastern North Atlantic freshening (Holliday et al., 2020) and Great Salinity Anomaly of the 1990s (Belkin, 2004), and instead highlights seasonal to interannual variability. To illustrate the temporal variability of runoff, sea ice production, and winds stress along southeast Greenland, we take the gridcell area weighted mean of alongshore wind stress and spatially integrate the FWFs and sea ice production.

Then a cumulative sum of the monthly data is computed each year starting in January (FWFs and sea ice production) and June (wind stress). The different start date for wind stress is selected to allow comparability with Castelao et al. (2019). The result is then used to obtain the members (individual years) for the FWC composites. Different months are chosen for each quantity to decide on the composite members: August for Greenland FWFs, May for sea ice production, and December for wind stress. These months are at or right after the peak of the cumulative sum of each quantity; only wind forcing continues to strengthen but we decided to focus on December for comparability with earlier studies.

For the respective months, each variable is grouped into categories of particularly anomalous years (15th and 85th percentile of the respective distribution). While these thresholds are too inclusive to consider the associated magnitudes as "extreme" (thresholds for cold spells/heat waves range from 10th/90th to 1st/99th percentiles (Frölicher et al., 2018; Hobday et al., 2018; Perkins-Kirkpatrick & Alexander, 2013)), some of the years included match such conditions. We determine the composite years for Greenland FWFs and sea ice production by subtracting: strong melt years minus reduced melt and weaker minus stronger alongshore wind stress. These composite years are used to compute the monthly FWC anomalies with implications discussed in Section 3.4.

3. Results

The following analysis aims at providing model-based evidence for a significant influence of glacial meltwater on the FWC of the EGC system in recent years. We begin with discussing variability of the FWC on the southeast Greenland shelf, where major outlet fjords are located. As internal variability proves large compared to such signal, we discuss the time varying export of freshwater from the Arctic Ocean through Fram Strait as an ultimate source of freshwater in the EGC, its southward propagation to Cape Farewell, the influence of local sea-ice melt, and the effect of the Ekman transport induced by differing wind stress magnitudes along the Greenland shelf. Lastly, a composite analysis looking at anomalous years of runoff, sea-ice melt and cumulative wind stress provides insight on magnitude and spatial distribution of these sources and factors driving low-salinity anomalies in the EGC system.

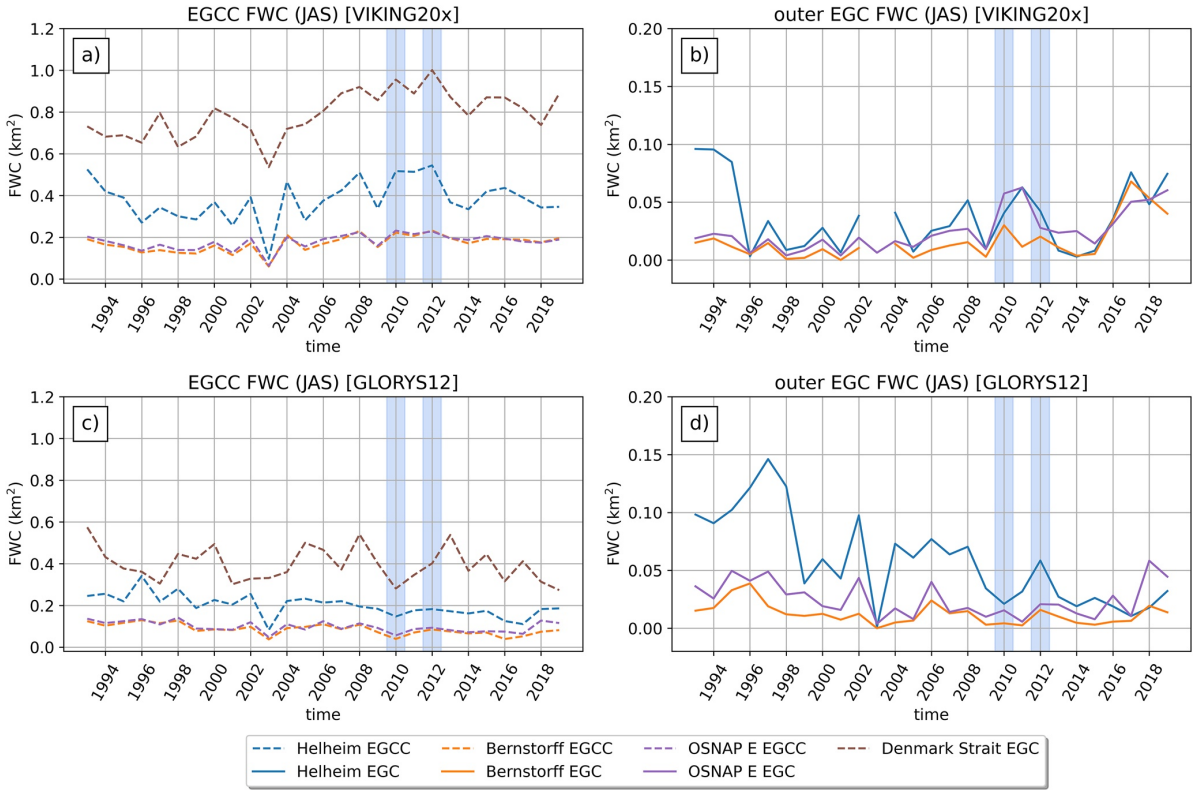

Figure 2. Time series of freshwater content (FWC) for VIKING20X and GLORYS per cross section. Panels (a) and (b) show the FWC from 1993 to 2019 for VIKING20X in the East Greenland Coastal Current (EGCC) and the outer East Greenland Current (EGC). The dashed lines indicate the EGCC, while the solid lines represent the outer EGC. Panels (c) and (d) show the same for GLORYS12. Note, *y*-axis ranges differ between left and right subfigures. The cross sections are south of Kangerlussuaq glacier at Denmark Strait (brown), south of Helheim glacier (blue), south of Bernstorff fjord (orange), and Overturning in the Subpolar North Atlantic Program East (purple). The two extreme runoff summers (2010 and 2012) are highlighted by the vertical blue thick lines.

3.1. Does Extreme Greenland Runoff Leave an Imprint on the East Greenland Shelf Hydrography?

3.1.1. Model Cross-Sections

Guided by the temporal evolution of the local runoff in southeast Greenland (Figure 1b), we select cross sections at Fram Strait (Arctic export gateway), Denmark Strait (south of Kangerlussuaq glacier), Helheim (south of Helheim glacier and at Sermilik trough), Bernstorff (south of Bernstorff Isfjord), and OSNAP East just off of Cape Farewell. These are all located within the nested area at 1/20° resolution, only Fram Strait at 78.5° is outside of the nest.

The major current pathways of the EGCC and outer EGC are marked in yellow in Figure 1. Foukal et al. (2020) observed that the EGCC intensifies as it passes through Denmark Strait. Surface drifters also revealed the presence of the EGCC further north, flowing all the way from Fram Strait to Cape Farewell. However in both VIKING20X and GLORYS12, the EGCC was detectable only south of Denmark Strait, based on the criteria for two distinct, along stream velocity cores to be present at the shelf and beyond the shelfbreak (Text S1 in Supporting Information S1). Figure 1a only depicts the model state.

A seasonally varying mask based on salinity and southward-only velocity thresholds is applied (method described in Text S1 in Supporting Information S1). The annual summer (July–September) FWC variability in the EGCC and EGC per cross section are shown in Figure 2. Most of the freshwater in summer is contained within the EGCC, seen in both VIKING20X and GLORYS12 (Figures 2a and 2c). The total FWC decreases southward for various reasons: the narrower shelf leads to larger meridional current speeds facilitating a faster export of

freshwater and an increased exchange with saltier waters from the interior basin. The shelf boundary is indicated by the 1,000 m isobath nearing the coastline south of 65°N in Figure 1a.

The EGCC FWC in VIKING20X in Figure 2a shows an increasing annual FWC and interannual peaks resembling those of the Greenland runoff forcing applied in the model, notably at Denmark Strait and Helheim cross sections. In Figure 1b, there is a steady increase in the FWF over southeast Greenland starting in the 1990s until the early 2010s. The FWC increases up to 2012 in VIKING20X's EGCC south of Denmark Strait and Helheim glacier. Thereafter, Greenland FWFs appear to decline after 2012 and level off as does the annual FWC in the EGCC in the VIKING20X simulation.

There are interannual extremes in the FWC occurring in 2010 and 2012 in the EGCC in VIKING20X which coincide with the extremes in Greenland runoff imposed in the model (see Figures 1b and 2a). Interannually varying runoff included in the JRA55-do atmospheric forcing ends in 2016 and consequently the melt event reported for 2019 (Slater et al., 2021b) is not present in this VIKING20X simulation. For the 2010 extreme it was observed that an early onset of melting was triggered by anomalously warm near surface air temperatures which reduced surface albedo (Tedesco et al., 2011). The high air temperatures persisted throughout the summer resulting in a positive albedo feedback loop and caused additional melting in west Greenland (Tedesco et al., 2011). The summer of 2012 was a year marked by exceptional Greenland melt runoff due to negative North Atlantic Oscillation (NAO) conditions which advected warm southerly winds resulting in widespread surface melting (Hanna et al., 2014).

In contrast, GLORYS12 lacks a realistically varying runoff as a surface boundary condition and shows an overall decrease in FWC (Figure 2c). The EGCC is identifiable in GLORYS12 but is saltier near the shelf and surface, suggesting increased lateral mixing with the interior basin. Similar to VIKING20X, the northernmost cross sections are fresher than those downstream. Although subtle, there is a slight decrease in FWC from the early 1990s to mid-2010s for the sections south of Denmark Strait. This may be due to a consequence of the weaker constrain from actual in situ data for the assimilation process due to lack of observations close to the coast and at lower resolution.

The annual summer FWC in the outer EGC (Figures 2b and 2d) for both VIKING20X and GLORYS12 show a strong reduction in FWC presumably caused by mixing with saltier, warmer waters from the interior basin. In particular, the FWC decreases over time in the outer EGC at the Helheim cross section. There is a clear difference in interannual variability and patterns on a decadal time scale in GLORYS12. Compared to VIKING20X GLORYS12 only has a weak representation of the freshening after 2015 in the outer EGC. This increase in FWC in the outer EGC may be related to the recent eastern North Atlantic fresh anomaly (Holliday et al., 2020), as discussed by Rühs et al. (2021).

It is in particular the presence of sea ice and icebergs on the Greenland shelf that limits obtaining observational data in this region, including near surface waters (top 50 m). This holds true for mooring data from the OSNAP East array which provides no data above 50 m depth. As most of the freshwater is contained with the upper water column, near surface measurements remain critical (Karpouzoglou et al., 2022) and likely reflects in the skill of the reanalysis from GLORYS12. When excluding the top 50 m for the FWC in the EGCC at the Helheim section, the FWC decreases by 30% for VIKING20X. The reduction in FWC is even greater for GLORYS12, decreasing by 70%. The outer EGC for both models undergoes an even greater difference with a 70% reduction in FWC, highlighting the importance of the thin, near-surface layer above 50 m depth, as the freshest water is contained there.

The analysis of the cross sections along East Greenland reveals significant differences in FWC near the shelf between VIKING20X and GLORYS12. For VIKING20X, the EGCC FWC contains an increasing pattern with two interannual extremes which correspond to strong Greenland melt years of observed runoff. Meanwhile the FWC along the EGCC and outer EGC for GLORYS12 shows the FWC generally decreasing with time. The outer EGC shows a minimal freshwater imprint, demonstrating that most of the freshwater is constrained to the shelf and upper water layer.

3.2. How Does Freshwater Propagate Along the East Greenland Shelf?

3.2.1. Arctic Freshwater Export

A large source of freshwater in the EGC system is the export of polar water from the Arctic Ocean through Fram Strait. Arctic-sourced freshwater comes in two forms: liquid and solid sea ice flowing both on the shelf

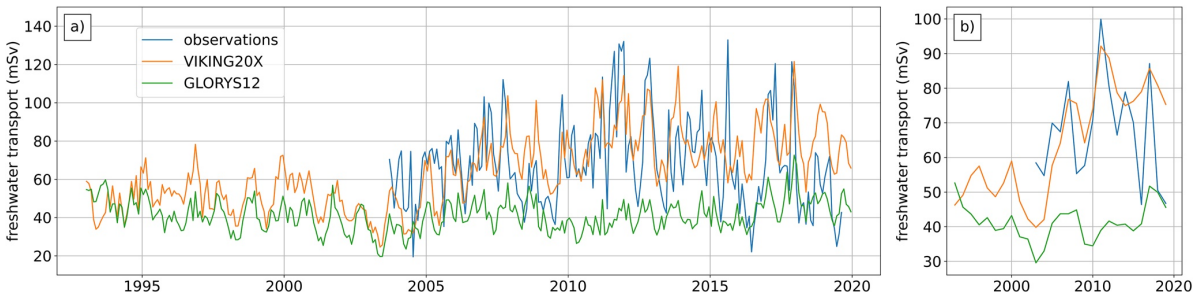

Figure 3. (a) The monthly Freshwater transport (FWT) from in situ observations at Fram Strait (78.5°) (blue), VIKING20X (orange), and GLORYS12 (green). (b) The annual mean FWT for the observations and models. Note the change in y limits on the vertical axis for the annual means.

and continental slope in the EGC (Holfort & Hansen, 2005). Sea ice export is primarily driven by alongshore, local winds (Smedsrud et al., 2008; Vinje, 2001). We investigate the FWT at Fram Strait as Arctic export sets the amount of low salinity polar water flowing south with the EGCC (Rudels et al., 2004). FWT differs from FWC in that it represents the volume of freshwater that is fluxed through the cross-sectional area, determined by both the flow velocity and salinity.

We compare the FWT estimates at Fram Strait between interpolated moored observations (Karpouzoglou et al., 2022), VIKING20X, and GLORYS12. The mooring line begins just off the shelfbreak from 8°W–2°W at 78.5°, but for both models we extend the region from the shelf to 2°W, due to the availability of the shelf extent and that the freshest water is contained near the coastal branch of the EGC system (Bacon et al., 2014; Foukal et al., 2020; Le Bras et al., 2018).

The long term annual means for liquid FWT of polar water at Fram Strait is approximately 69 mSv given a reference salinity of 34.9 psu (Karpouzoglou et al., 2022). We recompute the FWT using the 34.8 psu and excluding any northward velocities, where the transport is calculated by Equation 2 to obtain a mean FWT of 68 mSv. Note that the Fram Strait cross section is outside the high-resolution nest in VIKING20X remaining on the global host model at 1/4° resolution. Figure 3 shows the monthly and annual FWT for the observations, VIKING20X, and GLORYS12. The FWT is integrated from the shelf to 2°W (limit of the mooring array) for VIKING20X and GLORYS12, while the observations begin at the shelfbreak (Figure S3 in Supporting Information S1).

In Figure 3b, observational estimates from mooring data show an increased amount of FWT flowing across the section than VIKING20X and GLORYS12, particularly from 2003 to 2007. The long-term annual mean for the observations is 68 mSv, while VIKING20X and GLORYS12 have 62.7 and 41.4 mSv. GLORYS12 has lower FWT estimates due to freshwater reaching shallower depths in comparison to VIKING20X and the observations (Text S3 in Supporting Information S1). While closer to the observations in magnitude, the simulated temporal variability of VIKING20X resembles that of GLORYS12 more than that of the observations for the period 2003–2019 with correlation coefficients for monthly mean FWT of 0.64 to GLORYS12 and 0.45 to observations, while that for GLORYS to observations is only 0.27. The FWT estimates depend not only on salinity and velocity but also on the respective grid resolution. Freshwater does not extend as deep in the water column where the vertical grid cell sizes coarsen with increasing depth. Large grid cells may carry significant amounts of freshwater even when exceeding the constant threshold salinity only marginally; using partial grid cell volumes is not considered here.

On the other hand, the FWT for VIKING20X is comparable with the observations when the section includes the shelf (coastline to 2°W). There are deviations in interannual variability, particularly in Figure 3a, but the magnitudes appear consistent with observations. When the shelf is included, the FWT increases for VIKING20X suggesting that freshwater along Fram Strait remains near the shelf but freshwater offshore reach increased depths than GLORYS12.

Both models show an increase in the annual FWT from 2003, particularly in VIKING20X, which is not as evident in the observations as they begin in 2003 (Figure 3b). Although both models slightly underestimate the mean FWT at Fram Strait, in particular GLORYS12, there are differing biases in the models. VIKING20X has lower southward current speeds just off the shelfbreak at Fram Strait (Figure S3 in Supporting Information S1) but

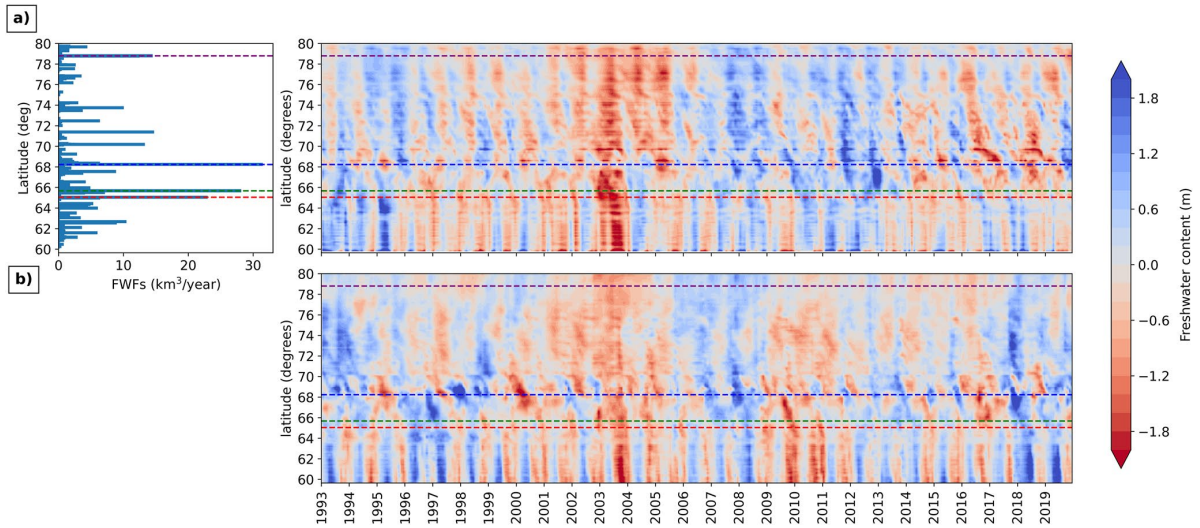

Figure 4. (a) The lefthand panel shows the annually integrated freshwater fluxes averaged over the period 1993–2016 from Greenland liquid and solid ice discharge (Bamber et al., 2018) per latitude. The dashed lines in purple, blue, green, and red indicate the top four largest runoff locations. The righthand top panel shows the evolution in freshwater content (FWC) anomalies over the reference period 1993–2019 per latitude for VIKING20X. (b) The FWC anomalies for GLORYS12.

comparable salinities to the observations across the section. Freshwater is transported downstream via Fram Strait closer onshore rather than offshore beyond the shelfbreak. Due to observational measurements lacking onshore, it is unclear if observations would result in an increased FWT provided on-shelf measurements were available however it would be of interest to see how magnitudes may vary if the entire shelf were included.

These discrepancies between the models and observations, particularly the reanalysis, highlight the need of obtaining a realistic representation of Fram Strait export, especially as this sets the amount of polar water flowing south with the EGCC (Rudels et al., 2004). The remaining analysis focuses on the origin and propagation of fresh anomalies and thus holds despite the described FWT biases at Fram Strait.

3.2.2. Downstream Freshwater Propagation From Fram Strait to Cape Farewell

As freshwater exported from the Arctic via Fram Strait plays a significant role in determining the initial low salinity near surface water of the EGC system, we investigate how freshwater propagates along the shelf from Fram Strait to Cape Farewell. Figure 4 shows Hovmoeller diagrams of the zonally integrated FWC on the east Greenland shelf for VIKING20X and GLORYS12. Given that Greenland FWFs enter through the surface and along the coastline, we determine the changes in FWC along the shelf computed from Equation 1 and integrated over the top 200 m. The mean FWC climatology over the EGC region (59–80°N) is calculated based on the reference period 1993–2019 and then the FWC anomalies are linearly detrended. The detrended FWC is used to focus on the salinity variations that arise from local melt and upstream freshwater sources on an interannual basis rather than any long-term evolution in Greenland runoff or Arctic export as discussed above (Figures 1b and 3b). Since the zonal extent of the 1000 m isobath varies in distance per latitude, the anomalies are standardized by dividing the total horizontal grid cell area per latitude, which reduces the overestimation of the FWC from changes in shelf width.

The righthand top panel of Figure 4a and the lower panel b show the monthly FWC anomalies for VIKING20X and GLORYS12, where positive FWC signifies fresher water than the climatology. There is strong interannual variability in VIKING20X and GLORYS12 with a period of greater salinities from 2003 to 2006. Since FWC was detrended, these do not originate from the long-term increase of Fram Strait FWT. Other differences between the models are in 2010 and 2012 when exceptional Greenland runoff occurred during those summers but the positive anomalies in FWC are not seen in GLORYS12.

In Figure 4a, the dashed lines indicate major runoff locations, displayed by the bar diagram of the land-sourced FWF (Bamber et al., 2018) per ≈0.2° latitude in 4a. The monthly FWFs are accumulated per year and then averaged

over 1993–2016. There is a maximum of FWF from Greenland at ≈68°N at Kangerlussuaq glacier; one of the largest glaciers along East Greenland. The next largest freshwater input comes from Helheim glacier (≈66°N) and at 79°N where the 79°N glacier and Zachariae Isstroem glacier is located (Rignot & Mouginot, 2012). In GLORYS12, coastal runoff is represented by a spatially varying climatological FWF in combination with an additional, uniformly distributed FWF in regions of observed iceberg occurrence.

FWC anomalies propagate south but considerable local variability imprints on this signal, where the anomalies are generally larger in VIKING20X than in GLORYS12. The advective time scale from Fram Strait to Cape Farewell ranges between 4 and 8 months. Thus freshwater anomalies leaving the Arctic Ocean in mid-winter to spring can potentially interfere with and mask runoff anomalies in southeast Greenland, which peak in summer (July–August). Local offshore advection and mixing with saltier interior waters in the Nordic and Irminger seas contribute to the erosion of the anomaly along the way. The maximum in Greenland meltwater input occurs at the Kangerlussuaq glacier (68°N), just north of Denmark Strait. (Foukal et al., 2020) observed that freshwater flowing southward along the EGC tended to converge at Denmark Strait where downwelling-favorable winds drive onshore flow due to widening of the shelf north of Denmark Strait. This suggests that any meltwater output from the Kangerlussuaq glacier likely mixes with the initial low-salinity polar waters propagating southward from Fram Strait and would explain why there is not a strong positive FWC anomaly south of 68°N (Figures 4a and 4b).

Recirculation occurs at the deeper Kangerlussuaq trough at ≈67°N where studies show that a net input of freshwater splits into the EGCC south of Denmark Strait with a return flow out of the trough (Foukal et al., 2020; Sutherland & Pickart, 2008). Arctic freshwater export and recirculation at the trough just south of the Kangerlussuaq glacier both contribute to FWC variability but likely obscure any additional signal from Greenland runoff.

After recirculation at the trough and freshwater convergence along the shelf due to strongly downwelling-favorable winds, meridional current speeds increase south of 65°N, reaching values up to 0.4 m/s in both models (Figure S1 in Supporting Information S1), which occurs where the 1,000 m isobath and shelfbreak steadily narrows. Given the high current velocities and the reduced distance freshwater travels, advection of freshwater from 65°N to 59°N happens within 1 month and hence the propagation of freshwater anomalies is not resolved by the monthly mean output of the models used here. This explains why in the Figures 4a and 4b Hovmoellers there are these vertical, instantaneous-like positive and negative FWC anomalies, implying a divergence of freshwater south of 64°N.

3.3. What Are the Processes Driving Salinity Variations and Freshwater Transport in the EGC?

3.3.1. Sea Ice Melt and Greenland Runoff

Apart from polar water and Greenland runoff, a significant freshening source is sea ice melting along the east Greenland shelf. We analyze the sea ice production output from VIKING20X (local freezing, when >0, and melting rates, <0), a quantity not provided for GLORYS12, which includes sea ice thickness as a variable but not thermodynamic thickness change, that is, melt or freezing. A provisional reconstruction of such an ice production field based on month-to-month sea ice thickness changes is prone to failure because sea ice thickness change is dominated by advection in this region. Further analysis concentrates on VIKING20X output.

Figure 5a shows the seasonal cycle of sea ice production (blue colors imply meltwater input) per zonal section (meridional resolution of 10–20 km, ORCA025 grid) from VIKING20X. Sea ice production is zonally integrated over the east Greenland shelf within the 1,000 m isobath. For comparison, the seasonal cycle of runoff along east Greenland is shown per coastline gridpoint (Figure 5b). There is primarily sea ice formation throughout winter and early spring from 67 to 80°N. Sea ice melt occurs from summer to late fall peaking in June (67–70°N) and July (north of ∼71°N). North of ∼71°N runoff begins to increase in late May, reaching a maximum in June/July then reduces in September. South of 70°N, there are some latitudes which have a positive Greenland FWF year-round (Figure 5b). The wintertime runoff is attributed to outlet glacier calving where solid ice discharge can enter the open ocean (Bamber et al., 2018) but have relatively lower magnitudes compared to summer runoff. Freshwater from sea ice melt coincides with the runoff peak but typically exceeds the latter, suggesting that additional freshwater from summertime sea ice melt further north propagating downstream can mask the local runoff signal.

Further south, from 65 to 67°N, sea ice melting occurs from late fall (November) to early summer (June). As there is no sea ice present in summer and early fall, most of the ice melting in this region originates further north and is

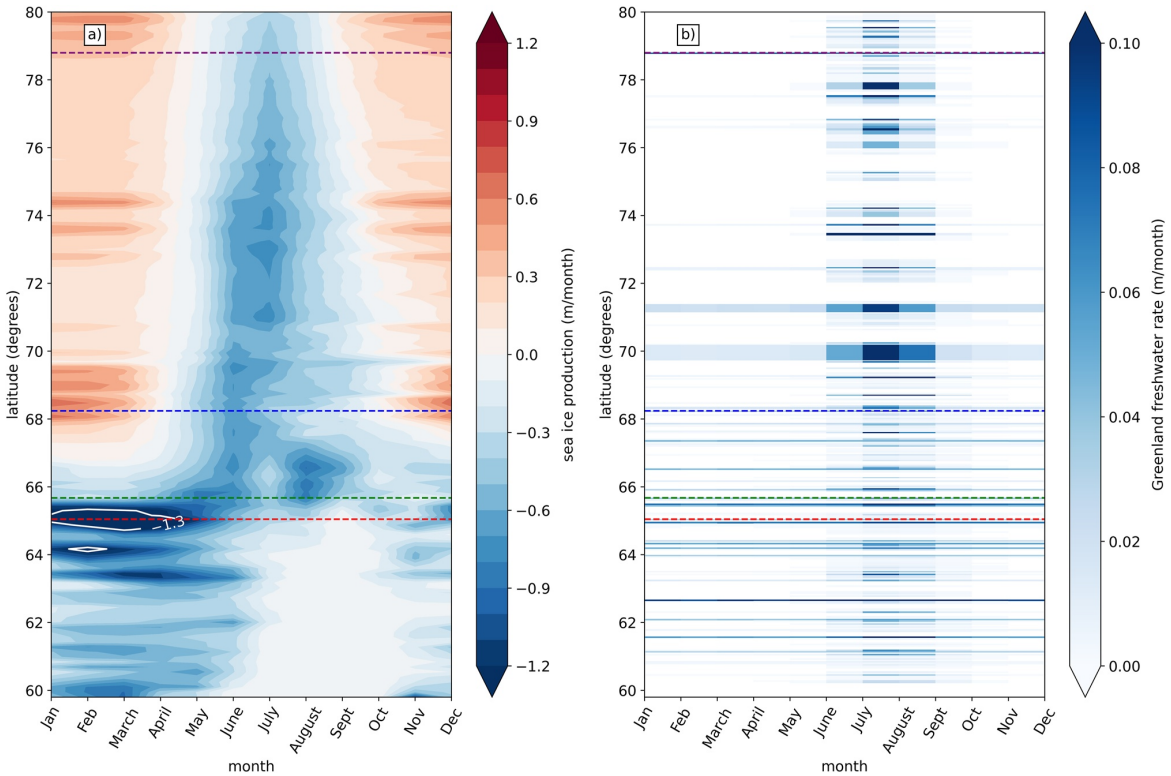

Figure 5. (a) Hovmoller plot showing the climatology of sea ice production (m/month) from VIKING20X over the reference period 1993–2019. Positive values indicate sea ice growth, while negative values signify melting. (b) Mean seasonal cycles of Greenland freshwater fluxe (FWF) (m/month) from Bamber et al. (2018) averaged over 1993–2019 per latitude band. The zonally integrated FWFs (km^3/month) are divided by the ocean model's grid cell area to convert to m/month for comparison with sea ice production depicted in panel (a). The white to blue colors indicate increasing FWFs per latitude (15° resolution). The dashed colored lines indicate the major Greenland runoff sources (see Figure 4a) showing the mean annual FWFs integrated over 1993–2016.

imported by the southward flow with only little formed and melted locally. This timing does not overlap with the runoff seasonal cycle featuring a marked summer peak. The melting of sea ice south from Cape Farewell (59°N) to Denmark Strait (66°N) during the late winter and early spring including the region of enhanced southward current speeds on the narrower shelf explains the persistent positive and negative freshwater volume anomalies that occur during early winter/spring in Figure 4.

South of Denmark Strait, we find that there has been a reduction in sea ice meltwater flux in the last 13 years with a linear trend of −40.48 km^3/year for the period 2006–2019. Interannual variability has strongly reduced from 217.6 km^3 (1993–2005) to 73.5 km^3 (2006–2019), likely from a reduction in the amount of sea ice available to melt. In VIKING20X sea ice export through Fram Strait declined from 1993 to 2019 by 11.86 km^3/yr with a stronger trend of 42 km^3/yr over the last 13 years, which matches recent observational estimates (Spreen et al., 2020; Wang et al., 2021).

Sea ice melt remains a significant source of freshwater entering the ocean locally but also being advected along the EGC. Freshwater from Greenland, Arctic export through Fram Strait, and sea ice melt on the Greenland shelf all contribute as freshwater sources to the EGC and EGCC systems, which carries the anomalies into the SPNA. Disentangling the individual signals remains a challenge, but the sources provide insight into how freshwater is transported and seasonally changes along the East Greenland shelf.

3.3.2. Effect of Wind Stress on Volume and Freshwater Transport

Alongshore winds play a large role on modulating cross-shelf transport of freshwater (Luo et al., 2016). The shallower EGCC in particular is observed to be both wind and buoyancy driven (Sutherland & Pickart, 2008).

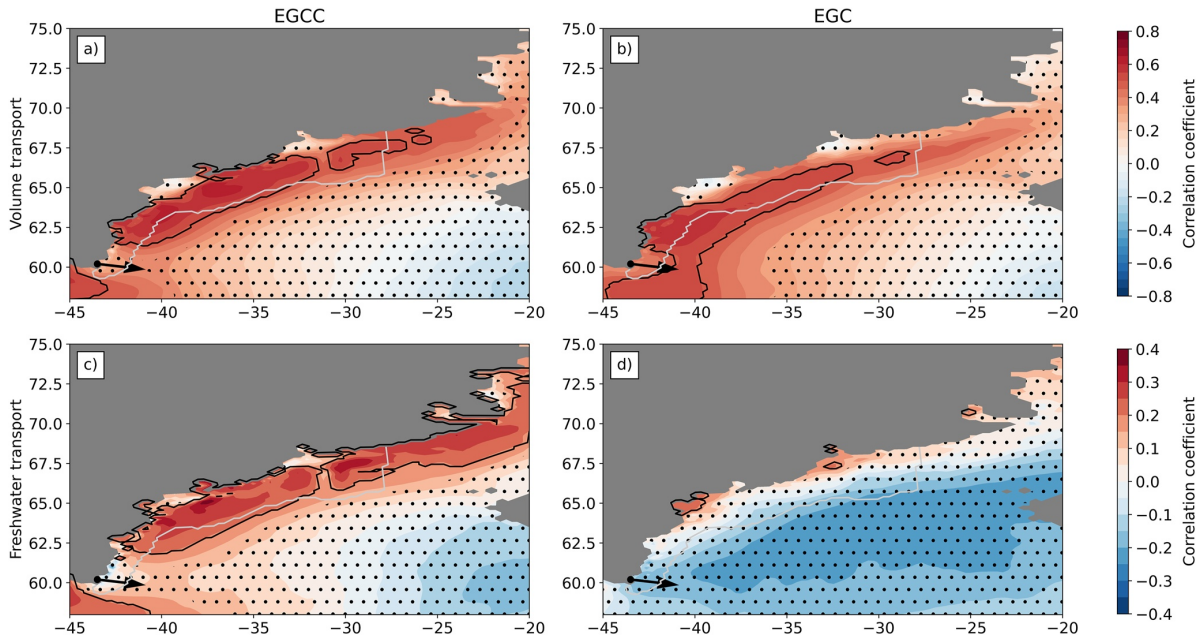

Figure 6. The following correlations are between the alongshore wind stress and the volume and Freshwater transport (FWT) at the Overturning in the Subpolar North Atlantic Program (OSNAP) East mooring line indicated by the black arrow. (a) Correlation between East Greenland Coastal Current (EGCC) volume transport from VIKING20X at OSNAP East mooring line location and alongshore wind stress. (b) correlation between alongshore wind stress and outer East Greenland Current (EGC) volume transport. For panels (a) and (b), the black contour shows coefficients greater than 0.5. (c) correlation between EGCC FWT with the wind stress. Note the change in colorbar limits. The black contour shows coefficients greater than 0.2. (d) Correlation between outer EGC FWT and alongshore wind stress. The gray contour indicates the southeast Greenland partition. Black dots indicate areas that are not significant.

We investigate the role of alongshore wind stress as being a driver of the EGCC and outer EGC transport variability in VIKING20X, as hypothesized by Le Bras et al. (2018). We focus on VIKING20X since surface wind stress is not provided for GLORYS12. GLORYS12 is forced with ERA-interim reanalysis wind speeds, but without detailed information on the bulk formulae used in GLORYS12 wind stress estimates would be associated with large uncertainty. Thus we only use VIKING20X output.

The OSNAP East EGCC and outer EGC monthly volume transport correlation is evaluated with the alongshore wind stress from 1993 to 2019 following similar analysis by Le Bras et al. (2018). We also evaluate the correlation of the FWT with the wind stress to investigate the effect of alongshore winds on salinity along the shelf. The correlation between the monthly alongshore wind stress and volume/FWT is computed at zero lag expecting no lag greater than 1 month between transport and wind forcing. We apply the method described in Section 2 to isolate the EGCC from the outer EGC at the location of OSNAP East. The correlations are evaluated at zero lag, where a one-tailed student t-test is used to determine the 99% confidence interval.

Figures 6a and 6b show the correlations between volume transport and alongshore wind stress for the EGCC and EGC. The correlation patterns agree well with those presented by Le Bras et al. (2018), (their Figure 10). The volume transport of the outer EGC shows further offshore correlations south of 65°N extending south of Cape Farewell. Upstream reaching positive correlations are explained by coherent high-speed northeasterly surface winds, which are maintained along the extent of the southeast Greenland coast (Moore, 2014). Le Bras et al. (2018) also noted that upstream wind stress may be transmitted southward by coastally trapped waves. The positive correlations between volume transport and alongshore winds show consistency with the mechanism that northerly alongshore winds result in primarily downwelling, where strong onshore Ekman transport steepens isopycnals, and southward flowing current velocities accelerate (Bacon et al., 2014; Harden et al., 2014; Le Bras et al., 2018; Sutherland & Pickart, 2008).

In VIKING20X, we find a larger spatial extent and higher positive correlations ($r \geq 0.5$) for the EGCC than reported by Le Bras et al. (2018). The correlation pattern of the EGCC presented here appears more similar to

that of the outer EGC in Le Bras et al. (2018), (their Figure 10). The EGCC's volume transport at OSNAP East is highly correlated with the alongshore wind stress further upstream and over the entire east Greenland shelf up to about 70°N. Interestingly, the correlation is not statistically significant directly at the mooring line. (Le Bras et al., 2018) noted that the mooring array may underestimate the EGCC volume transport, since the near-shelf velocity core is not consistently located below the CF1 mooring. There is only one CTD station located onshore, while in VIKING20X the entire shelf area is relatively well represented. On the other hand, VIKING20X may under-represent local, coastal processes, which could explain comparatively high and far upstream correlations with the wind stress.

To examine the wind's impact on freshwater anomalies, we present corresponding correlation maps with the FWT at OSNAP East in Figures 6c and 6d. Note that FWT contains volume transport and salinity anomalies (Equation 2). For the EGCC we find a similar correlation pattern but about 50% lower than for volume transport. Positive, significant correlation values extend just north of the OSNAP East cross section to north of Denmark Strait, indicating that alongshore winds strengthen the connectivity on the shelf. Stronger alongshore winds cause stronger onshore Ekman transport leading to a narrowing and acceleration of the EGCC. In consequence, freshwater is flushed faster downstream. There are positive correlations that reach south of 65° where the shelf is much narrower which is associated with further acceleration of the current. This is also evident in Figure 4 where the advective time scale for freshwater anomalies to travel downstream reduces to less than 1 month in both VIKING20X and GLORYS12 south of 65°N.

In contrast, FWT in the outer EGC is not significantly correlated with the wind stress. We find a rapid decrease from sparse positively correlated locations at the coast to widely negative ones in the interior Irminger Sea. Since FWT is a combination of volume transport and salinity anomalies, we conclude that FWT in the EGCC is partly wind- and partly salinity-driven whereas in the outer EGC it is mostly a function of salinity variations originating from mixing with either the fresher EGCC or the saltier Irminger current water adjacent to the outer EGC. FWC is larger on the shelf and increases toward the coast in both VIKING20X and GLORYS12 (see Figure 2) making the EGCC a significant freshwater conduit in southeast Greenland with alongshore winds influencing freshwater anomalies and their propagation around Cape Farewell.

3.4. What Is the Relative Importance of Freshwater Sources and Is It Changing Over Time?

Given the various freshwater sources along East Greenland, we will determine their relative impact on interannual variations in FWC in the EGC system. Please note that the following analysis focuses on VIKING20X, as neither wind stress nor sea ice production are available from GLORYS12. A composite analysis is done based on the cumulative Greenland runoff fluxes and sea ice production accumulated over the seasonal cycle (January–December) with alongshore wind stress accumulated from June–December (Castelao et al., 2019) (method described in Section 2).

We focus the composite analysis on southeast Greenland due to the immediate impact of additional freshwater input into the Irminger (Duyck et al., 2022; Holliday et al., 2007) and Labrador seas (Castelao et al., 2019; Gillard et al., 2016). This is justified by coherent large-scale atmospheric conditions, a short advective time scale and similar sea ice conditions (see sections above). The composite member years to determine the years of strong/weak meltwater from Greenland FWFs and sea ice melt alike are selected based the respective month in which the seasonal-based increase in freshwater input concludes that is, August for Greenland FWFs and May for sea ice production along southeast Greenland. The alongshore winds composite years are determined from December, as alongshore winds strengthen in winter and often drive near-surface FWT variability (Duyck et al., 2022; Sutherland & Pickart, 2008). The cumulative integral over the seasonal cycle for Greenland FWFs, sea ice production, and alongshore wind stress over southeast Greenland is shown in Figures 7a, 7c, and 7e. Resulting differences in FWC based on the composite analysis is presented in Figures 7b, 7d, and 7f. Additional information on a potential influence on stratification as preconditioning to deep convection later in January is provided in Text S4 in Supporting Information S1.

The cumulative time series from January to December for Greenland runoff shows strong seasonality with most runoff occurring from June to August indicated by the steeper, positive slope between those months (Figure 7a). Both the following winters after summers with exceptionally strong melt, 2010 and 2012, are included in the anomalously high runoff years. Notably, in southeast Greenland, the runoff in the summer of 2010 was greater than in 2012 (Figure 1b).

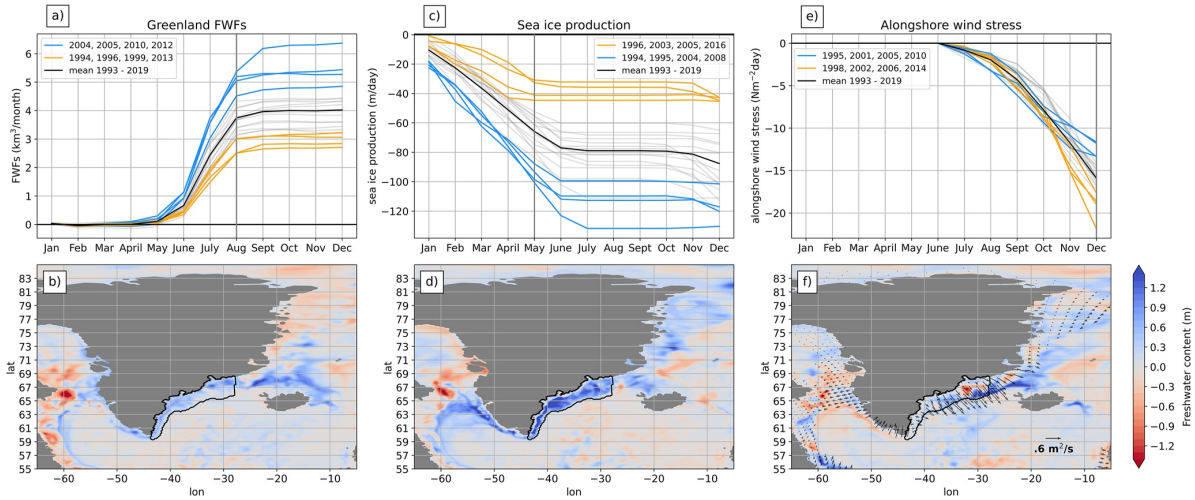

Figure 7. Panels (a), (c), and (e) show the cumulative Greenland melt, sea ice, and alongshore winds given the seasonal cycle starting over January/June–December. The gray line indicates the respective month which the composite to determine the freshwater content (FWC) anomalies are based on. The extreme years determined by a 15th percentile threshold are highlighted in yellow and blue. Panels (b), (d), and (f) show differences in FWC based on a composite analysis of Greenland freshwater fluxe and sea ice production (negative for melt) in August and for alongshore wind stress in December. Composite differences are computed by subtracting low runoff/melt years (orange lines in panels (a), (c)) from years with high rates (blue lines); for the wind stress based composite the mean of strong wind stress years (orange lines) is subtracted from weaker years (blue lines). The black contour shows the southeast Greenland partition. In panel (f) black vectors depict Ekman transport anomalies of December.

The spatial pattern of FWC composite differences (Figure 7b) shows enhanced FWC around the southeast Greenland shelf for strong runoff years compared to low years. There are patches of higher FWC anomalies particularly around Denmark Strait from 65 to 69°N, where the Kangerlussuaq glacier is located and where the EGC system is observed to converge at Denmark Strait and recirculation occurs at Kangerlussuaq trough. The composite difference reveals that this fresh anomaly is carried around Cape Farewell by the EGCC and outer EGC. The West Greenland Current, subsequent boundary current outlining the subpolar gyre, and further north along the shelf by Baffin Bay appear fresher in August just after the summertime peak in Greenland runoff. Years of increased freshwater release from the Greenland coastline show enhanced, positive FWC anomalies localized near the shelf and boundary current along southeast and West Greenland.

Figures 7c and 7d show the monthly cumulative sea ice production and the associated May FWC composite difference. In southeast Greenland region, sea ice melt occurs predominantly in winter and subsides in May (Figure 5a). Therefore, we find cumulative sea ice melt growing (steeper, negative slope) from November (strong melt years, blue lines in Figure 7c) and January (weak melt, orange lines) over winter. Interestingly, while both summers of 2010 and 2012 resulted in anomalous runoff, neither 2010 or 2012 is included in the composite years for sea ice production. We conclude there is no coherence between runoff and sea ice production. Instead, local sea ice melt is dominated by ice being advected into the southeast Greenland region.

For May we find a positive FWC anomaly from Cape Farewell up to Fram Strait for years of strong sea ice melt in southeast Greenland, suggesting that this is driven by a large-scale coherent forcing. There is a patch of positive anomalies by Denmark Strait, and south of 65°N where there are higher FWC anomalies along the boundary current which then follow along the west Greenland current and intrudes the northern Labrador sea. Sea ice melt results in increased FWC along the east and southwest Greenland shelf, reiterating that sea ice melting and formation plays a significant role in setting the FWC along the East Greenland shelf (de Steur et al., 2015). In contrast to the runoff composite, the positive, blue FWC anomaly on the southwest Greenland shelf is enhanced and connects to a fresh anomaly in the northern Labrador Sea, which otherwise is characterized by slightly reduced but comparable FWC anomaly magnitude.

We focus on the immediate impact on local FWC rather than freshwater having propagated from further upstream. It takes about 1 month for freshwater to be advected southward from 65°N but 4–8 months for freshwater to

propagate from Fram Strait to Cape Farewell (Figure 4). From the fast advection within a single month around Cape Farewell, southeast Greenland runoff anomalies will show as FWC anomalies on the southwestern shelf indicative of the known, strong influence of east Greenland runoff on the Labrador Sea. Similar for the wind, we look at the cumulative effect on FWC right at the end of its strengthening season in fall. Wind plays a dominant role in driving much of the near-surface freshwater on and offshore (Håvik & Våge, 2018).

Cumulative wind stress grows linearly from September onwards and hence contributes to FWC anomalies in December (Figure 7e) Negative alongshore wind stress values indicate primarily downwelling favorable winds (onshore Ekman transport), while values close to zero or positive indicate the potential for upwelling-favorable winds (offshore or weaker onshore transport). The December FWC anomaly is computed by subtracting the stronger alongshore winds from weaker northerly winds yielding anomalous offshore Ekman transport.

The December FWC and Ekman transport anomalies are shown in Figure 7f. We find a fresher EGC system particularly south of 65°N. Close to the shelfbreak, the FWC anomaly difference becomes minimal; over the interior Irminger and Labrador Sea it is weakly positive and negative. As indicated by the arrows, the associated Ekman transport anomaly points offshore, showing a weakening of the predominant onshore Ekman transport. This slackening of the wind forcing allows the fresh polar waters of the EGCC to expand over the shelf, and occasionally offshore across the shelf break. The composite shows that reduced onshore Ekman transport relaxes the EGCC and extends the width along which freshwater travels southward along the current. Meanwhile, strong onshore transport results in a steepening of isopycnals close to the shelf, restricting the freshwater and narrowing the boundary current, but allows for saline and warmer water from the interior basin to intrude on the outer EGC due to the strong winds pushing the water toward the shelf. Interestingly, we find 2005 and 2010 among the years with anomalously weak cumulative wind stress (favoring fresh conditions on the shelf), years that are also characterized by anomalously large runoff (cf. Figure 7a), which however occurred in summer prior to the wind stress anomaly. Here, we can only speculate that climate modes, such as the NAO, occasionally provide a link between these two factors in the EGCC freshening.

The Ekman transport anomalies show coherent behavior south of 71°N, which relates to the overlying large-scale atmospheric conditions but points at a different regime dominating farther north in the Greenland Sea. Here, the shelf is wider and eddy-driven mechanisms have been observed to dominate transport changes rather than the local wind stress, as westward transport of Atlantic water from the West Spitsbergen Current merges with the EGC via topographically steered eddies (Gascard et al., 1995; Richter et al., 2018). Approaching Cape Farewell, south of 63°N, Ekman transport anomalies tend to reduce. More importantly, on the southwestern side of Greenland the anomaly is rather onshore suggesting that in winters, in which the southeast Greenland shelf freshens due to anomalous winds, less freshwater actually enters the interior northern Labrador Sea under the same wind regime. We find a negative FWC anomaly off the shelf break in the northern Labrador Sea—the opposite signature of a sea ice melt freshened southeastern shelf (cf. Figures 7d and 7f).

The composite analysis reveals that a direct attribution of FWC anomalies to runoff, sea ice melt and wind stress and their implications for deep convection remains a challenge, because (a) FWC anomalies of different origin or cause have similar magnitudes, (b) years of anomalous runoff may also feature anomalous sea ice melt and/or wind conditions causing a similar freshening, and (c) runoff and sea ice melt peak long before the next deep convection season and varying wind regimes moderate their advection along and export from the boundary current into the interior Labrador and Irminger Seas.

4. Discussion and Conclusions

In this work we use the GLORYS12 reanalysis, an observational-assimilated model-based product, along with the high resolution, eddy-rich ocean model VIKING20X to compare freshwater propagation and variability along the east Greenland shelf and test their potential for identifying imprints of accelerated Greenland ice sheet melt. A mandatory requisite of the data being used for this is a well-resolved EGCC because freshwater is contained on and close to the shelf and surface. We find that the improvement of surface boundary conditions including interannually and seasonally varying, local estimates is crucial to realistically simulate the redistribution of meltwater and changes in FWC in the EGCC, which contains the first imprints of Greenland runoff. In line with earlier studies (Castelao et al., 2019; Gillard et al., 2016) we conclude that a sufficiently high spatial resolution should be used to simulate the dynamical interaction between the EGCC and outer EGC and the freshwater pathway along east Greenland and find 1/20° suitable to achieve this.

In the VIKING20X simulation forced with realistic interannually varying runoff, we find two FWC maxima in the EGCC at sections south of major glaciers (Helheim and Kangerlussuaq) in 2010 and 2012 (see Figure 2). During these summers, the Greenland ice sheet experiences extreme melt conditions yielding exceptionally large runoff (Hanna et al., 2014; Slater et al., 2021b; Tedesco et al., 2011). While similarly extreme conditions were observed during 2019 (Sasgen et al., 2020; Slater et al., 2021b), the runoff forcing applied to VIKING20X does include interannual variations in Greenland runoff only until 2016 based on the data from Bamber et al. (2018) and applies the monthly climatology from 2012 to 2016 thereafter (Tsujino et al., 2018) and thus lacks freshening in 2019 comparable to 2010 and 2012. The imprint of strong Greenland meltwater runoff seen in the EGCC is highly dependent on the freshwater forcing. Although local salinity observations are assimilated in GLORYS12, we could not find a comparable imprint in FWC on the east Greenland shelf and conclude that this is due to the runoff forcing applied to GLORYS12 lacking annual estimates of increased Greenland runoff (applying a linear trend instead) and the general lack of in situ observations on the shelf in the upper 50 m, where most of the freshwater is carried with the EGCC. Reanalysis products like GLORYS12 would greatly benefit from intensified Greenland shelf observations and it would be interesting to see whether such observations could compensate a lack in surface boundary conditions detail, such as interannually varying meltwater fluxes. Without such observations, the product relies on the capabilities of the model to simulate shelf processes demanding mesoscale dynamics permitting grid spacing.

Low salinity waters near the shelf are well represented in VIKING20X when compared with mooring data along the OSNAP East array, while GLORYS12 appears more saline close to the shelf (Figure S2 in Supporting Information S1). A significant source of freshwater in the EGC system is determined by Arctic Ocean export. GLORYS12 underestimated FWT through Fram Strait when compared to observations shown in Figure 3, while VIKING20X was comparable to observations. However model biases such as slower current speeds, freshwater export being further confined to the shelf in VIKING20X and higher salinities with freshwater observed at shallower depths in GLORYS12 result in the reduced transport. VIKING20X and GLORYS12 had a mean annual FWF of 44–62 mSv, while observational estimates yield 68 mSv. Since Arctic export is such a significant source of freshwater in the EGC system (Harden et al., 2014) it is crucial to accurately represent high Arctic sources of freshwater and the subsequent export to lower latitudes. Nevertheless, an analysis of freshwater anomalies, such as ours, is likely less affected by biases and variations at and upstream of Fram Strait.

We find that freshwater anomalies are advected from Fram Strait to Cape Farewell within 4–8 months, in agreement with Harden et al. (2014) observing a lag of approximately 4 months between the FWC seasonality at Fram Strait when measured at the mooring array by Sermilik fjord (≈65°N). Therefore, late wintertime freshwater anomalies at Fram Strait reach Denmark Strait just at beginning of summer when runoff from Greenland picks up (Figure 4). South of 65°N the Greenland shelf narrows and the boundary current velocity increases, reducing advective time scales to less than 1 month. Particularly in winter where the alongshore northerly winds strengthen, induce onshore transport, and speed up the current.

The overlapping seasonality from freshwater sources highlights the challenge of determining the imprint and impact of enhanced Greenland runoff, given the contribution from freshwater sources such as Arctic Ocean export and regional sea ice melt. Sea ice melt begins during summer at latitudes greater than 68°N, thus occurring at the same time as Greenland runoff is strongest along the coast. However, the VIKING20X simulation shows that south of 65°N, melting of sea ice is largest during late winter and early spring (Figure 5a) contributing to the FWC further downstream at a time well distinguishable from any runoff peak.

The correlation analysis based on Le Bras et al. (2018) shows the role that alongshore surface winds play in the EGCC and outer EGC transport variability. We find a higher correlation at the EGCC than (Le Bras et al., 2018) where the discrepancy may be due to mooring availability close to the shelf. When alongshore winds strengthen and strong onshore Ekman transport steepens the isopycnals speeding up the EGCC, most of the freshwater is constrained within the EGCC. Thus, the FWT variability in the EGCC is more correlated with the changes in wind stress versus the outer EGC. The correlations show that the volume transport variability in the EGCC and outer EGC is consistent with wind-driven mechanisms discussed in previous studies. The FWT correlation, with lower correlation coefficients but still statistically significant, confirmed that the freshest waters are contained within the EGCC close to the shelf whereas the outer EGC is more saline due to lateral mixing from warmer and saltier offshore waters. Most recently, Duyck and de Jong (2023) showed that any exchanges between the southeast Greenland shelf and interior seas, particularly at Cape Farewell, are driven primarily by alongshore winds.

Lastly we investigated the impact on FWC from Greenland runoff, sea ice melt, and alongshore wind stress from composites contrasting exceptionally weak and strong conditions (Figure 7). Increased Greenland runoff and sea ice melt resulted in a fresher boundary current, but the alongshore winds showed that weaker onshore Ekman transport results in a relaxation of the EGCC, where the freshwater constrained to the shelf can widen, laterally increasing the maximum extent beyond the shelf. While the opposite occurs during periods of strong, downwelling-favorable winds where the freshwater is pushed towards the shelf, narrowing the fresh boundary current but allowing saltier water from the interior to mix further with the outer EGC thus resulting in a salinification of the slope and EGCC. After the peak freshwater input from sea ice melt in May, there is a strong FWC anomaly along southeast Greenland which appears to follow the west Greenland current and intrudes into the northern Labrador sea with the anomaly eroding in the interior but results in a freshening of the interior Labrador sea.

In this study, it is evident that disentangling the signals of freshwater contributions by Greenland ice sheet melt, Arctic Ocean export, and sea ice melt still remains a challenge. The potential for enhanced Greenland runoff, longer freshening events in the future, and offshore transport of freshwater could all affect stratification in the interior subpolar gyre. While most of the freshwater from Greenland and the Arctic Ocean stays within the confines of the EGCC and boundary current system after rounding Cape Farewell, its potential to directly enter the deep convection sites in the Labrador Sea depends on the local wind regime and baroclinic instability of the current itself and is subject to strong interannual variability (Castelao et al., 2019; Rieck et al., 2019). The negative mass balance of the Greenland ice sheet has not yet persisted long enough to have a visible impact on the salinity budget and stratification, that is, the FWC, of the SPNA and to affect deep convection (Böning et al., 2016; Devilliers et al., 2021; Dukhovskoy et al., 2019; Luo et al., 2016). However with much more freshwater looming on Greenland (Slater et al., 2021a) or in the Beaufort Gyre of the Arctic Ocean (Proshutinsky et al., 2019; Solomon et al., 2021; Zhang et al., 2021), investigating how freshwater is transported along the EGC system is vital to understand future responses to global warming in the SPNA.

Data Availability Statement

All (processed) model data and scripts needed for Figures 1–7 are made available using the GEOMAR data management platform under the identifier: hdl.handle.net/20.500.12085/fd7a41ce-9cc1-46f9-8ed4-1339880c3c42 (Schiller-Weiss et al., 2023). The CMEMS global ocean physics reanalysis is made available on the Copernicus Marine Service: https://doi.org/10.48670/moi-00021. Fram Strait gridded monthly mean velocity and salinity data are available: https://data.npolar.no/dataset/049178d8-9bd3-42b3-a793-606690a5cd8a. OSNAP East CTD measurements at Cape Farewell were collected and made freely available by the OSNAP project: www.o-snap.org.

Acknowledgments
This work was supported by the Deutsche Forschungsgemeinschaft (DFG) as project G-Shocx (MA 4039/1-1). The authors wish to thank the Ocean Dynamics working group at GEOMAR. Thank you to Patricia Handmann for fruitful discussions on freshwater in the subpolar North Atlantic, Willi Rath for technical and scientific support, and Klaus Getzlaff for conducting the VIKING20X simulation. Finally, we want to thank the comments of the anonymous reviewers who helped to greatly improve this manuscript. Open Access funding enabled and organized by Projekt DEAL.

References

Bacon, S., Marshall, A., Holliday, N., Aksenov, Y., & Dye, S. (2014). Seasonal variability of the east Greenland coastal current. *Journal of Geophysical Research: Oceans*, *119*(6), 3967–3987. https://doi.org/10.1002/2013JC009279

Bacon, S., Reverfdin, G., Rigor, I., & Snaith, H. (2002). A freshwater jet on the east Greenland shelf. *Journal of Geophysical Research*, *107*(C7), 3068. https://doi.org/10.1029/2001JC000935

Bakker, P., Schmittner, A., Lenaerts, J., Abe-Ouchi, A., Bi, D., Van den Broeke, M., et al. (2016). Fate of the Atlantic meridional overturning circulation—Strong decline under continued warming and Greenland melting: AMOC projections for warming & GIS melt. *Geophysical Research Letters*, *43*(23), 12252–12260. https://doi.org/10.1002/2016GL070457

Bamber, J., Tedstone, A., King, M., Howat, I., Enderlin, E., Van den Broeke, M., & Noël, B. (2018). Land ice freshwater budget of the arctic and north Atlantic oceans. Part I: Data, methods and results. *Journal of Geophysical Research: Oceans*, *123*(3), 1827–1837. https://doi.org/10.1002/2017JC013605

Behrens, E. (2013). The oceanic response to Greenland melting: The effect of increasing model resolution (Unpublished doctoral dissertation). Retrieved from https://macau.uni-kiel.de/receive/diss_mods_00013684

Belkin, I. M. (2004). Propagation of the "great salinity anomaly" of the 1990s around the northern north Atlantic. *Geophysical Research Letters*, *31*(8), L08306. https://doi.org/10.1029/2003GL019334

Biastoch, A., Schwarzkopf, F., Getzlaff, K., Rühs, S., Martin, T., Scheinert, M., et al. (2021). Regional imprints of changes in the atlantic meridional overturning circulation in the eddy-rich ocean model viking20x. *Ocean Science*, *17*(5), 1177–1211. https://doi.org/10.5194/os-17-1177-2021

Böning, C., Behrens, E., Biastoch, A., Getzlaff, K., & Bamber, J. (2016). Emerging impact of Greenland meltwater on deepwater formation in the North Atlantic Ocean. *Nature Geoscience*, *9*(7), 523–527. https://doi.org/10.1038/ngeo2740

Castelao, R., Luo, H., Oliver, H., Rennermalm, A., Tedesco, M., Bracco, A., et al. (2019). Controls on the transport of meltwater from the southern Greenland ice sheet in the Labrador Sea. *Journal of Geophysical Research: Oceans*, *124*(6), 3551–3560. https://doi.org/10.1029/2019JC015159

Dai, A., Qian, T., Trenberth, K., & Milliman, J. (2008). Changes in continental freshwater discharge from 1948 to 2004. *Journal of Climate*, *22*(10), 2773–2792. https://doi.org/10.1175/2008JCLI2592.1

Debreu, L., Vouland, C., & Blayo, E. (2008). Agrif: Adaptive grid refinement in Fortran. *Computers & Geosciences*, *34*(1), 8–13. https://doi.org/10.1016/j.cageo.2007.01.009

de Steur, L., Peralta Ferriz, C., & Pavlova, O. (2018). Freshwater export in the east Greenland current freshens the North Atlantic. *Geophysical Research Letters*, *45*(24), 13359–13366. https://doi.org/10.1029/2018GL080207

de Steur, L., Pickart, R., Macrander, A., Våge, K., Harden, B., Jonsson, S., et al. (2016). Liquid freshwater transport estimates from the east Greenland current based on continuous measurements north of Denmark strait. *Journal of Geophysical Research: Oceans*, *122*, 93–109. https://doi.org/10.1002/2016JC012106

de Steur, L., Pickart, R., Torres, D., & Valdimarsson, H. (2015). Recent changes in the freshwater composition east of Greenland. *Geophysical Research Letters*, *42*(7), 2326–2332. https://doi.org/10.1002/2014GL062759

Devilliers, M., Swingedouw, D., Mignot, J., Deshayes, J., Garric, G., & Ayache, M. (2021). A realistic Greenland ice sheet and surrounding glaciers and ice caps melting in a coupled climate model. *Climate Dynamics*, *57*(9–10), 2467–2489. https://doi.org/10.1007/s00382-021-05816-7

Dickson, R., Meincke, J., Malmberg, S.-A., & Lee, A. (1988). The great salinity anomaly in the northern north Atlantic 1968-1982. *Progress in Oceanography*, *20*(2), 103–151. https://doi.org/10.1016/0079-6611(88)90049-3

Dickson, R., Rudels, B., Dye, S., Karcher, M., Meincke, J., & Yashayaev, I. (2006). Current estimates of freshwater flux through arctic and subarctic seas. *Progress in Oceanography*, *73*(3–4), 210–230. https://doi.org/10.1016/j.pocean.2006.12.003

Drévillon, M., Lellouche, J., Régnier, C., Garric, G., Bricaud, C., & R, H. (2021). Cmems-glo-quid-001-030, 1.4 edn., eu copernicus marine service information [online]. Retrieved from https://catalogue.marine.copernicus.eu/documents/QUID/CMEMS-GLO-QUID-001-030.pdf

Dukhovskoy, D., Myers, P., Platov, G., Timmermans, M.-L., Curry, B., Proshutinsky, A., et al. (2015). Greenland freshwater pathways in the sub-Arctic seas from model experiments with passive tracers. *Journal of Geophysical Research: Oceans*, *121*(1), 877–907. https://doi.org/10.1002/2015JC011290

Dukhovskoy, D., Yashayaev, I., Proshutinsky, A., Bamber, J., Bashmachnikov, I., Chassignet, E., et al. (2019). Role of Greenland freshwater anomaly in the recent freshening of the subpolar north Atlantic. *Journal of Geophysical Research: Oceans*, *124*(5), 3333–3360. https://doi.org/10.1029/2018JC014686

Duyck, E., & de Jong, M. F. (2023). Cross-shelf exchanges between the east Greenland shelf and interior seas. *Journal of Geophysical Research: Oceans*, *128*(7), e2023JC019905. https://doi.org/10.1029/2023JC019905

Duyck, E., Gelderloos, R., & de Jong, M. F. (2022). Wind-driven freshwater export at cape farewell. *Journal of Geophysical Research: Oceans*, *127*(5), e2021JC018309. https://doi.org/10.1029/2021JC018309

Fichefet, T., & Morales Maqueda, M. A. (1997). Sensitivity of a global sea ice model to the treatment of ice thermodynamics and dynamics. *Journal of Geophysical Research*, *1021*(C6), 12609–12646. https://doi.org/10.1029/97JC00480

Fischer, J., Karstensen, J., Oltmanns, M., & Schmidtko, S. (2018). Mean circulation and eke distribution in the Labrador Sea water level of the subpolar north Atlantic. *Ocean Science*, *14*(5), 1167–1183. https://doi.org/10.5194/os-14-1167-2018

Foukal, N., Gelderloos, R., & Pickart, R. (2020). A continuous pathway for fresh water along the east Greenland shelf. *Science Advances*, *6*(43). https://doi.org/10.1126/sciadv.abc4254

Friedman, A. R., Reverdin, G., Khodri, M., & Gastineau, G. (2017). A new record of Atlantic Sea surface salinity from 1896 to 2013 reveals the signatures of climate variability and long-term trends. *Geophysical Research Letters*, *44*(4), 1866–1876. https://doi.org/10.1002/2017GL072582

Frölicher, T., Fischer, E., & Gruber, N. (2018). Marine heatwaves under global warming. *Nature*, *560*(7718), 360–364. https://doi.org/10.1038/s41586-018-0383-9

Fuentes-Franco, R., & Koenigk, T. (2019). Sensitivity of the Arctic freshwater content and transport to model resolution. *Climate Dynamics*, *53*(3–4), 1765–1781. https://doi.org/10.1007/s00382-019-04735-y

Garcia, C., Comiso, J., Dinnat, E., & Brucker, L. (2017). Satellite observed salinity distributions at high latitudes in the northern hemisphere: A comparison of four products. *Journal of Geophysical Research: Oceans*, *122*(9), 7717–7736. https://doi.org/10.1002/2017JC013184

Gascard, J.-C., Richez, C., & Rouault, C. (1995). New insights on large-scale oceanography in Fram Strait: The West Spitsbergen Current. In W. O. Smith & J. M. Grebmeir (Eds.), *Arctic oceanography: Marginal ice zones and continental shelves*. https://doi.org/10.1029/CE049p0131

Gillard, L., Hu, X., Myers, P., & Bamber, J. (2016). Meltwater pathways from marine terminating glaciers of the Greenland ice sheet: Meltwater pathways from the GrIS. *Geophysical Research Letters*, *43*(20), 10873–10882. https://doi.org/10.1002/2016GL070969

Good, S., Martin, M., & Rayner, N. (2013). En4: Quality controlled ocean temperature and salinity profiles and monthly objective analyses with uncertainty estimates. *Journal of Geophysical Research: Oceans*, *118*(12), 6704–6716. https://doi.org/10.1002/2013JC009067

Guinehut, S., Dhomps, A.-L., Gilles, L., & Traon, P.-Y. (2012). High resolution 3-d temperature and salinity fields derived from in situ and satellite observations. *Ocean Science*, *8*(5), 845–857. https://doi.org/10.5194/os-8-845-2012

Haine, T., Curry, B., Gerdes, R., Hansen, E., Karcher, M., Lee, C., et al. (2015). Arctic freshwater export: Status, mechanisms, and prospects. *Global and Planetary Change*, *125*, 13–35. https://doi.org/10.1016/j.gloplacha.2014.11.013

Handmann, P. (2019). Deep water formation and spreading dynamics in the subpolar north Atlantic from observations and high-resolution ocean models (Unpublished doctoral dissertation). Retrieved from https://macau.uni-kiel.de/receive/macau_mods_00000258

Hanna, E., Fettweis, X., Mernild, S., Cappelen, J., Ribergaard, M., Shuman, C., et al. (2014). Atmospheric and oceanic climate forcing of the exceptional Greenland ice sheet surface melt in summer 2012. *International Journal of Climatology*, *34*(4), 1022–1037. https://doi.org/10.1002/joc.3743

Hanna, E., Huybrechts, P., Steffen, K., Cappelen, J., Huff, R., Shuman, C., et al. (2008). Increased runoff from melt from the Greenland ice sheet: A response to global warming. *Journal of Climate*, *21*(2), 331–341. https://doi.org/10.1175/2007JCLI1964.1

Harden, B., Straneo, F., & Sutherland, D. (2014). Moored observations of synoptic and seasonal variability in the east Greenland coastal current. *Journal of Geophysical Research: Oceans*, *119*(12), 8838–8857. https://doi.org/10.1002/2014JC010134

Håvik, L., Pickart, R., Våge, K., Torres, D., Thurnherr, A., Beszczynska-Moeller, A., et al. (2017). Evolution of the east Greenland current from fram strait to Denmark strait: Synoptic measurements from summer 2012. *Journal of Geophysical Research: Oceans*, *122*(3), 1974–1994. https://doi.org/10.1002/2016JC012228

Håvik, L., & Våge, K. (2018). Wind-driven coastal upwelling and downwelling in the shelfbreak east Greenland current. *Journal of Geophysical Research: Oceans*, *123*(9), 6106–6115. https://doi.org/10.1029/2018JC014273

Hobday, A., Oliver, E., Gupta, A., Benthuysen, J., Burrows, M., Donat, M., et al. (2018). Categorizing and naming marine heatwaves. *Oceanography*, *31*(2). https://doi.org/10.5670/oceanog.2018.205

Holfort, J., & Hansen, E. (2005). Timeseries of polar water properties in fram strait. *Geophysical Research Letters*, *32*(19), L19601. https://doi.org/10.1029/2005GL022957

Holliday, N., Bersch, M., Berx, B., Chafik, L., Cunningham, S., Florindo-López, C., et al. (2020). Ocean circulation causes the largest freshening event for 120 years in eastern subpolar north Atlantic. *Nature Communications*, *11*(1), 585. https://doi.org/10.1038/s41467-020-14474-y

Holliday, N., Meyer, A., Bacon, S., Alderson, S., & Cuevas, B. (2007). Retroflection of part of the east Greenland current at cape farewell. *Geophysical Research Letters*, *340*(7), L07609. https://doi.org/10.1029/2006GL029085

Jackson, L., & Wood, R. (2018). Timescales of AMOC decline in response to fresh water forcing. *Climate Dynamics*, *51*(4), 1333–1350. https://doi.org/10.1007/s00382-017-3957-6

Karpouzoglou, T., de Steur, L., Smedsrud, L., & Sumata, H. (2022). Observed changes in the Arctic freshwater outflow in fram strait. *Journal of Geophysical Research: Oceans*, *127*(3), e2021JC018122. https://doi.org/10.1029/2021JC018122

Koehler, J., Sena-Martins, M., Serra, N., & Stammer, D. (2014). Quality assessment of spaceborne sea surface salinity observations over the northern north Atlantic. *Journal of Geophysical Research: Oceans*, *120*(6), 4306–4323. https://doi.org/10.1002/2014JC010067

Le Bras, I., Straneo, F., Holte, J., & Holliday, N. (2018). Seasonality of freshwater in the east Greenland current system from 2014 to 2016. *Journal of Geophysical Research: Oceans*, *123*(12), 8828–8848. https://doi.org/10.1029/2018JC014511

Lellouche, J.-M., Greiner, E., Bourdallé-Badie, R., Garric, G., Melet, A., Drevillon, M., et al. (2021). The copernicus global 1/12° oceanic and sea ice GLORYS12 reanalysis. *Frontiers in Earth Science*, *9*, 698876. https://doi.org/10.3389/feart.2021.698876

Locarnini, R. A., Mishonov, A. V., Antonov, J. I., Boyer, T. P., Garcia, H. E., Baranova, O. K., et al. (2013). In S. Levitus (Ed.), A. Mishonov (Technical Ed.), *World Ocean Atlas 2013 volume 1: Temperature*. *NOAA Atlas NESDIS 73* (40 pp,). https://doi.org/10.7289/V55X26VD

Lozier, M., Li, F., Bacon, S., Bahr, F., Bower, A., Cunningham, S., et al. (2019). A sea change in our view of overturning in the subpolar north Atlantic. *Science*, *363*(6426), 516–521. https://doi.org/10.1126/science.aau6592

Luo, H., Castelao, R., Rennermalm, A., Tedesco, M., Bracco, A., Yager, P., & Mote, T. (2016). Oceanic transport of surface meltwater from the southern Greenland ice sheet. *Nature Geoscience*, *9*(7), 528–532. https://doi.org/10.1038/ngeo2708

Madec, G., Bourdallé-Badie, R., Bouttier, P. A., Bricaud, C., Bruciaferri, D., Calvert, D., & Vancoppenolle, M. (2016). Nemo ocean engine. *Scientific notes of climate modeling center (27)*. Institut Pierre Simon Laplace (IPSL). https://doi.org/10.5281/zenodo.8167700

Marshall, J., Scott, J., & Proshutinsky, A. (2017). Climate response functions for the Arctic Ocean: A proposed coordinated modelling experiment. *Geoscientific Model Development*, *10*(7), 2833–2848. https://doi.org/10.5194/gmd-10-2833-2017

Martin, T., & Biastoch, A. (2023). On the ocean's response to enhanced Greenland runoff in model experiments: Relevance of mesoscale dynamics and atmospheric coupling. *Ocean Science*, *19*(1), 141–167. https://doi.org/10.5194/os-19-141-2023

Moore, G. (2012). A new look at Greenland flow distortion and its impact on barrier flow, tip jets and coastal oceanography. *Geophysical Research Letters*, *39*(22), L22806. https://doi.org/10.1029/2012gl054017

Moore, G. (2014). In *A new look at Southeast Greenland barrier winds and katabatic flow* (Vol. 12). US CLIVAR Variations Newsl.

Mulet, S., Rio, M.-H., Mignot, A., Guinehut, S., & Morrow, R. (2012). A new estimate of the global 3d geostrophic ocean circulation based on satellite data and in-situ measurements. *Deep Sea Research Part II: Topical Studies in Oceanography*, *77–80*, 70–81. https://doi.org/10.1016/j.dsr2.2012.04.012

Myers, P., Donnelly, C., & Ribergaard, M. (2009). Structure and variability of the west Greenland current in summer derived from 6 repeat standard sections. *Progress in Oceanography*, *80*(1–2), 93–112. https://doi.org/10.1016/j.pocean.2008.12.003

Olmedo, E., Gabarro, C., González-Gambau, V., Martinez, J., Ballabrera, J., Turiel, A., et al. (2018). Seven years of SMOS sea surface salinity at high latitudes: Variability in arctic and sub-arctic regions. *Remote Sensing*, *10*(11), 1772. https://doi.org/10.3390/rs10111772

Oltmanns, M., Karstensen, J., & Fischer, J. (2018). Increased risk of a shutdown of ocean convection posed by warm north Atlantic summers. *Nature Climate Change*, *8*(4), 300–304. https://doi.org/10.1038/s41558-018-0105-1

Perkins-Kirkpatrick, S., & Alexander, L. (2013). On the measurement of heat waves. *Journal of Climate*, *26*(13), 4500–4517. https://doi.org/10.1175/JCLI-D-12-00383.1

Proshutinsky, A., Krishfield, R., Toole, J., Timmermans, M., Williams, W., Zimmerman, S., et al. (2019). Analysis of the beaufort gyre freshwater content in 2003–2018. *Journal of Geophysical Research: Oceans*, *124*(12), 9658–9689. https://doi.org/10.1029/2019JC015281

Rahmstorf, S., Box, J., Feulner, G., Mann, M., Robinson, A., Rutherford, S., & Schaffernicht, E. (2015). Exceptional twentieth-century slowdown in Atlantic ocean overturning circulation. *Nature Climate Change*, *5*, 475–480. https://doi.org/10.1038/nclimate2554

Richter, M., von Appen, W.-J., & Wekerle, C. (2018). Does the east Greenland current exist in the northern fram strait? *Ocean Science*, *14*(5), 1147–1165. https://doi.org/10.5194/os-14-1147-2018

Rieck, J., Böning, C., & Getzlaff, K. (2019). The nature of eddy kinetic energy in the Labrador Sea: Different types of mesoscale eddies, their temporal variability, and impact on deep convection. *Journal of Physical Oceanography*, *49*(8), 2075–2094. https://doi.org/10.1175/jpo-d-18-0243.1

Rignot, E., & Mouginot, J. (2012). Ice flow in Greenland for the international polar year 2008-2009. *Geophysical Research Letters*, *39*(11), L11501. https://doi.org/10.1029/2012GL051634

Rignot, E., Velicogna, I., Van den Broeke, M., Monaghan, A., & Lenaerts, J. (2011). Acceleration of the contribution of the Greenland and Antarctic ice sheets to sea level rise. *Geophysical Research Letters*, *38*(5), L05503. https://doi.org/10.1029/2011GL046583

Rudels, B., Jones, E., Schauer, U., & Eriksson, P. (2004). Atlantic sources of the Arctic Ocean surface and halocline waters. *Polar Research*, *23*(2), 181–208. https://doi.org/10.1111/j.1751-8369.2004.tb00007.x

Rühs, S., Oliver, E., Biastoch, A., Böning, C., Dowd, M., Getzlaff, K., et al. (2021). Changing spatial patterns of deep convection in the subpolar north Atlantic. *Journal of Geophysical Research: Oceans*, *126*(7). https://doi.org/10.1029/2021JC017245

Sasgen, I., Wouters, B., Gardner, A., King, M., Tedesco, M., Landerer, F., et al. (2020). Return to rapid ice loss in Greenland and record loss in 2019 detected by the grace-fo satellites. *Communications Earth & Environment*, *1*, 8. https://doi.org/10.1038/s43247-020-0010-1

Schiller-Weiss, I., Martin, T., Karstensen, J., & Biastoch, A. (2023). Supplementary material to: Do salinity variations along the east Greenland shelf show imprints of increasing meltwater runoff? [Dataset]. GEOMAR Helmholtz Centre for Ocean Research Kiel [distributor]. https://hdl.handle.net/20.500.12085/fd7a41ce-9cc1-46f9-8ed4-1339880c3c42

Slater, T., Lawrence, I., Otosaka, I., Shepherd, A., Gourmelen, N., Jakob, L., et al. (2021a). Review article: Earth's ice imbalance. *The Cryosphere*, *15*(1), 233–246. https://doi.org/10.5194/tc-15-233-2021

Slater, T., Shepherd, A., McMillan, M., Leeson, A., Gilbert, L., Muir, A., et al. (2021b). Increased variability in Greenland ice sheet runoff from satellite observations. *Nature Communications*, *12*(1), 6069. https://doi.org/10.1038/s41467-021-26229-4

Smedsrud, L., Sorteberg, A., & Kloster, K. (2008). Recent and future changes of the arctic sea-ice cover. *Geophysical Research Letters*, *35*(20), L20503. https://doi.org/10.1029/2008GL034813

Solomon, A., Heuzé, C., Rabe, B., Bacon, S., Bertino, L., Heimbach, P., et al. (2021). Freshwater in the Arctic Ocean 2010–2019. *Ocean Science*, *17*(4), 1081–1102. https://doi.org/10.5194/os-17-1081-2021

Spreen, G., de Steur, L., Divine, D., Gerland, S., Hansen, E., & Kwok, R. (2020). Arctic sea ice volume export through fram strait from 1992 to 2014. *Journal of Geophysical Research: Oceans*, *125*(6), e2019JC016039. https://doi.org/10.1029/2019JC016039

Sutherland, D., & Pickart, R. (2008). The east Greenland coastal current: Structure, variability, and forcing. *Progress in Oceanography*, *78*(1), 58–77. https://doi.org/10.1016/j.pocean.2007.09.006

Swingedouw, D., Houssais, M.-N., Herbaut, C., Blaizot, A.-C., Devilliers, M., & Deshayes, J. (2022). AMOC recent and future trends: A crucial role for oceanic resolution and Greenland melting? *Frontiers in Climate*, *4*. https://doi.org/10.3389/fclim.2022.838310

Swingedouw, D., Rodehacke, C., Behrens, E., Menary, M., Olsen, S., Gao, Y., et al. (2012). Decadal fingerprints of freshwater discharge around Greenland in a multi-model ensemble. *Climate Dynamics*, *41*(3–4), 695–720. https://doi.org/10.1007/s00382-012-1479-9

Tedesco, M., Fettweis, X., Van den Broeke, M., Wal, R., Smeets, P., Berg, W., et al. (2011). The role of albedo and accumulation in the 2010 melting record in Greenland. *Environmental Research Letters*, *6*(1), 014005. https://doi.org/10.1088/1748-9326/6/1/014005

Tesdal, J.-E., Abernathey, R., Goes, J., Gordon, A., & Haine, T. (2018). Salinity trends within the upper layers of the subpolar north Atlantic. *Journal of Climate*, *31*(7), 2675–2698. https://doi.org/10.1175/JCLI-D-17-0532.1

Tournadre, J., Bouhier, N., Girard-Ardhuin, F., & Rémy, F. (2015). Antarctic icebergs distributions 1992–2014. *Journal of Geophysical Research: Oceans*, *121*(1), 327–349. https://doi.org/10.1002/2015JC011178

Tsujino, H., Urakawa, S., Nakano, H., Small, R., Kim, W., Yeager, S., et al. (2018). Jra-55 based surface dataset for driving ocean—Sea-ice models (jra55-do). *Ocean Modelling*, *130*, 79–139. https://doi.org/10.1016/j.ocemod.2018.07.002

Våge, K., Papritz, L., Håvik, L., Spall, M., & Moore, G. (2018). Ocean convection linked to the recent ice edge retreat along east Greenland. *Nature Communications*, *9*(1), 1287. https://doi.org/10.1038/s41467-018-03468-6

Vinje, T. (2001). Fram strait ice fluxes and atmospheric circulation: 1950-2000. *Journal of Climate*, *14*(16), 3508–3517. https://doi.org/10.1175/1520-0442(2001)014<3508:FSIFAA>2.0.CO;2

Wang, Q., Ricker, R., & Mu, L. (2021). Arctic sea ice decline preconditions events of anomalously low sea ice volume export through fram strait in the early 21st century. *Journal of Geophysical Research: Oceans*, *126*(2), e2020JC016607. https://doi.org/10.1029/2020JC016607

Zhang, J., Weijer, W., Steele, M., Cheng, W., Verma, T., & Veneziani, M. (2021). Labrador sea freshening linked to beaufort gyre freshwater release. *Nature Communications*, *12*(1), 1229. https://doi.org/10.1038/s41467-021-21470-3

Zou, S., Lozier, M., Li, F., Abernathey, R., & Jackson, L. (2020). Density-compensated overturning in the Labrador sea. *Nature Geoscience*, *13*(2), 1–6. https://doi.org/10.1038/s41561-019-0517-1

Zweng, M. M., Reagan, J. R., Antonov, J. I., Locarnini, R. A., Mishonov, A. V., Boyer, T. P., et al. (2013). In S. Levitus (Ed.), A. Mishonov (Technical Ed.), *World Ocean Atlas 2013 volume 2: Salinity*. *NOAA Atlas NESDIS 74* (39 pp.). https://doi.org/10.7289/V5251G4D

3

Study 2: Emerging influence of enhanced Greenland melting on boundary currents and deep convection regimes in the Labrador and Irminger Seas

This study shifts from east to the west of Greenland comparing two model simulations with differing inputs of Greenland runoff. One experiment consists of realistic, interannually varying freshwater input from Greenland, and the other contains reduced runoff based on a climatological mean. A local freshening and cooling is found primarily along the Greenland boundary currents with an associated increase in the current velocities, particularly at OSNAP West. The increased speeds show a tendency for increased eddy formation into the interior Labrador Sea. Greenland meltwater has propagated into two deep convection regions, with implications for deeper mixed layers found in the eastern Irminger Sea, evident in years 2015–2018.

This chapter is a print of the manuscript "*Emerging influence of enhanced Greenland melting on boundary currents and deep convection regimes in the Labrador and Irminger Seas*", accepted for publication on April 20th, 2024 in Geophysical Research Letters.

Emerging influence of enhanced Greenland melting on boundary currents and deep convection regimes in the Labrador and Irminger Seas

Ilana Schiller-Weiss[1], Torge Martin[1], Franziska U. Schwarzkopf[1]

[1]GEOMAR Helmholtz Centre for Ocean Research Kiel, Kiel, Germany

Key Points:

- The West Greenland Current (WGC) freshens and cools with the observed recent increase in meltwater runoff from Greenland
- The density gradient across the boundary current intensifies, strengthening the WGC and increasing local eddy formation
- Deep mixing of meltwater at shallower depths in the Labrador Sea contributes a shift in deep convection into the Irminger Sea (2015–2018)

Corresponding author: Ilana Schiller-Weiss, ischiller-weiss@geomar.de

Abstract

Freshwater input from Greenland ice sheet melt has been increasing in the past decades from warming temperatures. To identify the impacts from enhanced meltwater input into the subpolar North Atlantic from 1997–2021, we use output from two nearly identical simulations in the eddy-rich model VIKING20X (1/20°) only differing in the freshwater input from Greenland: one with realistic interannually varying runoff increasing in the early 2000s and the other with climatologically (1961–2000) continued runoff. The majority of the additional freshwater remains within the boundary current enhancing the density gradient towards the warm and salty interior waters yielding increased current velocities. The accelerated boundary current shows a tendency towards eddy shedding into the Labrador Sea interior. Further, the experiments allow to attribute higher stratification and shallower mixed layers southwest of Greenland and deeper mixed layers in the Irminger Sea, particularly in 2015–2018, to the runoff increase in the early 2000s.

Plain Language Summary

Global warming has accelerated the melting of the Greenland ice sheet over the past few decades resulting in enhanced freshwater input into the North Atlantic. The additional freshwater can potentially inhibit deep water formation and have future implications on ocean circulation. To determine the influence from Greenland melt, we compare two high-resolution model experiments all with the same forcing but differing input of Greenland freshwater fluxes from 1997–2021. We find that in the experiment with realistically increasing Greenland meltwater, the water becomes fresher and cooler along the continental shelf and boundary of the subpolar gyre. The density difference between the shelf and interior increases with more freshwater, resulting in faster West Greenland Current speeds and enhanced eddy formation. Deeper mixed layers are found in the eastern Irminger Sea, particularly in 2015–2018. From 2009–2013, there were shallower mixed layers in the Labrador Sea where less Greenland meltwater was mixed downwards and spread eastward, causing mixed layers to deepen in the Irminger Sea.

1 Introduction

The Greenland ice sheet has been losing mass over the last couple of decades as a result of global warming (Hanna et al., 2008; Fettweis et al., 2011; Bamber et al., 2018). With an increasing amount of freshwater input, there is interest in the impact it will have on circulation in the subpolar North Atlantic (SPNA), particularly whether additional freshwater will increase stratification and reduce deep water formation, which could weaken the Atlantic Meridional Overturning Circulation (AMOC) (Rahmstorf et al., 2015; Bakker et al., 2016; Böning et al., 2016; Swingedouw et al., 2022). Freshwater from Greenland melt will first appear in the East and West Greenland Currents (EGC/WGC) along with Arctic sourced fresh Polar Water (de Steur et al., 2009, 2018). Both the EGC and WGC consist of two surface intensified double current cores with a coastal current and outer slope current just beyond the shelfbreak (Bacon et al., 2002; Håvik et al., 2017; Sutherland & Pickart, 2008; Le Bras et al., 2018; Myers et al., 2009; Pacini et al., 2020; Gou et al., 2021). We will use the term boundary current to address both cores together as one system.

The EGC is observed to be fairly coherent with minimal freshwater export along east Greenland; strong alongshore winds constrain the majority of fresh and cool water near the shelf (Sutherland & Pickart, 2008; Le Bras et al., 2018; Duyck et al., 2022; Schiller-Weiss et al., 2023). Along southeast Greenland at Cape Farewell, tip jets, northeasterly winds, and a retroflection can export freshwater into the central Irminger Sea (Duyck et al., 2022; Holliday et al., 2007). The WGC consists of near surface buoyant and fresh waters with warmer and salty Irminger water at depth (Gou et al., 2022; Myers et al.,

2007; Fratantoni & Pickart, 2007; Pacini et al., 2020). Freshwater can be transported by the WGC, northward into Baffin Bay, or cyclonically around the Labrador basin (Pacini et al., 2021; Gou et al., 2021). Freshwater from the WGC can be fluxed into the central Labrador Sea via offshore Ekman transport (Luo et al., 2016; Castelao et al., 2019; Schulze Chretien & Frajka-Williams, 2018) and eddies (Lilly et al., 2003; Katsman et al., 2004; Rieck et al., 2019; Pacini & Pickart, 2022). The Labrador and Irminger Sea will be referred to as LAB and IRM respectively throughout the manuscript.

Eddies shed from the boundary current into LAB have different origins. Irminger Rings are formed from steep topographic differences in the slope south of Cape Desolation (CD) (Lilly et al., 2003; Bracco et al., 2008; Luo et al., 2011; de Jong & de Steur, 2016; Rieck et al., 2019). Eddies are generated near the shelf in the WGC and Labrador Current via baroclinic instabilities which intensify in winter as the lateral temperature gradient increases between the boundary current and interior (Katsman et al., 2004; Spall, 2004; Chanut et al., 2008; Rieck et al., 2019). Eddies are observed to play a significant role in determining the magnitude and location of deep convection, restratification, and preconditioning processes by transporting heat and freshwater into the interior (Gelderloos et al., 2011; Chanut et al., 2008; Rieck et al., 2019). An eastward shift in deep convection occurred from 2015–2018 (Zunino et al., 2020; Piron et al., 2017; Rühs et al., 2021), which Rühs et al. (2021) hypothesized may partially be attributed to accelerated Greenland melting. As more freshwater enters the boundary currents, it is important to understand and identify associated hydrographic and potential dynamical changes.

In this study, we investigate the influence of Greenland freshwater input between two nearly identical high-resolution, eddying ocean model runs from 1997–2021 but with differing Greenland freshwater fluxes (FWFs). We break down the question for an observable imprint by enhanced Greenland melting onto the ocean into the following subtopics: (1) hydrographic changes i.e. in near-surface salinity and temperature (2) dynamical changes i.e. changes in density and its influence on boundary current strength and eddy formation, and (3) changes in mixed layer depth (MLD) with a particular focus on additional freshwater contributing to the eastward shift of deep convection.

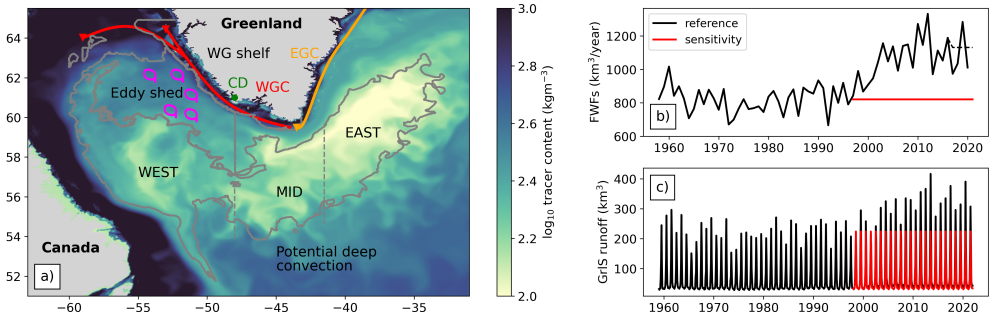

Figure 1. (a) Snapshot of passive tracer integrated over the top 200m and schematic of surface currents. The three gray contours show the West Greenland shelf, eddy shedding region (eddies marked by fuchsia rings), and the area of potential deep convection split into three subregions: LAB (WEST), south of Cape Farewell (MID), and IRM (EAST). Cape Desolation (CD) location marked in green. (b) Total, annual FWFs from Greenland runoff from 1960–2021. (c) Monthly varying FWFs. Black line shows interannually varying FWF of REF, dashed line shows 2012–2016 mean; the red line shows the reduced, climatological FWF from SENS.

2 Ocean Model Experiments

The analysis is based on the ocean/sea-ice general circulation model NEMO configuration VIKING20X (Biastoch et al., 2021) (model details described in Supporting Information). The model has been evaluated extensively for the representation of AMOC (Biastoch et al., 2021), SPNA deep convection (Rühs et al., 2021), deep water formation and pathways (Handmann et al., 2018), and successfully applied to identifying the mechanisms of the recent Eastern North Atlantic freshening (Fox et al., 2022).

We compare two nearly identical model simulations of VIKING20X: one including the observed increase in Greenland runoff (referred to as "reference", short REF) and a "sensitivity" experiment (SENS), where the Greenland FWFs is reduced to the 1961–2000 climatology. In REF Greenland FWFs are interannually varying with an increasing trend shown in the total annual FWFs (black line of Figure 1b), based on (Bamber et al., 2018; Slater et al., 2021). The FWFs are monthly varying with a prominent seasonal cycle (Figure 1c) and are released at the surface and coastline, tagged by an accumulated passive tracer (Figure 1a) (more details given in the Supporting Information). Greenland FWFs from Bamber et al. (2018) do not extend beyond 2016 and runoff in the JRA55-do forcing is continued by a daily varying 2012–2016 climatology (Tsujino et al., 2018). To include a fair representation of the years after 2016, in particular the record runoff year 2019 (Tedesco & Fettweis, 2020), an annually varying scaling factor is applied based on a linear regression of the total annual Greenland FWF of (Bamber et al., 2018) and runoff estimates of (Slater et al., 2021) data. The spatial pattern and daily variability of the JRA55-do climatological values are maintained but scaled by a single value, varying per year. While the scaling is based on the total Greenland runoff, the factor is applied to local FWFs per model grid cell to generate the forcing, where the spatial pattern of the Greenland FWF is still tied to the 2012–2016 mean.

Greenland FWFs in SENS are represented as daily climatology from 1961–2000 (red line in Figure 1b, c). The cumulative difference in Greenland runoff between REF and SENS amounts to about 6300 km^3 from 1997-2021. The increase in FWF in the late 1990s and early 2000s is about 0.01 Sv over one year (cf. (Bamber et al., 2018), Fig. 3), which is 1–2 orders of magnitude smaller than the typical amount applied in hosing experiments (Jackson & Wood, 2018).

3 Results

The following analysis focuses on significant changes between REF and SENS. We investigate significant sea surface salinity (SSS) and temperature (SST) differences, then changes in the West Greenland boundary current strength, followed by differences in eddy kinetic energy (EKE) to investigate the potential for enhanced eddy formation from changes in the boundary current. We attribute a deepening of mixed layers in IRM to the enhanced FWF in REF (particularly in 2015–2018) and discuss the mechanisms leading to a contribution by Greenland meltwater to the recent eastward shift of deep convection.

3.1 Surface freshening and cooling

The first imprint of enhanced Greenland FWFs in the hydrography appears along the Greenland shelf. We focus on the last 20 years of the simulation (2002–2021) to allow for additional freshwater to quasi-equilibrate (the linear trend in total Greenland FWFs applied to REF is nearly zero over these two decades). We focus on annual means and compute differences (REF minus SENS) showing a significant freshening and cooling in SSS and SST particularly along the continental shelves (Figure 2a, b). Freshening and cooling appear throughout the year, with fresher near shelf water in summer associated with the seasonal peak in Greenland runoff (Bamber et al., 2018) (Figure S1a, c).

Significant areas of the SSS difference, purple in Figure 2a implying lower salinities in REF compared to SENS, are found primarily in the WGC, LAB shelf, and eddy shedding region. We define the WGC boundaries by the 1000 m isobath and the eddy shedding region by the EKE field (further limited by the 1000 m and 2000 m isobaths towards the east and north, respectively). (Figure 1a). The southern boundary is limited by the potential deep convection area (pDCA), defined as any grid point where MLDs exceed $z_{critical}$ = 1000 m at least once (Rühs et al., 2021) between 2002–2021 (Figure 1a). Statistical significance is computed from bootstrap resampling (Bertino et al., 2003) where areas are significant when the difference between the resampled means are larger than the total standard deviation of the two bootstrapped runs.

The coolest SSTs occur near the shelves and eddy shedding region where LAB's shelf boundary exhibits anomalously colder SSTs in REF (Figure 2b). The strong cooling around the northwest LAB boundary is associated with a greater extent of winter sea ice in REF (Figure S1a, c, e) attributed to local sea-ice formation and export from Baffin Bay (Våge et al., 2009; Kwok, 2007). Deser et al. (2002) observed that sea ice formation lagged changes in salinity along the WGC by 8 months suggesting that enhanced summer melt affects LAB's northern sea ice extent.

2010 and 2012 were two years of exceptional Greenland runoff (Tedesco et al., 2011; Hanna et al., 2014) (Figure 1b). This is most evident in the WGC where REF and SENS freshen from 2010–2012 (Figure 2c). Although 2019 was a year of anomalous Greenland melt, the majority of melt occurred further northwest of the ice sheet (Tedesco & Fettweis, 2020), thus the freshening is less than in 2010/2012. 2012 remains the year of strongest Greenland melt on record from higher humidity and air temperature over the ice sheet (Tedesco & Fettweis, 2020).

Annual mean salinity in the WGC begins to diverge in 2004 with REF developing significantly lower salinity than in SENS, some years after the rapid increase in Greenland FWFs from 2000 onwards (Figure 1b). The eddy shedding region exhibits less of a difference in SSS annual means than in the WGC. The strong reduction in SSS begins in 2011 rather than 2010, a year with record runoff. Alongshore winds were downwelling favorable in the winter of 2010 following the exceptional summer runoff and hence offshore transport of fresher waters was even less than in 2011 (Figure S2) (Myers et al., 2021), highlighting the importance of wind forcing over runoff for freshening events offshore the WGC.

The VIKING20X-JRA OMIP hindcast run from which both REF and SENS are branched off in 1997, shows quasi multi-decadal variability with lower/higher salinities in the 1970s and 2000s/1980s–1990s. The sharp decrease in salinity in the WGC and eddy shedding region in 1969 is identified as the Great Salinity anomaly from 1968–1982 (GSA'70s) resulting from anomalous Arctic export via Fram Strait (Dickson et al., 1988; Belkin et al., 1998). In REF, the period of 2010–2012 attributed to exceptional runoff reaches even lower SSS values than the GSA'70s emphasizing the significance that Greenland FWFs has on the boundary current.

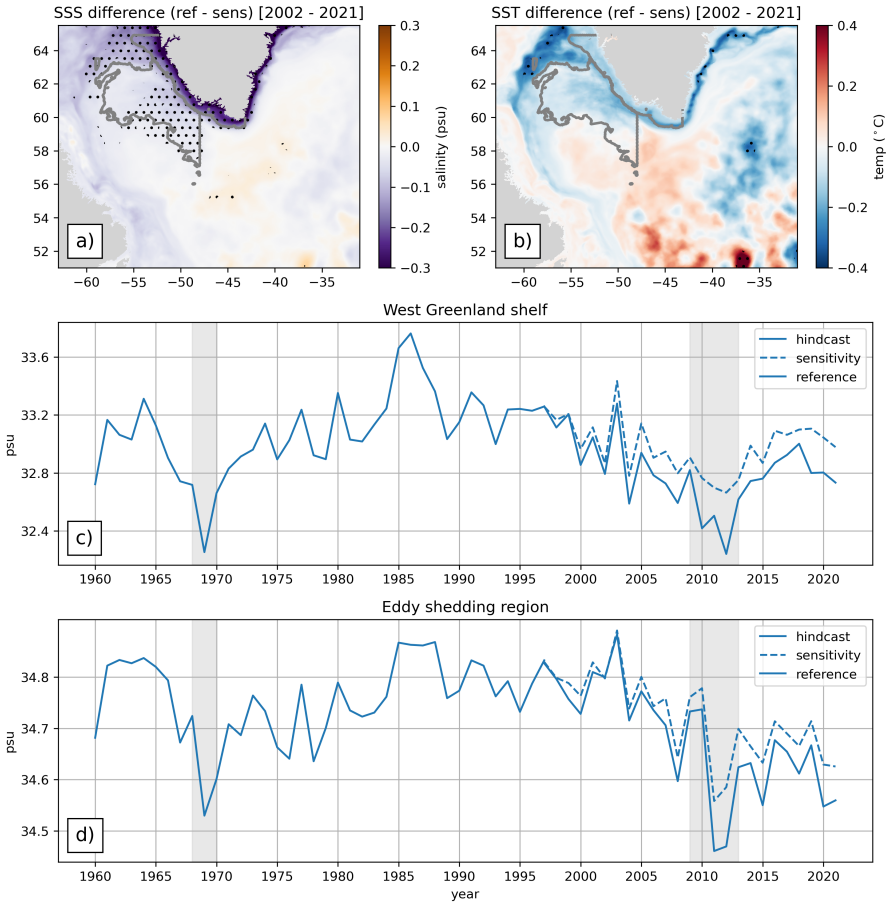

Figure 2. (a) Mean SSS response (REF minus SENS) and (b) mean SST difference. Black stippling indicates significant areas. Gray contours mark the West Greenland shelf and eddy shedding region. (c) Annual mean SSS over the West Greenland shelf. (d) Annual mean SSS over the eddy shedding region. The solid line is based on the hindcast simulation (1960–1996) and from REF (1997–2021); dashed line represents SENS. Gray vertical bars indicate the GSA'70s and 2010–2012 years of strong Greenland melt.

3.2 Strengthened boundary current

Enhanced Greenland runoff over the recent decades contributes to the fresh polar watermass carried by the Greenland boundary current system – with a density decrease along the boundaries primarily driven by the local freshening from enhanced meltwater (Figure S1e, f). The density decrease on the shelf intensifies the horizontal gradient towards the denser interior LAB and strengthens the WGC via thermal wind balance (Gou et al., 2022; Katsman et al., 2004). To investigate these changes in the boundary current system, we take an exemplary cross section at OSNAP West (Lozier et al., 2019) to obtain the WGC velocity structure in REF (Figure 3a). The current consists of two current cores both reaching velocity magnitudes up to 0.5 m/s: the West Greenland coastal current (WGCC) and just off the shelfbreak, the slope current. The WGCC contains the most polar water along with traces of Greenland meltwater (Lin et al., 2018; Pacini et al., 2020; Gou et al., 2022). The slope current is adjacent and lies above the saltier and warmer Irminger Current (Fratantoni & Pickart, 2007; Myers et al., 2009). We isolate the surface intensified WGCC and slope current by taking the top 100 m and northwest-

ward velocities only (black boxes in Figure 3a). We sample the WGC system by selecting only the top 100 m as a conservative choice to focus on the fresh and fast WGC (Gou et al., 2021).

The slope current (Figure 3b, orange lines) has greater annual mean velocities on average than the WGCC (blue lines) and appears to increase while the WGCC shows stronger interannual variability. At OSNAP West, slope current speed increases over the last two decades, also found by (Gou et al., 2022) south of Fylla Bank. Both the mean WGCC and slope current velocities are greater in REF than in SENS, particularly in 2011 where the speeds deviate more (Figure 3b). While the increase in REF is relatively small, the bootstrapped means are statistically significant where the resampled REF mean velocity for both currents are greater than the 90^{th} percentile of the resampled SENS velocities. As the spread increases towards 2021, we speculate that this signal will emerge more clearly over the next years. Note that in contrast to earlier hosing/freshwater-release experiments, the much smaller observed increase in Greenland FWF studied here can only drive a slight increase in the boundary current speed. We also do not find a significant increase in the boundary current velocity between REF and SENS at CD and Fylla Bank (Figure S3e, f).

Nevertheless, at OSNAP West there are significantly faster flow speeds increasing shear and the potential for local instabilities, which can increase eddy formation (Gou et al., 2023; Chanut et al., 2008; Katsman et al., 2004). We analyze the EKE after discussing the thermal wind balance effect. The surface density gradient between the shelf and interior increases due to enhanced runoff, resulting in a faster boundary current. We evaluate the correlation between the WGCC and slope current velocities at OSNAP West, CD, and Fylla Bank and the surface horizontal density gradient. The correlation maps from each of the sections per WGCC and slope current (Figure S3) are added together to obtain a "cumulative correlation" (capped at 1.0). The aim of this cumulative correlation is to provide a regional overview of the connection between the boundary currents and the density gradient along their pathway (Figure 3c, d). The current structure and correlation map per cross section are discussed in Supporting Information Text/Figure S3.

The WGCC shows a band of higher positive cumulative correlations surrounding the Greenland coast (Figure 3c), illustrating the strong link between a strengthening of the current speed and an increase in the density gradient across the shelf break. The dipole pattern created by a band of negative correlations just offshore suggests an inshore movement of the sharp density gradient following the shelf break in periods with intensified WGCC flow speeds. In contrast, the cumulative correlation between the slope current and the density gradient shows a less confined pattern (Figure 3d), where a patch of positive cumulative correlations is found in the northeast LAB and the eddy shedding region.

We argue that the greater area of positive correlations with the slope current is driven by enhanced eddy activity during increased flow speed along the shelf slope. Since horizontal density gradients are computed per model grid cell, the sharp fronts of mesoscale eddies dominate an area of otherwise smaller horizontal density fluctuations. The relatively strong correlation with the accelerating slope current (Figures 3b, d) hints at growing eddy activity in this region. Does this mean that EKE is enhanced in REF over SENS? Is there a change in eddy activity related to enhanced Greenland FWFs?

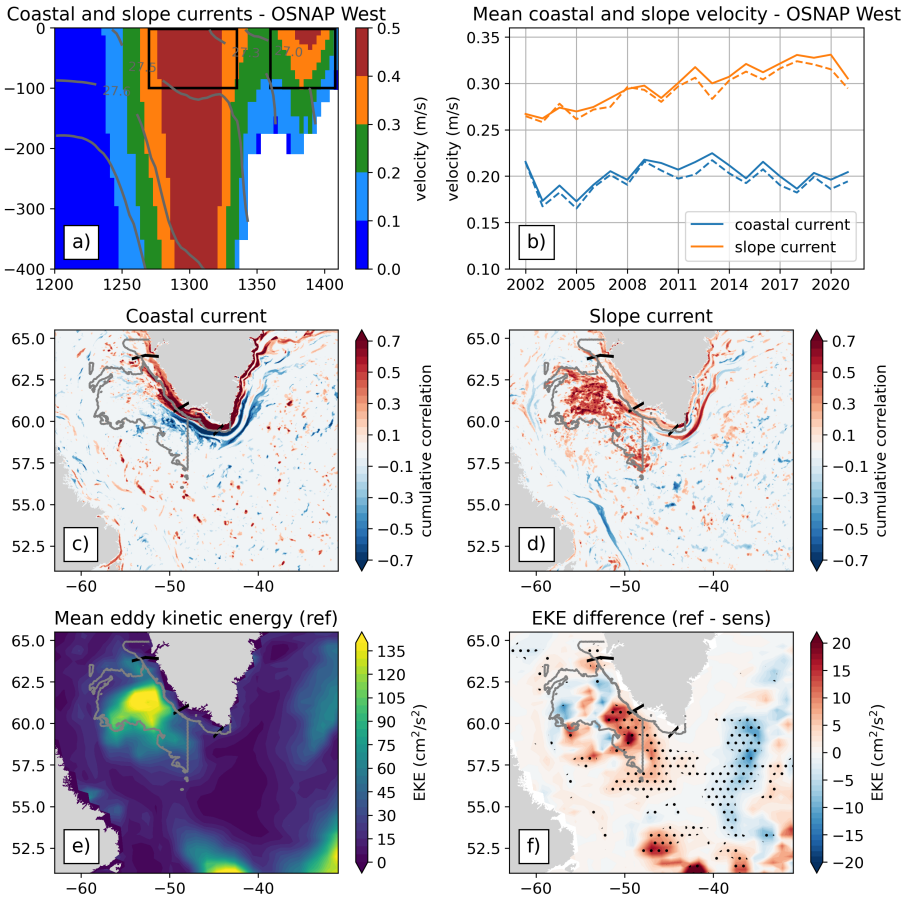

Figure 3. (a) Mean (2002–2021) current velocity magnitude at OSNAP West. Black boxes show the coastal and slope current cores. (b) Annual mean coastal/slope current velocity time series in blue/orange. Dashed/solid is SENS/REF. (c) Cumulative correlation between the horizontal density gradient and WGCC at OSNAP West, CD, and Fylla Bank (south to north sections in black lines). (d) Cumulative correlation at the slope current. (e) Mean EKE at 100m depth from REF. (f) Mean EKE difference (REF minus SENS). Stippling indicates the significant areas.

In both experiments, most eddies are formed in the northeast corner of LAB, at CD, marked in Figure 1a), from large topographic changes which generate Irminger Rings (Bracco et al., 2008), shown by the patch of high EKE (Figure 3e). As the eddy field is highly variable, we coarsen the EKE field to $\approx 1/4°$ for smoothing. When computing the mean EKE difference between REF and SENS (Figure 3f), we find significant positive EKE differences southwest of CD where lower salinities leak into the interior (Figure 2a). The positive difference does not extend over the whole eddy shedding region, particularly where the EKE is greatest at CD. Baroclinic instabilities arise as the boundary currents flow along the basin and from the strong hydrographic and velocity front between the shelf and interior. We interpret the significant enhancement of EKE southeast of the primary eddy shedding region as a possible earlier, upstream shedding of some of the eddies in REF from the enhanced density gradient. Changes in eddy activity in the main EKE region further north are likely masked by large internal variability at the mesoscale differing between REF and SENS.

Since eddies play an important role in preconditioning the LAB for deep convection (Gelderloos et al., 2011; Chanut et al., 2008), we ask whether the small but realistic increase in Greenland runoff has a significant effect on winter MLD in REF versus SENS.

3.3 Eastward deepening of mixed layer depth

We investigate the changes in MLD between the experiments to identify a potential impact from enhanced runoff over the recent two decades. Deep convection typically occurs yearly in LAB but differs in strength (Yashayaev & Clarke, 2008; Zunino et al., 2020). There are periods of deep convective activity in IRM, particularly in 2009, 2012, and 2015–2018 from favorable preconditioning the preceding years (Zunino et al., 2020; de Jong & de Steur, 2016; Piron et al., 2016; Yashayaev & Loder, 2017; Piron et al., 2017; Rühs et al., 2021). Labrador Sea Water (LSW) is formed at mid-depth (500–2000m) during convection and can spread eastward into IRM on time scales of 1–3 years (Lavender et al., 2000; Straneo et al., 2003; Yashayaev et al., 2007; Chafik et al., 2022; Böning et al., 2023). Rühs et al. (2021) speculated that freshening trends in the SPNA may have resulted in intensified convection in IRM from 2015–2018. While changes in MLD are primarily dominated by winter air-sea heat fluxes versus changes in stratification (de Jong et al., 2012; de Jong & de Steur, 2016; Piron et al., 2017), the question remains whether traces of Greenland melt has partially contributed to the deepening of mixed layers in the east. Note, the atmospheric forcing is the same for the experiments and surface fluxes are virtually equal. While there are subtle differences in surface ocean properties, i.e. REF has a slightly cooler SST in IRM (Figure 2b, Figure S4e), its impact is relatively minimal thus allowing attribution of MLD differences to the enhanced Greenland FWFs.

We focus on the years 2009–2013, a period of preconditioning,and 2015–2018, the period of strong deep convection. The long term mean (2002–2021) shows deepest MLDs primarily in the central LAB (Figure 4a). In 2009–2013 deep convection was confined to LAB (pink contour in 4a, b), while 2009 and 2012 were individual years where the MLDs reached depths greater than 1500m in LAB and ≈1000m south of Cape Farewell (MID, Figure 1a) (Figure S5a, c).

Deep convection occurred in both LAB and IRM (black contour in Figure 4a, b) in 2015–2018. When computing the maximum MLD difference (REF minus SENS) from 2015–2018, we find significantly deeper MLDs in IRM in REF than in SENS, with differences ranging from 200–600 m (Figure 4b). This is seen in the convective resistance (CR), defined by the amount of vertical integral buoyancy anomaly that must be removed in order to overcome stratification and mix down to a particular depth (h=1500m) (Gillard et al., 2022; Frajka-Williams et al., 2014; Holdsworth & Myers, 2015) (Text S6). Shallower MLDs dominate LAB in REF, particularly between WEST and MID (Figure 4b), coinciding with significant, higher CRs in REF in LAB (Figure S6b).

To investigate whether Greenland melting has contributed to an eastward deepening of MLDs in 2015–2018, we look at winter mean depth profiles averaged along the pDCA over maximum band of ±5° latitude from 2009–2013. Stratification increases up to 20% in REF with respect to SENS in LAB (WEST) below 300 m (Figure 4c).

Stratification differences between REF and SENS in IRM (EAST) show a prominent dipole with reduced stratification in REF up to 30% above 1000–1500 m and greater stratification below (Figure 4c, Figure S4a, f). There is an outstanding reduction in meltwater tracer concentration in EAST in REF compared to SENS below the same depth interface contoured by said stratification response dipole (red patch in Figure 4d, Figure S4g), aligned with the stronger stratification in REF. Tracer content is enhanced above this 1000–1500 m interface matching the weaker stratification (Figure S4a, b). For WEST and MID, the section shows enhanced tracer content over the entire column, as expected since FWFs are larger in REF than in SENS. Together, these patterns hint at freshwa-

ter being convected to greater depth in LAB in SENS prior to being exported to EAST with the LSW (deeper LAB MLDs in SENS in Figure 4c, d). Since we are averaging over 5 years, there is a smoothing over the annual maximum MLDs, where the MLD discrepancy between REF and SENS is strongest in 2009 and 2012 (Figure S5a, c).

We interpret these signals such that firstly, enhanced Greenland FWFs cause reduced deep mixing in LAB, leading to meltwater being entrained at a shallower depth before being exported to IRM. Secondly, the meltwater now residing between 200–1000 m (instead of further down) acts to decrease stratification between mid-depth and the surface, also illustrated by lower CRs in EAST in REF versus SENS (Figure S6c, green line). Thus, the water column in the central to eastern IRM was preconditioned for deeper mixing prior to the occurrence of favorable atmospheric conditions triggering convection in 2015 and following years. A shift in deep convection center from LAB to IRM under enhanced freshwater input from Greenland appears to be a common response among coupled climate models (e.g., Devilliers et al., 2021; Martin et al., 2022; Martin & Biastoch, 2023).

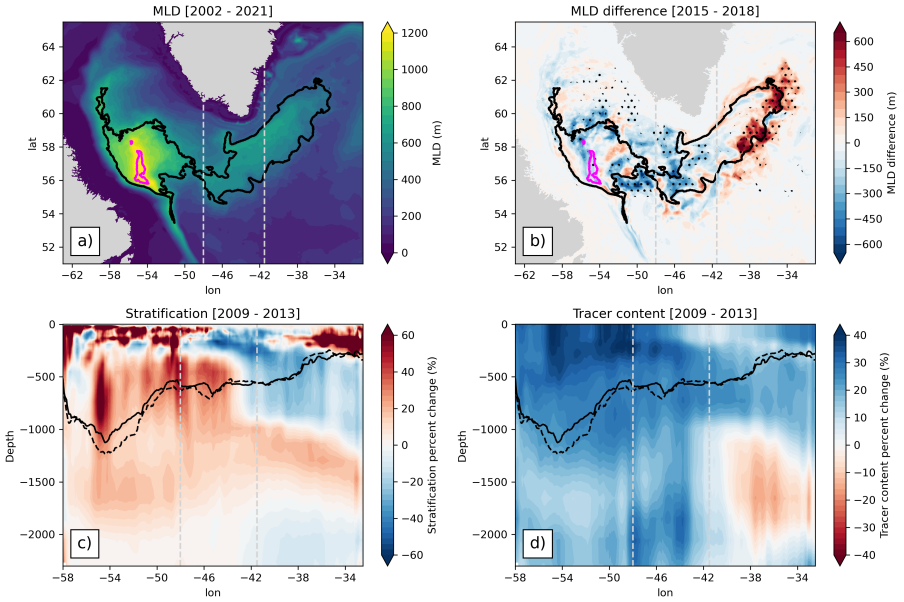

Figure 4. (a) The maximum 2002–2021 mean MLD (REF). (b) The MLD difference (REF minus SENS) in 2015–2018. Stippling indicates significant areas, the pink/black contour shows the deep convection area in 2009–2013/2015–2018. (c) The winter mean (2008–2013) stratification percent change of REF compared to SENS averaged over the pDCA. (d) The Greenland tracer content percent change. Black solid/dashed line indicates the mean maximum MLD of the REF/SENS. The gray dashed, vertical lines indicate the WEST/MID/EAST separations.

We suggest that preconditioning of IRM at mid-depth began in 2009–2013 when LAB's MLDs exceeded $z_{critical}$ allowing for deep entrainment of meltwater. This process preceded the propagation of fresher waters into IRM in 2017–2018 (Biló et al., 2022) originating from the Eastern North Atlantic salinity anomaly of 2012–2016 (Holliday et al., 2020). It is noteworthy that the comparatively small but realistic increase in FWFs in REF helped reduce CR to as low as 0.2 m^2/s^2 in EAST, as low as during the GSA in the early 1980s. In contrast, the minimum CR in WEST was twice as strong in recent years than during the early 1980s and 1990s (Figure S6c). We highlight that: 1) en-

hanced runoff of Greenland meltwater is not vertically mixed deeper from increased CRs and shallower MLDs in LAB, 2) stratification in IRM decreases upon more freshwater entering the upper 1000 m enabling deeper MLDs, and 3) increasing Greenland FWFs reduces IRM's CR after 2009 reaching even lower levels than LAB.

4 Conclusions

In this study we analyze two 1/20° ocean/sea-ice model simulations with the same surface forcing except for Greenland freshwater input: REF containing realistically varying FWFs, and SENS with reduced FWFs based on a climatological mean (1961–2000). We conclude that while there has not yet been a significant impact by accelerated Greenland melting on large scale circulation, the most notable emerging imprints are:

1) The boundary current shows the largest signal in hydrographic changes. There is a significant freshening around the WGC system which intrudes into the eddy shedding region, reducing the density on and near the shelf. Cooler temperatures dominate the boundary currents, with enhanced sea ice coverage in the northwest perimeter of the Labrador basin.

2) The shelf's reduced density increases the density gradient between the slope current and interior Labrador/Irminger seas, where the coastal and slope currents strengthen i.e. at OSNAP West. The increase in density gradients and current strength can result in barotropic and baroclinic instabilities leading to intensified eddy shedding. The increased eddy activity southwest of Greenland favors an enhanced "leaking" of meltwater into the Labrador Sea.

3) The intrusion of relatively fresher waters into the deep convection region reduces—but does not prohibit—deep mixing in the Labrador Sea. The signal is entrained to shallower depths only and is exported into the Irminger Sea via LSW, reducing stratification between the surface and mid-depth. We argue that our experiment demonstrates that by this process, enhanced Greenland runoff has contributed to a lowering of convective resistance in Irminger Sea and an eastward shift of deep convection in 2015–2018.

In this model-sensitivity study, we find a series of early but subtle impacts from enhanced meltwater runoff. Hydrographic changes remain localized with the strongest signal along Greenland's continental shelves. The boundary current strengthens incrementally only in the vicinity of OSNAP West, and surface fluxes remain the dominant driver of changes in deep convection for now. The distribution of Greenland meltwater in the simulations, applied at the surface and along the coastlines, the lack of an interactive ice sheet and the missing representation of proper fjord circulation, may obscure how meltwater is distributed throughout the water column. Nevertheless, more extremes in runoff like in summers 2010 and 2012 may occur in the future with rising air temperatures. However, deep convection occurs in winter, so despite the amount of summer meltwater, the wind regimes from summer to winter likely dominates the fate of freshwater and its potential for impeding deep water formation. With the onset of enhanced Greenland runoff, there is an increased potential for intermediate waters to freshen which may have persisting impacts on stratification and thus could support a continued eastward shift to and strengthening of deep convection in the Irminger Sea.

Open Research

All (processed) model data and scripts needed for Figures 1–4 are made available using the GEOMAR data management platform under the identifier: `hdl.handle.net/20.500.12085/e3cd8f8c-07bd-4955-b77a-504377e299ac` (Schiller-Weiss et al., 2024).

Acknowledgments

This work was carried out in the G-Shocx project (MA 4039/1-1) supported by the Deutsche Forschungsgemeinschaft (DFG). The authors thank Willi Rath and Tobias Schulzki for technical and scientific support. Finally, we want to thank the comments of the anonymous reviewers who helped to greatly improve this manuscript.

References

Bacon, S., Reverdin, G., Rigor, I. G., & Snaith, H. M. (2002). A freshwater jet on the east Greenland shelf. *Journal of Geophysical Research: Oceans*, *107*(C7), 5–1–5–16. doi: 10.1029/2001JC000935

Bakker, P., Schmittner, A., Lenaerts, J. T. M., Abe-Ouchi, A., Bi, D., van den Broeke, M. R., ... Yin, J. (2016). Fate of the Atlantic Meridional Overturning Circulation: Strong decline under continued warming and Greenland melting. *Geophysical Research Letters*, *43*(23), 12,252–12,260. doi: 10.1002/2016GL070457

Bamber, J. L., Tedstone, A. J., King, M. D., Howat, I. M., Enderlin, E. M., van den Broeke, M. R., & Noel, B. (2018). Land Ice Freshwater Budget of the Arctic and North Atlantic Oceans: 1. Data, Methods, and Results. *Journal of Geophysical Research: Oceans*, *123*(3), 1827–1837. doi: 10.1002/2017JC013605

Belkin, I. M., Levitus, S., Antonov, J., & Malmberg, S.-A. (1998, January). "Great Salinity Anomalies" in the North Atlantic. *Progress in Oceanography*, *41*(1), 1–68. doi: 10.1016/S0079-6611(98)00015-9

Bertino, L., Evensen, G., & Wackernagel, H. (2003). Sequential Data Assimilation Techniques in Oceanography. *International Statistical Review*, *71*(2), 223–241. doi: 10.1111/j.1751-5823.2003.tb00194.x

Biastoch, A., Schwarzkopf, F. U., Getzlaff, K., Rühs, S., Martin, T., Scheinert, M., ... Böning, C. W. (2021, September). Regional imprints of changes in the Atlantic Meridional Overturning Circulation in the eddy-rich ocean model VIKING20X. *Ocean Science*, *17*(5), 1177–1211. doi: 10.5194/os-17-1177-2021

Biló, T. C., Straneo, F., Holte, J., & Le Bras, I. a.-A. (2022). Arrival of New Great Salinity Anomaly Weakens Convection in the Irminger Sea. *Geophysical Research Letters*, *49*(11), e2022GL098857. doi: 10.1029/2022GL098857

Bracco, A., Pedlosky, J., & Pickart, R. S. (2008, September). Eddy Formation near the West Coast of Greenland. *Journal of Physical Oceanography*, *38*(9), 1992–2002. doi: 10.1175/2008JPO3669.1

Böning, C. W., Behrens, E., Biastoch, A., Getzlaff, K., & Bamber, J. L. (2016, July). Emerging impact of Greenland meltwater on deepwater formation in the North Atlantic Ocean. *Nature Geoscience*, *9*(7), 523–527. doi: 10.1038/ngeo2740

Böning, C. W., Wagner, P., Handmann, P., Schwarzkopf, F. U., Getzlaff, K., & Biastoch, A. (2023, August). Decadal changes in Atlantic overturning due to the excessive 1990s Labrador Sea convection. *Nature Communications*, *14*(1), 4635. doi: 10.1038/s41467-023-40323-9

Castelao, R. M., Luo, H., Oliver, H., Rennermalm, A. K., Tedesco, M., Bracco, A., ... Medeiros, P. M. (2019). Controls on the Transport of Meltwater From the Southern Greenland Ice Sheet in the Labrador Sea. *Journal of Geophysical Research: Oceans*, *124*(6), 3551–3560. doi: 10.1029/2019JC015159

Chafik, L., Holliday, N. P., Bacon, S., & Rossby, T. (2022). Irminger Sea Is the Center of Action for Subpolar AMOC Variability. *Geophysical Research Letters*, *49*(17), e2022GL099133. doi: 10.1029/2022GL099133

Chanut, J., Barnier, B., Large, W., Debreu, L., Penduff, T., Molines, J. M., & Mathiot, P. (2008, August). Mesoscale Eddies in the Labrador Sea and Their Contribution to Convection and Restratification. *Journal of Physical Oceanog-*

raphy, *38*(8), 1617–1643. doi: 10.1175/2008JPO3485.1

de Jong, M. F., & de Steur, L. (2016). Strong winter cooling over the Irminger Sea in winter 2014–2015, exceptional deep convection, and the emergence of anomalously low SST. *Geophysical Research Letters*, *43*(13), 7106–7113. doi: 10.1002/2016GL069596

de Jong, M. F., van Aken, H. M., Våge, K., & Pickart, R. S. (2012, May). Convective mixing in the central Irminger Sea: 2002–2010. *Deep Sea Research Part I: Oceanographic Research Papers*, *63*, 36–51. doi: 10.1016/j.dsr.2012.01.003

Deser, C., Holland, M., Reverdin, G., & Timlin, M. (2002). Decadal variations in Labrador Sea ice cover and North Atlantic sea surface temperatures. *Journal of Geophysical Research: Oceans*, *107*(C5), 3–1–3–12. doi: 10.1029/2000JC000683

de Steur, L., Hansen, E., Gerdes, R., Karcher, M., Fahrbach, E., & Holfort, J. (2009). Freshwater fluxes in the East Greenland Current: A decade of observations. *Geophysical Research Letters*, *36*(23). doi: 10.1029/2009GL041278

de Steur, L., Peralta-Ferriz, C., & Pavlova, O. (2018). Freshwater Export in the East Greenland Current Freshens the North Atlantic. *Geophysical Research Letters*, *45*(24), 13,359–13,366. (_eprint: https://onlinelibrary.wiley.com/doi/pdf/10.1029/2018GL080207) doi: 10.1029/2018GL080207

Devilliers, M., Swingedouw, D., Mignot, J., Deshayes, J., Garric, G., & Ayache, M. (2021, November). A realistic Greenland ice sheet and surrounding glaciers and ice caps melting in a coupled climate model. *Climate Dynamics*, *57*(9), 2467–2489. doi: 10.1007/s00382-021-05816-7

Dickson, R. R., Meincke, J., Malmberg, S.-A., & Lee, A. J. (1988, January). The "great salinity anomaly" in the Northern North Atlantic 1968–1982. *Progress in Oceanography*, *20*(2), 103–151. doi: 10.1016/0079-6611(88)90049-3

Duyck, E., Gelderloos, R., & de Jong, M. F. (2022). Wind-Driven Freshwater Export at Cape Farewell. *Journal of Geophysical Research: Oceans*, *127*(5), e2021JC018309. doi: 10.1029/2021JC018309

Fettweis, X., Tedesco, M., van den Broeke, M., & Ettema, J. (2011, May). Melting trends over the Greenland ice sheet (1958–2009) from spaceborne microwave data and regional climate models. *The Cryosphere*, *5*(2), 359–375. doi: 10.5194/tc-5-359-2011

Fox, A. D., Handmann, P., Schmidt, C., Fraser, N., Rühs, S., Sanchez-Franks, A., ... Yashayaev, I. (2022, October). Exceptional freshening and cooling in the eastern subpolar North Atlantic caused by reduced Labrador Sea surface heat loss. *Ocean Science*, *18*(5), 1507–1533. doi: 10.5194/os-18-1507-2022

Frajka-Williams, E., Rhines, P. B., & Eriksen, C. C. (2014, January). Horizontal Stratification during Deep Convection in the Labrador Sea. *Journal of Physical Oceanography*, *44*(1), 220–228. doi: 10.1175/JPO-D-13-069.1

Fratantoni, P. S., & Pickart, R. S. (2007, October). The Western North Atlantic Shelfbreak Current System in Summer. *Journal of Physical Oceanography*, *37*(10), 2509–2533. doi: 10.1175/JPO3123.1

Gelderloos, R., Katsman, C. A., & Drijfhout, S. S. (2011, November). Assessing the Roles of Three Eddy Types in Restratifying the Labrador Sea after Deep Convection. *Journal of Physical Oceanography*, *41*(11), 2102–2119. doi: 10.1175/JPO-D-11-054.1

Gillard, L. C., Pennelly, C., Johnson, H. L., & Myers, P. G. (2022, March). The Effects of Atmospheric and Lateral Buoyancy Fluxes on Labrador Sea Mixed Layer Depth. *Ocean Modelling*, *171*, 101974. doi: 10.1016/j.ocemod.2022.101974

Gou, R., Feucher, C., Pennelly, C., & Myers, P. G. (2021). Seasonal cycle of the coastal west greenland current system between cape farewell and cape desolation from a very high-resolution numerical model. *Journal of Geophysical*

Research: Oceans, *126*(5), e2020JC017017. doi: https://doi.org/10.1029/2020JC017017

Gou, R., Li, P., Wiegand, K. N., Pennelly, C., Kieke, D., & Myers, P. G. (2023, October). Variability of Eddy Formation off the West Greenland Coast from a 1/60° Model. *Journal of Physical Oceanography*, *53*(10), 2475–2490. doi: 10.1175/JPO-D-23-0004.1

Gou, R., Pennelly, C., & Myers, P. G. (2022). The Changing Behavior of the West Greenland Current System in a Very High-Resolution Model. *Journal of Geophysical Research: Oceans*, *127*(8), e2022JC018404. doi: 10.1029/2022JC018404

Handmann, P., Fischer, J., Visbeck, M., Karstensen, J., Biastoch, A., Böning, C., & Patara, L. (2018). The Deep Western Boundary Current in the Labrador Sea From Observations and a High-Resolution Model. *Journal of Geophysical Research: Oceans*, *123*(4), 2829–2850. doi: 10.1002/2017JC013702

Hanna, E., Fettweis, X., Mernild, S. H., Cappelen, J., Ribergaard, M. H., Shuman, C. A., ... Mote, T. L. (2014). Atmospheric and oceanic climate forcing of the exceptional Greenland ice sheet surface melt in summer 2012. *International Journal of Climatology*, *34*(4), 1022–1037. doi: 10.1002/joc.3743

Hanna, E., Huybrechts, P., Steffen, K., Cappelen, J., Huff, R., Shuman, C., ... Griffiths, M. (2008, January). Increased Runoff from Melt from the Greenland Ice Sheet: A Response to Global Warming. *Journal of Climate*, *21*(2), 331–341. doi: 10.1175/2007JCLI1964.1

Holdsworth, A. M., & Myers, P. G. (2015, June). The Influence of High-Frequency Atmospheric Forcing on the Circulation and Deep Convection of the Labrador Sea. *Journal of Climate*, *28*(12), 4980–4996. doi: 10.1175/JCLI-D-14-00564.1

Holliday, N. P., Bersch, M., Berx, B., Chafik, L., Cunningham, S., Florindo-López, C., ... Yashayaev, I. (2020, January). Ocean circulation causes the largest freshening event for 120 years in eastern subpolar North Atlantic. *Nature Communications*, *11*(1), 585. doi: 10.1038/s41467-020-14474-y

Holliday, N. P., Meyer, A., Bacon, S., Alderson, S. G., & de Cuevas, B. (2007). Retroflection of part of the east Greenland current at Cape Farewell. *Geophysical Research Letters*, *34*(7). doi: 10.1029/2006GL029085

Håvik, L., Pickart, R. S., Våge, K., Torres, D., Thurnherr, A. M., Beszczynska-Möller, A., ... von Appen, W.-J. (2017). Evolution of the East Greenland Current from Fram Strait to Denmark Strait: Synoptic measurements from summer 2012. *Journal of Geophysical Research: Oceans*, *122*(3), 1974–1994. doi: 10.1002/2016JC012228

Jackson, L. C., & Wood, R. A. (2018). Hysteresis and Resilience of the AMOC in an Eddy-Permitting GCM. *Geophysical Research Letters*, *45*(16), 8547–8556. doi: 10.1029/2018GL078104

Katsman, C. A., Spall, M. A., & Pickart, R. S. (2004, September). Boundary Current Eddies and Their Role in the Restratification of the Labrador Sea. *Journal of Physical Oceanography*, *34*(9), 1967–1983. doi: 10.1175/1520-0485(2004)034⟨1967:BCEATR⟩2.0.CO;2

Kwok, R. (2007). Baffin Bay ice drift and export: 2002–2007. *Geophysical Research Letters*, *34*(19). doi: 10.1029/2007GL031204

Lavender, K. L., Davis, R. E., & Owens, W. B. (2000, September). Mid-depth recirculation observed in the interior Labrador and Irminger seas by direct velocity measurements. *Nature*, *407*(6800), 66–69. doi: 10.1038/35024048

Le Bras, I. A.-A., Straneo, F., Holte, J., & Holliday, N. P. (2018). Seasonality of Freshwater in the East Greenland Current System From 2014 to 2016. *Journal of Geophysical Research: Oceans*, *123*(12), 8828–8848. doi: 10.1029/2018JC014511

Lilly, J. M., Rhines, P. B., Schott, F., Lavender, K., Lazier, J., Send, U., & D'Asaro, E. (2003, October). Observations of the Labrador Sea eddy field. *Progress in*

Oceanography, *59*(1), 75–176. doi: 10.1016/j.pocean.2003.08.013

Lin, P., Pickart, R. S., Torres, D. J., & Pacini, A. (2018, September). Evolution of the Freshwater Coastal Current at the Southern Tip of Greenland. *Journal of Physical Oceanography*, *48*(9), 2127–2140. doi: 10.1175/JPO-D-18-0035.1

Lozier, M. S., Li, F., Bacon, S., Bahr, F., Bower, A. S., Cunningham, S. A., ... Zhao, J. (2019, February). A sea change in our view of overturning in the subpolar North Atlantic. *Science*, *363*(6426), 516–521. doi: 10.1126/science.aau6592

Luo, H., Bracco, A., & Di Lorenzo, E. (2011, November). The interannual variability of the surface eddy kinetic energy in the Labrador Sea. *Progress in Oceanography*, *91*(3), 295–311. doi: 10.1016/j.pocean.2011.01.006

Luo, H., Castelao, R. M., Rennermalm, A. K., Tedesco, M., Bracco, A., Yager, P. L., & Mote, T. L. (2016, July). Oceanic transport of surface meltwater from the southern Greenland ice sheet. *Nature Geoscience*, *9*(7), 528–532. doi: 10.1038/ngeo2708

Martin, T., & Biastoch, A. (2023, February). On the ocean's response to enhanced Greenland runoff in model experiments: relevance of mesoscale dynamics and atmospheric coupling. *Ocean Science*, *19*(1), 141–167. doi: 10.5194/os-19-141-2023

Martin, T., Biastoch, A., Lohmann, G., Mikolajewicz, U., & Wang, X. (2022). On Timescales and Reversibility of the Ocean's Response to Enhanced Greenland Ice Sheet Melting in Comprehensive Climate Models. *Geophysical Research Letters*, *49*(5), e2021GL097114. doi: 10.1029/2021GL097114

Myers, P. G., Castro de la Guardia, L., Fu, C., Gillard, L. C., Grivault, N., Hu, X., ... Romanski, J. (2021). Extreme High Greenland Blocking Index Leads to the Reversal of Davis and Nares Strait Net Transport Toward the Arctic Ocean. *Geophysical Research Letters*, *48*(17), e2021GL094178. doi: 10.1029/2021GL094178

Myers, P. G., Donnelly, C., & Ribergaard, M. H. (2009, January). Structure and variability of the West Greenland Current in Summer derived from 6 repeat standard sections. *Progress in Oceanography*, *80*(1), 93–112. doi: 10.1016/j.pocean.2008.12.003

Myers, P. G., Kulan, N., & Ribergaard, M. H. (2007). Irminger Water variability in the West Greenland Current. *Geophysical Research Letters*, *34*(17). doi: 10.1029/2007GL030419

Pacini, A., & Pickart, R. S. (2022, January). Meanders of the West Greenland Current near Cape Farewell. *Deep Sea Research Part I: Oceanographic Research Papers*, *179*, 103664. doi: 10.1016/j.dsr.2021.103664

Pacini, A., Pickart, R. S., Bahr, F., Torres, D. J., Ramsey, A. L., Holte, J., ... Jong, M. F. d. (2020, September). Mean Conditions and Seasonality of the West Greenland Boundary Current System near Cape Farewell. *Journal of Physical Oceanography*, *50*(10), 2849–2871. doi: 10.1175/JPO-D-20-0086.1

Pacini, A., Pickart, R. S., Bras, I. A. L., Straneo, F., Holliday, N. P., & Spall, M. A. (2021, July). Cyclonic Eddies in the West Greenland Boundary Current System. *Journal of Physical Oceanography*, *51*(7), 2087–2102. doi: 10.1175/JPO-D-20-0255.1

Piron, A., Thierry, V., Mercier, H., & Caniaux, G. (2016, March). Argo float observations of basin-scale deep convection in the Irminger sea during winter 2011–2012. *Deep Sea Research Part I: Oceanographic Research Papers*, *109*, 76–90. doi: 10.1016/j.dsr.2015.12.012

Piron, A., Thierry, V., Mercier, H., & Caniaux, G. (2017). Gyre-scale deep convection in the subpolar North Atlantic Ocean during winter 2014–2015. *Geophysical Research Letters*, *44*(3), 1439–1447. doi: 10.1002/2016GL071895

Rahmstorf, S., Box, J. E., Feulner, G., Mann, M. E., Robinson, A., Rutherford, S., & Schaffernicht, E. J. (2015, May). Exceptional twentieth-century slowdown in

Atlantic Ocean overturning circulation. *Nature Climate Change*, *5*(5), 475–480. doi: 10.1038/nclimate2554

Rieck, J. K., Böning, C. W., & Getzlaff, K. (2019, August). The Nature of Eddy Kinetic Energy in the Labrador Sea: Different Types of Mesoscale Eddies, Their Temporal Variability, and Impact on Deep Convection. *Journal of Physical Oceanography*, *49*(8), 2075–2094. doi: 10.1175/JPO-D-18-0243.1

Rühs, S., Oliver, E. C. J., Biastoch, A., Böning, C. W., Dowd, M., Getzlaff, K., ... Myers, P. G. (2021). Changing Spatial Patterns of Deep Convection in the Subpolar North Atlantic. *Journal of Geophysical Research: Oceans*, *126*(7), e2021JC017245. doi: 10.1029/2021JC017245

Schiller-Weiss, I., Martin, T., Karstensen, J., & Biastoch, A. (2023). Do Salinity Variations Along the East Greenland Shelf Show Imprints of Increasing Meltwater Runoff? *Journal of Geophysical Research: Oceans*, *128*(10), e2023JC019890. doi: 10.1029/2023JC019890

Schiller-Weiss, I., Martin, T., & Schwarzkopf, F. (2024). *Supplementary material to: Emerging impacts of enhanced greenland melting on labrador sea dynamics.* (GEOMAR Helmholtz Centre for Ocean Research Kiel [distributor] [dataset], `hdl.handle.net/20.500.12085/e3cd8f8c-07bd-4955-b77a-504377e299ac`)

Schulze Chretien, L. M., & Frajka-Williams, E. (2018, October). Wind-driven transport of fresh shelf water into the upper 30 m of the Labrador Sea. *Ocean Science*, *14*(5), 1247–1264. doi: 10.5194/os-14-1247-2018

Slater, T., Shepherd, A., McMillan, M., Leeson, A., Gilbert, L., Muir, A., ... Briggs, K. (2021, November). Increased variability in Greenland Ice Sheet runoff from satellite observations. *Nature Communications*, *12*(1), 6069. doi: 10.1038/s41467-021-26229-4

Spall, M. A. (2004, May). Boundary Currents and Watermass Transformation in Marginal Seas. *Journal of Physical Oceanography*, *34*(5), 1197–1213. doi: 10.1175/1520-0485(2004)034⟨1197:BCAWTI⟩2.0.CO;2

Straneo, F., Pickart, R. S., & Lavender, K. (2003, June). Spreading of Labrador sea water: an advective-diffusive study based on Lagrangian data. *Deep Sea Research Part I: Oceanographic Research Papers*, *50*(6), 701–719. doi: 10.1016/S0967-0637(03)00057-8

Sutherland, D. A., & Pickart, R. S. (2008, July). The East Greenland Coastal Current: Structure, variability, and forcing. *Progress in Oceanography*, *78*(1), 58–77. doi: 10.1016/j.pocean.2007.09.006

Swingedouw, D., Houssais, M.-N., Herbaut, C., Blaizot, A.-C., Devilliers, M., & Deshayes, J. (2022). Amoc recent and future trends: A crucial role for oceanic resolution and greenland melting? *Frontiers in Climate*, *4*. doi: 10.3389/fclim.2022.838310

Tedesco, M., & Fettweis, X. (2020, April). Unprecedented atmospheric conditions (1948–2019) drive the 2019 exceptional melting season over the Greenland ice sheet. *The Cryosphere*, *14*(4), 1209–1223. doi: 10.5194/tc-14-1209-2020

Tedesco, M., Fettweis, X., Van den Broeke, M., Wal, R., Smeets, P., Berg, W., ... Box, J. (2011, January). The role of albedo and accumulation in the 2010 melting record in Greenland. *Environmental Research Letters*, *6*, 014005. doi: 10.1088/1748-9326/6/1/014005

Tsujino, H., Urakawa, S., Nakano, H., Small, R. J., Kim, W. M., Yeager, S. G., ... Yamazaki, D. (2018, October). JRA-55 based surface dataset for driving ocean–sea-ice models (JRA55-do). *Ocean Modelling*, *130*, 79–139. doi: 10.1016/j.ocemod.2018.07.002

Våge, K., Pickart, R. S., Thierry, V., Reverdin, G., Lee, C. M., Petrie, B., ... Ribergaard, M. H. (2009, January). Surprising return of deep convection to the subpolar North Atlantic Ocean in winter 2007–2008. *Nature Geoscience*, *2*(1), 67–72. doi: 10.1038/ngeo382

Yashayaev, I., Bersch, M., & van Aken, H. M. (2007). Spreading of the Labrador

Sea Water to the Irminger and Iceland basins. *Geophysical Research Letters*, *34*(10). doi: 10.1029/2006GL028999

Yashayaev, I., & Clarke, A. (2008, March). Evolution of North Atlantic Water Masses Inferred from Labrador Sea Salinity Series. *Oceanography*, *21*(1), 30–45. doi: 10.5670/oceanog.2008.65

Yashayaev, I., & Loder, J. W. (2017). Further intensification of deep convection in the Labrador Sea in 2016. *Geophysical Research Letters*, *44*(3), 1429–1438. doi: 10.1002/2016GL071668

Zunino, P., Mercier, H., & Thierry, V. (2020, January). Why did deep convection persist over four consecutive winters (2015–2018) southeast of Cape Farewell? *Ocean Science*, *16*(1), 99–113. doi: 10.5194/os-16-99-2020

5 References from the Supporting Information

Bailey, D. A., Rhines, P. B., & Häkkinen, S. (2005, October). Formation and pathways of North Atlantic Deep Water in a coupled ice–ocean model of the Arctic–North Atlantic Oceans. Climate Dynamics, 25 (5), 497–516. doi: 10.1007/s00382-005-0050-3

Bamber, J. L., Tedstone, A. J., King, M. D., Howat, I. M., Enderlin, E. M., van den Broeke, M. R., & Noel, B. (2018). Land Ice Freshwater Budget of the Arctic and North Atlantic Oceans: 1. Data, Methods, and Results. Journal of Geophysical Research: Oceans, 123 (3), 1827–1837. doi: 10.1002/2017JC013605

Biastoch, A., Schwarzkopf, F. U., Getzlaff, K., Rühs, S., Martin, T., Scheinert, M., . . . Böning, C. W. (2021, September). Regional imprints of changes in the Atlantic Meridional Overturn- ing Circulation in the eddy-rich ocean model VIKING20X. Ocean Science, 17 (5), 1177–1211. doi: 10.5194/os-17-1177-2021

Castelao, R. M., Luo, H., Oliver, H., Rennermalm, A. K., Tedesco, M., Bracco, A., . . . Medeiros, P. M. (2019). Controls on the Transport of Meltwater From the Southern Greenland Ice Sheet in the Labrador Sea. Journal of Geophysical Research: Oceans, 124 (6), 3551–3560. doi: 10.1029/2019JC015159

Debreu, L., Vouland, C., & Blayo, E. (2008, January). AGRIF: Adaptive grid refinement in Fortran. Computers & Geosciences, 34 (1), 8–13. doi: 10.1016/j.cageo.2007.01.009

de Jong, M. F., & de Steur, L. (2016). Strong winter cooling over the Irminger Sea in winter 2014–2015, exceptional deep convection, and the emergence of anomalously low SST. Geophysical Research Letters, 43 (13), 7106–7113. doi: 10.1002/2016GL069596

Frajka-Williams, E., Rhines, P. B., & Eriksen, C. C. (2014, January). Horizontal Stratification during Deep Convection in the Labrador Sea. Journal of Physical Oceanography, 44 (1), 220–228. doi: 10.1175/JPO-D-13-069.1

Gillard, L. C., Hu, X., Myers, P. G., & Bamber, J. L. (2016). Meltwater pathways from marine terminating glaciers of the Greenland ice sheet. Geophysical Research Letters, 43 (20), 10,873–10,882. doi: 10.1002/2016GL070969

Gillard, L. C., Pennelly, C., Johnson, H. L., & Myers, P. G. (2022, March). The Effects of Atmospheric and Lateral Buoyancy Fluxes on Labrador Sea Mixed Layer Depth. Ocean Modelling, 171 , 101974. doi: 10.1016/j.ocemod.2022.101974

Gou, R., Feucher, C., Pennelly, C., & Myers, P. G. (2021). Seasonal cycle of the coastal west greenland current system between cape farewell and cape desolation from a very high-resolution numerical model. Journal of Geophysical Research: Oceans, 126 (5), e2020JC017017. doi: https://doi.org/10.1029/2020JC017017

693 Gou, R., Pennelly, C., & Myers, P. G. (2022). The Changing Behavior of the West
694 Greenland Current System in a Very High-Resolution Model. Journal of Geophysical Re-
695 search: Oceans, 127 (8), e2022JC018404. doi: 10.1029/2022JC018404

696 Hallberg, R. (2013, December). Using a resolution function to regulate parameter-
697 izations of oceanic mesoscale eddy effects. Ocean Modelling, 72 , 92–103. doi: 10.1016/j.ocemod.2013.08.007

698 Holdsworth, A. M., & Myers, P. G. (2015, June). The Influence of High-Frequency
699 Atmospheric Forcing on the Circulation and Deep Convection of the Labrador Sea. Jour-
700 nal of Climate, 28 (12), 4980–4996. doi: 10.1175/JCLI-D-14-00564.1

701 Lozier, M. S., Li, F., Bacon, S., Bahr, F., Bower, A. S., Cunningham, S. A., . . .
702 Zhao, J. (2019, February). A sea change in our view of overturning in the subpolar North
703 Atlantic. Science, 363 (6426), 516–521. doi: 10.1126/science.aau6592

704 Luo, H., Castelao, R. M., Rennermalm, A. K., Tedesco, M., Bracco, A., Yager, P.
705 L., & Mote, T. L. (2016, July). Oceanic transport of surface meltwater from the south-
706 ern Greenland ice sheet. Nature Geoscience, 9 (7), 528–532. doi: 10.1038/ngeo2708

707 Madec, G., & NEMO System Team. (2016). NEMO Ocean Engine. Scientific notes
708 of climate modeling center (27). Institut Pierre Simon Laplace (IPSL). doi: 10.5281/zen-
709 odo.1464816

710 Martin, T. (2021, September). Runoff remapping for ocean model forcing [Software].
711 Retrieved 2024-03-25, from https://git.geomar.de/open-source/runoff remapping (Place:
712 Kiel, Germany Publisher: GEOMAR Helmholtz Centre for Ocean Research Kiel) doi:
713 10.3289/SW 2 2021

714 Mortensen, J. (2018). Report on hydrographic conditions off southwest greenland
715 june/july 2017. NAFO SCR Doc, 18 (005), 8.

716 Myers, P. G., Donnelly, C., & Ribergaard, M. H. (2009, January). Structure and
717 variability of the West Greenland Current in Summer derived from 6 repeat standard
718 sections. Progress in Oceanography, 80 (1), 93–112. doi: 10.1016/j.pocean.2008.12.003

719 Pacini, A., & Pickart, R. S. (2022, January). Meanders of the West Greenland Cur-
720 rent near Cape Farewell. Deep Sea Research Part I: Oceanographic Research Papers, 179
721 , 103664. doi: 10.1016/j.dsr.2021.103664

722 Pickart, R. S., Straneo, F., & Moore, G. W. K. (2003, January). Is Labrador Sea
723 Water formed in the Irminger basin? Deep Sea Research Part I: Oceanographic Research
724 Papers, 50 (1), 23–52. doi: 10.1016/S0967-0637(02)00134-6

725 Piron, A., Thierry, V., Mercier, H., & Caniaux, G. (2016, March). Argo float ob-
726 servations of basin-scale deep convection in the Irminger sea during winter 2011–2012.
727 Deep Sea Research Part I: Oceanographic Research Papers, 109 , 76–90. doi: 10.1016/j.dsr.2015.12.012

728 Piron, A., Thierry, V., Mercier, H., & Caniaux, G. (2017). Gyre-scale deep con-
729 vection in the subpolar North Atlantic Ocean during winter 2014–2015. Geophysical Re-
730 search Letters, 44 (3), 1439–1447. doi: 10.1002/2016GL071895

731 Rühs, S., Oliver, E. C. J., Biastoch, A., Böning, C. W., Dowd, M., Getzlaff, K., .
732 . . Myers, P. G. (2021). Changing Spatial Patterns of Deep Convection in the Subpo-
733 lar North Atlantic. Journal of Geophysical Research: Oceans, 126 (7), e2021JC017245.
734 doi: 10.1029/2021JC017245

735 Schiller-Weiss, I., Martin, T., Karstensen, J., & Biastoch, A. (2023). Do Salinity
736 Variations Along the East Greenland Shelf Show Imprints of Increasing Meltwater Runoff?
737 Journal of Geophysical Research: Oceans, 128 (10), e2023JC019890. doi: 10.1029/ 2023JC019890

738 Slater, T., Shepherd, A., McMillan, M., Leeson, A., Gilbert, L., Muir, A., . . . Briggs,
739 K. (2021, November). Increased variability in Greenland Ice Sheet runoff from satellite
740 observations. Nature Communications, 12 (1), 6069. doi: 10.1038/s41467-021-26229-4

741 Sterl, M. F., & de Jong, M. F. (2022). Restratification Structure and Processes in
742 the Irminger Sea. Journal of Geophysical Research: Oceans, 127 (12), e2022JC019126.
743 doi: 10.1029/2022JC019126

744 Stolzenberger, S., Rietbroek, R., Wekerle, C., Uebbing, B., & Kusche, J. (2022).
745 Simulated Signatures of Greenland Melting in the North Atlantic: A Model Compari-
746 son With Argo Floats, Satellite Observations, and Ocean Reanalysis. Journal of Geo-
747 physical Research: Oceans, 127 (11), e2022JC018528. doi: 10.1029/2022JC018528

748 Tedesco, M., Fettweis, X., Van den Broeke, M., Wal, R., Smeets, P., Berg, W., .
749 . . Box, J. (2011, January). The role of albedo and accumulation in the 2010 melting
750 record in Greenland. Environmental Research Letters, 6 , 014005. doi: 10.1088/1748-
751 9326/6/1/014005

752 Tsujino, H., Urakawa, S., Nakano, H., Small, R. J., Kim, W. M., Yeager, S. G., .
753 . . Yamazaki, D. (2018, October). JRA-55 based surface dataset for driving ocean–sea-
754 ice models (JRA55-do). Ocean Modelling, 130 , 79–139. doi: 10.1016/j.ocemod.2018.07.002

755 Yashayaev, I., & Loder, J. W. (2017). Further intensification of deep convection
756 in the Labrador Sea in 2016. Geophysical Research Letters, 44 (3), 1429–1438. doi: 10.1002/2016GL071668

757 Zunino, P., Mercier, H., & Thierry, V. (2020, January). Why did deep convection
758 persist over four consecutive winters (2015–2018) southeast of Cape Farewell? Ocean Sci-
759 ence, 16 (1), 99–113. doi: 10.5194/os-16-99-2020

Geophysical Research Letters

Supporting Information for

Emerging influence of enhanced Greenland melting on boundary currents and deep convection regimes in the Labrador and Irminger Seas

Ilana Schiller-Weiss[1,], Torge Martin[1], Franziska U. Schwarzkopf[1]

[1]GEOMAR Helmholtz Centre for Ocean Research Kiel, Kiel, Germany

Contents of this file

1. Text S1 to S5

2. Figures S1 to S6

Introduction

This supporting information includes the VIKING20X model description and complementing figures supporting the main text. In Addition to annual mean salinity and temperature in Figure 2, we here provide the winter and summer mean of surface salinity, temperature, and density anomalies in the subpolar North Atlantic (SPNA) (Text S1 and Figure S1). Text S2 and Figure S2 shows changes in the cumulative alongshore wind stress along the west Greenland shelf. The discussion on the current structure along the West Greenland Current (WGC) based on mooring locations is supported by Text and Figure S3, in which we present the temporal evolution of the mean WGC velocity and correlations between the current velocity and horizontal density gradient. Text and Figure S4 show the stratification and the Greenland meltwater passive tracer content percent change between the two model runs (REF and SENS) in 2009 and 2012, two years where deep convection was strong in the Labrador Sea (LAB) prior to the intensification of deep convection in both the east and west in 2015 - 2018 (de Jong et al., 2016, Piron et al., 2016, Piron et al., 2017, Ruehs et al., 2021). Text S5 and Figure S5 discuss the differences in convective resistance (CR) between REF and SENS and the temporal evolution of CR over the potential deep convection area (pDCA).

VIKING20X model description

VIKING20X employs the NEMO3.6 ocean engine (Madec et al., 2016) and utilizes a two-way nesting with Adaptive Grid Refinement in Fortran (AGRIF) (Debreu et al., 2008) with a regional horizontally refined grid at 1/20° over the south and north Atlantic oceans (34°S - 70°N) (see Figure 1 of Biastoch et al., 2021). The refinement permits the explicit simulation of mesoscale eddies (Hallberg et al., 2013) which improves the representation of deep convection in the LAB

and Atlantic Meridional Overturning Circulation variability (Biastoch et al., 2021, Ruehs et al., 2021). There needs to be adequate horizontal resolution particularly near the shelf to realistically simulate the impact from Greenland freshwater and role of mesoscale eddies therein (Gillard et al., 2016, Stolzenberger et al., 2022, Schiller-Weiss et al., 2023). The atmospheric forcing for both runs is JRA55-do (Tsujino et al., 2018) which includes estimates of Greenland freshwater fluxes provided as daily mean data and derived from monthly and spatially varying liquid runoff and solid discharge from Bamber et al., 2018 covering the period 1958 - 2016. The freshwater is released at the surface along the coastline and is tagged by a passive tracer.

The two model experiments, REF and SENS, are spun off from the hindcast VIKING20X-JRA-OMIP of (Biastoch et al., 2021), which starts from rest in 1958 initialized with climatological hydrographic conditions of the World Ocean Atlas. Both experiments start from January 1997 and run through December 2021. To overcome numerical instabilities with the passive tracer occurring along some steep topography, a regionally confined no-slip lateral boundary condition has been introduced in a 0.5° x 0.5° box in the South-East corner of Cat Island, Bahamas. Besides this change, REF is identical to VIKING20X-JRA-OMIP until 2016. For the years 2017 - 2021 the Greenland freshwater fluxes, which lack interannual variability in JRA55-do, are scaled to match the variability reported by Slater et al., 2021. For this we computed a linear regression for the Greenland total annual mean freshwater flux of Bamber et al., 2018 using the respective runoff estimates of Slater et al., 2021.

Runoff is remapped to coastal grid cells on the 1/4° global grid (Martin et al., 2021) and then interpolated to the 1/20° nest grid (see Biastoch et al., 2021, end of section 2.2) ensuring no runoff is lost to land grid cells. This yields a slightly wider band of about five 1/20° grid cells (approximately equalling one 1/4° grid cell) of runoff along the coast. Runoff is thus partly entering the ocean inside the fjords but mostly on the shelf following the coarser coast line (note at 1/4° major Greenland fjords are present). On neither grid is fjord circulation properly simulated but vertical mixing and diffusion yield a relatively rapid distribution over the top 100 to 200m. Not distributing the meltwater over depth may have some local implications but we consider the mixing in the boundary current sufficiently vigorous to yield a realistic salinity and density structure for the interaction of the boundary current with the interior and for eddy shedding. Nevertheless, we are working on a more realistic distribution for future simulations.

Text S1

Figure S1 shows the mean winter and summer sea surface salinity (SSS), temperature (SST), and potential density differences between REF and SENS over the period 2002 - 2021. There is a freshening along the east and west Greenland boundaries, particularly in summer when Greenland melting peaks (dark purple area around the shelf in Figure S1b). While there is cooling found along the Greenland shelf boundary in both seasons (Figure S1c, d), it is particularly strong in the very north of the Labrador basin towards Davis Strait (Figure S1c).

The red/cyan contours in Figure S1a, c, e mark the 15% sea ice concentration outline (i.e. the sea ice edge) in winter in REF/SENS, with REF sea ice coverage extending further south. Figure S1e, f show the winter and summer density differences. There is a strong seasonal cycle present with strong density and salinity differences along the Greenland boundary current in summer due to enhanced Greenland melt. Salinity appears to dominate the surface potential density with significantly lower differences found further offshore in winter (Figure S1a, e).

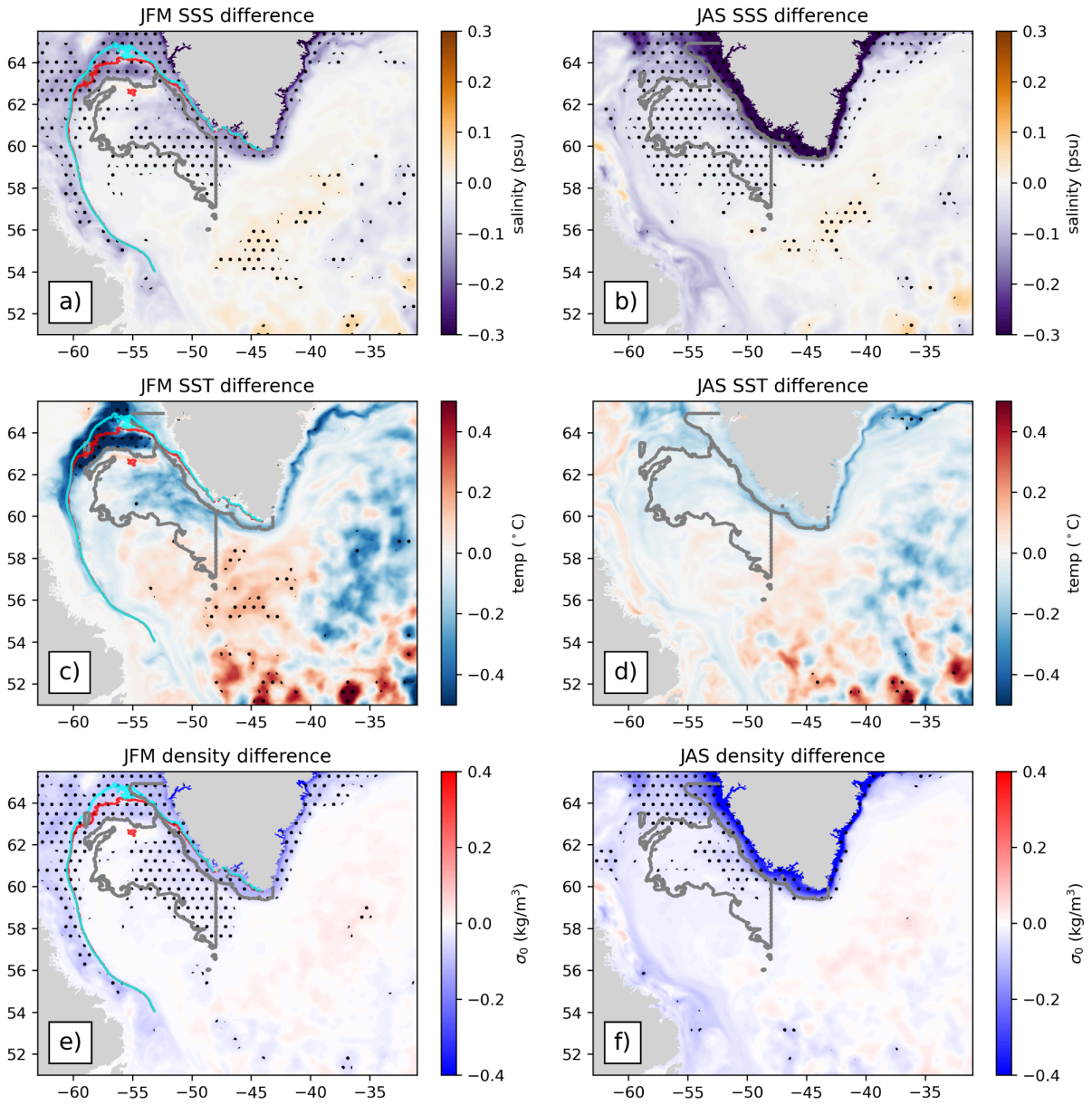

Figure S1: (a) Mean (2002 - 2021) winter (January - March) sea surface salinity (SSS) difference (REF minus SENS). (b) Mean summer (July - September) SSS differences. (c) Winter sea surface temperature (SST) difference. (d) Summer SST difference. (e) Winter surface potential density difference. (f) Summer potential density difference. In the winter SSS, SST, and density difference maps (subplots a, c, e), the red/cyan contour indicates the 15% sea ice concentration in REF/SENS. Black stippling indicates statistically significant areas. Gray contours indicate the west Greenland shelf and eddy shedding region.

Text S2

Figure S2 shows the cumulative alongshore wind stress from June - December averaged over the west Greenland shelf (gray contour along the shelf shown in Figure S1). Alongshore winds weaken in summer and increase in winter, where winds along west Greenland can be upwelling favorable and transport freshwater offshore (Castelao et al., 2019, Luo et al., 2016). As the wind stress shows strong instantaneous variability, computing the cumulative alongshore wind stress permits for substantial upwelling and downwelling favorable winters to be distinguished on an annual basis (Castelao et al., 2019). The cumulative alongshore wind stress is grouped into two categories of anomalous upwelling and downwelling favorable years (15th and 85th percentiles), shown in the blue (upwelling) and orange (downwelling) lines in Figure S2).

The summer of 2010 is where strong Greenland melting occurred (Tedesco et al., 2011). In the winter of 2010, winds were downwelling favorable where freshwater along the shelf is constrained to the coast and transported northward to Baffin Bay or follows the isobaths surrounding the LAB basin (Castelao et al., 2019).

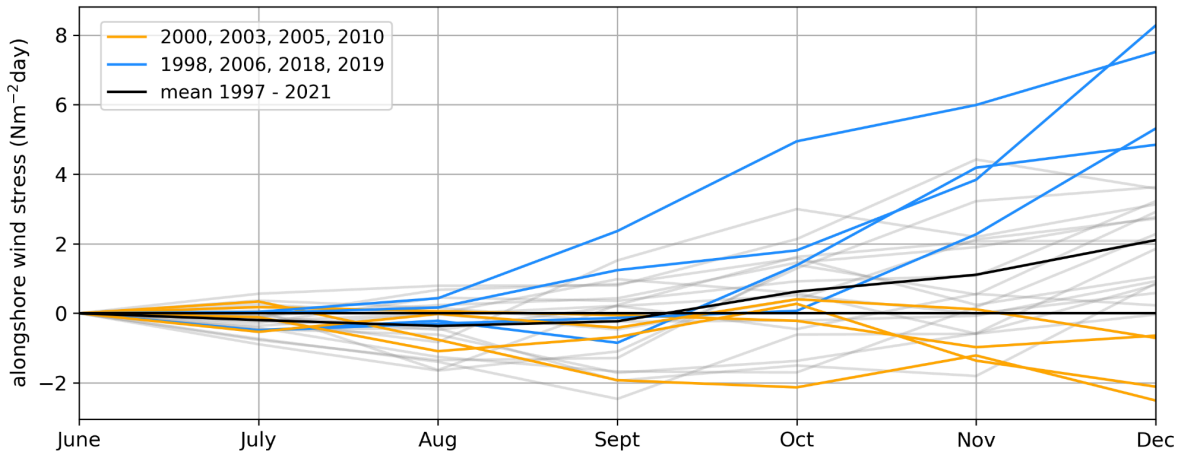

Figure S2: Cumulative alongshore wind stress from June - December averaged over the west Greenland shelf region. Black line indicates the mean alongshore wind stress, blue/orange lines indicate years with upwelling/downwelling favorable conditions outside the 15th/85th percentile.)

Text S3

The mean (2002 - 2021) West Greenland Current (WGC) velocity structure shown in Figure S3a. b, and c is taken over three repeat standard cross sections from the model output: OSNAP West (Lozier et al., 2019), Cape Desolation, and Fylla Bank (Mortensen 2018, Myers et al., 2009). The current velocity magnitude along the OSNAP West section (Figure S3a) shows two peaks in the velocity at the shelf and just off the shelfbreak along the slope. The coastal current is present at Cape Desolation (Figure S3b) but slightly weaker than at OSNAP West.

The annual mean current speed for the coastal and slope current per cross section is shown in Figure S3d, e, f. It is at OSNAP West where the coastal and slope current strength in REF

shows a significant increase compared to SENS (Figure S3d). At Cape Desolation, the coastal current for REF and SENS show the same variability where REF has slightly higher annual mean current velocities than SENS. However at the slope current, there is differing variability between the two runs. At Cape Desolation there are strong topographical differences and changes in alongshore wind stress that result in baroclinic instabilities (Gou et al., 2021, Gou et al., 2021, Pacini et al., 2022), potentially explaining for the lack of coherent variability between REF and sensitivity run in the slope current (Figure S3e). The coastal current speed in REF is slightly greater than in SENS at Fylla Bank, and the slope current speeds are slightly greater in REF. The speed in the coastal current between the three cross sections decrease further north, while the slope current increases from OSNAP West to Cape Desolation and decreases at Fylla Bank.

We evaluate the correlation of the coastal and slope current velocities at each cross section with the local surface horizontal density gradient at each grid node in REF. The correlation maps between the coastal current velocity and density gradient for OSNAP West, Cape Desolation, and Fylla Bank are shown in Figures S3g, h, i. For all the cross sections, there are significant, positive correlations between the density gradient and coastal current speed along the east and west Greenland shelves. There is a patch of negative correlations further offshore, showing a potential dipole pattern of near shelf changes in the density gradient suggesting an offshore meandering of the density front to be associated with a weaker coastal current.

Figure S3j, k, l show the same correlation but for the slope current velocity. For OSNAP West, there is a large patch of positive correlations in the eddy shedding region (Figure S3j), while for Cape Desolation there are positive correlations just off the section encircling the Labrador basin (Figure S3k). In contrast, for Fylla Bank, positive correlations are confined to the Greenland shelf (Figure S3l).

For a rather schematic illustration of the overall correlation between the boundary currents and the density gradient towards the LAB interior, we compute a “cumulative correlation”. We first set a threshold by retaining only correlations that are statistically significant (areas defined by the gray contour based on 1st/99th percentiles), and then we compute the sum of all correlation maps from each section:

$$R_{all} = \sum_{n=1}^{N} R_n \; with \; R_{all} \in [-1, 1], \qquad (1)$$

where R_n is the evaluated correlation coefficient between the coastal and slope current velocity with the surface horizontal density gradient for N number of cross sections. As the sum will be greater than $|\pm 1|$, we cap the cumulative correlation coefficient R_{all} at ± 1.

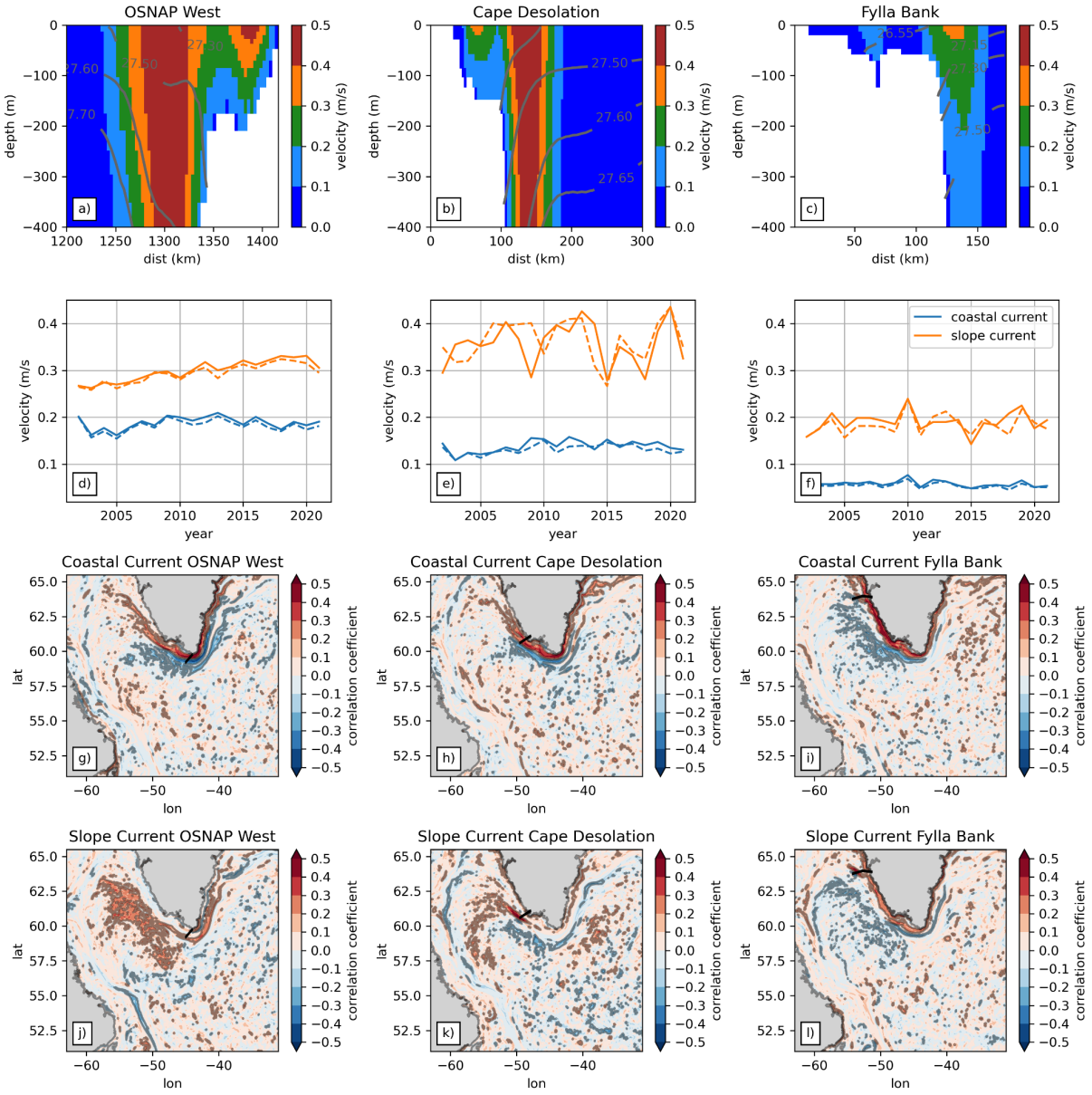

Figure S3: (a) Mean (2002 - 2021) current velocity magnitude at OSNAP West. (b) Cape Desolation. (c) Fylla Bank. Gray contours indicate the isopycnals referenced to the surface. (d) The annual mean current speed depth averaged the over the top 200m for the coastal (blue) and slope current (orange) for OSNAP West. Solid lines depict REF and dashed ones SENS. (e) Cape Desolation. (f) Fylla Bank. (g) Correlation between the coastal current velocity at OSNAP West and the horizontal surface density gradient. The gray contour indicates significant areas based on the 1st and 99th confidence intervals. The black line shows the specified cross section along the shelf. (h) Correlation at Cape Desolation. (i) Fylla Bank. (j) The correlation between slope current velocity and the surface density gradient at OSNAP West. (k) Cape Desolation. (l) Fylla Bank.

Text S4

In order to investigate how freshwater is distributed over the water column, we look at the depth profiles averaged over EAST defined by the pDCA and winter (January, February, March) from 2009 - 2013. The tracer content is larger in REF than in SENS (since we add more freshwater) but the distribution with depth is non-uniform and we identify three levels: above ~200m and—to a smaller amount—at 200 - 1000m REF shows larger content, but at 1000 - 2000m tracer content in SENS is greater than in REF (Figure S4b, g). Despite the greater meltwater tracer content, density in REF exceeds that of SENS above 1000m, especially above 300m (Figure S4c, h). The latter is due to waters being cooler in REF than in SENS (Figure S4e) despite also being fresher (Figure S4 d). We conclude that the meltwater does rather not affect density in EAST directly, as one may expect, but rather acts through altering the stratification with consequences for heat loss (stronger mixing with Polar Water of the boundary current would have a similar effect but we consider this less likely due to the distance and EGC/EGCC being strongly confined to the shelf/coast).

The stratification peak near 200m depth (Figure S4a) is indicative of a different water mass residing below this level and we argue that the meltwater tracer in the layer of 200-1000m is rather imported by intermediate waters from the Labrador Sea than locally mixed down by deep convection. Since REF contains more meltwater that is entrained in deep convection in the Labrador Sea, we also find larger amounts of meltwater tracer in REF than in SENS in this region at this depth range. The interesting part is that there is more meltwater tracer below 1000m in SENS than in REF. Although we think this meltwater is not mixed down locally, it is worth noting that deep convection in EAST reaches deeper in REF than in SENS in 2015 - 2018, which is contradictory to the tracer concentration. Deep convection in the Labrador Sea, however, is deeper in SENS than in REF since REF is overall fresher at/near the surface. We thus argue that the tracer concentration in EAST below 300m links to the deep convection in the Labrador Sea. And a shallower deep convection in the Labrador Sea yields a shallower meltwater-caused freshening in EAST, in the Irminger Sea, which significantly reduces stratification below 200m (Figure S4f) and is a preconditioning for deeper convection in the East.

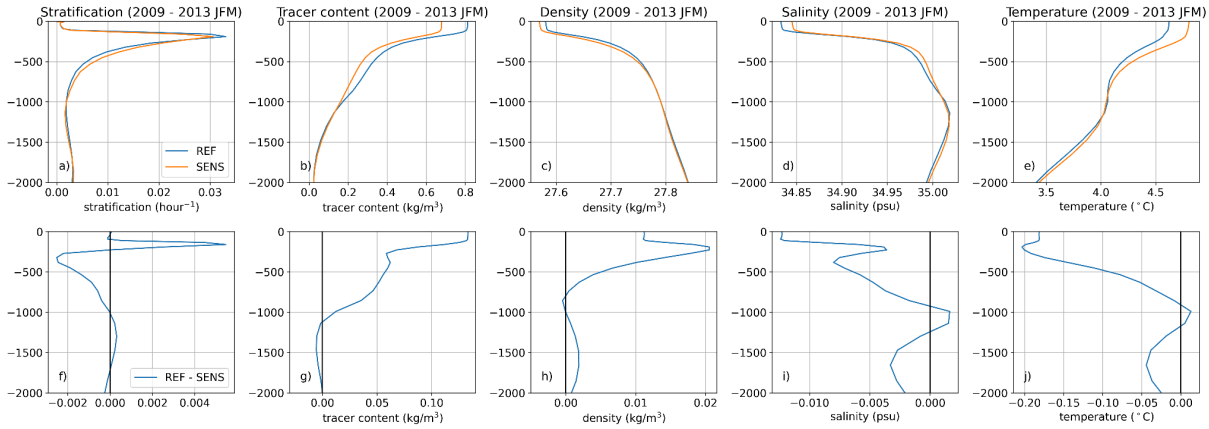

Figure S4: (a) The depth profile of stratification averaged over EAST and winter 2009 - 2013 between REF and SENS. (b) Depth profile of tracer content. (c) Density. (d) Salinity. (e) Temperature. The blue/orange line show REF/SENS respectively. (f) The depth profile of the

difference in stratification between REF and SENS. The black line indicates 0. (g) difference in tracer content. (h) Density. (i) Salinity. (j) Temperature.

We compute the stratification percent changes in REF due to the increase in Greenland freshwater fluxes with respect to the stratification in SENS for the winters (January - March) of 2009 and 2012 (Figures S5a, c). In 2009, there is a positive percent change (increase), in stratification in REF from 58 - 45°W in the depth range 200 - 1500m. Southeast of Cape Farewell (43 - 38°W), there is a negative percent change (decrease) in stratification (Figure S5a) at 200 - 1000m. The MLD in the LAB is deeper for SENS than REF, but both model runs feature deep convection with the MLD reaching depths greater than $z_{critical} = 1000m$. From 48 - 38°W REF has a slightly shallower MLD but around a depth of $z_{critical}$. The MLD becomes shallower up to depths of 500m east of 38°W. In support of the argument about Greenland-sourced freshwater being entrained at different depths in REF and SENS by the deep convection in the LAB, we present passive tracer concentration percent changes in Figure S5b, d. In 2009, there is a negative percent change of meltwater tracer content between 43 and 33°W from 1000 - 2000m depth in REF (red patch in Figure S5b). Especially in 2009, Greenland-sourced freshwater likely spread at greater depth into the Irminger Sea (IRM) from the LAB deep convection center.

In 2012, the decrease in stratification appears surface intensified south of Cape Farewell and then weakens but spreads further east (43 - 33°W) and in depth (Figure S5c). The MLD in both REF and sensitivity experiments are comparable with MLDs reaching up to 1500m in the LAB. In the IRM from 39 - 35°W REF has deeper MLDs with a difference of 400m compared to the SENS experiment. Less passive tracer content has spread further east and is mixed downward in 2012 (Figure S5d), with SENS containing higher amounts of Greenland meltwater there. The increase in meltwater presence coincides with the shallower MLD in SENS from 38 - 34°W.

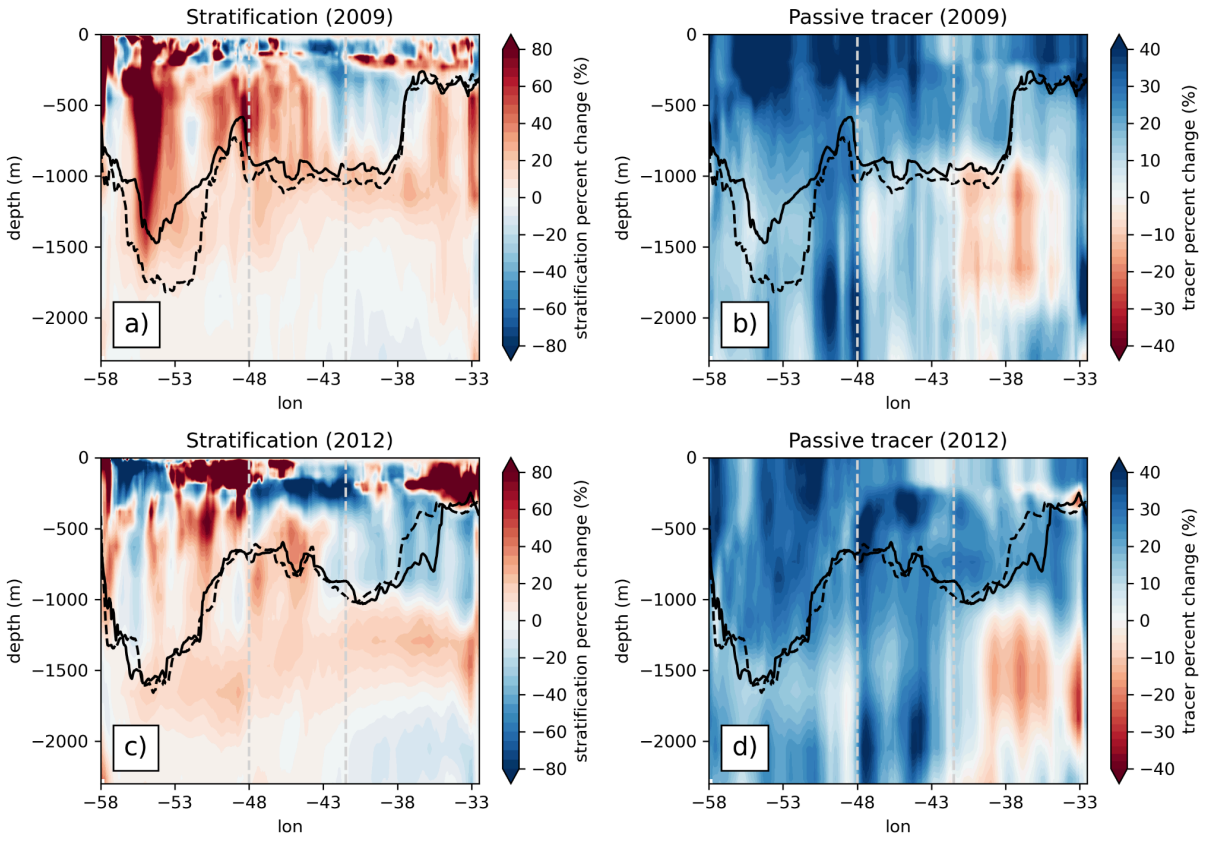

Figure S5: (a) The percent change in winter mean stratification in 2009 between REF and SENS. The annual maximum MLD from REF is the solid black line, while the dashed line is the sensitivity. (b) The percent change of Greenland meltwater passive tracer content in winter. (c) Same as (d) but for 2012. (d) Same as (b) but for 2012. The dashed vertical gray lines indicate the separation between WEST, MID, and EAST regions.

Text S5

Convective resistance (CR) is the quantification of water column stability to a particular depth (Gillard et al., 2022, Frajka-Williams et al., 2014, Holdsworth & Myers, 2015). The CR, based on Gillard et al., 2022, for each model grid cell is defined as:

$$CR(h) = \frac{g}{\rho_0}\left[h\sigma_0(h) - \int_0^h \sigma_0(z)dz\right] \quad (2)$$

where *g* is gravity (9.8 m/s^2), ρ_0 is REF density (1026 kg/m^3), σ_0 is the potential density referenced to the surface, and *h* is the mixing depth. Maximum MLDs have been observed to reach depths of 2000m in the IRM (Sterl & de Jong, 2022, Zunino et al., 2020) but we choose a depth (*h*) of 1500m as an upper limit of maximum MLDs in the IRM (Pickart et al., 2003). A high,

positive CR indicates a stronger resistance to convection (Gillard et al., 2022, Bailey et al., 2005) and stably stratified layers, zero CR indicates mixing, and a negative CR would indicates unstable stratification (Gillard et al., 2022, Frajka-Williams et al., 2014), which is unlikely to show in monthly mean model output used here since overturning would have been simulated.

Figure S6a and b show the difference in winter mean convective resistance between REF and sensitivity for years 2009 - 2013 and 2015 - 2018. Both show higher CR in the LAB and lower values in the IRM for REF. Positive/negative values signifying greater/smaller CR in REF. In 2009 - 2013, it appears that the majority of negative and significant CR occur just south of the potential deep convection contour in the IRM (EAST region) (Figure S6a). There are significant positive CR changes in the eddy shedding region and southeast of Cape Farewell.

In 2015 - 2018 (Figure S6b), there is greater CR in REF in the central LAB and within the pDCA. The majority of negative, significant CR differences occur outside the eastern boundary of the potential deep convection region but there is significantly lower CR in REF where the largest MLD differences occur in 2015 - 2018.

From 1997 onwards, CR differences start to slowly evolve as more Greenland-sourced freshwater begins to accumulate in REF than in SENS in all three regions WEST, MID, and EAST of the pDCA (Figure S5c). From about 2009 onwards, REF and SENS begin to separate. Particularly in EAST (green line), i.e. the IRM, CR systematically becomes smaller in REF than in SENS. This underlines a role of freshwater from Greenland in decreasing CR ultimately leading to an eastward shift or expansion of the deep convection region in 2015 - 2018.

There is less of a systematic spread in the LAB (WEST) and south of Cape Farewell (MID) between REF and SENS. From 2011 to 2018, REF shows elevated mean winter CR than SENS. Note that MLDs in the LAB can reach to depths of 2000m (Gillard et al., 2022, Yashayev & Loder, 2017) and thus there may not be an imprint on CR referenced to 1500m from the reduced deep convection discussed above. Interestingly and in agreement with an eastward shift of deep convection in 2015 - 2018, CR averaged over EAST reaches lower values than in WEST in both REF and SENS.

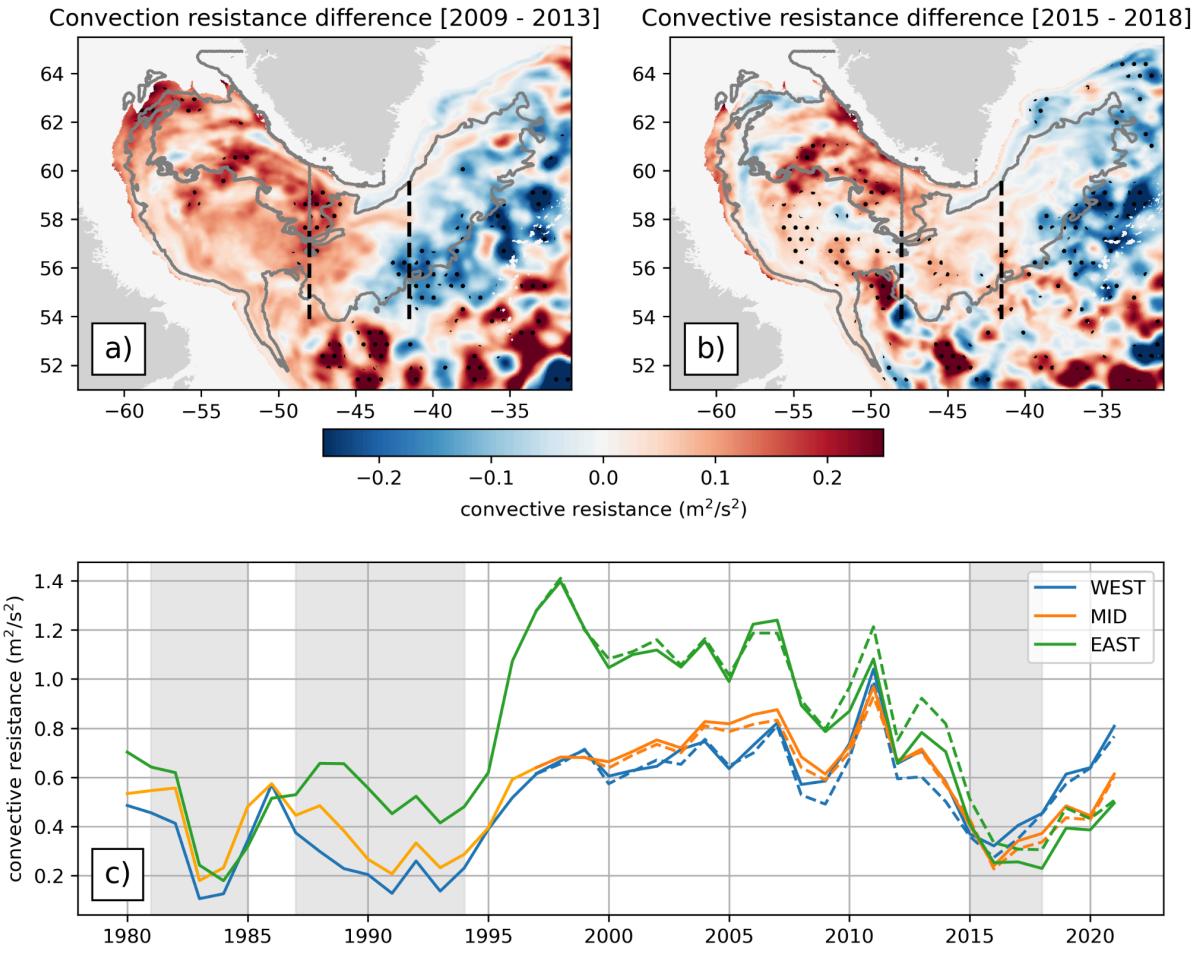

Figure S6: (a) The convective resistance difference (REF minus SENS) averaged over winter (January - March) from 2009 - 2013. (b) Winter convective resistance over 2015 - 2018. The gray contours indicate the west Greenland shelf, eddy shedding region, and pDCA. The dashed vertical, gray lines indicate the separation between WEST, MID, and EAST within the pDCA. (c) The convective resistance averaged over WEST (blue), MID (orange), and EAST (green). The solid line is a combination of the hindcast simulation (1980 - 1996) and REF (from 1997 onwards). The dashed line depicts SENS. The light grey vertical bars indicate associated periods of strong deep convection.

References

Bailey, D. A., Rhines, P. B., & Häkkinen, S. (2005, October). Formation and pathways of North Atlantic Deep Water in a coupled ice–ocean model of the Arctic–North Atlantic Oceans. Climate Dynamics, 25 (5), 497–516. doi: 10.1007/s00382-005-0050-3

Bamber, J. L., Tedstone, A. J., King, M. D., Howat, I. M., Enderlin, E. M., van den Broeke,M. R., & Noel, B. (2018). Land Ice Freshwater Budget of the Arctic and North AtlanticOceans: 1. Data, Methods, and Results. Journal of Geophysical Research: Oceans, 123 (3), 1827–1837. doi: 10.1002/2017JC013605

Biastoch, A., Schwarzkopf, F. U., Getzlaff, K., Rühs, S., Martin, T., Scheinert, M., . . . Böning, C. W. (2021, September). Regional imprints of changes in the Atlantic Meridional Overturning Circulation in the eddy-rich ocean model VIKING20X. Ocean Science, 17 (5), 1177–1211. doi: 10.5194/os-17-1177-2021

Castelao, R. M., Luo, H., Oliver, H., Rennermalm, A. K., Tedesco, M., Bracco, A., . . . Medeiros, P. M. (2019). Controls on the Transport of Meltwater From the Southern Greenland Ice Sheet in the Labrador Sea. Journal of Geophysical Research: Oceans, 124 (6), 3551–3560. doi: 10.1029/2019JC015159

Debreu, L., Vouland, C., & Blayo, E. (2008, January). AGRIF: Adaptive grid refinement in Fortran. Computers & Geosciences, 34 (1), 8–13. doi: 10.1016/j.cageo.2007.01.009

de Jong, M. F., & de Steur, L. (2016). Strong winter cooling over the Irminger Sea in winter 2014–2015, exceptional deep convection, and the emergence of anomalously low SST. Geophysical Research Letters, 43 (13), 7106–7113. doi: 10.1002/2016GL069596

Frajka-Williams, E., Rhines, P. B., & Eriksen, C. C. (2014, January). Horizontal Stratification during Deep Convection in the Labrador Sea. Journal of Physical Oceanography, 44 (1), 220–228. doi: 10.1175/JPO-D-13-069.1

Gillard, L. C., Hu, X., Myers, P. G., & Bamber, J. L. (2016). Meltwater pathways from marine terminating glaciers of the Greenland ice sheet. Geophysical Research Letters, 43 (20), 10,873–10,882. doi: 10.1002/2016GL070969

Gillard, L. C., Pennelly, C., Johnson, H. L., & Myers, P. G. (2022, March). The Effects of Atmospheric and Lateral Buoyancy Fluxes on Labrador Sea Mixed Layer Depth. Ocean Modelling, 171 , 101974. doi: 10.1016/j.ocemod.2022.101974

Gou, R., Feucher, C., Pennelly, C., & Myers, P. G. (2021). Seasonal cycle of the coastal west greenland current system between cape farewell and cape desolation from a very high-resolution numerical model. Journal of Geophysical Research: Oceans, 126 (5), e2020JC017017. doi: https://doi.org/10.1029/2020JC017017

Gou, R., Pennelly, C., & Myers, P. G. (2022). The Changing Behavior of the West Greenland Current System in a Very High-Resolution Model. Journal of Geophysical Research: Oceans, 127 (8), e2022JC018404. doi: 10.1029/2022JC018404

Hallberg, R. (2013, December). Using a resolution function to regulate parameterizations of oceanic mesoscale eddy effects. Ocean Modelling, 72 , 92–103. doi: 10.1016/j.ocemod.2013 .08.007

Holdsworth, A. M., & Myers, P. G. (2015, June). The Influence of High-Frequency Atmospheric Forcing on the Circulation and Deep Convection of the Labrador Sea. Journal of Climate, 28 (12), 4980–4996. doi: 10.1175/JCLI-D-14-00564.1

Lozier, M. S., Li, F., Bacon, S., Bahr, F., Bower, A. S., Cunningham, S. A., . . . Zhao, J. (2019, February). A sea change in our view of overturning in the subpolar North Atlantic. Science, 363 (6426), 516–521. doi: 10.1126/science.aau6592

Luo, H., Castelao, R. M., Rennermalm, A. K., Tedesco, M., Bracco, A., Yager, P. L., & Mote, T. L. (2016, July). Oceanic transport of surface meltwater from the southern Greenland ice sheet. Nature Geoscience, 9 (7), 528–532. doi: 10.1038/ngeo2708

Madec, G., & NEMO System Team. (2016). NEMO Ocean Engine. Scientific notes of climate modeling center (27). Institut Pierre Simon Laplace (IPSL). doi: 10.5281/zenodo.1464816

Martin, T. (2021, September). Runoff remapping for ocean model forcing [Software]. Retrieved 2024-03-25, from https://git.geomar.de/open-source/runoff remapping (Place: Kiel, Germany Publisher: GEOMAR Helmholtz Centre for Ocean Research Kiel) doi: 10.3289/SW 2 2021

Mortensen, J. (2018). Report on hydrographic conditions off southwest greenland june/july 2017. NAFO SCR Doc, 18 (005), 8.

Myers, P. G., Donnelly, C., & Ribergaard, M. H. (2009, January). Structure and variability of the West Greenland Current in Summer derived from 6 repeat standard sections. Progress in Oceanography, 80 (1), 93–112. doi: 10.1016/j.pocean.2008.12.003

Pacini, A., & Pickart, R. S. (2022, January). Meanders of the West Greenland Current near Cape Farewell. Deep Sea Research Part I: Oceanographic Research Papers, 179 , 103664. doi: 10.1016/j.dsr.2021.103664

Pickart, R. S., Straneo, F., & Moore, G. W. K. (2003, January). Is Labrador Sea Water formed in the Irminger basin? Deep Sea Research Part I: Oceanographic Research Papers, 50 (1), 23–52. doi: 10.1016/S0967-0637(02)00134-6

Piron, A., Thierry, V., Mercier, H., & Caniaux, G. (2016, March). Argo float observations of basin-scale deep convection in the Irminger sea during winter 2011–2012. Deep Sea Research Part I: Oceanographic Research Papers, 109 , 76–90. doi: 10.1016/j.dsr.2015.12.012

Piron, A., Thierry, V., Mercier, H., & Caniaux, G. (2017). Gyre-scale deep convection in the subpolar North Atlantic Ocean during winter 2014–2015. Geophysical Research Letters, 44 (3), 1439–1447. doi: 10.1002/2016GL071895

Rühs, S., Oliver, E. C. J., Biastoch, A., Böning, C. W., Dowd, M., Getzlaff, K., . . . Myers, P. G. (2021). Changing Spatial Patterns of Deep Convection in the Subpolar North Atlantic. Journal of Geophysical Research: Oceans, 126 (7), e2021JC017245. doi: 10.1029/2021JC017245

Schiller-Weiss, I., Martin, T., Karstensen, J., & Biastoch, A. (2023). Do Salinity Variations Along the East Greenland Shelf Show Imprints of Increasing Meltwater Runoff? Journal of Geophysical Research: Oceans, 128 (10), e2023JC019890. doi: 10.1029/2023JC019890

Slater, T., Shepherd, A., McMillan, M., Leeson, A., Gilbert, L., Muir, A., . . . Briggs, K. (2021, November). Increased variability in Greenland Ice Sheet runoff from satellite observations. Nature Communications, 12 (1), 6069. doi: 10.1038/s41467-021-26229-4

Sterl, M. F., & de Jong, M. F. (2022). Restratification Structure and Processes in the Irminger Sea. Journal of Geophysical Research: Oceans, 127 (12), e2022JC019126. doi: 10.1029/2022JC019126

Stolzenberger, S., Rietbroek, R., Wekerle, C., Uebbing, B., & Kusche, J. (2022). Simulated Signatures of Greenland Melting in the North Atlantic: A Model Comparison With Argo Floats, Satellite Observations, and Ocean Reanalysis. Journal of Geophysical Research: Oceans, 127 (11), e2022JC018528. doi: 10.1029/2022JC018528

Tedesco, M., Fettweis, X., Van den Broeke, M., Wal, R., Smeets, P., Berg, W., . . . Box, J. (2011, January). The role of albedo and accumulation in the 2010 melting record in Greenland. Environmental Research Letters, 6 , 014005. doi: 10.1088/1748-9326/6/1/014005

Tsujino, H., Urakawa, S., Nakano, H., Small, R. J., Kim, W. M., Yeager, S. G., . . . Yamazaki, D. (2018, October). JRA-55 based surface dataset for driving ocean–sea-ice models (JRA55-do). Ocean Modelling, 130 , 79–139. doi: 10.1016/j.ocemod.2018.07.002

Yashayaev, I., & Loder, J. W. (2017). Further intensification of deep convection in the Labrador Sea in 2016. Geophysical Research Letters, 44 (3), 1429–1438. doi: 10.1002/2016GL071668

Zunino, P., Mercier, H., & Thierry, V. (2020, January). Why did deep convection persist over four consecutive winters (2015–2018) southeast of Cape Farewell? Ocean Science, 16 (1), 99–113. doi: 10.5194/os-16-99-2020

4

Study 3: Relating sea surface height changes to decadal variability of the Atlantic Meridional Overturning Circulation: a multi-centennial ocean model study using repeated forcing cycles

This study investigates sea surface height (SSH) anomalies as a potential Atlantic Meridional Overturning Circulation (AMOC) fingerprint on decadal fingerprint from 1980–2021, using an ensemble of six ocean model hindcast simulations and two additional experiments with differing amounts of Greenland runoff spun from the first run of the ensemble. It is demonstrated that on decadal time scales, there is an inverse relationship between AMOC and SSH variability; as the AMOC strengthens (weakens), the regional SSH there decreases (increases) most clearly seen along the US East coast and western subpolar gyre. There is also an observed increase in SSH along the East and West Greenland shelf and Labrador Sea with enhanced Greenland melting. On longer, pentadal and decadal, time scales Greenland runoff variations appear inversely proportional to changes in the AMOC and North Atlantic Oscillation.

This chapter is part of and extension of a current manuscript in preparation with Tobias Schulzki, Franziska U. Schwarzkopf, Torge Martin, and Arne Biastoch but has not been published or submitted for publication.

Introduction

The Atlantic Meridional Overturning Circulation (AMOC) is a key driver of climate through its transport of heat and salt throughout the Atlantic (Ganachaud and Wunsch, 2000; Johnson and Wijffels, 2011; Jackson et al., 2022). It is composed of a large system of currents that transports northward flowing, warm waters and southward moving cold waters across the entire north and south Atlantic oceans (Frajka-Williams et al., 2019). Warm and salty water originating from the equatorial Atlantic and increasing in density by surface heat loss as it travels northward, making up the upper limb of the AMOC (Little et al., 2019; Thomas et al., 2015). Likewise, cold, dense but relatively fresh deep waters are brought southward forming the lower limb of the AMOC (Jackson et al., 2022; Frajka-Williams et al., 2019).

The upper and lower limb of the AMOC join in the high North Atlantic latitudes where warm, upper waters sink due to heat loss to the atmosphere, forming deep waters through deep mixing and convection (Spall and Pickart, 2001; Zou et al., 2020). A schematic of the currents making up the majority of AMOC transport in the northern hemisphere is shown in Figure 4.1, taken from Little et al., 2019: the upper limb defined by northward moving currents is highlighted in red, while the lower limb transporting dense and cool waters southward is in blue.

AMOC variability is observed to occur on a range from daily, seasonal, interannual, and decadal to multi-decadal timescales. On interannual timescales, studies show that the AMOC changes are attributed to wind forcing via changes in Ekman transport, wind stress curl (Biastoch et al., 2008; Zhao and Johns, 2014), and western boundary currents (Böning et al., 2006; McCarthy et al., 2012). On decadal time scales and longer, AMOC variability has been linked to deep water formation in the subpolar gyre and local buoyancy forcing in the Labrador Sea (Zhang, 2008; Lohmann et al., 2009a; Jackson et al., 2022; Böning et al., 2023). AMOC variability has been widely studied through observational mooring arrays (Meinen et al., 2013; Smeed et al., 2014; Lozier et al., 2019) and climate models (Cheng et al., 2013; Swingedouw, Mignot, et al., 2013). While observations are vital to understanding changes in AMOC, the relatively short record period limits the understanding of AMOC in the previous decades (Fu et al., 2020).

There have been observed periods of strengthening and weakening of AMOC. In a combination of moorings and satellite altimetry suggested a slow down of AMOC from 2002–2012 (Smeed et al., 2014), while since 1980 to the mid-1990s there was evidence a strengthening of the subpolar AMOC (Böning et al., 2023). The subtropical AMOC shows differing variability than the subpolar AMOC, strengthening in 2001–2005 and weakening from 2005–2014 (Jackson et al., 2022). These stronger and weaker phases of AMOC are consistent with observations of active deep convection in the Labrador Sea in the mid-1990s (Lohmann et al., 2021; Jackson et al., 2022), however there are still uncertainties about what is driving these changes.

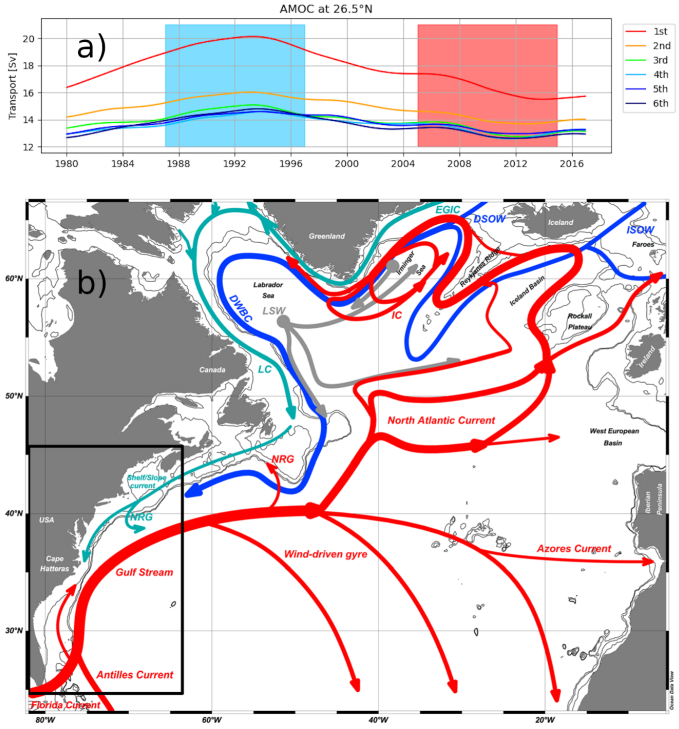

Fig. 4.1: (a) Decadally filtered AMOC at 26.5°N from 1980–2019 across the different cycles. Red is the 1st cycle, orange is the 2nd, green is the 3rd, blue is the 4th, dark blue is the 5th, and black is the 6th cycle. The blue/red vertical shading indicates the high/low phase of AMOC. (b) Schematic of AMOC from Little et al., 2019. Abbreviations: NRG = Northern Recirculation Gyre; LC = Labrador Current; DWBC = Deep Western Boundary Current; IC = Irminger Current; EGIC = East Greenland-Irminger Current.

An indicator of changes in AMOC was proposed to reflect in changes in regional sea surface height anomalies (Cromwell et al., 2007; Landerer et al., 2007; Bingham and Hughes, 2009; Hirschi et al., 2009; Lorbacher et al., 2010; Wang et al., 2015). Model studies have observed strong variability in SSH along the western North Atlantic by a pronounced dipole or tripole pattern centered along the subpolar gyre (SPG) and the Gulf Stream (GS) (Bryan, 1996; Häkkinen et al., 2013; Lorbacher et al., 2010). Zhang, 2008 found a similar pattern on interannual to decadal AMOC changes in the first empirical orthogonal function of SSH anomalies, suggesting that SSH anomalies can potentially link to variations in AMOC strength. Levermann et al., 2005 observed a considerably lower mean SSH in the northern North Atlantic than in the North Pacific, thought to be driven in part by formation of North Atlantic Deep Water and associated with AMOC (Levermann et al., 2005; Saenko et al., 2017).

They also proposed that there exists a connection between the AMOC strength and the SSH field, with a weaker AMOC corresponding to a positive change in SSH in the North Atlantic (Vellinga and Wood, 2008; Saenko et al., 2017). Since direct estimates of the AMOC transport with current meters and geostrophic moorings are very complex and only extend back to the early 2000s, an imprint of AMOC variability in other fields, known as AMOC fingerprints, could provide additional information about the past AMOC evolution (Zhang,

2008; Caesar et al., 2018). In particular, a robust SSH fingerprint could allow for an AMOC reconstruction from satellite observations and potentially even from tide gauges. While the first would allow for an AMOC reconstruction back to the early 90s the latter extend back to the mid 19th century at some locations. Furthermore, it would be possible to monitor the future AMOC evolution without relying exclusively on the very few direct transport measurements and thus increase confidence in the detected changes.

A question that follows is what influences AMOC variability and is there a particular time scale in which SSH anomalies can reflect changes in AMOC? Lorbacher et al., 2010 examined the changes of regional dynamic SSH patterns with a multidecadal decline in AMOC from artificially adding freshwater in the northern North Atlantic and comparing it with changes in SSH on intraseasonal to decadal time scales from atmospheric forcing and internal dynamics. They concluded that the difference in SSH patterns over varying time scales suggest that changes in AMOC transport depends strongly on the time scales of interest. Nevertheless, a limitation of these studies, especially those focusing on multi-decadal timescales, is their use of coarse resolution models. The model's horizontal resolution is of particular importance for resolving narrow boundary currents, which play a major role of sea-level variability along the coast (Little et al., 2019). Also, the AMOC pathways at subpolar latitudes and processes thought to impact the formation of deep water and AMOC variability are more realistic at eddying resolution (e.g. Rieck et al., 2019; Hirschi et al., 2020; Colombo et al., 2020). As a consequence, the circulation and SSH patterns associated with changes in the AMOC may not be realistic in coarse resolution models.

Furthermore, often freshwater or salt is artificially added to the North Atlantic in order to force AMOC changes and study their imprint on SSH (e.g. Levermann et al., 2005; Lorbacher et al., 2010). Artificially adding freshwater/salt itself has an impact on SSH through halosteric sea-level changes (e.g. Jackson and Wood, 2018). Adding freshwater adds mass, i.e. alters density in a typical volume conserving ocean models, and hence influences dynamcis. Kienert and Rahmstorf, 2012 found that the SSH pattern associated with AMOC changes could depend on the mechanism by which this change is forced. It is therefore necessary to not only derive the AMOC fingerprint itself, but also study the causal link between SSH, circulation, mass distribution and density changes. This provides additional information on the robustness of such a fingerprint on different timescales.

In this study, we investigate the influence of differing AMOC strengths on SSH variability on decadal time scales with eight high resolution, eddy resolving model runs with the same model configuration (VIKING20X). Each model run is forced by the same atmospheric reanalysis product but initial conditions evolve as the individual runs are spun off from the last time step of the preceding cycle. There are six cycles with two additional runs spun off the first cycle. The first cycle features the strongest AMOC signal, which then weakens over the following cycles.

We treat the set of consecutive experiments as an ensemble, each cycle being an ensemble member starting from differing initial conditions. The two additional runs, based off the first cycle, only differ in the amount of Greenland runoff. One of the runs has a realistic, interannually varying freshwater forcing representing Greenland meltwater, while the other contains reduced runoff based on a climatological mean. Since increasing Greenland

meltwater runoff is anticipated to have a significant influence on sea level and North Atlantic ocean dynamics (e.g. Martin et al., 2022) under global warming, an additional set of runs, in which this runoff is altered, will be analyzed. We aim to answer the following questions:

1) Can decadal SSH anomalies be attributed to AMOC variations and what is the link?

2) What is the contribution of thermal and haline components on steric sea level changes during high and low phases of AMOC strength? And does enhanced Greenland ice sheet melting over the past two decades already have an imprint on SSH?

3) Using the cycles as one long simulation instead, is there a link between AMOC strength and SSH on even longer time scales i.e. multidecadal?

The VIKING20X model configuration and OMIP protocol will be discussed in the following section. Results show the differences in SSH between decadal strong and weak periods of AMOC, the correlation between decadally filtered AMOC and SSH variability and the impact of differing AMOC strengths per model cycle, and lastly the influence of thermo vs halosteric changes on regional sea level change.

Data and Methods

VIKING20X Eddy-Rich Ocean/Sea Ice Model Configuration and OMIP cycles

VIKING20X employs the NEMO3.6 ocean engine (Madec and Team, 2016) and LIM2 sea-ice models on a tripolar Arakawa C grid. VIKING20X utilizes a two-way nesting with Adaptive Grid Refinement in Fortran (AGRIF) (Debreu et al., 2008) with a global host model at 1/4° (ORCA025) and a regional horizontally refined grid at 1/20° over the south and north Atlantic oceans (34°S–70°N) (see Figure 1 of Biastoch et al., 2021). This refinement permits the explicit simulation of mesoscale eddies (Hallberg, 2013), which improves the representation of Atlantic Meridional Overturning Circulation variability and deep convection in the subpolar gyre (Biastoch et al., 2021; Rühs et al., 2021). The nesting approach permits variability of mesoscale processes and how they may be impacted by large scale processes such as change in the AMOC (Rühs et al., 2021).

The atmospheric forcing is the JRA55-do version 1.4 surface data set (Tsujino et al., 2018), providing 3-hourly temporal resolution on a 1/2° grid up to 2019. JRA55-do also provides seasonally and interannually varying runoff at daily resolution including freshwater fluxes (FWFs) from Greenland (Bamber et al., 2018). There is a salinity restoring rate (50 m/year) applied to reduce model drift from missing feedbacks from the atmosphere, but no restoring flux applied in an 80 km radius from Greenland to avoid an instant compensation of the runoff from melting and facilitate the spread of enhanced meltwater from ice sheets (Biastoch et al., 2021).

The VIKING20X model runs are based on OMIP, an experimental protocol for global ocean/sea-ice models with a prescribed atmospheric forcing. OMIP is also a protocol for ocean diagnostics and contributes to CMIP6 by providing a framework to evaluate, improve, and understand climate and earth system models (Griffies et al., 2016). The VIKING20X JRA OMIP first cycle starts from rest in 1958 initialized with climatological hydrographic conditions from the World Ocean Atlas 2013 (WOA13, Locarnini et al., 2013; Zweng et al., 2013). The other 5 cycles follows the OMIP protocol (Griffies et al., 2016), where the following cycles (2–6), rather than starting from rest and initialized by the WOA13, starts at the last time step of the preceding cycle.

This allows additional time for the ocean model to spin up through each of the cycles. The OMIP protocol enables systematic diagnostics and comparisons to potential biases and differences per model cycle. For example, the model cycles 1–6 vary in AMOC strength (Figure 4.1b), where the first cycle has increased AMOC strength, and cycle 3–6 stabilize magnitude. The simulations begin in 1958–2021, but to allow time for the model to adjust, we consider only periods from 1980 onwards per cycle.

There is an additional set of twin experiments spun off from the 1st cycle of the OMIP runs beginning in 1997–2019, with the only difference between them being the freshwater forcing from Greenland (see Chapter 3). In one experiment, referred to as the "reference" run, includes an observed increase and interannually varying in Greenland runoff and a "sensitivity" experiment where Greenland FWFs are reduced to a climatology of 1961–2000. Both experiments differ from traditional hosing experiments where the North Atlantic is flooded with freshwater to halt the AMOC (Rahmstorf, 1995; Stouffer et al., 2006), by incrementally ramping of the Greenland FWFs based on current estimates consisting of realistic and interannually varying FWF magnitudes (Bamber et al., 2018; Slater et al., 2019). These two experiments consist of a stronger AMOC (spun from 1st OMIP cycle) with differing amounts of Greenland freshwater input, which can be used to determine local changes in SSH from Greenland runoff contribution alone.

Definition of AMOC

The AMOC is typically referenced at a particular latitude using a stream function Ψ and in units of Sverdrups. The AMOC consists of zonally and vertically integrated meridional volume transport (Frajka-Williams et al., 2019).

$$\Psi(z) = \int_{z}^{0} \int_{x_w}^{x_e} v(x,z) dx dz, \tag{4.1}$$

The AMOC stream function is shown in depth coordinates (4.1), where velocities are integrated over depth and across the latitudinal section from west (x_w) to east (x_e) (Frajka-Williams et al., 2019). The strength of the overturning is defined as the maximum depth below 500m of the AMOC streamfunction:

$$\text{AMOC}_z = \max\Psi(z). \tag{4.2}$$

We compute the AMOC strength over latitudes with known observational arrays, such as 57°N, 26.5°N, and 11°S. There was minimal difference on decadal time scales between each of the latitudes, thus we select 26.5°N as the reference latitude for AMOC changes. We then apply a low-pass filter to the AMOC and SSH anomalies to isolate the decadal signal.

Steric sea level change

As SSH levels are strongly linked to local changes in density from salinity and temperature anomalies (Landerer et al., 2007), we investigate regional steric sea level changes within the cycles. Note that in all cases regarding SSH, the long-term global mean per cycle is removed. We compute the steric sea level within each cycle as:

$$\zeta = \frac{1}{\rho_0}\int_{-H}^{0} \rho(T,S,p)dz, \tag{4.3}$$

where the reference density, ρ_0, is taken to be 1035 kg/m^3, ρ is density referenced to the surface, T, S, and P are temperature, salinity, and pressure. To understand the relative impact from thermal and haline contributions on steric SSH changes (Saenko et al., 2017), we split the steric sea level change into thermal and haline components. The thermosteric (ζ_{thermo}) and halosteric contribution (ζ_{halo}) of steric sea level change is computed as:

$$\Delta\zeta_{thermo} = -\frac{1}{\rho_0}\int_{-H}^{0} [\rho(T,S_{ref},P) - \rho_{ref}(S_{ref},T_{ref},p_{ref})]dz. \tag{4.4}$$

$$\Delta\zeta_{halo} = -\frac{1}{\rho_0}\int_{-H}^{0} [\rho(T_{ref},S,P) - \rho_{ref}(S_{ref},T_{ref},p_{ref})]dz. \tag{4.5}$$

In order to compute the thermo and halosteric changes within each cycle and compare between two decades, temperature and salinity are first locally detrended to remove model drift and the long term mean (1980–2021) of the cycle is then added denoted by a tilde above the variable i.e. $\tilde{S},\tilde{T}$. Thus the change in mean steric sea level compared to the long term mean per cycle is computed as:

$$\Delta\zeta(t,y,x)\frac{1}{\rho_0}[\rho(\tilde{T},\tilde{S},p) - \overline{\rho(\tilde{S},\tilde{T},p)}]dz, \tag{4.6}$$

where $\tilde{T}$ and $\tilde{S}$ is the detrended local temperature and salinity with the mean added. This can likewise be applied to the thermo and halosteric components, where the resulting steric

sea level change ($\zeta(t, y, z)$) can be averaged over particular decades and differences taken within the same cycle.

Results

High versus low AMOC phases

The magnitudes of AMOC mean strength and decadal variability differ between cycles (Figure 4.1a), where the first cycle consists of a stronger AMOC at 26.5°N compared to cycles 2–6. Note, in all cycles there are same periods in which the AMOC is particularly strong—from 1987–1997—and weak, from 2005–2015 (blue and red shaded areas in Figure 4.1a). Cycle 1 shows the strongest decadal variability, with a large increase in the late 80s to mid-90s, while the magnitude of low-frequent variability in cycles 2–6 decreases significantly. We compute mean differences in SSH (here, anomaly from global mean), ocean heat content (OHC), and freshwater content (FWC) between strong and weak phases of AMOC within each cycle with OHC and FWC linearly detrended prior to the differencing to account for internal model drift. Using these three parameter, we (1) show the fingerprint of AMOC variability on SSH and (2) demonstrate the robustness of the signal independent of the mean AMOC strength. We focus the discussion of the results on cycles 1 and 6, as the 6th cycle has a reduced AMOC strength and the model has the most time to spin up. The 6th cycle represents well cycles 3–5 as the mean AMOC and variability are nearly the same; cycles 2 and 3 are marked by strong transient AMOC change as the model adjusts to an equilibrium state.

In response to an AMOC weakening, i.e. low minus high AMOC phase, we find increased SSH in the western SPG and along the pathway of the GS, for cycle 1 and 6 (Figure 4.2a, b). The SSH differences are more pronounced in cycle 1 than 6 suggesting an impact by the magnitude of AMOC decadal variability. During lower AMOC phases, there is an increase in SSH particularly visible in the SPG, along the US East coast shelf break and—to a lesser degree—on the shelf, with the latter extending north all the way to Hudson Bay. A decrease in regional sea level is found further offshore, along the southern/eastern flank of the GS. Such a dipole pattern has been attributed to a distinctive fingerprint in AMOC changes (Mahajan et al., 2011), particularly in ocean-only models and coupled simulations (Zhang, 2008).

There has been evidence proposed by a number of studies (e.g. Böning et al., 2006; Yeager et al., 2012; Yeager and Danabasoglu, 2014) that changes in the AMOC and gyre circulations are fundamentally linked (Yeager, 2015). Assuming this is the case, an increase in SSH in the central SPG is indicative of a slow down of the gyre's circulation, which here can be linked to the multidecadal change from the 1990s to the 2000 but also to an overall weaker AMOC state (cycle 6 vs. 1). Cycle 1, which contains much stronger magnitude of decadal AMOC variability on average, shows a more pronounced SSH change compared to cycle 6 although differences are computing within each cycle between low and high AMOC phases. Note that the model-diagnosed SSH analyzed here is a direct function of the divergence of

the vertically integrated horizontal velocity. Hence, a weakening AMOC yielding a reduced northward transport must impose on the SSH field.

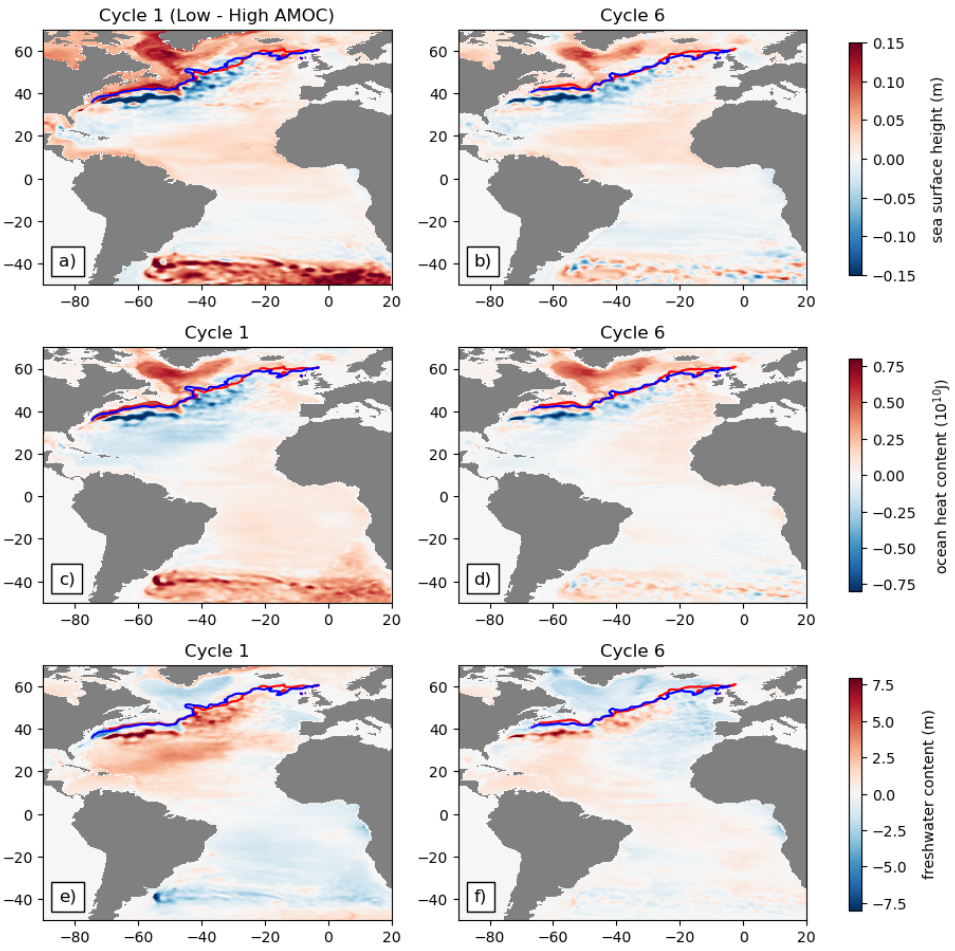

Fig. 4.2: (a). The SSH difference between lower (2005–2015) and higher (1987–1997) AMOC phases for cycle 1. (b) The SSH difference for cycle 6. Positive/negative values indicate an increase/decrease in regional SSH. (c) The difference in OHC (low minus high AMOC phase) for cycle 1. (d) The OHC difference in cycle 6. (e) FWC difference (low minus high AMOC) in cycle 1. (f) FWC difference in cycle 6. The blue/red contour shows the Gulf Stream axis during high/low AMOC phases.

We show that the SPG is more strongly affected than the subtropical gyre (STG) and hence the SSH gradient across the North Atlantic Current ought to weaken as well. Zhang, 2008 saw in a coupled simulation that the dipole pattern seen with a stronger AMOC is associated with an increased deep western boundary current, further increasing the northern recirculation gyre (marked on Figure 4.1b) causing GS to shift southwards (Zhang, 2008). In both, cycle 1 and 6 there are only small differences in the GS position between low and high AMOC phases. Here, we define the GS position by the 10°C isotherm at 100 m depth (red and blue contour in Figure 4.2). This is an often used criterion though it must be considered sub-optimal as, for instance, a coincident warming of GS waters sustains the more northward position of the isotherm and may mask an actual shift of the GS. The small changes in our case do make it difficult to identify a southward shift during a strong AMOC phase.

Within each cycle, there is a local increase in vertically integrated OHC of the entire water column in the SPG and near shore GS during the weaker AMOC phase in the early 2000s (Figure 4.2c, d), following a nearly identical pattern to the SSH differences. For both cycles 1 and 6 there is an increase in OHC in the most recent decade when AMOC decadal changes show a local weakening, but changes in OHC and FWC are primarily related to changes in the surface forcing. It is likely not caused by AMOC changes alone, which would affect the subsurface temperature and freshwater changes.

A stronger AMOC would lead to a warmer SPG from increased northward heat transport, while in this case there is a general cooling during the high AMOC phase. All cycles use the same atmospheric forcing, thus the differences between cycle 1 and 6 in OHC are minimal (Figure 4.2c, d), which is another indication of surface fluxes causing the OHC change between the two AMOC phases. Almost all ocean basins have seen an observed increase in warming since the 1990s (Cheng et al., 2017), where the most recent decades contains higher OHC in the SPG. However the similarity in both OHC and FWC patterns (Figure 4.2e, f) is likely due to the commonality of the surface forcing that is applied to each of the model cycles. The strong decrease in SSH and OHC but increase in FWC just south of the GS pathway, during the weaker AMOC phase is potentially from reduced convergence of heat and salt from reduced northward transport.

Cycle 1 shows increased OHCs, particularly along the GS extension and Labrador Sea (Figure 4.2c), where the GS is shifted just slightly southward. The recent warming partially explains for the increase in SSH in the subpolar gyre and near shore GS, as warmer waters expand locally increasing SSH. The western SPG appears to salinify in the recent years, during the weaker AMOC phase. It is in the western SPG which has a higher correlation to decadal changes in the North Atlantic Oscillation (NAO) than in the eastern SPNA where an opposite, recent cooling trend has been observed (Robson et al., 2016; Zhang and Yan, 2017). Megann et al., 2021 attributed these differences to a mixture of both NAO changes and large-scale ocean circulation.

In the Labrador and Irminger seas variability in OHC is dominated by surface heat flux variations and less influenced by AMOC changes (Megann et al., 2021). In fact, surface heat flux variations in these regions may imprint strongly on the AMOC (Böning et al., 2023). During the 1990s, when the NAO was positive, stronger winds and cold air outbreaks caused high surface heat loss and a strong AMOC, whereas in the mid-2000s, the lower AMOC phase coincided with a negative NAO phase. The AMOC strength associated with heat and salt transport into the SPG is rather inferior to the surface fluxes, which explains that the low AMOC state can be characterized by a positive OHC and negative FWC anomaly in both cycles 1 and 6 (Fig. 4.2c–f). Further, one would expect a greater disagreement between cycles 1 and 6 in the differences of OHC and FWC since the AMOC is considerably weaker in cycle 6. Thus variations in surface fluxes likely dominate the difference between low and high AMOC phases within each cycle, arguing that decadal variations in SSH can well be surface flux driven.

Decadal response of AMOC strength on sea surface height variability

To investigate whether there is a link between decadal variations in AMOC and SSH, we evaluate the correlation between the decadally filtered AMOC at 26.5°N and SSH per gridpoint. We find that the most robust signal occurs on decadal time scales (Figure 4.3a, b). In both cycles 1 and 6, significant highly negative correlations are found primarily in the western SPG and along the US East Coast. There are some positive correlations along the NAC pathway but their spatial extent is less. The evaluated correlations show a tripolar pattern of oscillating negative-positive-negative correlations in ech basin, the North and South Atlantic, divided by major frontal regions such as the GS/NAC. Since Lorbacher et al., 2010 found the same pattern for an interannually filtered SSH field, this suggests that decadal variability is concentrated in the same regions as high frequency variability.

The correlation between the SSH and AMOC at 26.5°N is larger in cycle 1 (Figure 4.3a) and has a correlation coefficient close to 1 everywhere along the western SPG and the Northwestern passages. Cycle 6 shows a similar pattern but with slightly lower correlation coefficients and with negative coefficients restricted primarily to the western SPG (Figure 4.3b). The magnitude of decadal AMOC variations reach greater amplitude in cycle 1, which could explain the larger correlation of decadal AMOC variability with SSH changes. The reminiscent tripole pattern in the North Atlantic seen in cycle 1 and 6, has been associated with gyre-scale oceanic heat convergence and the NAO, related to adjustment of large scale circulation from surface buoyancy and wind forcing (Volkov et al., 2019; Volkov et al., 2023). The tripole pattern is also a good proxy for OHC interannual variability in the North Atlantic (Volkov et al., 2023).

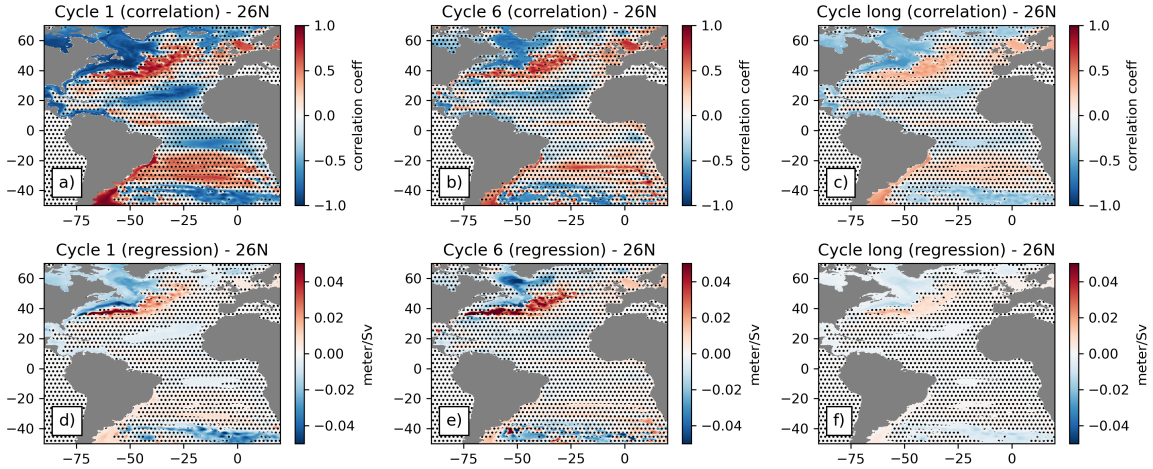

Fig. 4.3: (a). Correlation between the decadally filtered AMOC at 26.5°N and SSH for the 1st cycle. The black stippling indicates nonsignificant areas. (b) The correlation between the AMOC and SSH for the 6th cycle. (c). The correlation between the extended AMOC and SSH field, where the extended time series consists of 1980–2021 of the 1st cycle, then 1950–2021 of cycle 2–6. (d) The regression of the decadally filtered AMOC onto SSH for the 1st cycle. (e) The regression of the AMOC onto SSH for the 6th cycle. (f) The regression of the temporally extended AMOC onto the extended SSH field.

The correlation map suggests that on decadal time scales, changes in AMOC strength will be associated with local changes in SSH. Since a decadal filter is applied, higher frequency signals such as the interannual and daily variations from the wind forcing are smoothed out. While the correlation differs between the 1st and 6th cycle, the signal appears robust and significant near the western SPG and along the US East Coast. In order to validate whether this signal is indeed robust, rather than just a property of the individual cycles, we compute the correlation between the AMOC at 26.5°N and SSH of a longer extended time series combined of all 6 cycles (Figure 4.3c). The extended time series consists of the 1st cycle from 1980–2021, then cycles 2–6 from 1958–2021; the 1st cycle starts at 1980 to allow the 1st model run to spin up and adjust. The correlation between the extended AMOC time series and SSH field show significant, negative correlations as in the 1st and 6th cycle. The correlation coefficient magnitude is less than in the 1st and 6th cycles, however the time series is much longer and mimics longer term dedadal variability. The tripole is less visible, but there's a clear dipole in negative correlations in the North Atlantic with positive correlations southward of the GS.

There is an antiphase relationship when regressing the SSH field onto the AMOC at 26.5°N (Figure 4.3d, e). A strengthening/weakening of AMOC results in a decrease/increase in regional sea level along the western SPG and US east coast, whereas a strengthening in the AMOC results in a increase in SSH along the GS pathway, seen also by the positive correlations (Figure 4.3d, e). Interestingly, the regression appears weaker in the 1st cycle, despite the stronger AMOC signal (Figure 4.3d). The 6th cycle shows significant and more negative regression coefficients in the Labrador Sea, with stronger, positive regression coefficients along the GS track. The regression, while reduced in magnitude, is also visible in the extended time series and SSH field which includes all cycles (Figure 4.3f).

With a strengthened/weaker AMOC, there is a stronger/weaker Deep Western Boundary Current (DWBC) in the, interacting with steep topography along the US East coast, causing a southward/northward shift of the GS path (Zhang, 2008; Zhang et al., 2011; Sanchez-Franks and Zhang, 2015). From geostrophic balance, a weakening of AMOC and the associated northward GS shift in the upper ocean causes an increase in sea level along the western boundary of the Atlantic (Zhang et al., 2023). We find that on decadal time scales, there is a significant antiphase correlation between the AMOC at 26.5°N and SSH along the western SPG and US East coast. However the amplitudes of the correlation coefficients differ depending on the strength of the AMOC, with the 1st cycle containing higher correlation coefficients, but the 6th cycle having higher regression coefficients. This suggests that in the cycle with stronger decadal AMOC changes, the AMOC has a stronger impact on SSH compared to other processes. Further, the lower regression in cycle 1 could hint on an impact of non-linear adjustments, where a further weakening of the AMOC does not lead to a proportional change in SSH.

Steric sea level contributions within each cycle

Changes in SSH are strongly dependent on seawater density, which is influenced by sub-surface changes in temperature and salinity. Steric sea level change is associated with either the vertical expansion or contraction of water column from changes in local density

(Landerer et al., 2007). Steric sea level can be split up into two components: thermosteric and halosteric sea level changes (Hu et al., 2011; Henry et al., 2012; Li et al., 2016). SSH along the northeast US coast is closely linked to the horizontal gradient of steric sea level rise and mass redistribution in the ocean (Zhang et al., 2023). We determine the mean steric sea level changes and thermosteric and halosteric components between the low and high AMOC phases for both the 1st and 6th cycle (Figure 4.4). The steric sea level change patterns largely matches the difference patterns of the SSH model diagnostic showing a dipole in the North Atlantic (compare Fig. 4.4a, d with Fig. 4.2a, b). In both cycles, steric sea level increases in the SPG and along the US shelf break during the low AMOC state—on the continental shelf itself there is minimal steric sea level change due to the shallow water column (Landerer et al., 2007; Yin et al., 2009). Steric sea level is reduced to the south and east of the GS.

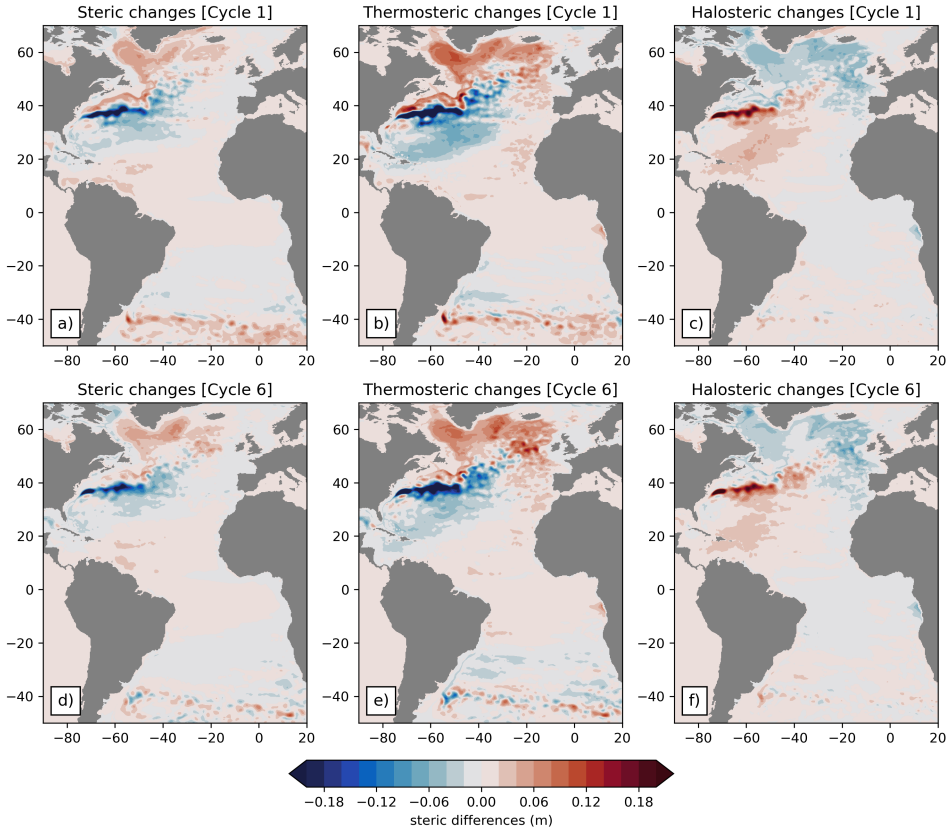

Fig. 4.4: (a) Steric sea level changes between the lower minus higher AMOC phase in the 1st cycle. Positive/negative values indicates greater/lower steric sea level changes in the lower AMOC phase compared to the higher AMOC phase. (b) The thermosteric sea level contribution between the two AMOC phases in the 1st cycle. (c) The halosteric sea level contribution for the 1st cycle. (d) The steric sea level change between weaker minus stronger AMOC phases in the 6th cycle. (e) The thermosteric sea level contribtion in the 6th cycle. (f) The halosteric sea level contribution in the 6th cycle.

The magnitudes do not differ much between the 1st and 6th cycle but there is an enhancement of slightly higher steric changes in the western SPG for the 1st cycle and in the Irminger Sea for the 6th cycle. In the recent decade when the AMOC was weaker, steric sea level

changes are positive indicating an expansion due to water column warming, which was already indicated by increased OHC (cf. Fig. 4.2a, d). Now, we can quantify the effect on the density by computing the differences in the thermosteric component. Figure 4.4b, e shows differences of about 10 cm for most of the SPG. Interestingly, this is more than the actual steric change of only 5–6 cm. Hence, we can expect a moderating contribution by haline contraction.

The halosteric component of steric sea level change, related to changes in salinity, show negative sea level changes in both cycles implying that during the weaker AMOC phase, there is a depression in halosteric sea level (Figure 4.4c, f). The low AMOC phase also showed a small salinification compared to the 1990s in the western SPG (Figure 4.2e, f), where thermosteric changes are partially compensated for halosteric sea level changes. Warmer (colder) seawater is usually saltier (fresher), where fresher (saline) water expands (contracts) (Johnson and Wijffels, 2011; Volkov et al., 2023). The magnitude of the thermosteric contribution exceeds that of the halosteric effect in most regions, indicating that the recent warming plays a dominant role over changes in salinity during a lower AMOC phase, except for the eastern North Atlantic, where thermal and haline effects seem to cancel out in total steric sea level. This is further evident in the positive increase in steric sea level over the SPG (Figure 4.4a, d).

There are minimal differences between the contributions of thermo- and halosteric sea level changes between the 1st and 6th cycle. The 1st cycle has a larger area of the eastern SPG, i.e. the Irminger Sea and south of Iceland, with negative halosteric sea level changes versus the 6th cycle. Overall, steric sea level was greater in the eastern SPG during the weaker AMOC period, indicated by the positive change between the two decades (Figure 4.4a, d), which also occurred during a negative NAO period. Studies have suggested the strong effect of NAO on steric sea level change in the SPG, where during a negative NAO phase where the AMOC was also weaker, westerlies are shifted southward, reducing transport and circulation in the SPNA (Llovel et al., 2011; Wang et al., 2015).

SSH changes and the relation to Greenland melting

While thermosteric changes appear to dominate steric sea level changes in the SPG and along the US East coast, changes in halosteric sea level are regionally important particularly with increased sea ice and land ice melt, changing precipitation patterns, and salt redistribution (Yin et al., 2010). Note, while sea ice melt does not add mass to the overall ocean mass, its regional redistribution by advection with winds and currents means a non-negligible freshwater transport. As the AMOC underwent a weakening period from 2005–2015, we ask whether the influence of Greenland melting at its current magnitudes may have also contributed to an overall increase in SSH. There are model experiments which explore the "hosing" of freshwater from Greenland to simulate a response or shut down of the AMOC. Sea level rise, cooling in the North Atlantic, and a general reduction in the ocean circulation are common responses (Jackson et al., 2015; Martin et al., 2022; Jackson et al., 2023).

As both experiments are spun from the 1st cycle, differing in FWFs from 1997 onwards, we do not compare the low (2005–2015) minus high (1987–1997) AMOC phases but rather

compare the differences between the two experiments during the weaker phase. Since the surface fluxes (apart from Greenland runoff) are nearly identical, and there are subtle differences in surface ocean properties between the two experiments only, the differences in SSH and hydrography are relatively small but—by means of the experimental setup—can be attributed directly to the enhancement of Greenland FWFs.

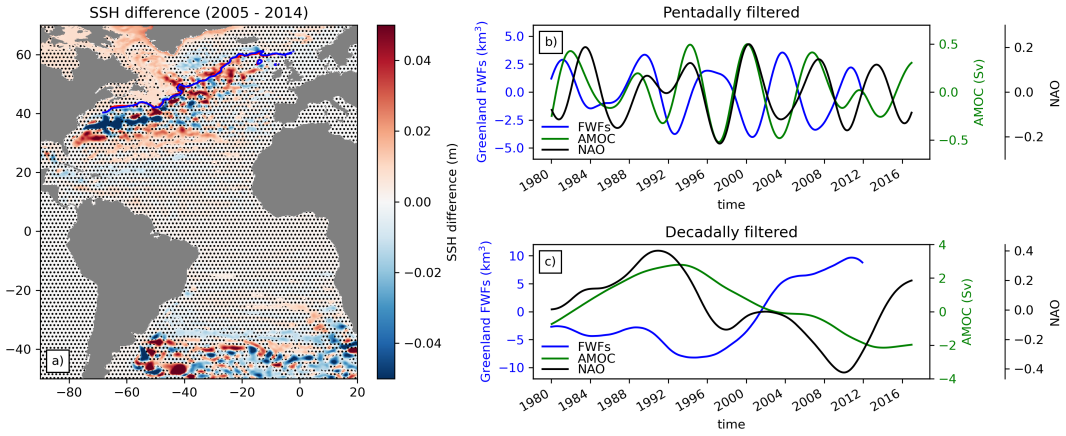

Fig. 4.5: (a). The SSH difference during the weaker AMOC phase (2005–2015) between the reference run with enhanced Greenland runoff as observed and the sensitivity experiment with reduced, climatological runoff. The black stippling indicates non-significant areas from bootstrapping. (b) Pentadally filtered Greenland FWFs (blue), AMOC at 26.5°N from the 1st cycle (Green), and the NAO (black). (c) Decadally filtered Greenland FWFs, AMOC at 26.5°, and the NAO from 1980–2016.

We find greater, localized SSHs in the reference experiment from enhanced Greenland runoff during the weaker AMOC phase, indicating that even at current magnitudes of increasing Greenland runoff, there's a mean, local increase in sea level (Figure 4.5a). The SSH increase is less in magnitude than between the low and high AMOC decadal phases within the 1st and 6th cycle (Figure 4.2a. b), but there is still an emerging response in increasing SSH given additional freshwater input from Greenland. In 2005–2015, the Northwest Atlantic Continental Shelf and Slope region (NWACSS) (area defined in Chen et al., 2020 and Holliday et al., 2020) shows a strong dipole response between positive SSH anomalies along NWASCSS and just south of the GS pathway shows a significant decrease in SSH where deeper waters are. These areas of negative and positive SSH difference along the GS pathway is significant, but these are likely due to internal variability and eddies, particularly as the GS is known to meander and a highly variable region. However the small but significant increase in SSH along the western SPG, East and West Greenland shelves are attributed to the enhanced freshwater input.

The next question we ask is how does meltwater compare with AMOC and NAO on longer time scales? We compute a pentadally and decadally filtered time series of Greenland FWFs from the Bamber et al., 2018 data set, the NAO, and AMOC at 26.5°N of the first cycle. There are two distinct regime shifts in the temporal variability of the Greenland FWFs in response to the AMOC and NAO, seen in the pentadally filtered time series (Figure 4.5b). From 1980–2000, there is a 1–2 year lag between the AMOC and NAO, with the AMOC leading. Llovel et al., 2011 found that shorter interannual time scales the North Atlantic

SSH variability was largely influenced by changes in ENSO from 1997–2004, but after 2004 the NAO dominated North Atlantic SSH changes (Llovel et al., 2011). This may be reflected in the pentadally filtered shift in Greenland FWFs and NAO changes, where there is an evident antiphase relationship with no lag (Figure 4.5b). Between the AMOC and NAO, there is a slight strengthening in the early 2000s and then weakening from 2008 onwards where the AMOC appears to lead Greenland FWFs, shifted by one year. Changes in the NAO have been linked to fluctuations in the surface mass balance of Greenland (Bevis et al., 2019), particularly the summer NAO index and melt events, where accelerated mass loss is attributed to negative phases of the NAO as air temperatures are warmer, prevalence of high pressure and clear-sky conditions, enhancing the melt-albedo feedback (Hanna et al., 2008; Bevis et al., 2019; Slater et al., 2021).

On longer, decadal time scales, there is barely one full cycle as the time series is relatively limited however there is an inverse relationship between AMOC and NAO changes vs. Greenland FWFs (Figure 4.5c). Both the NAO and AMOC show positive phase peaking in the early 90s, while Greenland FWFs show a decrease on the decadal time scales. Exceptionally cold winters in the Labrador Sea led to significantly reduced surface heat loss during the first half of the 1990s inducing a positive AMOC anomaly (Fox et al., 2022; Böning et al., 2023). This coincided with a positive NAO anomaly, conditions associated with cold winters and increased sea ice cover over the Labrador Sea and a strengthening in the SPG (Schulze et al., 2016), which on decadal time scales is associated with a strengthening of the AMOC. While Greenland melt is observed to fluctuate strongly with the summer NAO index on shorter time scales, the mean decadal AMOC and NAO phase show an antiphase relationship with Greenland FWFs. Melting is reduced in the early and mid-1990s likely from colder winter temperatures and in the early 2000s, the NAO and AMOC phase become more negative, associated with warmer conditions. Over the last two decades, Greenland melting is affected by both the overall increasing trend of global warming in conjunction with multidecadal variability over the Atlantic (Ruan et al., 2019).

Discussion and Conclusions

In this study, we employ a set of 6 OMIP cycle hindcast simulations of the VIKING20X model, all with the same atmospheric forcing but differing AMOC strengths and two additional ones with differing Greenland freshwater input, to assess the robustness of an AMOC fingerprint through decadal SSH changes. Our study reveals that on decadal time scales, there is a strong response between AMOC variability and regional SSH, particularly localized along the US East coast and western SPG. As the AMOC strengthens/weakens, the regional SSH decreases/increases in these regions. However the correlation coefficients differ depending on the strength of the AMOC within the model cycles. The 1st cycle contained the strongest AMOC, resulting in stronger SSH responses, with cycles 3–6 reducing in AMOC strength with minimal difference between them. Treating the OMIP cycle runs as an ensemble, where the primary difference between them is the strength of the AMOC due to the changing initial conditions per cycle, we find that strength of the AMOC within each cycle influences the magnitude of local SSH responses.

Two decadal periods of pronounced stronger and weaker AMOC were identified in the late 1980s to mid 1990s and the early to mid 2000s. Within each cycle, there is an observed response of increased SSH most prominent along the western SPG and US East Coast, associated with warmer subsurface temperatures and more saline water. The warming explains for the rise in SSH in the most recent decade, where thermosteric changes in the western SPG dominate over halosteric changes. However with warming temperatures and increased mass loss from Greenland, halosteric sea level changes may become more significant in the future.

Comparing the two decades within each model cycle, it becomes apperent that surface fluxes dominate over transport variations associated with the respective AMOC state in affecting OHC and FWC changes in the North Atlantic. Particularly as the surface fluxes are virtually the same between each of the model runs, given the common atmospheric forcing. However the prominent SSH response between these two decades, stronger and weaker AMOC phase, is a further implication that observed SSH changes may hint at a fingerprint of AMOC changes on decadal time scales, as seen by a number of studies (e.g. Zhang, 2008; Lorbacher et al., 2010; Mahajan et al., 2011).

Our study further compares two additional model runs, spun off the 1st cycle where one experiment has interannually varying and realistic Greenland-sourced freshwater forcing, while the other sensitivity experiment has suppressed runoff based on the climatological mean of 1961–2000. The AMOC strength is nearly the same between these two experiments, given the stronger magnitudes in the 1st cycle, but also the additional freshwater input is relatively small between the two experiments. However, we find that there is a significant although small increase in SSH along the East and West Greenland shelf and Labrador Sea from the additional freshwater. On slightly shorter pentadal time scales, there appears to be a regime shift between the NAO, AMOC, and Greenland FWFs, where prior to 2004 Greenland FWFs are leading but correlated with the NAO and AMOC. Whereas after 2004, the AMOC and particularly the NAO are anticorrelated with Greenland FWFs. On decadal time scales, this inverse relationship between Greenland melt and the NAO and AMOC are clearer, with negative NAO phases inducing further gradual melting of the Greenland ice sheet superimposed on additional warming from rising air temperatures.

We compare regional SSH changes between differing AMOC states and magnitudes on decadal time scales, finding a robust relationship between the two with a weaker/stronger AMOC resulting in greater/lower SSH primarily along the US East Coast and western SPG. Along with an imprint of additional Greenland meltwater increasing regional SSH during a weaker AMOC phase, primarily in the western SPG and East Greenland. Further questions also remain particularly on disentangling wind driven changes versus remotely forced buoyancy changes on AMOC variability. Since we focus on decadal time scales, the wind forcing and shorter time scales are relatively reduced from the filtering, however the influence and/or origin of decadal or low frequency wind changes is still yet to be explored, especially as the VIKING20X model is an ocean/sea-ice model not coupled to the atmosphere. It is also of major interest to better understand the connection between decadal AMOC variations and SSH, which are correlated but uncertainty is large about the causality of processes forcing SSH changes as surface heat fluxes and ocean heat transport both play a

role and hence atmospheric variability matters as much as variations in the GS and NAC (Little et al., 2019).

Lastly, it would be of interest to further investigate the strength of AMOC and its lagged effect on the SPG. Particularly as a stronger AMOC is associated with a stronger deep western boundary current, a local cooling and reduction in SSH, and a strengthening of the SPG (Zhang, 2008). However, as the SPG and AMOC mutually influence each other, a strong SPG also drives higher surface salinity and density where deep waters sink along the boundary, increasing the potential for deep convection and AMOC with a lag of a several years (Zhang, 2008, Sun et al., 2021). But as denser, deeper water propagates southward, the vertical stratification increases reducing the mixed layer depth in the SPG, causing a weakening of the SPG and a further warming/increase in SSH (Zhang, 2008). Understanding more of this lagged, feedback loop between the AMOC strength and its effect on the SPG is of interest particularly how the enhancement of warmer subsurface temperatures will likely influence Greenland runoff in the future.

5 Summary and Outlook

5.0.1 Synthesis

The aim of this thesis is to gain an improved understanding of the emerging impacts from enhanced runoff of meltwater from the Greenland ice sheet into the subpolar North Atlantic. The work is based primarily on output of the high resolution, strongly eddying ocean-sea ice model VIKING20X but also reanalysis products and observations are used for model validation and further insight into relevant processes. As mass loss and freshwater discharge from Greenland increase due to global warming, it is important to understand the hydrographic and dynamical changes from increased freshwater input into the subpolar North Atlantic. In the following, the primary findings and conclusions are documented from Chapters 2 to 4, along with a future outlook.

Chapter 2 focuses on freshwater propagation and variability along the East Greenland shelf from 1993–2019. As Greenland meltwater appears initially along the East and West Greenland Currents (EGC/WGC), a mixture of reanalysis, mooring observations, and high resolution model output is used to compare their representation of freshwater content variability along the EGC system and identify imprints of enhanced Greenland melt. Two strong melting events were detected in the coastal current in 2010 and 2012, with weaker magnitudes in the outer slope current. Freshwater is found to propagate from Fram Strait to Cape Farewell on time scales of 4–8 months, with the EGC system being fairly coherent with minimal offshore transport due to strong downwelling favorable winds. Weaker alongshore winds and less onshore Ekman transport, southeast of Greenland, result in a relaxation of the EGCC and lateral extension of current pathway, while enhanced onshore Ekman transport results in a narrowing of the current, pushing fresher water towards the shelf but allowing for saline intrusions from the interior.

The mixture of these processes further masks the input from Greenland runoff alone, particularly as Arctic export remains the dominant source of freshwater in the EGC system. In order to model these processes, sufficient horizontal grid resolution is required to properly represent mesoscale dynamics, particularly in resolving the narrow East Greenland boundary currents, as the EGCC contains the majority of freshwater. The surface boundary condition of having a realistically increasing and varying freshwater forcing representing Greenland runoff is also highly important for determining salinity changes along the EGC. The reanalysis GLORYS12 has sufficient resolution to distinguish the two East Greenland current cores, but a realistic representation of freshwater input from Greenland remains limited.

Chapter 3 transitions from East Greenland to West Greenland and the interior subpolar gyre (SPG). Freshwater along the EGC system remains relatively constrained near the shelf, with

some offshore export into the Nordic Seas and Irminger Sea (Duyck et al., 2022; Duyck and De Jong, 2023), while upwelling favorable winds and eddies can transport freshwater off West Greenland. In a model-sensitivity study tailored to quantify the potential impact of the observed increase in Greenland meltwater runoff two experiments only differing in the freshwater input were compared. It is found that with the observed enhancement beginning in the late 1990s, the most significant hydrographic changes form and emerge slowly along the boundary current system, which shows a local freshening and cooling. The intensifying density gradient from enhanced Greenland meltwater input between the less dense, fresh, cool shelf waters and the denser, saltier, warmer interior causes an increase in the boundary current, particularly at OSNAP West. The strong hydrographic and velocity front from the fast moving WGC system causes local instabilities leading to enhanced eddy formation, with increased eddy kinetic energy southeast of Cape Desolation.

From upwelling favorable winds, i.e. offshore Ekman transport, topographic differences particularly at Cape Desolation, and local instabilities, water can be transported off the shelf into the interior through eddies. The effect of increased Greenland runoff is then investigated on the winter mixed layer depth in the Labrador and Irminger Seas. Mixed layer depths in the eastern Irminger Sea are significantly deeper with enhanced meltwater, particularly seen in 2015–2018, a period of strong deep convection. Just prior to that period, in 2009–2013, relatively fresh waters reduce deep mixing in the Labrador Sea while still being entrained but now at shallower, mid to intermediate depths. These waters are then exported to the Irminger Sea as intermediate (subpolar mode) waters. This in turn contributed to a decrease in stratification between the surface and mid-depth in the eastern Irminger Sea, preconditioning it for deeper mixing prior to favorable atmospheric conditions triggering deep convection in 2015–2018. The realistic increase in freshwater input from Greenland has caused subtle but significant hydrographic changes, primarily along the boundary current from the observed near surface freshening and cooling. It is shown that freshwater from Greenland has affected, though not necessarily suppressed, deep mixing in the Labrador Sea from fresher water exported to the Irminger Sea at shallower depths, contributing to the deepening of winter mixed layer depth.

Lastly, in Chapter 4, a connection to the bigger picture of sea level rise and the Atlantic Meridional Overturning Circulation (AMOC) is drawn. While increasing Greenland meltwater runoff potentially has implications on the AMOC by enhancing stratification in the deep convection regions, it is investigated first that AMOC changes itself imprint on sea surface height in the Atlantic due to variations in heat and salt transport. In Chapter 4 larger scale variability from 1980–2021, focusing on SSH anomalies on decadal time scales as a potential AMOC fingerprint over the Atlantic Ocean is investigated. Using an ensemble of six ocean model hindcast simulations with differing AMOC strengths, we find that on decadal time scales, there is a strong, inverse relationship between AMOC and SSH variability specifically along the US East coast and western SPG. As the AMOC strengthens (weakens), the regional SSH there decreases (increases), but this relationship differs in magnitude depending on the strength of the AMOC per simulation. The AMOC strengthened in the late 1980s to mid 1990s and weakened in the early to mid 2000s. When computing SSH differences between these two periods (low minus high AMOC phases), there is a pronounced increase in SSH still seen along the western SPG and US East coast. The recent decade is associated with warmer temperatures and more saline water, opposite to what is expected under a weaker

AMOC (less northward heat and salt transport), indicating that ocean heat and freshwater content changes between the decades are directly related to the surface forcing.

As noted by other studies (e.g. Böning et al., 2016; Dukhovskoy et al., 2021; Swingedouw et al., 2022) and in Chapter 2 and 3, the amount of Greenland freshwater input at its current magnitudes has been too little to see a significant, far-reaching impact on large scale circulation changes in the SPNA or AMOC. However, comparing the SSH differences between the twin simulations but with varying inputs of runoff, there can be identified an increase in SSH along the east and west Greenland shelves and Labrador Sea. On decadal time scales, Greenland freshwater fluxes (FWFs) vary opposite to changes in the AMOC and North Atlantic Oscillation (NAO). During the 1990s, there was a positive NAO anomaly associated with cold winter conditions over the SPNA where the AMOC also strengthened during that period (Fox et al., 2022; Böning et al., 2023). Greenland FWFs largely reduced during that period, however this was also prior to the period in the early 2000s when runoff started to steadily increase (Bamber et al., 2018). This increase in runoff coincides with the lower AMOC and negative NAO phase but very likely was not of significant influence on such large-scale phenomena as stated above. On smaller, pentadal time scales, Greenland FWFs appear to vary with the AMOC and NAO but after 2004, there appears to be a regime shift where runoff becomes strongly anticorrelated with the NAO and in turn the AMOC, suggesting that Greenland runoff in recent years may be more susceptible to fluctuations in atmospheric variability, particularly as runoff may increase in the near distant future.

This thesis provides a look into the early impacts from increasing Greenland runoff, starting from changes along East and West Greenland boundary currents and then at larger scales focusing on SSH variability as a fingerprint of decadal AMOC changes and Greenland FWFs. There is still not yet a large imprint of Greenland meltwater alone on larger scale circulation changes, but in the future with the onset of even more mass loss from Greenland, these early impacts may have widespread consequences and changes for our future. In the following subsection, the key findings of this thesis are given, along with answers to the questions posed in the introduction. Then an outlook is provided along with emerging challenges and open questions for further research.

5.0.2 Summary of findings

The three research questions that were raised in the introduction are now answered as follows, utilizing the key findings summarized above:

What are the freshwater sources driving salinity changes along the Greenland boundary currents and how do they compare on seasonal time scales?

Freshwater sources include liquid and solid (icebergs) discharge from Greenland, liquid and solid (sea ice) export from the Arctic Ocean, and local sea ice melt. The first imprint of Greenland meltwater will be seen in the currents on and along the Greenland shelf. Along East Greenland, Arctic export remains the largest contributor to freshwater input thus having accurate magnitudes and variability of freshwater transport correctly represented in models

is of importance. The reanalysis GLORYS12 underestimates the liquid freshwater transport at Fram Strait by about 20 mSv. Greenland runoff peaks during summer (July, August, September) whereas the seasonality of sea ice melt differs depending on the location and latitude along the shelf. North of 67°N, sea ice melt occurs from summer to late fall, while along southeast Greenland south of 65°N, sea ice melt begins in late fall to early summer with no sea ice left to locally melt during summer. As freshwater propagates along the East Greenland shelf, it picks up additional freshwater from summer sea ice and meltwater along the way from glacier and fjord outlets. Alongshore winds constrain the majority of freshwater along East Greenland but weaken in summer when local melting is highest. It depends on the following winter and wind-driven conditions that will drive meltwater on or offshore, adjusting the lateral extent of the sharp salinity front of the EGC system. The differing and overlapping seasonality of sea ice melt and wind driven conditions also highlights the challenge of determining the imprint and signal from Greenland meltwater alone.

Are there observable changes in stratification and deep convection processes attributed to accelerated Greenland runoff?

Chapter 3 quantifies the direct impact from enhanced Greenland runoff in a model-sensitivity study. The primary concern of too much freshwater entering the SPNA from Greenland melt is from fresh and cool waters reaching deep convective areas where the low density waters may act as a lid, increasing stratification, and reducing the potential for vertical mixing. 2015–2018 was a period of strong deep convective activity in the Labrador and Irminger Seas with deeper mixed layers in the eastern Irminger Sea. Just prior to this period, in 2009–2013, it was found that Greenland meltwater runoff, which was tracked by a passive tracer in the model simulation, had accumulated in the Labrador Seas, and the model simulations using a passive tracer to track the meltwater show it well-distributed throughout the entire water column. A sensitivity experiment demonstrated not only that the accelerated meting of the Greenland ice sheet contributed to a greater freshwater content in the Labrador Sea deep convection region, but also indicated the advection of a fresher intermediate water mass at mid-depth to the Irminger Sea to occur at a shallower depth than in the case with climatological Greenland runoff. This led to a reduced stratification above 1000 m in the easter Irminger Sea, which now can be attributed to the input of additional meltwater prior to ∼2015. The combination of increased meltwater residing in the upper layers (200–1000 m) decreasing stratification plus favorable preconditioning for deep mixing in 2009–2013 certainly favored the eastward extension of the deep convection region and supported the reported shift into the Irminger Sea. This indicates the early imprint that Greenland runoff may have on stratification in deep convective processes.

What are the effects from increased meltwater runoff on large scale circulation changes i.e. AMOC and the SPG, particularly on pentadal to decadal time scales?

There is still too little additional freshwater input to see an imprint of Greenland melt associated with changes on the AMOC (Böning et al., 2016; Swingedouw et al., 2022). Chapter 4 investigates the fingerprint of AMOC variability on SSH on decadal time scales in an ensemble of models (OMIP cycles), including a detailed discussion of thermal and haline contributions to the steric sea level changes found in response to AMOC variations.

Thermal effects appear to dominate haline contributions to SSH changes, however with increased Greenland meltwater in the model-sensitivity study, we see a small, local response of rising SSHs in the experiment with enhanced Greenland runoff, during a phase of weaker AMOC (2005–2015). The elevation in regional SSH is found along the western SPG, East Greenland shelf, and US East coast, where the weakening in the AMOC is associated with an increase in SSH on decadal time scales based on a correlation and regression analysis. Strong internal variability from eddies were primarily seen along the Gulf Stream and the Antarctic Circumpolar Current. On pentadal time scales, after 2004, the NAO and AMOC showed a strong antiphase relationship with Greenland FWFs (Bamber et al., 2018), while on the decadal time scales there was also an associated but lagged antiphase relationship. Greenland FWFs are reduced in the early and mid-1990s, likely from colder winter temperatures and cold air outbreaks from the Canadian coast associated with positive NAO conditions. In the early 2000s, the NAO and AMOC phase become more negative, associated with warmer conditions. Note that, even though the model cycles have a relatively longer time series extending from 1958–2021, we only looked at 1980 onwards to allow time for model spin up. But even with a "longer" time series, on decadal time scales there is barely a full cycle, making it difficult to comment on the decadal changes between the AMOC and Greenland FWFs beyond speculation.

5.0.3 Emerging Challenges and Outlook

The framework of this thesis is split into three chapters, first focusing on the east and west Greenland boundary currents and then moving outward and investigating the AMOC on SSH variability in the North Atlantic on decadal time scales. It is evident that the freshwater contribution from Greenland runoff is relatively minimal compared to other freshwater fluxes, such as Arctic Ocean export and sea ice melt in the subpolar latitudes. One of the primary challenges in understanding and quantifying local changes from Greenland meltwater is adequately resolving of the fast and narrow boundary currents along the Greenland shelf. With regards to VIKING20X model simulations used, a sufficient resolution of finer than 1/20° is necessary for resolving the boundary currents. However, it is also the surface boundary conditions that significantly impact the realistic distribution and signal of Greenland meltwater as seen in salinity. Quantifying freshwater from Greenland runoff is a challenge, as freshwater content and transport are based on a local reference salinity, so one must already make an assumption. There are no physical constraints for determining a reference salinity, thus this can lead to ambiguities (Schauer and Losch, 2019).

There is not an interactive ice sheet or atmosphere coupled to the model, missing representation of fjord circulation, and the distribution of liquid meltwater being applied only to the surface and coastlines may all be obscuring how Greenland runoff is distributed throughout the water column and SPNA. There are also no icebergs present in the simulation and additional freshwater input, which underestimates the amounts of freshwater, especially as icebergs represent about half of Greenland's yearly mass loss (Marson et al., 2018). Icebergs can carry freshwater far from the coast (Martin and Adcroft, 2010) and are more likely to be relevant for open ocean convection (Marson et al., 2018).

This thesis has focused primarily on the western Labrador Sea when determining local impacts from enhanced freshwater (Chapter 3 and 4), but recent studies have shown that subpolar overturning and AMOC are primarily composed of waters formed east of Greenland in the Irminger Sea, Iceland basins and Nordic Seas (Lozier et al., 2019; Petit et al., 2020; Li et al., 2021). Despite substantial convection and deep water formation in the Labrador Sea, it was found that this region contributes minimally to the total overturning (Lozier et al., 2019), thus it is crucial to further investigate freshwater exchanges east of Greenland.

There is still much that is unknown about the emerging impacts of Greenland runoff, particularly how the freshwater input will evolve over time. As mesoscale eddies play a large role in transporting freshwater offshore, it would be of interest to quantify how much of Greenland meltwater is propagated offshore via mesoscale dynamics. Distinguishing the individual amounts of freshwater from Greenland melt, sea ice, liquid Arctic export alone would be of interest to determine the relative contribution of each freshwater component. Spall et al., 2024 explored the dominant mechanisms exporting solid and liquid freshwater from the EGC but used an idealized numerical model.

While this thesis primarily analyzes ocean/sea-ice model output, continued observations along with further model development are critical to understand and monitor the freshwater changes associated with Greenland runoff in the subpolar North Atlantic and its potential effect on the large scale circulation.

6 Acknowledgement

Thank you first and foremost to Torge Martin for your supervision, trust, and support. This journey has had its challenges but without your encouragement and guidance it would have had many more. Thank you for always having an open door for "pop-in hours" and patience for when I was wandering astray. I would like to thank Arne Biastoch and Johannes Karstensen for your invaluable feedback during the Thesis Advisory Committee meetings. Arne, thank you for all these opportunities to jump onboard the AMOC project, joining the DRAKKAR workshops, and making the trip to Greenland possible. I've always admired the way you gracefully lead OD. Johannes, your expertise in the North Atlantic and honest feedback has been crucial; you really guided me along the wavy and windy East Greenland Current.

Thank you to Joakim Kjellsson for being the second reviewer of this thesis; I really enjoyed your climDAT tutorials way back when! Thank you to Willi Rath aka Willi the wizard, coined by others, for finding clarity in my mired analysis. Your kindness, patience, support, and just knowledge of all things, science, technical, and life in general are just incredible. I always enjoyed our coffee breaks and lunches in the kitchen and I honestly don't know if I could have made it to this point without you, so I thank you from the bottom of my heart. Thank you Franziska Schwarzkopf for sharing and enlightening me with your genius on ocean modeling. I wish we could have gotten to know each other better earlier on in the PhD but am very honored to have been able to work on two projects (one still ongoing) with you!

I would like to express particular thanks to the Ocean Dynamics team – it really takes a village; without each and everyone one of your consistent support, expertise, and kindness, I would not be here. I would like to also acknowledge all the colleagues who've become friends at GEOMAR: Lara Schmittman – best office-mate! You are a big inspiration to me in science; our talks ranging from navigating academia to scheduling yoga classes together have deeply impacted me. I am so happy you found your way to OD. Mathias Zeller – it has been so nice getting to know you over the years. I remember the day we first met on the west shore rooftop and what a long way we've come since then. I've always loved our wraps dinners and game nights. Sweety Mohanty – I've always enjoyed our talks, walks, and dinners; you've always been a breath of fresh air. Tobias Schulzki – thank you for bearing with all my messages on Mattermost, answering all my random questions, and for reading large parts of this thesis. I'll always remember fondly of our fun times in Grenoble and celebrating your birthday on those occasions. The ME crew: Sedat Gözlet, Abhishek Savita, Malin Ödalen, amongst others – you all made me wish I were a part of ME sometimes! Fehmi Dilmahamod – for all the discussions on eddies and freshwater in the Labrador Sea and the fun chats on the ferry. Thank you for reading parts of this thesis too.

I would like to thank the ACDC-GRISO and Bad Honnef summer school communities; from mind-bending scientific discussions to late night shenanigans, I am very grateful to have met such incredible and inspiring people. Thank you to the NEMO ocean modeling/DRAKKAR

workshop community for all the feedback, insight, and knowledge on all things ocean, climate and modeling related. What a fun and inspiring group!

Thank you to the fabulous DR community and DokTeam here at GEOMAR, particularly Naveen, Isabel, Louis-Maxime, Bruna, and Daniel, for all the fun times from late nights at Phollkomplex to organizing the DR retreat: a beer, a shot, and be home by midnight! I would like to express my thanks to this beautiful, tight-knit community in Kiel, particularly "core Kiel": the bouldering, Winterschwimmen, spikeball groups... just to name a few. I love our many Whatsapp group chats with all the same people. You have all made my experience in Kiel extremely special and in large part, why I have come to call Kiel home. I know that even if we're spread out across the world, we'll always have each other. Particular shout out to Clara, Neha, Alexa, and Inga for all the lovely times. Cheers to many more!

I am deeply grateful to Irene and Evelyn for always rooting for me; our memorable summer nights on the terrace from Bremen to Crete, and just knowing when I'd see you both again, always keeps me going. Thank you to all my east coast family, friends, and fellow Smithies. I love you all so much and while I've been away for longer periods of time than I'd like, I never felt out of touch. Special thanks to Bella and Ya, so proud and in awe of you both, and to my parents Andrea and Greta for your unwavering support, love, care and for being my talk radio during the quieter moments.

Lastly, thank you to Ishan for being my home away from home and thank you to this magical little city called Kiel.

References

Bacon, S., Reverdin, G., Rigor, I. G., & Snaith, H. M. (2002). A freshwater jet on the east Greenland shelf. *Journal of Geophysical Research: Oceans*, *107*(C7), 5–1–5–16. https://doi.org/10.1029/2001JC000935

Bakker, P., Schmittner, A., Lenaerts, J. T. M., Abe-Ouchi, A., Bi, D., van den Broeke, M. R., Chan, W.-L., Hu, A., Beadling, R. L., Marsland, S. J., Mernild, S. H., Saenko, O. A., Swingedouw, D., Sullivan, A., & Yin, J. (2016). Fate of the Atlantic Meridional Overturning Circulation: Strong decline under continued warming and Greenland melting. *Geophysical Research Letters*, *43*(23), 12, 252–12, 260. https://doi.org/10.1002/2016GL070457

Bamber, J. L., Tedstone, A. J., King, M. D., Howat, I. M., Enderlin, E. M., van den Broeke, M. R., & Noel, B. (2018). Land Ice Freshwater Budget of the Arctic and North Atlantic Oceans: 1. Data, Methods, and Results. *Journal of Geophysical Research: Oceans*, *123*(3), 1827–1837. https://doi.org/10.1002/2017JC013605

Belkin, I. M. (2004). Propagation of the "Great Salinity Anomaly" of the 1990s around the northern North Atlantic. *Geophysical Research Letters*, *31*(8). https://doi.org/10.1029/2003GL019334

Belkin, I. M., Levitus, S., Antonov, J., & Malmberg, S.-A. (1998). "Great Salinity Anomalies" in the North Atlantic. *Progress in Oceanography*, *41*(1), 1–68. https://doi.org/10.1016/S0079-6611(98)00015-9

Bersch, M., Yashayaev, I., & Koltermann, K. P. (2007). Recent changes of the thermohaline circulation in the subpolar North Atlantic. *Ocean Dynamics*, *57*(3), 223–235. https://doi.org/10.1007/s10236-007-0104-7

Bevis, M., Harig, C., Khan, S. A., Brown, A., Simons, F. J., Willis, M., Fettweis, X., van den Broeke, M. R., Madsen, F. B., Kendrick, E., Caccamise, D. J., van Dam, T., Knudsen, P., & Nylen, T. (2019). Accelerating changes in ice mass within Greenland, and the ice sheet's sensitivity to atmospheric forcing. *Proceedings of the National Academy of Sciences*, *116*(6), 1934–1939. https://doi.org/10.1073/pnas.1806562116

Biastoch, A., Böning, C. W., Getzlaff, J., Molines, J.-M., & Madec, G. (2008). Causes of Interannual–Decadal Variability in the Meridional Overturning Circulation of the Midlatitude North Atlantic Ocean. *Journal of Climate*, *21*(24), 6599–6615. https://doi.org/10.1175/2008JCLI2404.1

Biastoch, A., Schwarzkopf, F. U., Getzlaff, K., Rühs, S., Martin, T., Scheinert, M., Schulzki, T., Handmann, P., Hummels, R., & Böning, C. W. (2021). Regional imprints of changes in the Atlantic Meridional Overturning Circulation in the eddy-rich ocean model VIKING20X. *Ocean Science*, *17*(5), 1177–1211. https://doi.org/10.5194/os-17-1177-2021

Bingham, R. J., & Hughes, C. W. (2009). Signature of the Atlantic meridional overturning circulation in sea level along the east coast of North America. *Geophysical Research Letters*, *36*(2). https://doi.org/10.1029/2008GL036215

Böning, C. W., Behrens, E., Biastoch, A., Getzlaff, K., & Bamber, J. L. (2016). Emerging impact of Greenland meltwater on deepwater formation in the North Atlantic Ocean. *Nature Geoscience*, *9*(7), 523–527. https://doi.org/10.1038/ngeo2740

Böning, C. W., Scheinert, M., Dengg, J., Biastoch, A., & Funk, A. (2006). Decadal variability of subpolar gyre transport and its reverberation in the North Atlantic overturning. *Geophysical Research Letters*, *33*(21). https://doi.org/10.1029/2006GL026906

Böning, C. W., Wagner, P., Handmann, P., Schwarzkopf, F. U., Getzlaff, K., & Biastoch, A. (2023). Decadal changes in Atlantic overturning due to the excessive 1990s Labrador Sea convection. *Nature Communications*, *14*(1), 4635. https://doi.org/10.1038/s41467-023-40323-9

Bracco, A., Pedlosky, J., & Pickart, R. S. (2008). Eddy Formation near the West Coast of Greenland. *Journal of Physical Oceanography*, *38*(9), 1992–2002. https://doi.org/10.1175/2008JPO3669.1

Brandt, P., Schott, F. A., Funk, A., & Martins, C. S. (2004). Seasonal to interannual variability of the eddy field in the Labrador Sea from satellite altimetry. *Journal of Geophysical Research: Oceans*, *109*(C2). https://doi.org/10.1029/2002JC001551

Brearley, J. A., Pickart, R. S., Valdimarsson, H., Jonsson, S., Schmitt, R. W., & Haine, T. W. N. (2012). The East Greenland boundary current system south of Denmark Strait. *Deep Sea Research Part I: Oceanographic Research Papers*, *63*, 1–19. https://doi.org/10.1016/j.dsr.2012.01.001

Brodeau, L., & Koenigk, T. (2016). Extinction of the northern oceanic deep convection in an ensemble of climate model simulations of the 20th and 21st centuries. *Climate Dynamics*, *46*(9), 2863–2882. https://doi.org/10.1007/s00382-015-2736-5

Bryan, K. (1996). The steric component of sea level rise associated with enhanced greenhouse warming: A model study. *Climate Dynamics*, *12*(8), 545–555. https://doi.org/10.1007/BF00207938

Buckley, M. W., & Marshall, J. (2016). Observations, inferences, and mechanisms of the Atlantic Meridional Overturning Circulation: A review. *Reviews of Geophysics*, *54*(1), 5–63. https://doi.org/10.1002/2015RG000493

Caesar, L., Rahmstorf, S., Robinson, A., Feulner, G., & Saba, V. (2018). Observed fingerprint of a weakening Atlantic Ocean overturning circulation. *Nature*, *556*(7700), 191–196. https://doi.org/10.1038/s41586-018-0006-5

Castelao, R. M., Luo, H., Oliver, H., Rennermalm, A. K., Tedesco, M., Bracco, A., Yager, P. L., Mote, T. L., & Medeiros, P. M. (2019). Controls on the Transport of Meltwater From the Southern Greenland Ice Sheet in the Labrador Sea. *Journal of Geophysical Research: Oceans*, *124*(6), 3551–3560. https://doi.org/10.1029/2019JC015159

Chafik, L., Penny Holliday, N., Bacon, S., Baker, J. A., Desbruyères, D., Frajka-Williams, E., & Jackson, L. C. (2023). Observed mechanisms activating the recent subpolar North Atlantic Warming since 2016. *Philosophical Transactions of the Royal Society A: Mathematical, Physical and Engineering Sciences*, *381*(2262), 20220183. https://doi.org/10.1098/rsta.2022.0183

Chanut, J., Barnier, B., Large, W., Debreu, L., Penduff, T., Molines, J. M., & Mathiot, P. (2008). Mesoscale Eddies in the Labrador Sea and Their Contribution to Convection and Restratification. *Journal of Physical Oceanography*, *38*(8), 1617–1643. https://doi.org/10.1175/2008JPO3485.1

Chen, Z., Kwon, Y.-O., Chen, K., Fratantoni, P., Gawarkiewicz, G., & Joyce, T. (2020). Long-Term SST Variability on the Northwest Atlantic Continental Shelf and Slope. *Geophysical Research Letters*, *47*. https://doi.org/10.1029/2019GL085455

Cheng, L., Trenberth, K. E., Fasullo, J., Boyer, T., Abraham, J., & Zhu, J. (2017). Improved estimates of ocean heat content from 1960 to 2015. *Science Advances*, *3*(3), e1601545. https://doi.org/10.1126/sciadv.1601545

Cheng, W., Chiang, J. C. H., & Zhang, D. (2013). Atlantic Meridional Overturning Circulation (AMOC) in CMIP5 Models: RCP and Historical Simulations. *Journal of Climate*, *26*(18), 7187–7197. https://doi.org/10.1175/JCLI-D-12-00496.1

Colombo, P., Barnier, B., Penduff, T., Chanut, J., Deshayes, J., Molines, J.-M., Le Sommer, J., Verezemskaya, P., Gulev, S., & Treguier, A.-M. (2020). Representation of the Denmark Strait overflow in a z-coordinate eddying configuration of the NEMO (v3.6) ocean model: Resolution and parameter impacts. *Geoscientific Model Development*, *13*(7), 3347–3371. https://doi.org/10.5194/gmd-13-3347-2020

Crivellari, S. (2018, January). *Effects of abrupt changes in the Atlantic meridional overturning circulation over the Amazon Basin: An isotopic and elemental approach* [Doctoral dissertation]. https://doi.org/10.13140/RG.2.2.32595.20000

Cromwell, D., Shaw, A. G. P., Challenor, P., Houseago-Stokes, R. E., & Tokmakian, R. (2007). Towards measuring the meridional overturning circulation from space. *Ocean Science*, *3*(2), 223–228. https://doi.org/10.5194/os-3-223-2007

Debreu, L., Vouland, C., & Blayo, E. (2008). AGRIF: Adaptive grid refinement in Fortran. *Computers & Geosciences*, *34*(1), 8–13. https://doi.org/10.1016/j.cageo.2007.01.009

DeGrandpre, M. D., Körtzinger, A., Send, U., Wallace, D. W. R., & Bellerby, R. G. J. (2006). Uptake and sequestration of atmospheric CO2 in the Labrador Sea deep convection region. *Geophysical Research Letters*, *33*(21). https://doi.org/10.1029/2006GL026881

de Jong, M. F., Oltmanns, M., Karstensen, J., & de Steur, L. (2018). Deep Convection in the Irminger Sea Observed with a Dense Mooring Array. *Oceanography*, *31*(1), 50–59. https://doi.org/10.5670/oceanog.2018.109

de Jong, M. F., van Aken, H. M., Våge, K., & Pickart, R. S. (2012). Convective mixing in the central Irminger Sea: 2002–2010. *Deep Sea Research Part I: Oceanographic Research Papers*, *63*, 36–51. https://doi.org/10.1016/j.dsr.2012.01.003

de Jong, M. F., & de Steur, L. (2016). Strong winter cooling over the Irminger Sea in winter 2014–2015, exceptional deep convection, and the emergence of anomalously low SST. *Geophysical Research Letters*, *43*(13), 7106–7113. https://doi.org/10.1002/2016GL069596

Desbruyères, D., Chafik, L., & Maze, G. (2021). A shift in the ocean circulation has warmed the subpolar North Atlantic Ocean since 2016. *Communications Earth & Environment*, *2*(1), 1–9. https://doi.org/10.1038/s43247-021-00120-y

Deshayes, J., & Frankignoul, C. (2008). Simulated Variability of the Circulation in the North Atlantic from 1953 to 2003. *Journal of Climate*, *21*(19), 4919–4933. https://doi.org/10.1175/2008JCLI1882.1

Dickson, R., Lazier, J., Meincke, J., Rhines, P., & Swift, J. (1996). Long-term coordinated changes in the convective activity of the North Atlantic. *Progress in Oceanography*, *38*(3), 241–295. https://doi.org/10.1016/S0079-6611(97)00002-5

Dickson, R. R., Meincke, J., Malmberg, S.-A., & Lee, A. J. (1988). The “great salinity anomaly” in the Northern North Atlantic 1968–1982. *Progress in Oceanography*, *20*(2), 103–151. https://doi.org/10.1016/0079-6611(88)90049-3

Dukhovskoy, D. S., Yashayaev, I., Chassignet, E. P., Myers, P. G., Platov, G., & Proshutinsky, A. (2021). Time Scales of the Greenland Freshwater Anomaly in the Subpolar North Atlantic. *Journal of Climate*, *34*(22), 8971–8987. https://doi.org/10.1175/JCLI-D-20-0610.1

Dukhovskoy, D. S., Yashayaev, I., Proshutinsky, A., Bamber, J. L., Bashmachnikov, I. L., Chassignet, E. P., Lee, C. M., & Tedstone, A. J. (2019). Role of Greenland Freshwater Anomaly in the Recent Freshening of the Subpolar North Atlantic. *Journal of Geophysical Research: Oceans*, *124*(5), 3333–3360. https://doi.org/10.1029/2018JC014686

Dukhovskoy, D. S., Myers, P. G., Platov, G., Timmermans, M.-L., Curry, B., Proshutinsky, A., Bamber, J. L., Chassignet, E., Hu, X., Lee, C. M., & Somavilla, R. (2016). Greenland freshwater pathways in the sub-Arctic Seas from model experiments with passive tracers. *Journal of Geophysical Research: Oceans*, *121*(1), 877–907. https://doi.org/10.1002/2015JC011290

Duyck, E., & De Jong, M. F. (2023). Cross-Shelf Exchanges Between the East Greenland Shelf and Interior Seas. *Journal of Geophysical Research: Oceans*, *128*(7), e2023JC019905. https://doi.org/10.1029/2023JC019905

Duyck, E., Gelderloos, R., & de Jong, M. F. (2022). Wind-Driven Freshwater Export at Cape Farewell. *Journal of Geophysical Research: Oceans*, *127*(5), e2021JC018309. https://doi.org/10.1029/2021JC018309

Duyck, E., & De Jong, M. F. (2021). Circulation Over the South-East Greenland Shelf and Potential for Liquid Freshwater Export: A Drifter Study. *Geophysical Research Letters*, *48*(5), e2020JB020886. https://doi.org/10.1029/2020GL091948

Eden, C., & Böning, C. (2002). Sources of Eddy Kinetic Energy in the Labrador Sea. *Journal of Physical Oceanography*, *32*(12), 3346–3363. https://doi.org/10.1175/1520-0485(2002)032<3346:SOEKEI>2.0.CO;2

Fettweis, X., Hanna, E., Lang, C., Belleflamme, A., Erpicum, M., & Gallée, H. (2013). *Brief communication* "Important role of the mid-tropospheric atmospheric circulation in the recent surface melt increase over the Greenland ice sheet". *The Cryosphere*, *7*(1), 241–248. https://doi.org/10.5194/tc-7-241-2013

Fichefet, T., Poncin, C., Goosse, H., Huybrechts, P., Janssens, I., & Le Treut, H. (2003). Implications of changes in freshwater flux from the Greenland ice sheet for the climate of the 21st century. *Geophysical Research Letters*, *30*(17). https://doi.org/10.1029/2003GL017826

Fischer, J., Schott, F. A., & Dengler, M. (2004). Boundary Circulation at the Exit of the Labrador Sea. *Journal of Physical Oceanography*, *34*(7), 1548–1570. https://doi.org/10.1175/1520-0485(2004)034<1548:BCATEO>2.0.CO;2

Flatau, M. K., Talley, L., & Niiler, P. P. (2003). The North Atlantic Oscillation, Surface Current Velocities, and SST Changes in the Subpolar North Atlantic. *Journal of Climate*, *16*(14), 2355–2369. https://doi.org/10.1175/2787.1

Foukal, N. P., Gelderloos, R., & Pickart, R. S. (2020). A continuous pathway for fresh water along the East Greenland shelf. *Science Advances*, *6*(43), eabc4254. https://doi.org/10.1126/sciadv.abc4254

Fox, A. D., Handmann, P., Schmidt, C., Fraser, N., Rühs, S., Sanchez-Franks, A., Martin, T., Oltmanns, M., Johnson, C., Rath, W., Holliday, N. P., Biastoch, A., Cunningham, S. A., & Yashayaev, I. (2022). Exceptional freshening and cooling in the eastern subpolar North Atlantic caused by reduced Labrador Sea surface heat loss. *Ocean Science*, *18*(5), 1507–1533. https://doi.org/10.5194/os-18-1507-2022

Fox-Kemper, B., Hewitt, H. T., Xiao, C., Aðalgeirsdóttir, G., Drijfhout, S. S., Edwards, T. L., Golledge, N. R., Hemer, M., Kopp, R. E., Krinner, G., Mix, A., Notz, D., Nowicki, S., Nurhati, I. S., Ruiz, L., Sallée, J.-B., Slangen, A. B. A., & Yu, Y. (2021). Ocean, cryosphere and sea level change. In *Climate change 2021: The physical science basis* (pp. 1211–1362). Cambridge University Press. https://doi.org/10.1017/9781009157896.011

Frajka-Williams, E., Ansorge, I. J., Baehr, J., Bryden, H. L., Chidichimo, M. P., Cunningham, S. A., Danabasoglu, G., Dong, S., Donohue, K. A., Elipot, S., Heimbach, P., Holliday, N. P., Hummels, R., Jackson, L. C., Karstensen, J., Lankhorst, M., Le Bras, I. A., Lozier, M. S., McDonagh, E. L., … Wilson, C. (2019). Atlantic Meridional Overturning Circulation: Observed Transport and Variability. *Frontiers in Marine Science*, *6*.

Frajka-Williams, E., Rhines, P. B., & Eriksen, C. C. (2014). Horizontal Stratification during Deep Convection in the Labrador Sea. *Journal of Physical Oceanography*, *44*(1), 220–228. https://doi.org/10.1175/JPO-D-13-069.1

Frankignoul, C., Deshayes, J., & Curry, R. (2009). The role of salinity in the decadal variability of the North Atlantic meridional overturning circulation. *Climate Dynamics*, *33*(6), 777–793. https://doi.org/10.1007/s00382-008-0523-2

Fratantoni, D. M. (2001). North Atlantic surface circulation during the 1990's observed with satellite-tracked drifters. *Journal of Geophysical Research: Oceans*, *106*(C10), 22067–22093. https://doi.org/10.1029/2000JC000730

Fratantoni, P. S., & Pickart, R. S. (2007). The Western North Atlantic Shelfbreak Current System in Summer. *Journal of Physical Oceanography*, *37*(10), 2509–2533. https://doi.org/10.1175/JPO3123.1

Fu, Y., Li, F., Karstensen, J., & Wang, C. (2020). A stable Atlantic Meridional Overturning Circulation in a changing North Atlantic Ocean since the 1990s. *Science Advances*, *6*(48), eabc7836. https://doi.org/10.1126/sciadv.abc7836

Ganachaud, A., & Wunsch, C. (2000). Improved estimates of global ocean circulation, heat transport and mixing from hydrographic data. *Nature*, *408*(6811), 453–457. https://doi.org/10.1038/35044048

Gelderloos, R., Katsman, C. A., & Drijfhout, S. S. (2011). Assessing the Roles of Three Eddy Types in Restratifying the Labrador Sea after Deep Convection. *Journal of Physical Oceanography*, *41*(11), 2102–2119. https://doi.org/10.1175/JPO-D-11-054.1

Gelderloos, R., Straneo, F., & Katsman, C. A. (2012). Mechanisms behind the Temporary Shutdown of Deep Convection in the Labrador Sea: Lessons from the Great Salinity Anomaly Years 1968–71. *Journal of Climate*, *25*(19), 6743–6755. https://doi.org/10.1175/JCLI-D-11-00549.1

Gerdes, R., Hurlin, W., & Griffies, S. M. (2006). Sensitivity of a global ocean model to increased run-off from Greenland. *Ocean Modelling*, *12*(3), 416–435. https://doi.org/10.1016/j.ocemod.2005.08.003

Gillard, L. C., Hu, X., Myers, P. G., & Bamber, J. L. (2016). Meltwater pathways from marine terminating glaciers of the Greenland ice sheet. *Geophysical Research Letters*, *43*(20), 10, 873–10, 882. https://doi.org/10.1002/2016GL070969

Goddard, P. B., Yin, J., Griffies, S. M., & Zhang, S. (2015). An extreme event of sea-level rise along the Northeast coast of North America in 2009–2010. *Nature Communications*, *6*(1), 6346. https://doi.org/10.1038/ncomms7346

Gou, R., Feucher, C., Pennelly, C., & Myers, P. G. (2021). Seasonal Cycle of the Coastal West Greenland Current System Between Cape Farewell and Cape Desolation From a Very High-Resolution Numerical Model. *Journal of Geophysical Research: Oceans*, *126*(5), e2020JC017017. https://doi.org/10.1029/2020JC017017

Gou, R., Pennelly, C., & Myers, P. G. (2022). The Changing Behavior of the West Greenland Current System in a Very High-Resolution Model. *Journal of Geophysical Research: Oceans*, *127*(8), e2022JC018404. https://doi.org/10.1029/2022JC018404

Griffies, S. M., Danabasoglu, G., Durack, P. J., Adcroft, A. J., Balaji, V., Böning, C. W., Chassignet, E. P., Curchitser, E., Deshayes, J., Drange, H., Fox-Kemper, B., Gleckler, P. J., Gregory, J. M., Haak, H., Hallberg, R. W., Heimbach, P., Hewitt, H. T., Holland, D. M., Ilyina, T., ... Yeager, S. G. (2016). OMIP contribution to CMIP6: Experimental and diagnostic protocol for the physical component of the Ocean Model Intercomparison Project. *Geoscientific Model Development*, *9*(9), 3231–3296. https://doi.org/10.5194/gmd-9-3231-2016

Haine, T. W. N., Curry, B., Gerdes, R., Hansen, E., Karcher, M., Lee, C., Rudels, B., Spreen, G., de Steur, L., Stewart, K. D., & Woodgate, R. (2015). Arctic freshwater export: Status, mechanisms, and prospects. *Global and Planetary Change*, *125*, 13–35. https://doi.org/10.1016/j.gloplacha.2014.11.013

Häkkinen, S., Rhines, P. B., & Worthen, D. L. (2013). Northern North Atlantic sea surface height and ocean heat content variability. *Journal of Geophysical Research: Oceans*, *118*(7), 3670–3678. https://doi.org/10.1002/jgrc.20268

Hallberg, R. (2013). Using a resolution function to regulate parameterizations of oceanic mesoscale eddy effects. *Ocean Modelling*, *72*, 92–103. https://doi.org/10.1016/j.ocemod.2013.08.007

Hanna, E., Huybrechts, P., Steffen, K., Cappelen, J., Huff, R., Shuman, C., Irvine-Fynn, T., Wise, S., & Griffiths, M. (2008). Increased Runoff from Melt from the Greenland Ice Sheet: A Response to Global Warming. *Journal of Climate*, *21*(2), 331–341. https://doi.org/10.1175/2007JCLI1964.1

Hanna, E., McConnell, J., Das, S., Cappelen, J., & Stephens, A. (2006). Observed and Modeled Greenland Ice Sheet Snow Accumulation, 1958–2003, and Links with Regional Climate Forcing. *Journal of Climate*, *19*(3), 344–358. https://doi.org/10.1175/JCLI3615.1

Hanna, E., Mernild, S. H., Cappelen, J., & Steffen, K. (2012). Recent warming in Greenland in a long-term instrumental (1881–2012) climatic context: I. Evaluation of surface air temperature records. *Environmental Research Letters*, *7*(4), 045404. https://doi.org/10.1088/1748-9326/7/4/045404

Håvik, L., Pickart, R. S., Våge, K., Torres, D., Thurnherr, A. M., Beszczynska-Möller, A., Walczowski, W., & von Appen, W.-J. (2017). Evolution of the East Greenland Current from Fram Strait to Denmark Strait: Synoptic measurements from summer 2012. *Journal of Geophysical Research: Oceans*, *122*(3), 1974–1994. https://doi.org/10.1002/2016JC012228

Henry, O., Prandi, P., Llovel, W., Cazenave, A., Jevrejeva, S., Stammer, D., Meyssignac, B., & Koldunov, N. (2012). Tide gauge-based sea level variations since 1950 along the Norwegian and Russian coasts of the Arctic Ocean: Contribution of the steric and mass components. *Journal of Geophysical Research (Oceans)*, *117*, C06023. https://doi.org/10.1029/2011JC007706

Hirschi, J. J.-M., Barnier, B., Böning, C., Biastoch, A., Blaker, A. T., Coward, A., Danilov, S., Drijfhout, S., Getzlaff, K., Griffies, S. M., Hasumi, H., Hewitt, H., Iovino, D., Kawasaki, T., Kiss, A. E., Koldunov, N., Marzocchi, A., Mecking, J. V., Moat, B., … Xu, X. (2020). The Atlantic Meridional Overturning Circulation in High-Resolution Models. *Journal of Geophysical Research: Oceans*, *125*(4), e2019JC015522. https://doi.org/10.1029/2019JC015522

Hirschi, J. J.-M., Killworth, P. D., Blundell, J. R., & Cromwell, D. (2009). Sea Surface Height Signals as Indicators for Oceanic Meridional Mass Transports. *Journal of Physical Oceanography*, *39*(3), 581–601. https://doi.org/10.1175/2008JPO3923.1

Holland, D. M., Thomas, R. H., De Young, B., Ribergaard, M. H., & Lyberth, B. (2008). Acceleration of Jakobshavn Isbr triggered by warm subsurface ocean waters. *Nature Geoscience*, *1*(10), 659–664. https://doi.org/10.1038/ngeo316

Holliday, N. P., Bersch, M., Berx, B., Chafik, L., Cunningham, S., Florindo-López, C., Hátún, H., Johns, W., Josey, S. A., Larsen, K. M. H., Mulet, S., Oltmanns, M., Reverdin, G., Rossby, T., Thierry, V., Valdimarsson, H., & Yashayaev, I. (2020). Ocean circulation causes the largest freshening event for 120 years in eastern subpolar North Atlantic. *Nature Communications*, *11*(1), 585. https://doi.org/10.1038/s41467-020-14474-y

Holliday, N. P., Meyer, A., Bacon, S., Alderson, S. G., & de Cuevas, B. (2007). Retroflection of part of the east Greenland current at Cape Farewell. *Geophysical Research Letters*, *34*(7). https://doi.org/10.1029/2006GL029085

Hu, A., Meehl, G. A., Han, W., & Yin, J. (2011). Effect of the potential melting of the Greenland Ice Sheet on the Meridional Overturning Circulation and global climate in the future. *Deep Sea Research Part II: Topical Studies in Oceanography*, *58*(17), 1914–1926. https://doi.org/10.1016/j.dsr2.2010.10.069

Hurrell, J. W. (1995). Decadal Trends in the North Atlantic Oscillation: Regional Temperatures and Precipitation [Publisher: American Association for the Advancement of Science]. *Science*, *269*(5224), 676–679. https://doi.org/10.1126/science.269.5224.676

Hurrell, J. W., & Deser, C. (2010). North Atlantic climate variability: The role of the North Atlantic Oscillation. *Journal of Marine Systems*, *79*(3), 231–244. https://doi.org/10.1016/j.jmarsys.2009.11.002

Hurrell, J. W., Kushnir, Y., Ottersen, G., & Visbeck, M. (2003). An Overview of the North Atlantic Oscillation. In *The North Atlantic Oscillation: Climatic Significance and Environmental Impact* (pp. 1–35). American Geophysical Union (AGU). https://doi.org/10.1029/134GM01

Jackson, L. C., Kahana, R., Graham, T., Ringer, M. A., Woollings, T., Mecking, J. V., & Wood, R. A. (2015). Global and European climate impacts of a slowdown of the AMOC in a high resolution GCM. *Climate Dynamics*, *45*(11), 3299–3316. https://doi.org/10.1007/s00382-015-2540-2

Jackson, L. C., & Wood, R. A. (2018). Hysteresis and Resilience of the AMOC in an Eddy-Permitting GCM. *Geophysical Research Letters*, *45*(16), 8547–8556. https://doi.org/10.1029/2018GL078104

Jackson, L. C., Alastrué de Asenjo, E., Bellomo, K., Danabasoglu, G., Haak, H., Hu, A., Jungclaus, J., Lee, W., Meccia, V. L., Saenko, O., Shao, A., & Swingedouw, D. (2023). Understanding AMOC stability: The North Atlantic Hosing Model Intercomparison Project. *Geoscientific Model Development*, *16*(7), 1975–1995. https://doi.org/10.5194/gmd-16-1975-2023

Jackson, L. C., Biastoch, A., Buckley, M. W., Desbruyères, D. G., Frajka-Williams, E., Moat, B., & Robson, J. (2022). The evolution of the North Atlantic Meridional Overturning Circulation since 1980. *Nature Reviews Earth & Environment*, *3*(4), 241–254. https://doi.org/10.1038/s43017-022-00263-2

Johnson, G., & Wijffels, S. (2011). Ocean Density Change Contributions to Sea Level Rise. *Oceanography*, *24*(2), 112–121. https://doi.org/10.5670/oceanog.2011.31

Josey, S. A., & Marsh, R. (2005). Surface freshwater flux variability and recent freshening of the North Atlantic in the eastern subpolar gyre. *Journal of Geophysical Research: Oceans*, *110*(C5). https://doi.org/10.1029/2004JC002521

Jungclaus, J. H., Haak, H., Esch, M., Roeckner, E., & Marotzke, J. (2006). Will Greenland melting halt the thermohaline circulation? *Geophysical Research Letters*, *33*(17). https://doi.org/10.1029/2006GL026815

Katsman, C. A., Spall, M. A., & Pickart, R. S. (2004). Boundary Current Eddies and Their Role in the Restratification of the Labrador Sea. *Journal of Physical Oceanography*, *34*(9), 1967–1983. https://doi.org/10.1175/1520-0485(2004)034<1967:BCEATR>2.0.CO;2

Kienert, H., & Rahmstorf, S. (2012). On the relation between Meridional Overturning Circulation and sea-level gradients in the Atlantic. *Earth System Dynamics*, *3*(2), 109–120. https://doi.org/10.5194/esd-3-109-2012

Koenigk, T., Fuentes-Franco, R., Meccia, V. L., Gutjahr, O., Jackson, L. C., New, A. L., Ortega, P., Roberts, C. D., Roberts, M. J., Arsouze, T., Iovino, D., Moine, M.-P., & Sein, D. V. (2021). Deep mixed ocean volume in the Labrador Sea in HighResMIP models. *Climate Dynamics*, *57*(7), 1895–1918. https://doi.org/10.1007/s00382-021-05785-x

Kopp, R. E., Mitrovica, J. X., Griffies, S. M., Yin, J., Hay, C. C., & Stouffer, R. J. (2010). The impact of Greenland melt on local sea levels: A partially coupled analysis of dynamic and static equilibrium effects in idealized water-hosing experiments. *Climatic Change*, *103*(3), 619–625. https://doi.org/10.1007/s10584-010-9935-1

Koul, V., Tesdal, J.-E., Bersch, M., Hátún, H., Brune, S., Borchert, L., Haak, H., Schrum, C., & Baehr, J. (2020). Unraveling the choice of the north Atlantic subpolar gyre index. *Scientific Reports*, *10*(1), 1005. https://doi.org/10.1038/s41598-020-57790-5

Kuhlbrodt, T., Griesel, A., Montoya, M., Levermann, A., Hofmann, M., & Rahmstorf, S. (2007). On the driving processes of the Atlantic meridional overturning circulation. *Reviews of Geophysics*, *45*(2). https://doi.org/10.1029/2004RG000166

Landerer, F. W., Jungclaus, J. H., & Marotzke, J. (2007). Regional Dynamic and Steric Sea Level Change in Response to the IPCC-A1B Scenario. *Journal of Physical Oceanography*, *37*(2), 296–312. https://doi.org/10.1175/JPO3013.1

Lazier, J. (1980). Oceanographic conditions at Ocean Weather Ship Bravo, 1964–1974. *Atmosphere-Ocean*, *18*(3), 227–238. https://doi.org/10.1080/07055900.1980.9649089

Lazier, J., Hendry, R., Clarke, A., Yashayaev, I., & Rhines, P. (2002). Convection and restratification in the Labrador Sea, 1990–2000. *Deep Sea Research Part I: Oceanographic Research Papers*, *49*(10), 1819–1835. https://doi.org/10.1016/S0967-0637(02)00064-X

Le Bras, I. A.-A., Straneo, F., Holte, J., de Jong, M. F., & Holliday, N. P. (2020). Rapid Export of Waters Formed by Convection Near the Irminger Sea's Western Boundary. *Geophysical Research Letters*, *47*(3), e2019GL085989. https://doi.org/10.1029/2019GL085989

Le Bras, I. A.-A., Straneo, F., Holte, J., & Holliday, N. P. (2018). Seasonality of Freshwater in the East Greenland Current System From 2014 to 2016. *Journal of Geophysical Research: Oceans*, *123*(12), 8828–8848. https://doi.org/10.1029/2018JC014511

Levermann, A., Griesel, A., Hofmann, M., Montoya, M., & Rahmstorf, S. (2005). Dynamic sea level changes following changes in the thermohaline circulation. *Climate Dynamics*, *24*(4), 347–354. https://doi.org/10.1007/s00382-004-0505-y

Li, F., Lozier, M. S., Bacon, S., Bower, A. S., Cunningham, S. A., de Jong, M. F., deYoung, B., Fraser, N., Fried, N., Han, G., Holliday, N. P., Holte, J., Houpert, L., Inall, M. E., Johns, W. E., Jones, S., Johnson, C., Karstensen, J., Le Bras, I. A., … Zhou, C. (2021). Subpolar North Atlantic western boundary density anomalies and the Meridional Overturning Circulation. *Nature Communications*, *12*(1), 3002. https://doi.org/10.1038/s41467-021-23350-2

Li, J., Tan, W., Chen, M., Zuo, J., & Yang, Y. (2016). The regional patterns of the global dynamic and steric sea level variation in twenty-first century projections. *Global and Planetary Change*, *146*, 133–139. https://doi.org/10.1016/j.gloplacha.2016.10.005

Lilly, J. M., Rhines, P. B., Schott, F., Lavender, K., Lazier, J., Send, U., & D'Asaro, E. (2003). Observations of the Labrador Sea eddy field. *Progress in Oceanography*, *59*(1), 75–176. https://doi.org/10.1016/j.pocean.2003.08.013

Lilly, J. M., Rhines, P. B., Visbeck, M., Davis, R., Lazier, J. R. N., Schott, F., & Farmer, D. (1999). Observing Deep Convection in the Labrador Sea during Winter 1994/95. *Journal of Physical Oceanography*, *29*(8), 2065–2098. https://doi.org/10.1175/1520-0485(1999)029<2065:ODCITL>2.0.CO;2

Lin, P., Pickart, R. S., Heorton, H., Tsamados, M., Itoh, M., & Kikuchi, T. (2023). Recent state transition of the Arctic Ocean's Beaufort Gyre. *Nature Geoscience*, *16*(6), 485–491. https://doi.org/10.1038/s41561-023-01184-5

Little, C. M., Hu, A., Hughes, C. W., McCarthy, G. D., Piecuch, C. G., Ponte, R. M., & Thomas, M. D. (2019). The Relationship Between U.S. East Coast Sea Level and the Atlantic Meridional Overturning Circulation: A Review. *Journal of Geophysical Research: Oceans*, *124*(9), 6435–6458. https://doi.org/10.1029/2019JC015152

Liu, W., Fedorov, A. V., Xie, S.-P., & Hu, S. (2020). Climate impacts of a weakened Atlantic Meridional Overturning Circulation in a warming climate. *Science Advances*, *6*(26), eaaz4876. https://doi.org/10.1126/sciadv.aaz4876

Llovel, W., Meyssignac, B., & Cazenave, A. (2011). Steric sea level variations over 2004–2010 as a function of region and depth: Inference on the mass component variability in the North Atlantic Ocean. *Geophysical Research Letters*, *38*(15). https://doi.org/10.1029/2011GL047411

Locarnini, R. A., Mishonov, A. V., Antonov, J. I., Boyer, T. P., Garcia, H. E., Baranova, O. K., Zweng, M. M., Paver, C. R., Reagan, J. R., Johnson, D. R., Hamilton, M., & Seidov, D. (2013). World ocean atlas 2013. Volume 1, Temperature. https://doi.org/10.7289/V55X26VD

Lohmann, K., Putrasahan, D. A., von Storch, J.-S., Gutjahr, O., Jungclaus, J. H., & Haak, H. (2021). Response of Northern North Atlantic and Atlantic Meridional Overturning Circulation to Reduced and Enhanced Wind Stress Forcing. *Journal of Geophysical Research: Oceans*, *126*(11), e2021JC017902. https://doi.org/10.1029/2021JC017902

Lohmann, K., Drange, H., & Bentsen, M. (2009a). A possible mechanism for the strong weakening of the North Atlantic subpolar gyre in the mid-1990s. *Geophysical Research Letters*, *36*(15). https://doi.org/10.1029/2009GL039166

Lohmann, K., Drange, H., & Bentsen, M. (2009b). Response of the North Atlantic subpolar gyre to persistent North Atlantic oscillation like forcing. *Climate Dynamics*, *32*(2), 273–285. https://doi.org/10.1007/s00382-008-0467-6

Lorbacher, K., Dengg, J., Böning, C. W., & Biastoch, A. (2010). Regional Patterns of Sea Level Change Related to Interannual Variability and Multidecadal Trends in the Atlantic Meridional Overturning Circulation. *Journal of Climate*, *23*(15), 4243–4254. https://doi.org/10.1175/2010JCLI3341.1

Lozier, M. S., Li, F., Bacon, S., Bahr, F., Bower, A. S., Cunningham, S. A., de Jong, M. F., de Steur, L., deYoung, B., Fischer, J., Gary, S. F., Greenan, B. J. W., Holliday, N. P., Houk, A., Houpert, L., Inall, M. E., Johns, W. E., Johnson, H. L., Johnson, C., … Zhao, J. (2019). A sea change in our view of overturning in the subpolar North Atlantic. *Science*, *363*(6426), 516–521. https://doi.org/10.1126/science.aau6592

Luo, H., Bracco, A., & Di Lorenzo, E. (2011). The interannual variability of the surface eddy kinetic energy in the Labrador Sea. *Progress in Oceanography*, *91*(3), 295–311. https://doi.org/10.1016/j.pocean.2011.01.006

Luo, H., Castelao, R. M., Rennermalm, A. K., Tedesco, M., Bracco, A., Yager, P. L., & Mote, T. L. (2016). Oceanic transport of surface meltwater from the southern Greenland ice sheet. *Nature Geoscience*, *9*(7), 528–532. https://doi.org/10.1038/ngeo2708

Madec, G., & Team, N. S. (2016). NEMO Ocean Engine. *Scientific Notes of Climate Modeling Center*, *27*. https://doi.org/10.5281/zenodo.1464816

Mahajan, S., Zhang, R., Delworth, T. L., Zhang, S., Rosati, A. J., & Chang, Y.-S. (2011). Predicting Atlantic meridional overturning circulation (AMOC) variations using subsurface and surface fingerprints. *Deep Sea Research Part II: Topical Studies in Oceanography*, *58*(17), 1895–1903. https://doi.org/10.1016/j.dsr2.2010.10.067

Marsh, R., Desbruyères, D., Bamber, J. L., de Cuevas, B. A., Coward, A. C., & Aksenov, Y. (2010). Short-term impacts of enhanced Greenland freshwater fluxes in an eddy-permitting ocean model. *Ocean Science*, *6*(3), 749–760. https://doi.org/10.5194/os-6-749-2010

Marshall, J., & Schott, F. (1999). Open-ocean convection: Observations, theory, and models. *Reviews of Geophysics*, *37*(1), 1–64. https://doi.org/10.1029/98RG02739

Marson, J. M., Myers, P. G., Hu, X., & Le Sommer, J. (2018). Using Vertically Integrated Ocean Fields to Characterize Greenland Icebergs' Distribution and Lifetime. *Geophysical Research Letters*, *45*(9), 4208–4217. https://doi.org/10.1029/2018GL077676

Martin, T., & Adcroft, A. (2010). Parameterizing the fresh-water flux from land ice to ocean with interactive icebergs in a coupled climate model. *Ocean Modelling*, *34*(3), 111–124. https://doi.org/10.1016/j.ocemod.2010.05.001

Martin, T., & Biastoch, A. (2023). On the ocean's response to enhanced Greenland runoff in model experiments: Relevance of mesoscale dynamics and atmospheric coupling. *Ocean Science*, *19*(1), 141–167. https://doi.org/10.5194/os-19-141-2023

Martin, T., Biastoch, A., Lohmann, G., Mikolajewicz, U., & Wang, X. (2022). On Timescales and Reversibility of the Ocean's Response to Enhanced Greenland Ice Sheet Melting in Comprehensive Climate Models. *Geophysical Research Letters*, *49*(5), e2021GL097114. https://doi.org/10.1029/2021GL097114

McCarthy, G., Frajka-Williams, E., Johns, W. E., Baringer, M. O., Meinen, C. S., Bryden, H. L., Rayner, D., Duchez, A., Roberts, C., & Cunningham, S. A. (2012). Observed interannual variability of the Atlantic meridional overturning circulation at 26.5°N. *Geophysical Research Letters*, *39*(19). https://doi.org/10.1029/2012GL052933

Megann, A., Blaker, A., Josey, S., New, A., & Sinha, B. (2021). Mechanisms for Late 20th and Early 21st Century Decadal AMOC Variability. *Journal of Geophysical Research: Oceans*, *126*(12), e2021JC017865. https://doi.org/10.1029/2021JC017865

Meinen, C. S., Speich, S., Perez, R. C., Dong, S., Piola, A. R., Garzoli, S. L., Baringer, M. O., Gladyshev, S., & Campos, E. J. D. (2013). Temporal variability of the meridional overturning circulation at 34.5°S: Results from two pilot boundary arrays in the South Atlantic. *Journal of Geophysical Research: Oceans*, *118*(12), 6461–6478. https://doi.org/10.1002/2013JC009228

Moore, G. W. K. (2003). Gale force winds over the Irminger Sea to the east of Cape Farewell, Greenland. *Geophysical Research Letters*, *30*(17). https://doi.org/10.1029/2003GL018012

Moore, G. W. K., & Renfrew, I. A. (2005). Tip Jets and Barrier Winds: A QuikSCAT Climatology of High Wind Speed Events around Greenland. *Journal of Climate*, *18*(18), 3713–3725. https://doi.org/10.1175/JCLI3455.1

Mouginot, J., Rignot, E., Bjørk, A. A., van den Broeke, M., Millan, R., Morlighem, M., Noël, B., Scheuchl, B., & Wood, M. (2019). Forty-six years of Greenland Ice Sheet mass balance from 1972 to 2018. *Proceedings of the National Academy of Sciences*, *116*(19), 9239–9244. https://doi.org/10.1073/pnas.1904242116

Myers, P. G. (2005). Impact of freshwater from the Canadian Arctic Archipelago on Labrador Sea Water formation. *Geophysical Research Letters*, *32*(6). https://doi.org/10.1029/2004GL022082

Myers, P. G., Donnelly, C., & Ribergaard, M. H. (2009). Structure and variability of the West Greenland Current in Summer derived from 6 repeat standard sections. *Progress in Oceanography*, *80*(1), 93–112. https://doi.org/10.1016/j.pocean.2008.12.003

Myers, P. G., Kulan, N., & Ribergaard, M. H. (2007). Irminger Water variability in the West Greenland Current. *Geophysical Research Letters*, *34*(17). https://doi.org/10.1029/2007GL030419

Neff, W., Compo, G. P., Martin Ralph, F., & Shupe, M. D. (2014). Continental heat anomalies and the extreme melting of the Greenland ice surface in 2012 and 1889. *Journal of Geophysical Research: Atmospheres*, *119*(11), 6520–6536. https://doi.org/10.1002/2014JD021470

Nummelin, A., Ilicak, M., Li, C., & Smedsrud, L. H. (2016). Consequences of future increased Arctic runoff on Arctic Ocean stratification, circulation, and sea ice cover. *Journal of Geophysical Research: Oceans*, *121*(1), 617–637. https://doi.org/10.1002/2015JC011156

Ortega, P., Robson, J., Sutton, R. T., & Andrews, M. B. (2017). Mechanisms of decadal variability in the Labrador Sea and the wider North Atlantic in a high-resolution climate model. *Climate Dynamics*, *49*(7), 2625–2647. https://doi.org/10.1007/s00382-016-3467-y

Orvik, K. A., & Niiler, P. (2002). Major pathways of Atlantic water in the northern North Atlantic and Nordic Seas toward Arctic. *Geophysical Research Letters*, *29*(19), 2–1–2–4. https://doi.org/10.1029/2002GL015002

Pacini, A., & Pickart, R. S. (2022). Meanders of the West Greenland Current near Cape Farewell. *Deep Sea Research Part I: Oceanographic Research Papers*, *179*, 103664. https://doi.org/10.1016/j.dsr.2021.103664

Pacini, A., & Pickart, R. S. (2023). Wind-Forced Upwelling Along the West Greenland Shelfbreak: Implications for Labrador Sea Water Formation. *Journal of Geophysical Research: Oceans*, *128*(3), e2022JC018952. https://doi.org/10.1029/2022JC018952

Pacini, A., Pickart, R. S., Bahr, F., Torres, D. J., Ramsey, A. L., Holte, J., Karstensen, J., Oltmanns, M., Straneo, F., Bras, I. A. L., Moore, G. W. K., & Jong, M. F. d. (2020). Mean Conditions and Seasonality of the West Greenland Boundary Current System near Cape Farewell. *Journal of Physical Oceanography*, *50*(10), 2849–2871. https://doi.org/10.1175/JPO-D-20-0086.1

Pacini, A., Pickart, R. S., Bras, I. A. L., Straneo, F., Holliday, N. P., & Spall, M. A. (2021). Cyclonic Eddies in the West Greenland Boundary Current System. *Journal of Physical Oceanography*, *51*(7), 2087–2102. https://doi.org/10.1175/JPO-D-20-0255.1

Parsons, L. A., Yin, J., Overpeck, J. T., Stouffer, R. J., & Malyshev, S. (2014). Influence of the Atlantic Meridional Overturning Circulation on the monsoon rainfall and carbon balance of the American tropics. *Geophysical Research Letters*, *41*(1), 146–151. https://doi.org/10.1002/2013GL058454

Petit, T., Lozier, M. S., Josey, S. A., & Cunningham, S. A. (2020). Atlantic Deep Water Formation Occurs Primarily in the Iceland Basin and Irminger Sea by Local Buoyancy Forcing. *Geophysical Research Letters*, *47*(22), e2020GL091028. https://doi.org/10.1029/2020GL091028

Pickart, R. S., Spall, M. A., Ribergaard, M. H., Moore, G. W. K., & Milliff, R. F. (2003). Deep convection in the Irminger Sea forced by the Greenland tip jet. *Nature*, *424*(6945), 152–156. https://doi.org/10.1038/nature01729

Pickart, R. S., Torres, D. J., & Clarke, R. A. (2002). Hydrography of the Labrador Sea during Active Convection. *Journal of Physical Oceanography*, *32*(2), 428–457. https://doi.org/10.1175/1520-0485(2002)032<0428:HOTLSD>2.0.CO;2

Piron, A., Thierry, V., Mercier, H., & Caniaux, G. (2017). Gyre-scale deep convection in the subpolar North Atlantic Ocean during winter 2014–2015. *Geophysical Research Letters*, *44*(3), 1439–1447. https://doi.org/10.1002/2016GL071895

Piron, A., Thierry, V., Mercier, H., & Caniaux, G. (2016). Argo float observations of basin-scale deep convection in the Irminger sea during winter 2011–2012. *Deep Sea Research Part I: Oceanographic Research Papers*, *109*, 76–90. https://doi.org/10.1016/j.dsr.2015.12.012

Proshutinsky, A., Krishfield, R., Timmermans, M.-L., Toole, J., Carmack, E., McLaughlin, F., Williams, W. J., Zimmermann, S., Itoh, M., & Shimada, K. (2009). Beaufort Gyre freshwater reservoir: State and variability from observations. *Journal of Geophysical Research: Oceans*, *114*(C1). https://doi.org/10.1029/2008JC005104

Rahmstorf, S. (1995). Bifurcations of the Atlantic thermohaline circulation in response to changes in the hydrological cycle. *Nature*, *378*(6553), 145–149. https://doi.org/10.1038/378145a0

Reverdin, G., Niiler, P. P., & Valdimarsson, H. (2003). North Atlantic Ocean surface currents. *Journal of Geophysical Research: Oceans*, *108*(C1), 2–1–2–21. https://doi.org/10.1029/2001JC001020

Rhein, M., Kieke, D., Hüttl-Kabus, S., Roessler, A., Mertens, C., Meissner, R., Klein, B., Böning, C. W., & Yashayaev, I. (2011). Deep water formation, the subpolar gyre, and the meridional overturning circulation in the subpolar North Atlantic. *Deep Sea Research Part II: Topical Studies in Oceanography*, *58*(17), 1819–1832. https://doi.org/10.1016/j.dsr2.2010.10.061

Rhein, M., Steinfeldt, R., Kieke, D., Stendardo, I., & Yashayaev, I. (2017). Ventilation variability of Labrador Sea Water and its impact on oxygen and anthropogenic carbon: A review. *Philosophical Transactions of the Royal Society A: Mathematical, Physical and Engineering Sciences*, *375*(2102), 20160321. https://doi.org/10.1098/rsta.2016.0321

Rieck, J. K., Böning, C. W., & Getzlaff, K. (2019). The Nature of Eddy Kinetic Energy in the Labrador Sea: Different Types of Mesoscale Eddies, Their Temporal Variability, and Impact on Deep Convection. *Journal of Physical Oceanography*, *49*(8), 2075–2094. https://doi.org/10.1175/JPO-D-18-0243.1

Rignot, E., Fenty, I., Xu, Y., Cai, C., & Kemp, C. (2015). Undercutting of marine-terminating glaciers in West Greenland. *Geophysical Research Letters*, *42*(14), 5909–5917. https://doi.org/10.1002/2015GL064236

Rignot, E., Koppes, M., & Velicogna, I. (2010). Rapid submarine melting of the calving faces of West Greenland glaciers. *Nature Geoscience*, *3*(3), 187–191. https://doi.org/10.1038/ngeo765

Robson, J., Ortega, P., & Sutton, R. (2016). A reversal of climatic trends in the North Atlantic since 2005. *Nature Geoscience*, *9*(7), 513–517. https://doi.org/10.1038/ngeo2727

Rossby, T. (1996). The North Atlantic Current and surrounding waters: At the crossroads. *Reviews of Geophysics*, *34*(4), 463–481. https://doi.org/10.1029/96RG02214

Ruan, R., Chen, X., Zhao, J., Perrie, W., Mottram, R., Zhang, M., Diao, Y., Du, L., & Wu, L. (2019). Decelerated Greenland Ice Sheet Melt Driven by Positive Summer North Atlantic Oscillation. *Journal of Geophysical Research: Atmospheres*, *124*(14), 7633–7646. https://doi.org/10.1029/2019JD030689

Rudels, B. (2011). Volume and freshwater transports through the Canadian Arctic Archipelago–Baffin Bay system. *Journal of Geophysical Research: Oceans*, *116*(C8). https://doi.org/10.1029/2011JC007019

Rudels, B., Fahrbach, E., Meincke, J., Budéus, G., & Eriksson, P. (2002). The East Greenland Current and its contribution to the Denmark Strait overflow. *ICES Journal of Marine Science*, *59*(6), 1133–1154. https://doi.org/10.1006/jmsc.2002.1284

Rühs, S., Oliver, E. C. J., Biastoch, A., Böning, C. W., Dowd, M., Getzlaff, K., Martin, T., & Myers, P. G. (2021). Changing Spatial Patterns of Deep Convection in the Subpolar North Atlantic. *Journal of Geophysical Research: Oceans*, *126*(7), e2021JC017245. https://doi.org/10.1029/2021JC017245

Saenko, O. A., Yang, D., & Myers, P. G. (2017). Response of the North Atlantic dynamic sea level and circulation to Greenland meltwater and climate change in an eddy-permitting ocean model. *Climate Dynamics*, *49*(7), 2895–2910. https://doi.org/10.1007/s00382-016-3495-7

Sanchez-Franks, A., & Zhang, R. (2015). Impact of the Atlantic meridional overturning circulation on the decadal variability of the Gulf Stream path and regional chlorophyll and nutrient concentrations. *Geophysical Research Letters*, *42*(22), 9889–9887. https://doi.org/10.1002/2015GL066262

Schauer, U., & Losch, M. (2019). "Freshwater" in the Ocean is Not a Useful Parameter in Climate Research. *Journal of Physical Oceanography*, *49*(9), 2309–2321. https://doi.org/10.1175/JPO-D-19-0102.1

Schulze, L. M., Pickart, R. S., & Moore, G. W. K. (2016). Atmospheric forcing during active convection in the Labrador Sea and its impact on mixed-layer depth. *Journal of Geophysical Research: Oceans*, *121*(9), 6978–6992. https://doi.org/10.1002/2015JC011607

Schulze Chretien, L. M., & Frajka-Williams, E. (2018). Wind-driven transport of fresh shelf water into the upper 30 m of the Labrador Sea. *Ocean Science*, *14*(5), 1247–1264. https://doi.org/10.5194/os-14-1247-2018

Slater, D. A., & Straneo, F. (2022). Submarine melting of glaciers in Greenland amplified by atmospheric warming. *Nature Geoscience*, *15*(10), 794–799. https://doi.org/10.1038/s41561-022-01035-9

Slater, D. A., Straneo, F., Felikson, D., Little, C. M., Goelzer, H., Fettweis, X., & Holte, J. (2019). Estimating Greenland tidewater glacier retreat driven by submarine melting. *The Cryosphere*, *13*(9), 2489–2509. https://doi.org/10.5194/tc-13-2489-2019

Slater, T., Shepherd, A., McMillan, M., Leeson, A., Gilbert, L., Muir, A., Munneke, P. K., Noël, B., Fettweis, X., van den Broeke, M., & Briggs, K. (2021). Increased variability in Greenland Ice Sheet runoff from satellite observations. *Nature Communications*, *12*(1), 6069. https://doi.org/10.1038/s41467-021-26229-4

Smeed, D. A., McCarthy, G. D., Cunningham, S. A., Frajka-Williams, E., Rayner, D., Johns, W. E., Meinen, C. S., Baringer, M. O., Moat, B. I., Duchez, A., & Bryden, H. L. (2014). Observed decline of the Atlantic meridional overturning circulation 2004–2012. *Ocean Science*, *10*(1), 29–38. https://doi.org/10.5194/os-10-29-2014

Smith, R. S., & Gregory, J. M. (2009). A study of the sensitivity of ocean overturning circulation and climate to freshwater input in different regions of the North Atlantic. *Geophysical Research Letters*, *36*(15). https://doi.org/10.1029/2009GL038607

Spall, M. A., & Pickart, R. S. (2001). Where Does Dense Water Sink? A Subpolar Gyre Example. *Journal of Physical Oceanography*, *31*(3), 810–826. https://doi.org/10.1175/1520-0485(2001)031<0810:WDDWSA>2.0.CO;2

Spall, M. A., Semper, S., & Våge, K. (2024). Mechanisms of Offshore Solid and Liquid Freshwater Flux from the East Greenland Current. *Journal of Physical Oceanography*, *54*(2), 379–397. https://doi.org/10.1175/JPO-D-23-0120.1

Stammer, D. (2008). Response of the global ocean to Greenland and Antarctic ice melting. *Journal of Geophysical Research: Oceans*, *113*(C6). https://doi.org/10.1029/2006JC004079

Sterl, M. F., & de Jong, M. F. (2022). Restratification Structure and Processes in the Irminger Sea. *Journal of Geophysical Research: Oceans*, *127*(12), e2022JC019126. https://doi.org/10.1029/2022JC019126

Stouffer, R. J., Yin, J., Gregory, J. M., Dixon, K. W., Spelman, M. J., Hurlin, W., Weaver, A. J., Eby, M., Flato, G. M., Hasumi, H., Hu, A., Jungclaus, J. H., Kamenkovich, I. V., Levermann, A., Montoya, M., Murakami, S., Nawrath, S., Oka, A., Peltier, W. R., … Weber, S. L. (2006). Investigating the Causes of the Response of the Thermohaline Circulation to Past and Future Climate Changes. *Journal of Climate*, *19*(8), 1365–1387. https://doi.org/10.1175/JCLI3689.1

Stramma, L., Kieke, D., Rhein, M., Schott, F., Yashayaev, I., & Koltermann, K. P. (2004). Deep water changes at the western boundary of the subpolar North Atlantic during 1996 to 2001. *Deep Sea Research Part I: Oceanographic Research Papers*, *51*(8), 1033–1056. https://doi.org/10.1016/j.dsr.2004.04.001

Straneo, F., & Cenedese, C. (2015). The Dynamics of Greenland's Glacial Fjords and Their Role in Climate. *Annual Review of Marine Science*, *7*, 89–112. https://doi.org/10.1146/annurev-marine-010213-135133

Straneo, F., & Heimbach, P. (2013). North Atlantic warming and the retreat of Greenland's outlet glaciers. *Nature*, *504*(7478), 36–43. https://doi.org/10.1038/nature12854

Sun, J., Latif, M., & Park, W. (2021). Subpolar Gyre–AMOC–Atmosphere Interactions on Multidecadal Timescales in a Version of the Kiel Climate Model. *Journal of Climate*, *34*(16), 6583–6602. https://doi.org/10.1175/JCLI-D-20-0725.1

Sutherland, D. A., & Cenedese, C. (2009). Laboratory Experiments on the Interaction of a Buoyant Coastal Current with a Canyon: Application to the East Greenland Current. *Journal of Physical Oceanography*, *39*(5), 1258–1271. https://doi.org/10.1175/2008JPO4028.1

Sutherland, D. A., & Pickart, R. S. (2008). The East Greenland Coastal Current: Structure, variability, and forcing. *Progress in Oceanography*, *78*(1), 58–77. https://doi.org/10.1016/j.pocean.2007.09.006

Swingedouw, D., Bopp, L., Matras, A., & Braconnot, P. (2007). Effect of land-ice melting and associated changes in the AMOC result in little overall impact on oceanic CO2 uptake. *Geophysical Research Letters*, *34*(23). https://doi.org/10.1029/2007GL031990

Swingedouw, D., Braconnot, P., & Marti, O. (2006). Sensitivity of the Atlantic Meridional Overturning Circulation to the melting from northern glaciers in climate change experiments. *Geophysical Research Letters*, *33*(7). https://doi.org/10.1029/2006GL025765

Swingedouw, D., Houssais, M.-N., Herbaut, C., Blaizot, A.-C., Devilliers, M., & Deshayes, J. (2022). AMOC Recent and Future Trends: A Crucial Role for Oceanic Resolution and Greenland Melting? *Frontiers in Climate*, *4*. https://doi.org/10.3389/fclim.2022.838310

Swingedouw, D., Mignot, J., Labetoulle, S., Guilyardi, E., & Madec, G. (2013). Initialisation and predictability of the AMOC over the last 50 years in a climate model. *Climate Dynamics*, *40*(9), 2381–2399. https://doi.org/10.1007/s00382-012-1516-8

Swingedouw, D., Rodehacke, C. B., Behrens, E., Menary, M., Olsen, S. M., Gao, Y., Mikolajewicz, U., Mignot, J., & Biastoch, A. (2013). Decadal fingerprints of freshwater discharge around Greenland in a multi-model ensemble. *Climate Dynamics*, *41*(3), 695–720. https://doi.org/10.1007/s00382-012-1479-9

Talley, L., Pickard, G., Emery, W., & Swift, J. (2011). *Descriptive Physical Oceanography: An Introduction*. Academic Press.

Tedesco, M., Fettweis, X., Mote, T., Wahr, J., Alexander, P., Box, J. E., & Wouters, B. (2013). Evidence and analysis of 2012 Greenland records from spaceborne observations, a regional climate model and reanalysis data. *The Cryosphere*, *7*(2), 615–630. https://doi.org/10.5194/tc-7-615-2013

The Lab Sea Group. (1998). The Labrador Sea Deep Convection Experiment. *Bulletin of the American Meteorological Society*, *79*(10), 2033–2058. https://doi.org/10.1175/1520-0477(1998)079<2033:TLSDCE>2.0.CO;2

Thomas, M. D., Tréguier, A.-M., Blanke, B., Deshayes, J., & Voldoire, A. (2015). A Lagrangian Method to Isolate the Impacts of Mixed Layer Subduction on the Meridional Overturning Circulation in a Numerical Model. *Journal of Climate*, *28*(19), 7503–7517. https://doi.org/10.1175/JCLI-D-14-00631.1

Toole, J. M., Curry, R. G., Joyce, T. M., McCartney, M., & Peña-Molino, B. (2011). Transport of the North Atlantic Deep Western Boundary Current about 39°N, 70°W: 2004–2008. *Deep Sea Research Part II: Topical Studies in Oceanography*, *58*(17), 1768–1780. https://doi.org/10.1016/j.dsr2.2010.10.058

Trenberth, K. E., Zhang, Y., Fasullo, J. T., & Cheng, L. (2019). Observation-Based Estimates of Global and Basin Ocean Meridional Heat Transport Time Series. *Journal of Climate*, *32*(14), 4567–4583. https://doi.org/10.1175/JCLI-D-18-0872.1

Tsujino, H., Urakawa, S., Nakano, H., Small, R. J., Kim, W. M., Yeager, S. G., Danabasoglu, G., Suzuki, T., Bamber, J. L., Bentsen, M., Böning, C. W., Bozec, A., Chassignet, E. P., Curchitser, E., Boeira Dias, F., Durack, P. J., Griffies, S. M., Harada, Y., Ilicak, M., … Yamazaki, D. (2018). JRA-55 based surface dataset for driving ocean–sea-ice models (JRA55-do). *Ocean Modelling*, *130*, 79–139. https://doi.org/10.1016/j.ocemod.2018.07.002

Vellinga, M., & Wood, R. A. (2008). Impacts of thermohaline circulation shutdown in the twenty-first century. *Climatic Change*, *91*(1), 43–63. https://doi.org/10.1007/s10584-006-9146-y

Visbeck, M. H., Hurrell, J. W., Polvani, L., & Cullen, H. M. (2001). The North Atlantic Oscillation: Past, present, and future. *Proceedings of the National Academy of Sciences*, *98*(23), 12876–12877. https://doi.org/10.1073/pnas.231391598

Volkov, D. L., Lee, S.-K., Domingues, R., Zhang, H., & Goes, M. (2019). Interannual Sea Level Variability Along the Southeastern Seaboard of the United States in Relation to the Gyre-Scale Heat Divergence in the North Atlantic. *Geophysical Research Letters*, *46*(13), 7481–7490. https://doi.org/10.1029/2019GL083596

Volkov, D. L., Zhang, K., Johns, W. E., Willis, J. K., Hobbs, W., Goes, M., Zhang, H., & Menemenlis, D. (2023). Atlantic meridional overturning circulation increases flood risk along the United States southeast coast. *Nature Communications*, *14*(1), 5095. https://doi.org/10.1038/s41467-023-40848-z

Wang, Q., Wekerle, C., Danilov, S., Koldunov, N., Sidorenko, D., Sein, D., Rabe, B., & Jung, T. (2018). Arctic Sea Ice Decline Significantly Contributed to the Unprecedented Liquid Freshwater Accumulation in the Beaufort Gyre of the Arctic Ocean. *Geophysical Research Letters*, *45*(10), 4956–4964. https://doi.org/10.1029/2018GL077901

Wang, Z., Lu, Y., Dupont, F., W. Loder, J., Hannah, C., & G. Wright, D. (2015). Variability of sea surface height and circulation in the North Atlantic: Forcing mechanisms and linkages. *Progress in Oceanography*, *132*, 273–286. https://doi.org/10.1016/j.pocean.2013.11.004

Westen, R. M. v., Kliphuis, M., & Dijkstra, H. A. (2024). Physics-based early warning signal shows that AMOC is on tipping course. *Science Advances*, *10*(6). https://doi.org/10.1126/sciadv.adk1189

Wu, P., Wood, R., & Stott, P. (2005). Human influence on increasing Arctic river discharges. *Geophysical Research Letters*, *32*(2). https://doi.org/10.1029/2004GL021570

Yashayaev, I., & Loder, J. W. (2016). Recurrent replenishment of Labrador Sea Water and associated decadal-scale variability. *Journal of Geophysical Research: Oceans*, *121*(11), 8095–8114. https://doi.org/10.1002/2016JC012046

Yashayaev, I., & Loder, J. W. (2017). Further intensification of deep convection in the Labrador Sea in 2016. *Geophysical Research Letters*, *44*(3), 1429–1438. https://doi.org/10.1002/2016GL071668

Yeager, S. (2015). Topographic Coupling of the Atlantic Overturning and Gyre Circulations. *Journal of Physical Oceanography*, *45*(5), 1258–1284. https://doi.org/10.1175/JPO-D-14-0100.1

Yeager, S., & Danabasoglu, G. (2014). The Origins of Late-Twentieth-Century Variations in the Large-Scale North Atlantic Circulation. *Journal of Climate*, *27*(9), 3222–3247. https://doi.org/10.1175/JCLI-D-13-00125.1

Yeager, S., Karspeck, A., Danabasoglu, G., Tribbia, J., & Teng, H. (2012). A Decadal Prediction Case Study: Late Twentieth-Century North Atlantic Ocean Heat Content. *Journal of Climate*, *25*(15), 5173–5189. https://doi.org/10.1175/JCLI-D-11-00595.1

Yin, J., Griffies, S. M., & Stouffer, R. J. (2010). Spatial Variability of Sea Level Rise in Twenty-First Century Projections. *Journal of Climate*, *23*(17), 4585–4607. https://doi.org/10.1175/2010JCLI3533.1

Yin, J., Schlesinger, M. E., & Stouffer, R. J. (2009). Model projections of rapid sea-level rise on the northeast coast of the United States. *Nature Geoscience*, *2*(4), 262–266. https://doi.org/10.1038/ngeo462

Zhang, J., Weijer, W., Steele, M., Cheng, W., Verma, T., & Veneziani, M. (2021). Labrador Sea freshening linked to Beaufort Gyre freshwater release. *Nature Communications*, *12*(1), 1229. https://doi.org/10.1038/s41467-021-21470-3

Zhang, L., Delworth, T. L., Yang, X., & Zeng, F. (2023). Skillful multiyear to decadal predictions of sea level in the North Atlantic Ocean and U.S. East Coast. *Communications Earth & Environment*, *4*(1), 1–10. https://doi.org/10.1038/s43247-023-01093-w

Zhang, R. (2008). Coherent surface-subsurface fingerprint of the Atlantic meridional overturning circulation. *Geophysical Research Letters*, *35*(20). https://doi.org/10.1029/2008GL035463

Zhang, R., Delworth, T. L., Rosati, A., Anderson, W. G., Dixon, K. W., Lee, H.-C., & Zeng, F. (2011). Sensitivity of the North Atlantic Ocean Circulation to an abrupt change in the Nordic Sea overflow in a high resolution global coupled climate model. *Journal of Geophysical Research: Oceans*, *116*(C12). https://doi.org/10.1029/2011JC007240

Zhang, W., & Yan, X.-H. (2017). The Subpolar North Atlantic Ocean Heat Content Variability and its Decomposition. *Scientific Reports*, *7*(1), 13748. https://doi.org/10.1038/s41598-017-14158-6

Zhao, J., & Johns, W. (2014). Wind-forced interannual variability of the Atlantic Meridional Overturning Circulation at 26.5°N. *Journal of Geophysical Research: Oceans*, *119*(4), 2403–2419. https://doi.org/10.1002/2013JC009407

Zou, S., Lozier, M. S., Li, F., Abernathey, R., & Jackson, L. (2020). Density-compensated overturning in the Labrador Sea. *Nature Geoscience*, *13*(2), 121–126. https://doi.org/10.1038/s41561-019-0517-1

Zunino, P., Mercier, H., & Thierry, V. (2020). Why did deep convection persist over four consecutive winters (2015–2018) southeast of Cape Farewell? *Ocean Science*, *16*(1), 99–113. https://doi.org/10.5194/os-16-99-2020

Zweng, M. M., Reagan, J. R., Antonov, J. I., Locarnini, R. A., Mishonov, A. V., Boyer, T. P., Garcia, H. E., Baranova, O. K., Johnson, D. R., Seidov, D., & Biddle, M. M. (2013). World ocean atlas 2013. Volume 2, Salinity. https://doi.org/10.7289/V5251G4D

List of Figures

1.1 Schematic of current pathways from AMOC. The northward/southward branch highlighted in red/blue. The areas of deep water formation are marked. Source: Crivellari, 2018. 3

1.2 The evolution of AMOC volume transport given in Sverdrups (Sv) at 26°N in a CSEM model version 1.0.5, after freshwater is fluxed into the North Atlantic (area marked by light blue rectangle in the globe inset). The proposed tipping point is indicated by the red arrow (source: Westen et al., 2024). 5

1.3 Schematic of major surface currents and basins. Atlantic-origin pathways in red and yellow, Arctic-origin freshwater pathways marked in blue. The dynamic thinning of Greenland is superimposed (source: Straneo and Heimbach, 2013). 7

1.4 Schematic of circulation along the East and West Greenland boundary system. EGCC: East Greenland Coastal Current, EGC/IC: East Greenland Current/Irminger Curent, WGCC: West Greenlannd coastal current, WGC: West Greenland Current (source: Pacini and Pickart, 2023). 8

1.5 (a) Composite map of ice speed over the Greenland ice sheet (source: Mouginot et al., 2019). (b) Annual Greenland freshwater fluxes (km^3/year) split up into runoff components (D is solid ice discharge, R_t is tundra, R_{GRIS} is Greenland ice sheet runoff, and R_{GIC} is glaicer and ice cap runoff outside of Greenland). Solid lines are 5 years moving averages (left-hand y axis), the total freshwater fluxes in the solid black line (right-hand y axis) (source: Bamber et al., 2018). 12

1.6 Greenland meltwater as passive tracer content in a meltwater release experiment in a high-resolution, eddy resolving model. Largescale current pathways are marked in white, with eddies denoted by small circles. (source: Martin and Biastoch, 2023). 13

4.1 (a) Decadally filtered AMOC at 26.5°N from 1980–2019 across the different cycles. Red is the 1st cycle, orange is the 2nd, green is the 3rd, blue is the 4th, dark blue is the 5th, and black is the 6th cycle. The blue/red vertical shading indicates the high/low phase of AMOC. (b) Schematic of AMOC from Little et al., 2019. Abbreviations: NRG = Northern Recirculation Gyre; LC = Labrador Current; DWBC = Deep Western Boundary Current; IC = Irminger Current; EGIC = East Greenland-Irminger Current. 75

4.2 (a). The SSH difference between lower (2005–2015) and higher (1987–1997) AMOC phases for cycle 1. (b) The SSH difference for cycle 6. Positive/negative values indicate an increase/decrease in regional SSH. (c) The difference in OHC (low minus high AMOC phase) for cycle 1. (d) The OHC difference in cycle 6. (e) FWC difference (low minus high AMOC) in cycle 1. (f) FWC difference in cycle 6. The blue/red contour shows the Gulf Stream axis during high/low AMOC phases. 81

4.3 (a). Correlation between the decadally filtered AMOC at 26.5°N and SSH for the 1st cycle. The black stippling indicates nonsignificant areas. (b) The correlation between the AMOC and SSH for the 6th cycle. (c). The correlation between the extended AMOC and SSH field, where the extended time series consists of 1980–2021 of the 1st cycle, then 1950–2021 of cycle 2–6. (d) The regression of the decadally filtered AMOC onto SSH for the 1st cycle. (e) The regression of the AMOC onto SSH for the 6th cycle. (f) The regression of the temporally extended AMOC onto the extended SSH field. 83

4.4 (a) Steric sea level changes between the lower minus higher AMOC phase in the 1st cycle. Positive/negative values indicates greater/lower steric sea level changes in the lower AMOC phase compared to the higher AMOC phase. (b) The thermosteric sea level contribution between the two AMOC phases in the 1st cycle. (c) The halosteric sea level contribution for the 1st cycle. (d) The steric sea level change between weaker minus stronger AMOC phases in the 6th cycle. (e) The thermosteric sea level contribtion in the 6th cycle. (f) The halosteric sea level contribution in the 6th cycle. 85

4.5 (a). The SSH difference during the weaker AMOC phase (2005–2015) between the reference run with enhanced Greenland runoff as observed and the sensitivity experiment with reduced, climatological runoff. The black stippling indicates non-significant areas from bootstrapping. (b) Pentadally filtered Greenland FWFs (blue), AMOC at 26.5°N from the 1st cycle (Green), and the NAO (black). (c) Decadally filtered Greenland FWFs, AMOC at 26.5°, and the NAO from 1980–2016. 87